An Investigation into the Decontamination of Carbon-14 from Irradiated Graphite

James Gill, B.Sc. (Hons)

A thesis submitted in partial fulfilment for the requirements of the degree of Doctor of Philosophy at the University of Central Lancashire

Forensic and Investigative Science Department

Centre for Materials Science

University of Central Lancashire

Dec/2014

DECLARATION

I declare that no material contained in the thesis has been used in any other submission for an academic award and is solely my own work. The work described in this thesis was conducted at the Centre for Materials Science, University of Central Lancashire, between October 2010 and Dec 2014.

Signature: 

James Richard Gill

Dec 2014

ABSTRACT

The decommissioning of nuclear power plants around the world will produce a major waste stream of irradiated graphite. Graphite has been used extensively as a reactor moderator and reflector material that becomes irradiated and contaminated over time. In the coming years ~250,000 tonnes of irradiated graphite will require management making this a significant waste management issue worldwide. Irradiated graphite is categorised as Intermediate Level Waste mostly due to its content of Carbon-14 (C-14) which is a long-lived radioisotope which could be released into the biosphere. In addition the Low Level Waste (LLW) repository at Drigg has very strict guidelines regarding C-14 authorisation and there is currently no deep geological repository available in the UK. Varying amounts of carbonaceous deposits have been identified on irradiated graphite samples removed from reactor cores. If these deposits are rich in C-14, treatment of the waste graphite by oxidation could reduce the C-14 inventory of the remaining graphite. This is the primary focus of this research.

In order to investigate a technique that would decontaminate graphite from the carbonaceous deposits it was necessary to produce a range of carbonaceous deposits on virgin graphite material to act as a simulant for the deposits present on reactor graphite. Two deposition techniques were investigated: microwave plasma assisted chemical vapour deposition and a combination of solution deposition and charring. C-13 precursors were used as they facilitate the study of the selective removal of the deposit by mass spectrometry and spectroscopy. Using C-13 analogues instead of C-14 prevents the need to work in active laboratories and allows higher concentrations of deposit to be used which is beneficial when developing a technique for selective removal. A thermal treatment which utilised the application of a vacuum was investigated to determine whether the carbonaceous deposits could be selectively removed with minimal oxidation to the underlying graphite. As carbon deposits were more amorphous than crystalline graphite it was thought that they would oxidise quicker at lower temperatures than graphite. Virgin graphite and samples with deposits were characterised before and after thermal treatment using Scanning Electron Microscopy, Raman Spectroscopy, Thermal Gravimetric Analysis and Mass Spectrometry.

An additional area of investigation was conducted using thermogravimetric studies of the oxidation of irradiated graphite which was carried out at the National Nuclear Laboratory's Preston Lab. This would determine the distribution of C-14 in the carbonaceous deposits and underlying irradiated graphite which could be a key factor in the determination of possible treatments and eventual storage/disposal routes of the waste graphite.

CONTENTS

TABLE OF FIGURES

LIST OF TABLES

ABBREVIATIONS

AGR	Advanced Gas-cooled Reactor
AVR	Arbeitsgemeinschaft Versuchs Reacktor
BEPO	British Energy Pile O
BWR	Boiling Water Reactor
CASE	Collaborative Awards in Science and Engineering
CCD	Charge Coupled Device
CEA	Commissariat a l'Energie Atomique
CoRWM	Committee on Radioactive Waste Management
CVD	Chemical Vapour Deposition
DFR	Dounreay Fast Reactor
DMTR	Dounreay Materials Test Reactor
DSRL	Dounreay Site Restoration Limited
DTG	Differential Thermal Gravimetry
EDF	Electricité de France
EURATOM	European Atomic Energy Community
FIB	Focused Ion Beam
GIF	Generation IV International Forum
GLEEP	Graphite Low Energy Experimental Pile
HLW	High Level Waste
HTR	High Temperature Reactor
ILW	Intermediate Level Waste
ISO	International Organisation for Standardisation
LLW	Low Level Waste
MDA	Minimum Detectable Activity

MERLIN	Medium Energy Research Light Water Moderated Industrial Nuclear Reactor
MID	Multiple Ion Detection
NDA	Nuclear Decommissioning Authority
NNL	National Nuclear Laboratory
PFR	Prototype Fast Reactor
PGA	Pile Grade A
PWR	Pressurised Water Reactors
RBMK-1000	Reaktor Bolshoy Moshchnosti Kanalnyy-1000
RSRL	Research Sites Restoration Limited
SEM	Scanning Electron Microscopy
SIMS	Secondary Ion Mass Spectrometry
TGA	Thermal Gravimetric Analysis
THOR	Thermal Organic Reduction
UKAEA	United Kingdom Atomic Energy Authority
UKAS	United Kingdom Accreditation Service
UKRWI	United Kingdom Radioactive Waste Inventory
UNGG	Uranium Natural Graphite Gaz Reactor
VHTR	Very High Temperature Reactor
VLLW	Very Low Level Waste
VPPM	Parts Per Million per Volume
WPPM	Parts Per Million per Weight
WAGR	Windscale Advanced Gas-cooled Reactor

ACKNOWLEDGEMENTS

I would like to extend my gratitude to my supervisors Professors Gary Bond of the Centre for Materials Science and Harry Eccles of the School of Computing, Engineering and Physical Sciences at the University of Central Lancashire, for their inspiration, guidance and support throughout this project. Without their insight and in-depth knowledge this work could not have been carried out. I would also like to thank Jim Donnelly and Dr Runjie Moa for assistance in using and understanding the equipment. In addition I would like to thank fellow post graduate researchers in particular the Graphite Research Team for assistance and support throughout my study.

Externally I would like to extend my thanks to Martin Metcalfe and Nassia Tzelepi from the National Nuclear Laboratory (NNL) for their support, insight and assistance with the interpretation of the C-14 results. I would also like to thank Dr Nick Hodge with the NNL Preston Laboratory Process Development team for assistance provided throughout the course of the mini project at Springfields as well as the Measurement and Analysis Team based at NNL Preston Laboratory for analytical assistance.

Finally a special thanks to my family and friends whose combined support has been invaluable over the years of my study. My mum and dad for providing in me the desire to succeed through the threat of having to join the army, Heather for your support and patience and my daughter Ava to whom this work is dedicated.

I am indebted to the EPSRC and NNL for financial support throughout my research.

1. INTRODUCTION

This chapter provides an insight into the use of graphite as a moderator in nuclear reactors, along with a summary of the structure and properties of graphite. A review of waste management opportunities and repository options in the United Kingdom (UK) for the disposal of irradiated graphite waste will also be discussed.

1.1 Graphite and the Nuclear Industry

Graphite is widely used in the nuclear industry as a moderator, reflector and fuel matrix in various types of reactors worldwide. Although not part of a nuclear reaction itself it plays a key role in slowing down neutron bombardment meaning the chain reaction is maintained longer. The unique combination of graphite properties means that it remains chemically and structurally stable at high temperatures.

1.2 Key Components of a Nuclear Reactor

A nuclear reactor generates electricity by producing steam which drives turbines similar to those found in most fossil fuel plants. However the steam is produced using the thermal energy generated from the splitting of the atoms of certain elements. The fuel used in nuclear reactors is uranium, more specifically the isotope uranium-235 (U-235). Naturally occurring uranium is made up predominantly of the non-fissile isotope uranium-238 (U-238), with U-235 only making up 0.7 % of the total uranium. Whilst this percentage of U-235 is adequate for some reactors (e.g. Magnox), others require an increased proportion of fissile material (U-235) through a process known as enrichment. Enriched uranium hexafluoride gas is then fabricated into uranium oxide powder, which in turn is pressed into pellets, which are arranged in tubes known as fuel rods. Control rods are also present in the reactor and can be withdrawn or inserted from the core to control the reaction rate or to stop it all together. Control rods are made up of neutron absorbing material such as boron, cadmium or hafnium. The reactor core is located within a steel pressure vessel along with the moderator and coolant. The coolant is circulated through the reactor core, to transfer heat from it, and is usually water or carbon dioxide (CO_2) gas. The function of the moderator is to slow down the neutrons released from fission, to initiate further fission, and thus sustaining the chain reaction for longer. The moderator can be water, heavy water or graphite. All of these components are housed within a metre thick structure made of concrete and steel which acts

as a biological shield. This is designed to protect anyone outside it from radiation and to protect the reactor from any outside influence[1].

1.3 A Brief History of Graphite Reactors

The use of graphite in the development of nuclear reactors will be described in this section, from the first sustained chain reaction, through to current reactors and plans for the future.

1.3.1 Origin

On December 2nd 1942 a team led by Enrico Fermi achieved the world's first controlled nuclear chain reaction which lasted only 28 minutes and produced 0.5 watts of power. The reactor was built in a squash court underneath a football stadium on the University of Chicago campus and was known as Chicago Pile 1 (CP-1). The reactor cost $1 million to build and was constructed from 12,400 pounds (US) of uranium metal and 80,590 pounds of uranium oxide as the fuel along with 771,000 pounds of graphite. This project formed the early stages of the Manhattan project which produced the first atomic bombs during World War 2[2,3].

1.3.2 Gas Cooled Reactors - Magnox

The first nuclear reactor opened commercially was in the UK and was opened by Her Majesty the Queen on 17th Oct 1956. This power station was known as Calder Hall and consisted of two graphite moderated reactors to begin with but increased to four over the years. Graphite was preferred as a moderator because of the existing knowledge available but also because the alternative, which was heavy water and beryllium, were not manufactured on a commercial scale in Great Britain. These reactors used natural uranium metal as the fuel and were gas cooled using CO_2. Gas cooling was selected over liquid cooling because gases absorb a smaller amount of neutrons. This early reactor design (Figure 1) was known as a Magnox reactor because the fuel element is enclosed in a casing made of a magnesium non oxidising alloy[4].

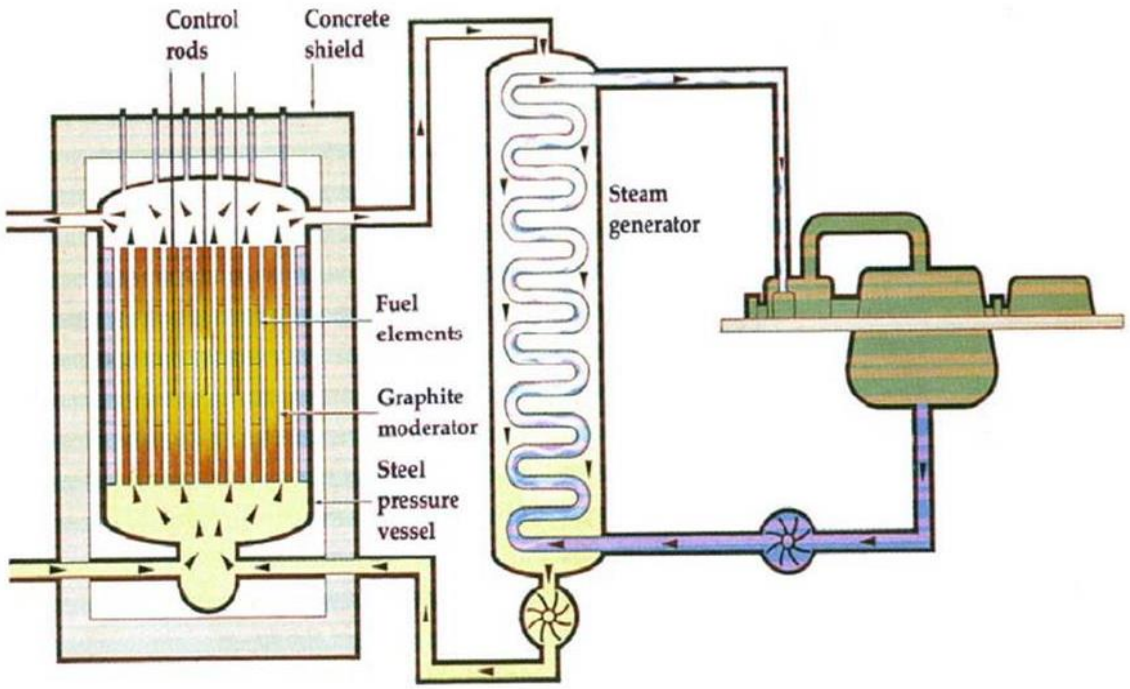

Figure 1 - Schematic of Magnox reactor design[5]

Calder hall consisted of four graphite moderated reactors which produced a gross electrical output of 4 x 46 MWe. The gas inlet temperature was 140°C compared with the outlet temperature of 336°C[6]. The primary objective of Calder hall was to produce plutonium for military purposes. The production of plutonium from uranium generates a lot of heat, so the production of electricity using steam created from the heat to drive turbines was seen as a free by-product. By 1959 the 2nd Magnox power station was opened in south-west Scotland known as Chapelcross and had 4 reactors and by 1971 a further nine Magnox power stations had been commissioned in the UK[7].

1.3.3 Advanced Gas-Cooled Reactors

In 1964 the government announced plans for the second generation of nuclear power stations. Opting to diverge away from other nuclear nations who favoured using water as a coolant, such as the American Boiling-Water Reactor (BWR), the British instead chose an improvement on the Magnox design known as the Advanced Gas-cooled Reactor (AGR). This new design required changing the fuel cladding from Magnox to stainless steel and an increase in pressure of the gas coolant. The fuel was also changed from uranium metal fuel with 0.7% U-235 to enriched uranium dioxide pellets with 2.5-3.5% U-235. This new reactor design (Figure 2) increased cost effectiveness by using a higher temperature (outlet gas

temperature ~650°C) to achieve higher thermal efficiencies and power densities to reduce capital costs[5].

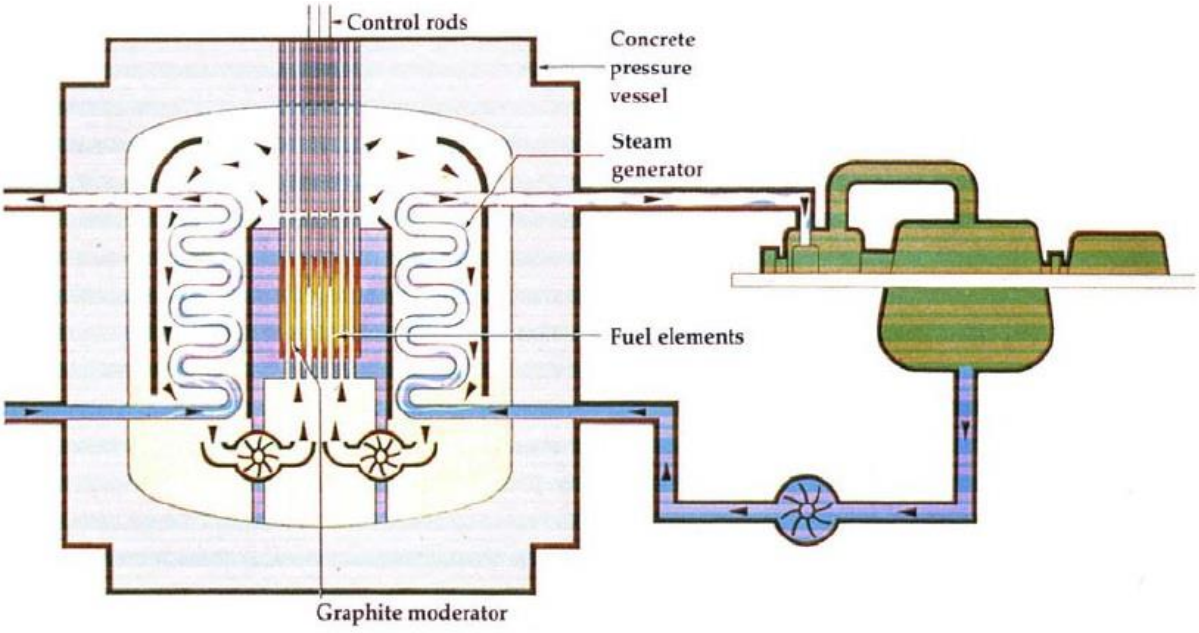

Figure 2 - Schematic of AGR design[5]

Along with control rods which penetrate the graphite moderator there is a secondary shutdown system which involves injecting nitrogen into the coolant. Much like the Magnox reactor design graphite was chosen as the moderator, as was the use of CO_2 gas as the coolant and the use of steam generators and gas circulators within a pressure vessel was retained[1,5,7]. The thermal efficiency is increased to 41% in AGRs compared to only 32% in Magnox reactors due to the higher running temperatures of 650°C being used. In order to avoid excessive thermal oxidation of the graphite bricks the moderator temperature is kept below 450°C. This is achieved by using re-entrant coolant flow where a portion of the coolant flows from the top of the core downwards between the bricks to the bottom of the fuel channels[8] (Figure 2).

1.3.4 High Temperature Gas Cooled Reactors

A number of high temperature gas-cooled reactors are currently in development although the first that will be commercially available will be in China, South Africa and the United States. The UK's current plans are most likely to use Pressurised Water Reactors (PWR) which will use water as a moderator and so will not be looked at in depth within this text[9].

1.3.5 Pebble Bed Modular Reactors

The pebble bed modulated reactor design (Figure 3) is a High Temperature Reactor (HTR) where the core is located within a pressurised steel vessel and the fuel comprises of enriched uranium dioxide (17% U-235) which has been encapsulated into graphite spheres. Unlike other graphite moderated reactors mentioned previously, helium is used as a coolant in this case and can reach temperatures of 950°C. Running at a higher temperature than previous reactor designs increases the thermal efficiency. Furthermore these reactors have a long life time due to the fact that spent fuel elements can be removed from the bottom of the core whilst new spheres can be added to the top[9].

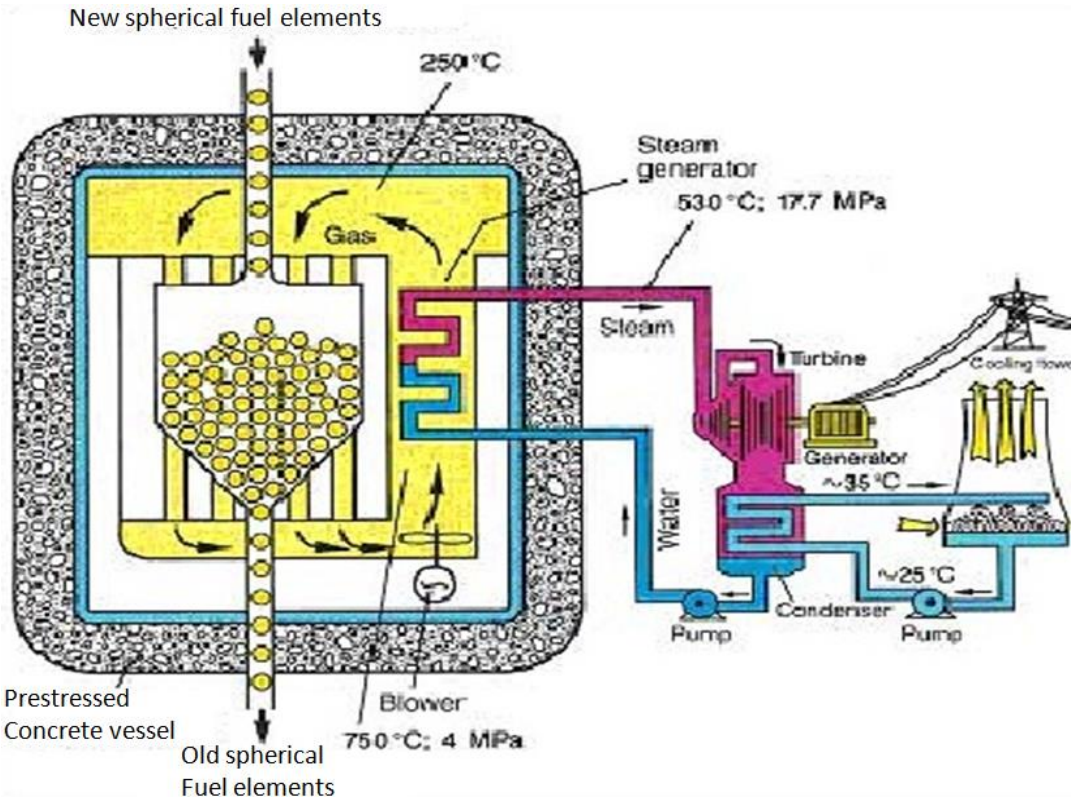

Figure 3 - Schematic of pebble bed modular reactor[10]

1.3.6 Future Builds

Having agreed that nuclear power would be required to meet energy needs in the future the Generation IV International Forum (GIF) was established in 2001. GIF is a multinational consortium tasked with the undertaking of research and development of the next generation of nuclear energy systems[11]. Six different nuclear energy systems were identified to develop

further however only one still uses graphite as a moderator and that is the Very High Temperature Reactor (VHTR) (Figure 4).

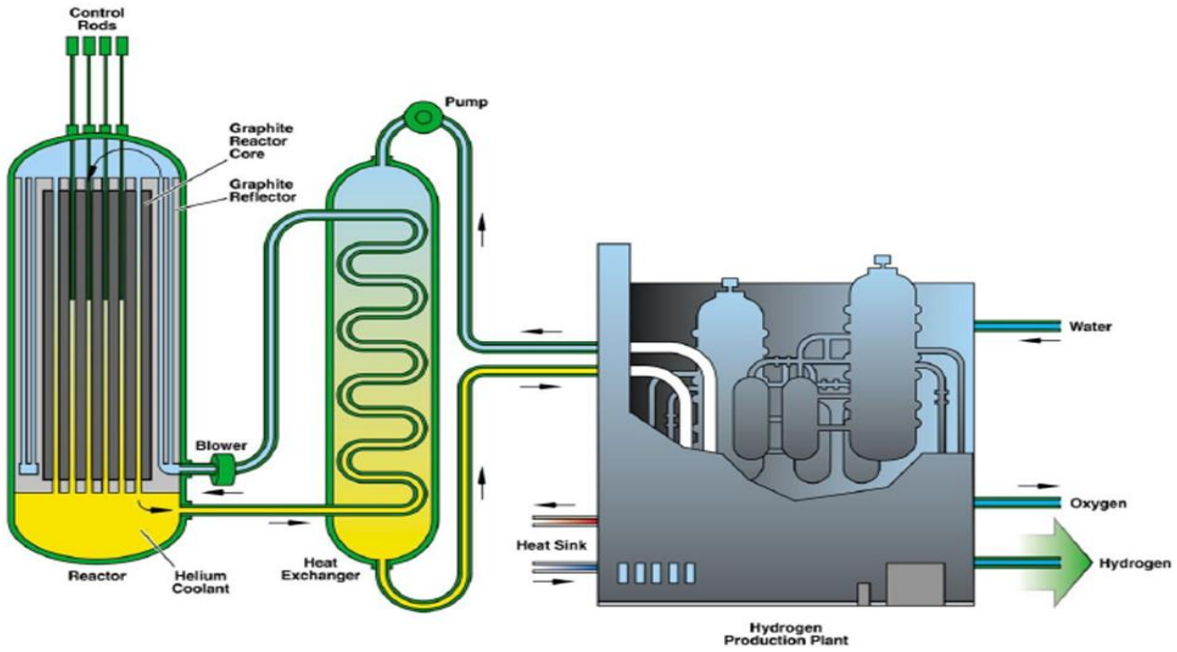

Figure 4 - Schematic of very high temperature reactor[12]

The basic technology of this design has already been established because this is the evolutionary development of the high temperature gas-cooled reactor design. Using helium gas as the coolant and graphite as the moderator the VHTR will have an outlet temperature of >900°C. Along with a high thermal efficiency this design has the added advantage of producing hydrogen by thermo-chemical processes as well as electricity[12].

1.4 The Properties of Graphite

In order to understand why graphite is used in the nuclear industry it is important to understand the unique properties that this allotrope of carbon exhibits. The following section will provide the reader with information on the structure and manufacturing of graphite along with its beneficial properties.

1.4.1 Natural Graphite

Natural graphite is a relatively abundant mineral found all over the world. It is classified as either amorphous, crystalline or flake depending on the type of precursor material present, either coal, oil or other carbonaceous material. The difference in precursor along with the

natural process which forms the graphite are factors which lead to the variance of chemical composition, impurities, appearance and physical properties of the different forms of natural graphite. Its uses in industry include lubricating oils and greases, batteries, conductive coatings, paints, pencil manufacture and more but the majority of graphite products are synthetic[13].

1.4.2 Nuclear Grade Graphite Manufacture

Nuclear grade graphite is a form of synthetic graphite which is manufactured using techniques for the production of graphite electrodes but with additional steps for the removal of impurities[14]. A schematic of the manufacture of nuclear grade graphite can be seen in (Figure 5) below.

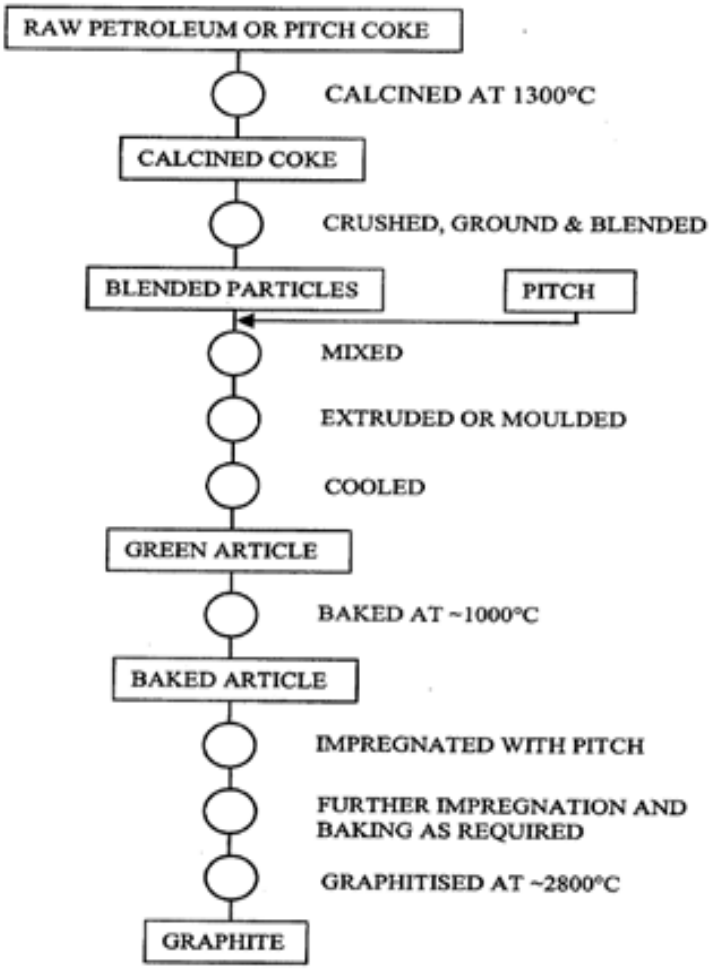

Figure 5 - Flowchart of the graphite manufacturing process[15]

The first stage in the graphite manufacturing process is the selection of a suitable coke. Needle coke is a product of the petroleum industry and because of its purity and availability, it was chosen for the production of Pile Grade A and B graphite, which was the graphite chosen to be the moderator for Magnox reactors in the UK. The coke used in AGRs is known as Gilsonite pitch coke and is formed from naturally occurring asphalt located in Utah USA. This form of coke contains spherical particulates with an onion skin structure[16].

The next stage of manufacturing involves the breaking up of the cokes and calcination at temperatures of 900-1300°C. These calcined cokes are then crushed, milled and graded where they can then be distributed to graphite manufacturers. The calcination procedure decreases the volume of shrinkage in later stages of the process and also removes volatile material.

The coke particles, commonly known as filler particles are then blended with a binding medium often a coal tar pitch, and in some cases some crushed graphite flour will be included in the mixture. The formation stage involves transforming this mixture into solid blocks referred to as the green article. Several forming methods can be adopted which may alter the final products properties. Many of the methods involve applying pressure to the mixture which is in a mould. AGR graphite was produced by moulding and pressing the mixture from one or two directions simultaneously. Other moulding techniques include using vibrations to compact the mixture or applying a uniform pressure to all sides of the coke mixture whilst situated in a rubber bag. However the most popular formation method is extrusion where the mixture, whilst under pressure, is forced through a template known as a die.

The newly formed green article is immersed in water for cooling however this can lead to internal cracks being produced, though the addition of the crushed graphite flour to the mix minimises this problem. Once cooled the green article is baked at 800°C in order to coke the binding material and drive off additional volatile material. It is necessary to surround the green article with a granular packing, commonly a coke in order to prevent oxidation during baking. During this bake gas evolution pores are produced throughout the material so it is important to increase the density of the blocks by impregnating them under vacuum with a pitch in an autoclave. Multiple impregnations may be required with the blocks being baked for a short period of time between each dose. This material can now be defined as carbon black and may be utilised as furnace liner or insulation after being subsequently baked at 1100°C.

The final stage of the manufacturing process is the graphitisation of the carbon blocks by either; covering them with an electrical conducting coke and applying a large electrical current to the coke covering or by applying the current directly to the carbon blocks having covered them with an oxidation protection coke. The graphitisation process is carried out at temperatures up to 3000°C and removes many impurities whilst improving the electrical and thermal conductivity as the graphite crystals are formed. The graphite blocks can now be machined into the required designs and can be utilised appropriately as a moderator in nuclear reactors[15].

1.4.3 Graphite as a Moderator

The moderator present in a nuclear reactor is essential to maintaining the chain reaction. During the fission of U-235 in the fuel, fast high energy neutrons are ejected from the nuclei and without the moderator these would be absorbed by the most abundant and more stable uranium isotope U-238. However the presence of a moderator will slow down enough of the fast neutrons to allow them to cause additional fissions with more U-235 nuclei and thus sustain a chain reaction for longer.

A good moderator must exhibit two important properties in order to be effective. They must have a low absorption cross section which is the probability that a neutron will be absorbed by the material. Furthermore its important that the moderator has a high scatter cross section which is the probability that a neutron will collide with an atom. The most suitable materials which possess these properties and are widely used in the nuclear industry are graphite, light water and heavy water, the properties of which can be seen in Table 1.

Heavy water has the lowest absorption cross section and so is technically the most suitable choice; however it's much more expensive than both light water and graphite which has restricted its use. Light water has the highest scattering cross section and is cheap but also has the highest absorption cross section which necessitates the use of enriched uranium fuel in the reactor which increases costs overall[17]. The advantages of using graphite are that it is inexpensive, thermally stable at high temperatures and relatively chemically inert. Furthermore graphite can be used as major structural components of nuclear plants and is a good neutron reflector[18].

Table 1 - The properties of moderator material[17]

Material	Absorption cross section (b)	Scattering cross section (b)
Graphite	0.0045	4.7
Light Water	0.66	49.2
Heavy Water	0.001	10.6

1.4.4 The Structure of Graphite

Graphite is a polycrystalline material meaning it's made up of a number of crystallites of varying size and orientation. The majority of graphite crystals exhibit what is known as hexagoanl stacking, where the planes are arranged in a ABAB stacking arrangment where carbon atoms in every other layer are superimposed over each other[13] (Figure 6).

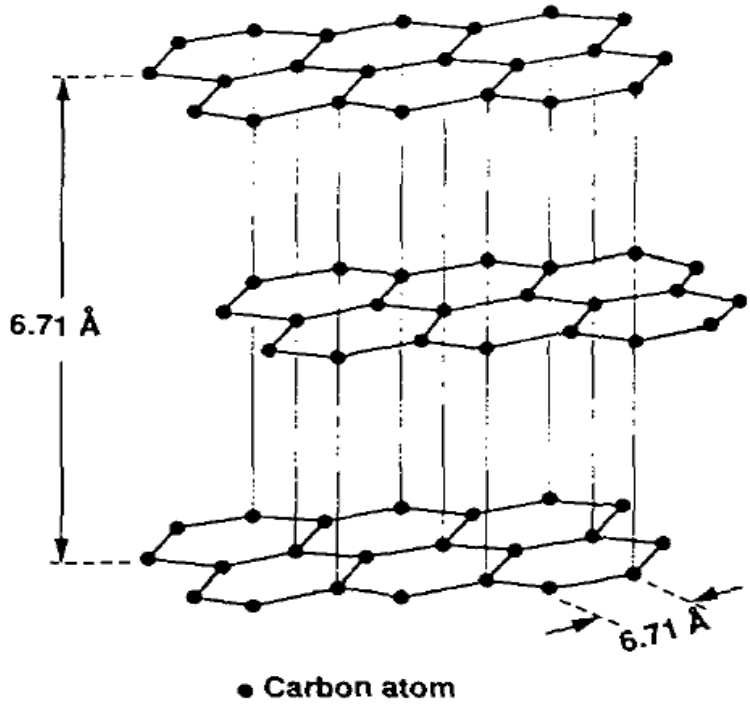

Figure 6 - Three-dimensional schematic of the graphite structure[13]

The covalent bonding between the carbon atoms that make up graphite are described as having trigonal sp^2 bonding. A valency of four is exhibited by carbon bonded this way from the promotion of an electron from the 2s orbital to combine with two of the 2p orbitals (hence sp^2), in order to produce three sp^2 orbitals and a delocalised p orbital. The sp^2 orbital has a

configuration which is lopsided which leads to extensive overlap with other sp^2 orbitals. This overlap is known as a sigma (σ) bond. Graphite exhibits a hexagonal structure as each of the sp^2 hybridised carbon atoms can combine with three other sp^2 hybridised carbon atoms (Figure 6).These parallel hexagonal planes are held together by the free delocalised electron (known as the pi (π) bond) which is orientated perpendicular to the sigma bonds in the hexagonal planes (Figure 7). The delocalised electrons are able to move easily from one side of the plane to the other but not so easily move from one layer to another. This means that graphite exhibits anisotropic properties, which in this case is a variance in the thermal and electrical properties depending on whether measurements are taken in the direction along the hexagonal plane or the direction perpendicular to the plane. The covalent sigma bonds have a high stregth (524 KJ/mol) and short length (0.141 nm) compared to the pi bonds held together by *Van der Waals* which have a low strength (7 KJ/mol) and are therefore longer (0.335 nm)[13].

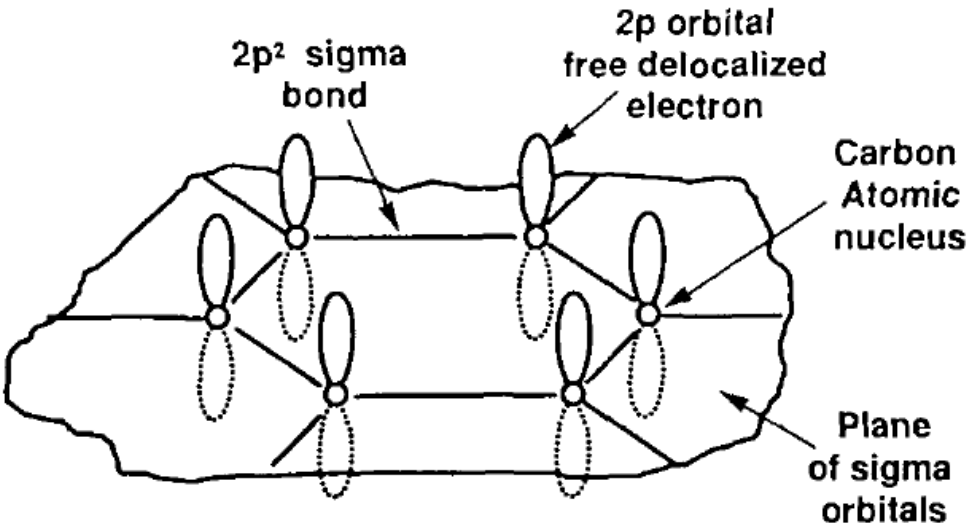

Figure 7 - Schematic of the sp^2 hybridised structure of graphite showing the sigma and pi bonds[13]

The crystallites can exhibit a number of imperfections which will in turn alter the properties of the bulk material. These defects include vacancies in the lattice structure, stacking faults in the ABAB structure or where the planes are no longer parallel, or growth defects such as edge dislocations. Therefore different graphite material will demonstrate differences in the shape, size and orientation of crystallites as well as the degree of imperfections present. Plus variation in porosity and amount of impurities means that graphite samples will display substantial differences in the properties they possess[13].

1.5 The Irradiated Graphite Challenge

The decommissioning of nuclear facilities around the world will produce a major waste stream of irradiated graphite. Graphite has been used extensively around the world as reactor moderator and reflector material and will become irradiated and contaminated over time. In the coming years ~250,000 tonnes of irradiated graphite will require management making this a serious problem worldwide[19]. When considering the management options it's necessary to characterise and understand the amount of variation of irradiated graphite waste. The neutron activation of graphite and its impurities leads to a variable radionuclide inventory because different types of graphite, with varying impurity contents, are used in different reactor designs with differing operation temperatures and coolants[20]. Furthermore there will be a proportion of the graphite waste which has been contaminated with actinides and fission products as a consequence of fuel element failures[21]. The presence of several long-lived isotopes makes the management of irradiated graphite waste problematic. Taking into consideration stored Wigner energy, graphite dust explosibility and the possible release of radioactive gases then making decisions regarding the treatment, disposal and storage options of irradiated graphite becomes a very challenging endeavour[19].

1.6 Volume of Waste

As stated above the estimated world-wide irradiated graphite inventory will be ~250,000 tonnes. Graphite is not only used in the large power producing reactors but has also been used extensively in prototype and experimental reactors such as HTRs and a number of plutonium producing reactors. Its used for structural components as well as neutron reflector and moderator material. The three nations within Europe with the largest quantities of irradiated graphite waste are France, Russia and the UK. Their waste volumes will be described in more detail in the following sections in order to provide the reader with an understanding of the scale of the irradiated graphite waste problem[22].

1.6.1 France

France has a total irradiated graphite inventory of about ~23,000 tonnes. This figure is divided between the three operators Electricité de France (EDF), Commissariat a l'Energie Atomique (CEA) and Areva. These three operators are responsible for the decommissioning of their nuclear facilities and financing the management of their produced waste. The

majority of the irradiated graphite waste comes from the operator EDF, the electrical utilities company who ran six natural-uranium gas cooled reactors (known in French as Uranium Naturel Graphite Gaz or UNGG reactors). The UNGG reactors are graphite moderated, CO_2 cooled and has natural uranium as fuel and their design is most similar to the British Magnox design. One of the main differences is that the fuel cladding used in the UNGG reactors is made of a magnesium-zirconium alloy as opposed to the magnesium-aluminium alloy used in Magnox reactors. These six UNGG reactors have all been shut down and their dismantling will produce about 17,000 tonnes of irradiated graphite waste including graphite sleeves temporarily stored at Saint-Laurent. The research group CEA will produce the 2nd largest proportion of French graphite waste of ~4,700 tonnes, from three UNGG reactors and some experimental reactors. Lastly the business corporation AREVA who work with used fuel treatment have temporarily stored ~1,000 tonnes of graphite sleeve[23].

1.6.2 Russia

There is presently only one operating organisation in Russia known as the Concern Rosenergoatom with an estimated volume of irradiated graphite waste of ~55,000 tonnes. This organisation is currently running 15 graphite-moderated water-cooled power reactors (4 EGP-6 reactors and 11 RBMK-1000 reactors). Three first generation reactors have been permanently shut down whereas in 2006 plans were put in place to extend the lifetime of the 11 RBMK reactors. A 45 year lifetime extension was considered realistic following extensive refurbishment including the replacement of fuel channels in addition to significant design modifications made after the Chernobyl accident**.** There were also 13 high-capacity weapons grade plutonium production reactors in operation which have all been shut down. These have been decommissioned by dismantling low activity structures, sealing off and filling all reactor spaces with concrete and Bentonite compounds, to ensure a sufficient protection barrier between the reactor and the environment is maintained[24].

1.6.3 United Kingdom

Commercial reactors that are currently in operation and generating electricity in the UK (as of 2014) include fourteen AGR reactors currently owned and operated by EDF Energy. There is also a single PWR (Sizewell B) which is also owned and operated by EDF Energy. Additionally Wylfa is the last remaining Magnox site operational, with one reactor retired in 2012 and one reactor expected to operate until late 2014[25]. Presently there are twenty-five

Magnox reactors in the UK which have been shut down and are awaiting decommissioning (Table 2). In the UK the Government, regulator and the producers of the irradiated graphite waste are responsible for its management[26].

A number of prototype, experimental and fuel production plants also containing graphite waste were once the responsibility of the UK Atomic Energy Authority (UKAEA) with ~6,000 tonnes of irradiated graphite waste to dispose of (Table 3). The UKAEA has since been divided into a number of subsidiary companies each responsible for sites around the UK. The Windscale AGR (WAGR) and the Windscale Piles now fall under the responsibility of Sellafield Limited. The subsidiary company Dounreay Site Restoration Limited (DSRL) is accountable for the Dounreay Fast Reactor (DFR) and the Dounreay Materials Test Reactor (DMTR). Whilst Research Sites Restoration Limited (RSRL) is responsible for the British Energy Pile O (BEPO), neutron reflector graphite from the two water moderated DIDO and PLUTO research reactors at Harwell as well as the high temperature DRAGON reactor at Winfrith[27,28]. The Graphite Low Energy Experimental Pile (GLEEP) has already been fully decommissioned, since the irradiation of the graphite and activation of impurities were both very low, the graphite core was crushed and treated in a commercial incinerator[29].

In order to obtain the most accurate figures for total graphite mass, raw volume and packaged volume the data from the UK Radioactive Waste Inventory (UKRWI) 2010[30] was corrected for the proportion of graphite present in mixed waste streams. Furthermore the value for packaged graphite volume is based on the proposed packaging plans from UKRWI 2010. The majority of graphite waste is produced from Magnox sites with over 56,000 tonnes of graphite waste to dispose of, with a further 24,000 tonnes attributed to AGR waste streams (Table 4). Combined with the graphite waste from the research reactors the total graphite waste will amass to over 85,000 tonnes of graphite and a packaged volume of almost 110,000 m^3 requiring appropriate disposal. With the addition of operational graphite waste to the decommissioned core graphite waste on a packaged volume basis, this amount will increase ~136,000 m^3 [28].

Table 2 - Summary of nuclear reactors containing graphite in the UK[26]

Reactor	Operation began	Operation ceased	Output per reactor MWe	Status
Experimental, Production and Prototype Reactors				
GLEEP	1947	1990	3 kWt	Decommissioned
BEPO	1948	1968	6 MWt	Shutdown
DIDO	1956	1990	26 MWt	Shutdown
PLUTO	1957	1990	26 MWt	Shutdown
DRAGON	1962	1975	20 MWt	Shutdown
Windscale Pile 1	1950	1957	180 MWt	Shutdown
Windscale Pile 2	1950	1957	180 MWt	Shutdown
WAGR	1962	1981	33	Partly decommissioned
Magnox Reactors				
Calder Hall	1956	2003	50 (x4) (D)	Shutdown
Chapelcross	1959	2004	49 (x4) (D)	Shutdown
Berkeley	1962	1989	150 (x2) (D)	Shutdown
Bradwell	1962	2002	121 (x2) (D)	Shutdown
Hunterston A	1964	1989	180 (x2) (D)	Shutdown
Hinkley Point A	1965	2000	250 (x2) (D)	Shutdown
Trawsfynydd	1965	1991	250 (x2) (D)	Shutdown
Dungeness A	1965	2006	275 (x2) (D)	Shutdown
Sizewell A	1966	2006	290 (x2) (D)	Shutdown
Oldbury	1967	2012	300 (x2) (D)	Shutdown
Wylfa	1971		590 (x2) (D)	Operating
Advanced Gas-cooled Reactors				
Dungeness B	1983/85		545 (x2) (A)	Operating
Hartlepool	1983/85		595 (x2) (A)	Operating
Heysham 1	1983/84		580 (x2) (A)	Operating
Heysham 2	1988		615 (x2) (A)	Operating
Hinkley Point B	1976		430 (x2) (A)	Operating
Hunterston B	1977		420 (x2) (A)	Operating
Torness	1988		625 (x2) (A)	Operating
Period of operation and current status (D=design, A=actual at Dec 2008)				

Table 3 - shows a summary of UKAEA graphite waste (2001)[27]

Reactor	Quantity of Graphite (te)	Purpose of the Graphite
GLEEP	505	Moderator and reflector
BEPO	766	Moderator and reflector
Windscale Pile 1	1966	Moderator and reflector
Windscale Pile 2	1966	Moderator and reflector
DFR	200	Borated graphite neutron shield
PFR	To be assessed	Neutron Shield
DIDO	17	Reflector only
PLUTO	17	Reflector only
DMTR	17	Reflector only
WAGR	210	Moderator and reflector

Table 4 - Mass and volume of core graphite wastes[28]

	Graphite mass t(e)	Raw graphite volume (m^3)	Graphite packaged volume (m^3)
Magnox reactors	56,555	45,244	59,190
EDF Energy AGR reactors	24,307	20,069	42,130
Sellafield reactors	3,967	2,890	6,493
RSRL research reactors	693	397	1,058
DSRL research reactors	296	124	623
Totals for all UK	**85,818**	**68,724**	**109,494**

1.7 Classification of Waste

In the UK legislation defines radioactive waste as material which incorporates or is contaminated by radioactivity above 40 kBq of beta/gamma activity for single items or 400 kBq for each cubic metre of material. Any materials below these levels of activity are classed as Very Low Level Waste (VLLW) and can be disposed of with ordinary refuse.

Any other radioactive material can be divided into three categories Low Level Waste (LLW), Intermediate Level Waste (ILW) and High Level Waste (HLW). LLW is specified as material whose activity does not exceed 12 GBq per tonne of beta/gamma activity or 4 GBq per tonne of alpha activity. LLW can be accepted for authorised disposal at landfill sites such as the Low Level Waste Repository near Drigg. HLW includes materials which have an activity which exceeds that specified for LLW and where the temperature of the waste may rise significantly as a result of their radioactivity. The possibility of a temperature rise in the waste is an important factor needed to be considered when designing disposal and storage facilities. ILW is classified as any material which exceeds the limits of LLW and where temperature change does not have to be taken into consideration[30,31].

Although the activity of irradiated graphite is below the limits established for LLW the majority of irradiated graphite waste produced is categorised as ILW. This is due to the fact that it cannot be accepted at the LLW Repository near Drigg due to additional radiological constraints placed on the disposal of LLW. Relating to the disposal of graphite the main restriction is the C-14 content of the waste. Using irradiated graphite waste from Windscale Pile 1 which has a C-14 content of 6.9 TBq as an example, its disposal as LLW would exceed the C-14 restriction of 1.5 TBq by a factor of 4.6[21,27].

With an estimated inventory of over 85,000 tonnes predicted to arise over the years irradiated graphite waste makes up 30% of the total inventory of ILW in the UK[28]. There is also an additional 15,000 tonnes of irradiated graphite classed as LLW[30]. Due to the restrictive C-14 regulation at the LLW Repository as well as a volume restriction in place it would not be possible to dispose of the majority of irradiated graphite as LLW. This means that a waste management strategy must be put in place for the large volume of ILW graphite waste[21,27].

1.8 Isotopic Inventory

Although graphite used in the nuclear industry is considered pure it does contain residual impurities within its structure which will undergo neutron activation to produce radioisotopes. The likelihood of contamination in the reactors coolant circuit may also contribute to the isotopic inventory of graphite. Possible sources of contamination include fission products from defective fuel, spalled oxides from steel components and fuel cladding as well as any uranium present from the fuel elements. The concentration of elements present in graphite have been studied using the chemical analysis of virgin graphite as well as some measurements made on irradiated graphite with known irradiation histories. This analysis displayed a large amount of variation from sample to sample and so the best estimate of the mean values were used. Magnox reactors and AGRs both use various grades of graphite. The elemental differences between different grades of graphite were shown to be no different from the differences of graphite samples within the same grade. Therefore only two sets of data outlining the impurity composition were provided; one for Magnox graphite and one for AGR graphite (Table 5)[32].

Table 5 - Graphite impurity levels in Magnox and AGR graphite (ppm)[32]

Element	Magnox	AGR	Element	Magnox	AGR	Element	Magnox	AGR
Li	0.05	0.05	**V**	12	0.4	**Sn**	0.05	1.0
Be	0.02	0.02	**Cr**	0.35	0.4	**Ba**	1.5	0.5
B	0.1	0.5	**Mn**	0.04	0.25	**Sm**	0.04	0.05
N	10	10	**Fe**	10	28	**Eu**	0.004	0.005
Na	1.0	4.0	**Co**	0.02	0.70	**Gd**	0.005	0.01
Mg	0.1	0.4	**Ni**	1.0	6.0	**Dy**	0.008	0.006
Al	1.0	4.0	**Zn**	0.13	1.0	**W**	0.12	0.15
Si	35	35	**Sr**	0.4	0.4	**Pb**	0.12	0.8
S	50	60	**Mo**	0.1	2.5	**Bi**	0.08	0.05
Cl	2.0	4.0	**Ag**	0.001	0.001			
Ca	35	25	**Cd**	0.04	0.07			
Ti	3	0.7	**In**	0.05	0.06			

There are several radioactive isotopes that are of particular concern relating to the disposal of irradiated graphite waste, which are namely Hydrogen-3 (also known as Tritium), C-14, Chlorine-36, Calcium-41, Iron-55, Nickel-63, Cobalt-60, Europium-152, Strontium-90, Barium-133, and Caesium-137 in addition to some transuranics[33]. The level of significance relating to these isotopes is based on their half-life (Table 6), free neutron kinetic energy and quantity[34].

Table 6 - Types of radiation and half-lives for the radionuclides in nuclear graphite[34]

Radioisotope	Radiation energy				Half-life
	α	β	γ	Electron Capture	(years)
H-3		Yes			12.3
C-14		Yes			5730
Cl-36		Yes			300 000
Ca-41				Yes	130 000
Co-60		Yes	Yes		5.3
Kr-85		Yes			10.8
Nb-94		Yes	Yes		20 000
Nb-95		Yes	Yes		0.096
Ba-133			Yes	Yes	10.5
Cs-134		Yes	Yes		2.06
Cs-137		Yes	Yes		30.2
Eu-152			Yes	Yes	13.3
Eu-154			Yes	Yes	8.5
Eu-155		Yes	Yes		4.96
Pu-238	Yes				87.75
Pu-239	Yes				24 390
Pu-240	Yes				6537
Am-241	Yes		Yes		433
Pu-241	Yes	Yes			14.89

The dominant isotope at reactor shutdown in terms of radiation dose is cobalt-60 (Co-60) which has a half-life of 5.3 years and emits both beta and gamma radiation. Co-60 will continue to be of concern for ~60 years until the dose rates stabilise at four orders of magnitude less than the level at shutdown. Tritium (H-3) is another radionuclide of key importance during reactor shutdown due to its activity. H-3 has a half-life of 12.3 years and a number of production routes, with the neutron activation of Lithium-6 (Li-6) producing the majority. Smaller amounts of H-3 are also produced from the neutron activation of hydrogen, helium and boron (Table 7). Due to the fact that H-3 is a low energy beta emitter additional problems may arise relating to detection limitations and contamination[34,35].

Table 7 - Neutron activation reactions which produce H-3[35]

Reaction
H-2 (n,γ) H-3
He-3 (n,p) H-3
Li-6 (n,α) H-3
B-10 (n,2α) H-3

When considering the long term disposal of graphite waste other radioisotopes that are of importance due to their long half-lives are C-14 and Cl-36. Once ~30 years have passed the H-3 will have decayed sufficiently so that C-14 will become the predominant isotope present in terms of activity. With a half-life of 5730 years C-14 is a long-lived beta emitter and its production in the nuclear industry and naturally will be discussed in depth in the next section. In addition Cl-36 has a very long half-life of 300,000 years and is primarily formed through the neutron activation of Cl-35, which is present in the graphite structure from the purification stage of graphite manufacture. Despite being the radionuclide with the longest half-life the hazards associated with Cl-36 are limited because it has a low specific activity, in addition to a reasonably low energy beta particle and minimal gamma radiation[34,35].

1.9 The Origin of C-14

With a high production rate and present in nearly all areas of a nuclear reactor, one of the radionuclides of considerable interest to the nuclear industry is C-14. It is a long-lived isotope with a half-life of 5730 years and decays into nitrogen-14 (N-14) through the emission of a beta particle. It can be released into the environment through the disposal of solid radioactive waste in addition to discharges of liquid and gaseous waste. The fact that C-14 is released into the atmosphere as CO_2 and through photosynthesis is easily incorporated into plant tissues means that it will reach people through the food chain as well as by direct inhalation[36]. This has led to extensive research evaluating its production in the nuclear industry and its potential release during decommissioning.

1.10 Naturally Occurring C-14

There are three isotopes of carbon which are naturally occurring. Carbon-12 (C-12) has six protons and neutrons (and so a mass of 12) and is the most abundant isotope, making up 98.89% of naturally occurring carbon. Carbon-13 (C-13) is present naturally with a 1.11% occurrence and has an additional neutron to C-12. Whilst these two forms of carbon are stable the third, C-14, is radioactive and has two additional neutrons than C-12[37].

The production of C-14 is happening constantly in the upper atmosphere and involves high velocity collisions between cosmic radiation and gases. These collisions produce neutrons which react with nitrogen atoms in the air, causing the emission of protons to form C-14. The level of C-14 present in the atmosphere almost doubled in the mid-1960s due to atmospheric nuclear bomb tests which lead to a massive influx of radiocarbon. However this concentration is decreasing over time and will return back to pre-nuclear bomb test levels within the next decade[38]. The fact that fossil fuels were formed millions of years ago means that any C-14 present will have long since decayed. This means that their combustion will actually dilute the amount of C-14 present in the atmosphere and lower the specific activity of C-14. Additionally C-14 can be produced naturally by burning wood, plants and other organic material. 1000 TBq is the annual production rate of C-14 by cosmic rays along with 140,000 TBq in the atmosphere and 10 million TBq in the deep oceans. Naturally occurring C-14 is very high compared to the total discharge from Magnox stations which has fallen from 12 TBq to 8 TBq between 1999 and 2004, due to the closure of reactors[35].

1.11 Formation of C-14 in a Reactor

Various radioisotopes are unavoidably formed during the normal operation of nuclear reactors from neutron activation of structural components and coolant to fission within the fuel. The majority of C-14 is produced from the neutron activation of: N-14 in fuels, moderators and coolants; C-13 in graphite moderators and oxygen-17 (O-17) in the oxide fuels, moderators and coolants[39] (Table 8).

Table 8 - Main routes of C-14 production in nuclear reactors[40]

Reaction	Capture cross section barns (10^{-24} cm^2)	Abundance of Isotope in natural element (%)
$^{14}N(n,p)^{14}C$	1.86	99.63 ^{14}N/Nitrogen
$^{13}C(n,\gamma)^{14}C$	0.00137	1.11 ^{13}C/Carbon
$^{17}O(n,\alpha)^{14}C$	0.235	0.037 ^{17}O/Oxygen

Using this data and a graphite sample with an assumed nitrogen impurity concentration of 50 parts per million per weight (wppm) the rate of production of C-14 from the three main sources N-14: C-13: O-17 is in the ratio 305:33:1 with the majority produced from N-14 impurity in the graphite structure. Whilst this is true for some reactors the amount of N-14 impurity will vary from batch to batch of material and will differ between different types of graphite used in different reactors around the UK[41,42].

Although C-13 has a low capture cross section its abundance within the graphite moderator structure leads to quite a high production route for C-14. A large quantity of the C-14 present in the coolant gas is produced from the reactions with O-17. The rates of C-14 production in the coolant from O-17: N-14: C-13 is in the ratio 25: 21: 1 assuming a 50 parts per million per volume (vppm) nitrogen impurity in the CO_2/1% CO coolant[41]. C-14 can also be produced from N-15 and O-16 however these isotopes have very low capture cross sections and are deemed unimportant in thermal reactors[39]. C-14 is retained in the graphite and any carbonaceous deposits present primarily as elemental carbon although there will be some carbon oxides present on the surface of graphite as well as in deposits[43].

1.12 Carbonaceous Deposits

Varying amounts of carbonaceous deposits have been identified on irradiated graphite samples removed from the reactor cores of both AGR and Magnox reactors[41,44]. With the exception of Sizewell B which is water moderated all commercial nuclear reactors in the UK use graphite as a moderator and are cooled using CO_2 gas[45]. Through reactions between the irradiated CO_2 coolant and the graphite moderator a high amount of mass loss can occur as well as the build-up of carbonaceous deposits. Another route is the radiolytic oxidation of graphite which can lead to the production of high levels of CO, which under gamma irradiation polymerises to produce sooty carbon deposits. Radiolytic oxidation can be

inhibited by regulating the chemical composition of the reactor coolant[41,44]. In Magnox reactors this process is controlled by the presence of hydrogen which is maintained at a minimum of 25-45 vppm, whereas in AGRs the addition of methane is used as an inhibitor. However the radiolytic decomposition of methane has also been shown to form undesired carbonaceous deposit build-up. Carbonaceous deposits can also be formed from CO in the presence of water in addition to methane from oil ingress reacting with oxidising species[41].

An investigation using isotopically labelled gas mixtures have shown that the majority of carbonaceous deposits produced are from the decomposition of methane. Furthermore this method of deposition can only occur when the gas is radiolysed, a process which generates several deposition precursors which may be catalytically decomposed to give carbon[46,47]. However this statement can only be made in relation to AGRs which use methane gas in their coolant.

During routine graphite trepanning campaigns deposit concentration measurements are undertaken. The level of deposit is expressed as material with a higher oxidation rate than underlying graphite. Therefore it should be taken into consideration that the figures recorded for deposit concentration may include graphite with a higher rate of oxidation due to catalytic contamination as well as carbonaceous deposits[41]. Studies have a shown a wide variation in the concentration of the deposits present in Magnox reactors, which relate to axial height within the core. Adjacent to the fuel-channel surfaces at the lower positions in the core, deposit concentrations have been reported to be in the excess of 15,000 wppm, with lower concentrations of deposit present at higher locations in the core. There has even been evidence of deposit concentrations reaching 30,000 wppm in some Magnox plants[48]. Although average values are significantly lower than this. In order to evaluate deposit reactivity the oxidation at 450°C of irradiated graphite samples with carbonaceous deposits present was undertaken. The interpretation of the curves produced displays that the carbonaceous deposits have a variable reactivity ranging between 0.1-1.0 g of deposit per g of sample per hour ($g.g^{-1}.h^{-1}$), with some carbonaceous deposits found to be 100 times more reactive than the underlying graphite[44]. These experiments are undertaken in order to assess the reactivity of the deposits during the event of air ingress into the reactor to determine the safety implications.

Through the investigation of particulate release the majority of carbonaceous deposits were found to be well adhered to the graphite surface. Material would only be released under

conditions with a severe atmospheric disturbance, or where graphite itself was abraded, or through the oxidation of graphite[43]. More recent studies involving the use of Focused Ion Beam (FIB) Microscopy have described the deposits to be an agglomeration of irregular spheres of up to 2 µm in diameter and resembling a cauliflower[49](Figure 8).

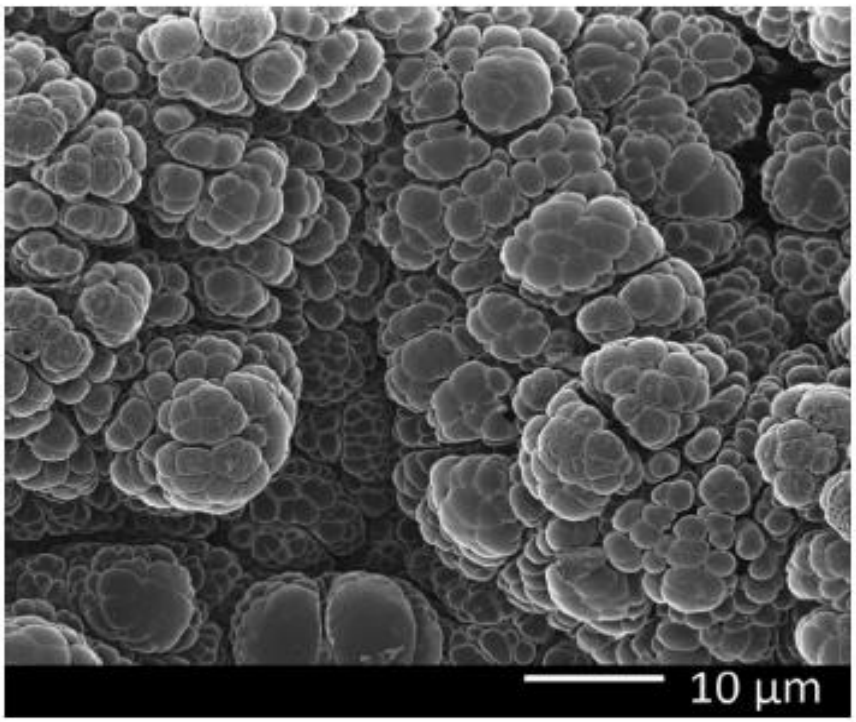

Figure 8 - FIB images of the surface of a fuel channel wall with carbonaceous deposits present[49]

Reactor operators have been investigating how carbonaceous deposits are formed and how to regulate them for many years and studies are on-going in this area due to the fact the chemistry of these processes are still not fully understood[41]. Additionally there has been no investigation into the C-14 content of these carbonaceous deposits. If they are rich in C-14 their removal with oxidation could significantly reduce the C-14 inventory of the remaining graphite.

1.13 Waste Management and Disposal Options in the UK

In order to make progress on the management of the large inventory of radioactive waste in the UK the government set up the Committee on Radioactive Waste Management (CoRWM). They were tasked with providing recommendations on the long-term management of some of the UK's higher activity level waste streams. CoRWM produced a report in 2006 using a combination of scientific advice, overseas experience and public and stakeholder engagement

as well as placing key consideration on ethical issues. They produced 15 recommendations, and concluded that the best available approach for the long-term management of irradiated waste would be geological disposal. However they also recognised the importance of examining alternative non-geological treatment options which will be discussed in a later section[50].

1.14 UK Geological Repository

Whilst there are currently no plans in place for a deep geological disposal facility in the UK there have been several strategies developed and published over recent years[28,29,51-53]. After the recommendations produced by CoRWM the government produced a white paper in which they accepted the recommendations made by CoRWM as well as responding to them. One response was that they would explore the concept of voluntarism for the site of the geological disposal facility[54]. By placing this consideration local councils have the power to reject any government proposals for the production of a geological disposal facility despite whether or not its geologically suitable. This has occurred most recently in Jan 2013 where the possibility of a deep geological disposal site to be located in West Cumbria was voted against by the Cumbria County Council and the process was brought to a close, despite the positive votes from the two Borough councils involved[55].

In more recent years it is the role of the Nuclear Decommissioning Authority (NDA) to advise on radioactive waste management strategies and oversee decommissioning in the UK. In documents published 2013-14 the NDA have produced a number of reports outlining the specific strategies and detailing credible options for the management of irradiated graphite waste. They have estimated that nearly 30% of the volumetric inventory of ILW in the UK is composed of irradiated graphite. However its placement in the planned geological disposal facility would only occupy 2% of the facilities footprint. The majority of the footprint is taken up by HLW which must be suitably separated to allow for heat dissipation[28].

1.15 Problems with Graphite Storage and Decommissioning

Although the majority of irradiated graphite waste falls below the limits for ILW it is still categorised in this way due to the presence of certain long-lived radioisotopes (C-14 and Cl-36). These isotopes are the reason why graphite waste cannot be accepted at a Low Level Waste Repository and must be encapsulated for deep geological disposal[21,27]. Not only does

this encapsulation process increase the already large volume of ILW from 68,724 m^3 to 109,494 m^3 [28], but the costs involved are significantly increased as well. An example of the costs involved for various waste management options has been proposed for the ILW of Magnox power station Hunterston A (Table 9)[51].

Table 9 - Summary of the costs involved for various waste management options for Hunterston Site A[51]

Option Description	Near-term Cost	Lifecycle Cost	Lifecycle Cost- 200 year storage
Encapsulate (on-site) prior to interim storage	£50.1M	£85.7M	£130.8M
Temporary containerisation then encapsulation immediately prior to disposal	£50.1M	£85.7M	£130.8M
Unencapsulated disposal	£11.9M	£47.5M	£92.6M
Prompt disposal at a near-surface facility at the site of origin	£38M	£39M	£39M

Furthermore there are significant issues that may arise during the long-term storage of radioactive waste which will be discussed in the following sections, paying particular attention to the problems arising with irradiated graphite waste.

1.15.1 Release of Radioisotopes

One of the main problems arising during the long-term storage of irradiated graphite waste in a deep geological facility is the mobility and possible release of long-lived radioisotopes C-14 and Cl-36. Using C-14 as an example there are two scenarios in which C-14 can be released; either by dissolving into the groundwater to be released into the biosphere in solution or released directly into the biosphere as methane gas[56]. There is reasonable confidence that any C-14 labelled CO_2 that is produced will be trapped in the near field through carbonation reactions[21]. However the production of C-14 labelled methane gas is of particular concern and is still under investigation in order to improve understanding of its production and to assess the safety implications involved[53].

1.15.2 Radiolytic Oxidation

Radiolytic oxidation is where the decomposition of the CO_2 coolant by ionising radiation produces oxidising species which are then absorbed onto the graphite surface and lead to the oxidation of graphite. There is a large amount of variation in the extent of radiolytic oxidation that occurs in different reactors graphite. This is because the dominant influence on oxidation rate appears to be the pore size and distribution, and as this varies between different graphite, there will be divergences in oxidation rate even under identical conditions[57].

An example which displayed a significant amount of radiolytic corrosion is the French Bugey-1 reactor which showed some graphite core samples reaching >40% mass loss[58]. In most cases oxidation inhibitors are pumped directly into the coolant in order to reduce the amount of corrosion taking place. Hydrogen was selected as an inhibitor in some early Magnox reactors (Oldbury and Wylfa), whilst the increased radiation flux in AGRs required the use of Methane. However the addition of methane may lead to the deposition of reactive carbonaceous material onto the graphite surface. These deposits can also be caused by the polymerisation of CO, another by-product of radiolytic oxidation[59].

Radiolytic oxidation is a key concern as it results in a significant mass loss in the graphite along with an increase in the porosity of the graphite. This in turn can lead to several changes to the properties of graphite including a decrease in thermal conductivity as well as changes in the strength and density which may cause cracking and degradation of the reactor graphite[45,60].

1.15.3 Wigner Energy Release

Stored energy (also known as Wigner energy after its discoverer) is produced in graphite when carbon atoms are displaced from their lattice positions into configurations of higher potential energy during neutron irradiation. The return of these atoms to their original state (known as annealing) causes a release of thermal energy[61-65]. The magnitude of Wigner energy that accumulates in the graphite lattice is a function of irradiation time, fast neutron flux and temperature which produces a unique distribution of different energies throughout the graphite lattice. This unique distribution of energy means that is difficult to reliably predict the release of the stored energy, so as a general rule it is stated that the stored energy can be released through the heating of graphite above the temperature at which it was

irradiated. However in order to remove the entirety of stored energy from irradiated graphite temperatures in excess of 2000°C may be required. This is because during irradiation over a long time period some carbon atoms will be displaced to even higher energy levels requiring higher temperatures to release the energy[62].

Furthermore stored Wigner energy is of particular concern in relation to graphite samples which have become irradiated at low temperatures. An increase in temperature could release the stored energy at a sufficient rate which would exceed the specific heat capacity of graphite, consequentially producing a potentially self-propagating irradiated graphite sample[66]. An example of the risks involved in relation to Wigner energy took place in the UK in 1957 where during a routine operation to remove the stored Wigner energy a fire was caused which led to the shutdown of both Windscale Piles 1 and 2[61].

It seems the higher the irradiation temperature the less Wigner energy that is produced, meaning that it is less of a problem for HTRs and AGRs. Whilst there is a substantial amount of Wigner energy present in some Magnox graphite some studies have shown the rate of release does not exceed the specific heat capacity of graphite and so would not be self-propagating[63]. However when designing a waste management strategy for the disposal of irradiated graphite the potential risk of an uncontrolled release of Wigner energy must be given some serious consideration. As Wigner energy is a potential heat source it will influence the development of future safety cases and immobilisation techniques[61].

1.15.4 Irradiation Damage

In addition to the production of Wigner energy the displacement of atoms in the graphite lattice from neutron irradiation causes lattice defects due to the inelastic and elastic scattering of carbon atoms. The result on individual crystallites of graphite is an expansion perpendicular to the basal planes and shrinkage parallel to the planes[67]. These defects will have a significant effect on various physical, mechanical and thermal properties of graphite. Electrical and thermal conductivity will be altered and internal stresses generated may lead to cracking and degradation of graphite bricks. The assessment of irradiation damage is important when it comes to the disassembly of graphite reactors at the end of their operating lifetime as dimensional changes could have led to the distortion of structural components and damage which may limit dismantling options prior to delivery to a geological repository[68].

1.15.5 Graphite Dust Explosibility

The introduction of an International Organisation of Standardisation (ISO) standard test has now categorised graphite dust as being weakly explosible and the decommissioning of graphite components in nuclear power plants may lead to the disruption and subsequent explosion of graphite dust. In order for a deflagration to occur the dust must be airborne in an atmosphere with sufficient oxygen to support combustion. The concentration of the dust must fall within an explosible range with an optimized particle size for combustion. Furthermore the dust must come into contact with an ignition source with enough energy to initiate flame propagation. This could be anything from a naked flame or electrical spark to a heated surface. Whilst the risk of an explosion of graphite dust is thought to be minimal, measures should be taken during decommissioning in order to eliminate the chance of an incident occurring[69].

1.16 Decontamination Processes

With the aim to provide an alternative to deep geological disposal there have been several investigations carried out over the years in order to supply possible treatment methodology to deal with the large volume of irradiated graphite waste worldwide. The aims of these procedures can include volume reduction, the removal of a significant proportion of the radionuclide inventory or the reclassification of waste. The approaches involved include thermal treatments and chemical leaching and will be discussed in the following sections[20].

1.16.1 The CARBOWASTE Consortium

Launched in 2008 under the 7th EURATOM Framework programme was the European project entitled "Treatment and Disposal of Irradiated graphite and other Carbonaceous Waste" more commonly referred to as CARBOWASTE. The aim of this collaboration was the development of the best practices for the retrieval, treatment and disposal of irradiated graphite and other carbonaceous waste addressing both legacy waste and future arisings. The CARBOWASTE project involves 30 partners with complementary multi-disciplinary scientific and industrial backgrounds from 10 different European countries and South Africa[70] (Figure 9).

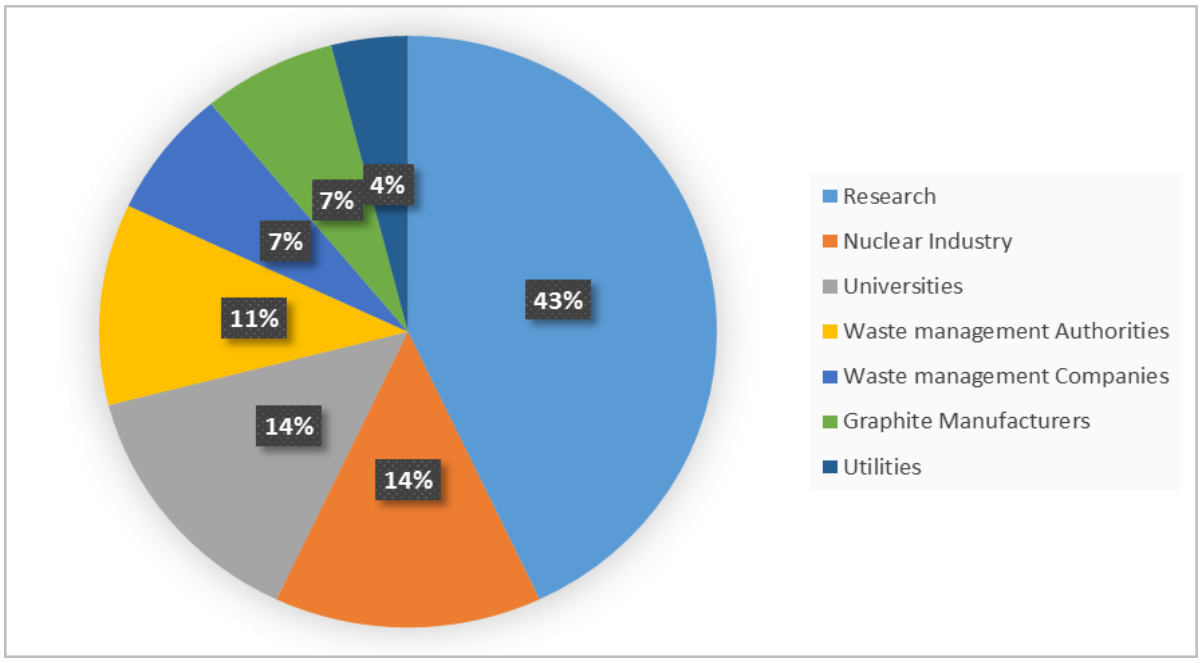

Figure 9 - Chart illustrating the backgrounds and percentage involvement of the CARBOWASTE consortium partners[71]

The CARBOWASTE project was separated into six technical work packages which would cover the life cycle of irradiated graphite from its use in a reactor to its eventual disposal or reuse. These work packages are as follows; Integrated waste management approach (WP1), Retrieval and segregation (WP2), Characterisation and modelling (WP3), Treatment and purification (WP4), Recycling and new products (WP5) and Disposal behaviour (WP6)[72]. As this project is involved with the treatment options for graphite waste, only methods from WP4 will be discussed in detail. The CARBOWASTE project took place between April 2008 and March 2013 and in that time was able to identify a number of potential treatment methods some of which will be included in the following sections.

1.16.2 Thermal Treatments

The thermal treatment procedures for irradiated graphite will involve heating the graphite to a temperature which will cause the graphite structure to either breakdown (e.g. incineration), react chemically with the environment (e.g. with water in steam reformation) or so that volatile contaminants are removed (e.g. roasting).

By heating graphite in these different ways it is possible to selectively remove certain nuclides (C-14 and H-3) from the graphite structure. These isotopes may accumulate on the surface of the graphite pores during a reactors operation through the activation of species

absorbed to the graphite surface during manufacture or from exposure to air. Additionally they may be produced from the deposition of isotopes in the gas phase having diffused into the pore volume of graphite. These mechanisms may form pore surface layers of irradiated graphite which are enriched in radioactive isotopes (such as C-14 and H-3) which could be released through gasification during thermal treatments. Whilst these procedures would remove only a small amount of graphite, the gases released could make up a significant proportion of the isotopic inventory meaning that the majority of graphite waste could be partially decontaminated[20].

An example where the use of a thermal treatment method has been successful in reducing the quantities of C-14 and H-3 would be the incineration of the graphite used in the GLEEP reactor. This was thought to be an appropriate treatment route as the irradiation of GLEEP graphite was very low with the resulting activation of impurities equally so. The graphite was placed into an industrial incinerator at 1150°C for a period of ~3 hours in the presence of a forced air supply. This process achieved the removal of 87% of the H-3 and 63% of the C-14 with only 6% of graphite mass loss due to thermal oxidation. This observation implies that the majority of the C-14 that has been removed was originally from the surface of the GLEEP graphite possibly in the form of sooty deposits[44].

The evaluation of the factional release of both C-14 and H-3 from irradiated graphite as a function of time and temperature, and during oxidation in both inert and steam conditions with varying flow rates has been studied comprehensively[73-75]. Comparisons were made between two different graphite samples originating from German reactors. Solid and ground powder graphite samples from a MERLIN (Medium Energy Research Light Water Moderated Industrial Nuclear Reactor) research reactor's thermal column were analysed in addition to reflector graphite powder from an AVR (Arbeitsgemeinschaft VersuchsReaktor) which was a prototype pebble bed reactor also from Germany. The results from all of the experimental conditions used showed that H-3 and C-14 was released faster than the graphite could oxidise. These experiments were conducted between the temperatures 870-1060°C. Graphite samples were heated in inert conditions using argon for 15 hours with the highest isotopic release observed from MERLIN graphite powder at temperatures of 1060°C. With a total graphite mass loss of 1.36%, a release rate of 43% was observed for H-3 whilst C-14 displayed a release rate of 20% compared to the release of C-12 which was <1.5%[73,74]. The

high release of C-14 under inert conditions can be attributed to the reaction of graphite with oxygen that has physisorbed and/or chemisorbed onto the graphite surface[75].

During experiments oxidising graphite in a steam environment almost all of the H-3 was removed from both solid and powder MERLIN graphite after 10 hours heating at 1060°C, whilst only 60% was released from AVR graphite. These experiments were carried out between 400-1060°C with the lowest H-3 release exhibited at 400°C which was 1.3% after 5 hours. The measurements for C-14 were carried out at higher temperatures with the highest release rate for C-14 being 70% at 1060°C with a C-12 release of 20%. This significant difference between C-12 and C-14 release was explained by the notion that C-14 was not uniformly distributed through the graphite lattice most likely due to the variability of the nitrogen impurity present in virgin graphite. The results indicated that C-14 was more concentrated on the graphite surface and decreased with depth. Another interesting result found during this study was that more C-14 was released from the solid samples compared to the powder samples. Again it was concluded that this resulted from the outer and inner porous surfaces being enriched with C-14 and that the milling process used to produce the powdered graphite samples increased the surface area of graphite which was not enriched with C-14. From these studies it can be deduced that C-14 and H-3 can be effectively released using an oxidation treatment however in order to provide minimal mass loss to the overall graphite mass a low temperature oxidation should be used[73,74].

Pyrolysis and steam reformation has also been studied for the volume reduction of graphite waste most notably in the patented Thermal Organic Reduction (THOR) process, which utilises a fluidised bed treatment system in combination with pyrolysis and steam reforming technology. The reaction of graphite with steam produces carbon monoxide (CO) and hydrogen which can then be converted to less hazardous CO_2 and water *via* supplementary oxidation through the addition of oxygen or air into the system. The THOR process also provides the procedure to convert the CO_2 product into a solid carbonate salt which can then go on to fill void spaces in existing disposal containers containing radioactive waste. Additional benefits that this process provides include the dissipation of Wigner energy from the graphite structure as well as the separation of other radioactive elements from the carbon in the graphite resulting in less strict handling procedures. The processing of ion exchange resins have reliably demonstrated weight reductions of 100:1 and volume reductions of 80:1[42]. However the sheer volume of CO_2 produced from graphite waste and its

transformation into a carbonate salt may lead to an increase in volume. For example 1,200 tonnes of graphite could be transformed into 10,000 tonnes of calcium carbonate, and whilst preventing the release of radionuclides to the environment and being insoluble it does not provide a solution to the volume problem[66].

The socio-economic implications of graphite incineration has been evaluated in order to put into perspective the global C-14 dose. By using the theoretical incineration data of a Magnox reactor a computer model was produced for the global dispersion of C-14 release into the atmosphere as CO_2. The model was validated using available experimental data. Based on the proposal of the incineration of one Magnox reactor every year for twenty years the work concluded that the peak annual dose would be three orders of magnitude smaller than the annual cosmic-ray induced C-14 background dose, and a further six orders of magnitude smaller than the average background dose from all UK sources. This study shows that a thermal treatment method for the disposal of irradiated graphite waste may be a viable treatment option[36], however the local dose in the vicinity of the incineration plant and the surrounding areas may prove to be more significant[66].

1.16.3 Chemical Treatments

Chemical treatments have been investigated in order to decontaminate irradiated graphite waste. Analysis has included the use of varying combinations of alkaline solutions, dissolved oxidising agents, mineral acids and organic washing detergents. Two mechanisms have been identified in the chemical decontamination of graphite; the destruction of the binding material and the selective removal of the surface layer of graphite[20]. Furthermore chemical treatments are also examined to evaluate the potential release of radionuclides from graphite waste during prolonged periods of time (geological disposal). If water were to come into contact with the waste then leaching would be a possible route for radiological release into the environment and so the leachability of several radioisotopes have been extensively researched with varying results.

An early study identified that the mechanism for the leaching of C-14 from graphite was due to a water-catalysed oxidation, where oxygen dissolved in water reacted with graphite to produce CO_2[76]. A continuation of this work led to a series of leaching experiments using both irradiated graphite from the Hanford site in America and French graphite supplied by the CEA. The leaching experiments carried out on the Hanford graphite were conducted over 8

weeks at temperatures of 20, 50 and 90°C using both de-ionised water and Hanford groundwater as a leachant, whereas the conditions used for the French graphite were 20°C for 13 weeks in de-ionised water. Both sets of experiments set out to monitor the leaching of both C-14 and Cl-36 from irradiated graphite.

Although there was a small degree of scatter with some data sets they all exhibited a decrease in leach rate over time with two possible mechanisms given as an explanation. One mechanism would be the depletion of the C-14 and Cl-36 sources which would be unlikely due to such a small fraction of the total activity being removed. However it may be possible that areas of readily accessible or more reactive sources may become depleted. This is particularly probable for C-14 which has a significant concentration on the surface layers of graphite which would be more reactive and accessible than C-14 within the graphite lattice. Once the more reactive areas have been depleted the leaching rate should decrease until it reaches the normal rate for C-12 which is in fact the case for both types of graphite. An alternative mechanism which explains the decrease in reaction rate over time may be due to diffusion through the graphite pores. The diffusion of a reactant such as oxygen through the leachant may limit the amount of graphite oxidation which can occur. Furthermore the diffusion of leached species in the graphite pores could limit the amount that reaches the bulk solution which is analysed. The total C-14 inventory leached from the Hanford graphite samples was $3.6x10^{-5}$ - $9.2x10^{-5}$. When compared to the total C-14 inventory leached from the French graphite which was much higher at $2.6x10^{-3}$ - $8.5x10^{-3}$, thus indicating that the French graphite was much more reactive than the American graphite[77,78].

Leaching studies have also been carried out in the UK using Magnox graphite samples at various temperatures using demineralised water, simulated groundwater and simulated sea water as leachants. The total inventory of C-14 leached from the Magnox samples was $8.8x10^{-4}$ - $1.4x10^{-3}$ which is fairly similar to the French graphite samples discussed previously. The results also confirmed the steady decrease in release rate over time exhibited by other experimental work carried out. However this study was carried out for a longer period of time (150 days) and found that the leach rates decreased by a factor of 50 to 100 after 100 days which is a far greater decrease than was observed with the Hanford and French graphite. These variances could be due to any number of differences between the graphite samples including temperature of the graphite during operational time, atmosphere that the graphite is exposed to (e.g. coolants used), differences in neutron flux or sample preparation

before the leaching experiments were carried out. Other radionuclides were also detected in the leachants used during the Magnox graphite leaching experiments. These included H-3, Ba-133, Co-60 and Cs-134 which all displayed a similar trend as C-14 where leach rates decreased over time, apart from Co-60 whose leach rate actually increased[32].

Another leaching study conducted on French graphite using de-ionised water was able to detect H-3, C-14, Cl-36, Co-60, Ni-63, Ba-133, Cs-177 and Eu-154. However the aim of this study was to evaluate ways to decrease the leaching of radionuclides from irradiated graphite for the purposes of long-term storage. The results showed that by impregnating the graphite samples with an epoxy resin pitch, which would fill all graphite pores larger than 0.1 µm, then all elements showed an improved resistance to leaching, with some leach rates reduced by a factor of 1,000[79].

A study on the leachability of C-14 from irradiated graphite was carried out over 720 days using alkaline conditions. The results showed that only a minimal amount of C-14 activity (18.4 Bq) had been removed from the total C-14 activity of the graphite sample (2.72×10^5 Bq). In order to accelerate the leaching process a leaching solution of sulphuric acid and potassium permanganate was used however the results for all six samples showed that over 90% of the C-14 activity remained in the graphite. This study also involved the identification of nitrogen impurity in nuclear grade graphite by measuring the thermal conductivity of gases produced from graphite treated in tin alloy at 2800°C. The distribution of nitrogen through the structure was evaluated using Secondary Ion Mass Spectrometry (SIMS). The study goes on to conclude that the C-14 that was released from the samples during leaching had originated from the surface of the graphite and that the bulk of the C-14 activity remains quite stable in the graphite lattice[80].

The comparison of the results quoted from various leaching studies are difficult to make due to the variation in leaching methodology used, irradiated graphite sample history, sample geometry and porosity and leachant sampling frequency to name a few. Furthermore it is difficult to realistically predict the long term leaching behaviour of samples due to the possibility of undesirable chemical reactions taking place during storage. Lastly whilst possible leaching mechanisms have been predicted they have not been widely validated thus highlighting the need for additional research in this area.

1.17 Summary of Introduction

The structural and mechanical properties of graphite have led to its extensive use in the nuclear industry. The decommissioning of nuclear reactors will produce ~90,000 tonnes of irradiated graphite waste in the UK for appropriate disposal. Whilst present waste management strategies involve the long-term storage of the waste in a deep geological facility there are currently no plans for its construction nor has an appropriate site been established, largely down to public opinion. The information provided from the characterisation of irradiated graphite, both structurally and its radionuclide inventory is vital when making considerations for the planning of a repository. The location of C-14 in the graphite structure and its possible release into the biosphere is one of the main challenges in relation to the disposal of irradiated graphite. There has been extensive research into processes which could decontaminate irradiated graphite waste from certain radionuclides in addition to reducing the large volumes of waste. Whilst chemical treatments have shown that minimal amounts of the activity of certain isotopes can be reduced, the successful incineration of GLEEP graphite indicates that thermal treatments may be a viable option in the disposal of graphite waste.

1.18 Objectives of this Research

The work carried out in this study is concerned with investigating the removal of carbonaceous deposits from graphite samples. In order to study this phenomenon a number of graphite samples with different carbonaceous deposits had to be generated followed by the study of their removal.

1.18.1 Deposition Techniques

In order to evaluate processes to remove carbonaceous deposits it was necessary to investigate deposition procedures which would produce a variety of carbon deposits onto the graphite surface which were comparable with the carbonaceous deposits found on reactor graphite. Two different deposition techniques were investigated; Solution deposition and Microwave Plasma assisted Chemical Vapour deposition. The former is where a solid carbonaceous precursor is dissolved in an appropriate solvent and added to the graphite sample under vacuum. Using a rotary evaporator the solvent is removed leaving the carbon precursor on the surface of the graphite and in the pores. These samples would then have to

undergo a charring procedure where they were placed in a furnace at a high temperature in an inert atmosphere to produce volatile gases (hydrogen and oxygen would be driven off) leaving a residue composed of carbon fixed to the graphite surface[42]. Another technique investigated was chemical vapour deposition which uses microwave plasma to produce carbonaceous deposits from a methane gas precursor. The charring stage is not necessary for the microwave method as the carbon precursor will be broken down during the process.

1.18.2 Deposition with C-13 Precursors

The analysis of irradiated graphite samples is limited to the presence of active laboratories on site as well as appropriate health and safety regulations in place. In addition the difficulties with the acquisition and transport of radioactive samples along with the problems of safe waste disposal lead to an alternative approach in analysis.

When the deposition and removal techniques have been standardised then carbonaceous deposits will be prepared using C-13 precursors. C-13 was selected to be a non-radioactive supplement for C-14 as they facilitate the study of the selective removal of the deposit by mass spectrometry and spectroscopy. It also meant that the samples could be handled safely at the available facilities and there was no safety restriction when it came to sample size or concentration of deposit formed. Using Mass Spectrometry and Raman Spectroscopy its possible to clearly distinguish between carbon from the graphite structure (C-12) and carbon from the deposit present (C-13) and therefore determine the effectiveness of the removal techniques.

1.18.3 Removal of Carbonaceous Deposits

When the successful deposition of various carbonaceous deposits was achieved the next stage was to develop a process which would selectively remove the deposits. A process of combusting the large volume of irradiated graphite with carbonaceous deposits in its entirety may produce too much C-14 CO_2 to make it a viable treatment option. However if the carbonaceous deposits are rich in C-14 then their removal from the graphite surface may be beneficial for future storage and disposal routes.

The selective removal of carbonaceous deposits from graphite samples will be investigated using the application of a vacuum to the thermal treatment of the samples. When a vacuum is applied to the experimental set up the partial pressure of oxygen will be less which will limit

the rate of oxidation[81]. This could mean that by heating the samples at high temperatures with a vacuum applied, the carbonaceous deposits on the surface of the graphite samples could be removed with limited oxidation to the underlying graphite. The amorphous deposits are more disordered and should be more reactive than the more crystalline graphite[82] due to having a higher surface area and more active sites available to react with oxygen[83]. The selectivity of this process will be determined using graphite samples with C-13 deposits which will be characterised using spectroscopy and spectrometry techniques.

1.18.4 Carbon-14 Content of Carbonaceous Deposits and Reactor Graphite

The work carried out during this project also involved an additional area of study which was an Industrial CASE award mini-project which was carried out at the National Nuclear Laboratory's Preston Lab based on Springfields Site. This work involved using irradiated graphite samples with the aim to investigate of the distribution of C-14 activities present in irradiated graphite and the carbonaceous deposits present.

2. MATERIALS AND METHODOLOGY

This chapter provides the description of the methods used during the project including experimental designs and techniques employed, as well as the characteristics of the samples used during the study. At all stages of experimental work, steps were taken to ensure the quality of data. The balances used were calibrated on a regular basis, as were the different analytical techniques utilised. Analyses were repeated frequently and control samples were used when appropriate.

2.1 Virgin Graphite Samples

A number of different graphite samples were attained from various sources during the course of this study. Using virgin graphite samples for the majority of the work alleviated the need to work in active laboratories. They are also more readily available than irradiated graphite samples, in addition to being easier to analyse and handle in the facilities available. Several non-irradiated or virgin graphite samples were acquired during the course of the project. These graphite samples were archived at the time of a reactor's construction for research purposes. Four different graphite samples were attained from different locations, at different time periods of the project and with varying volumes (Table 10). Initially 0.160 kg of Pile Grade A (PGA) graphite which was used in Magnox reactors was supplied consisting of five separate beam fragments. This sample was from Oldbury reactor 1 moderator brick. Subsequently a 10 kg block of Magnox graphite was also obtained. Furthermore two samples of Gilsocarbon which were used in AGRs were acquired, a 3 kg fuel sleeve and a 5 kg block originating from Hunterston B.

Table 10 - Virgin graphite sample information

Graphite Type	Origin	Information and Reference codes	Weight
Magnox – Pile Grade A (PGA)	Oldbury Reactor 1 – Moderator Brick	5 separate beam fragments – R3903 Heat Batch 514(R1) 8, 14, 16, 20, 27	0.160 kg
Magnox – Pile Grade A (PGA)	Sellafield	Brick Ref 0559761/8/7491	10 kg
AGR - Gilsocarbon	Springfields – Fuel Sleeve	Westinghouse Serial no: 5365	3 kg
AGR - Gilsocarbon	Hunterston B reactor graphite	Heat Batch -84, IM1-24, 19/1/B1/19/1/B2	5 kg

2.2 Sample Preparation

The majority of the virgin graphite samples received were in the form of a large single block weighing several kilograms. Initially, the as received graphite samples were wrapped in plastic to minimise contamination and then broken into smaller pieces using a hammer. It was decided to use a graphite particle size of 1-2 mm for the majority of experiments. This sample size was achieved by using a variety of methods which included a hammer, pliers and a hydraulic press. A series of sieves were used to ensure a reliable particle size was achieved. Samples were stored in glass Duran bottles or plastic Eppendorf tubes depending on sample size.

2.3 Solution Deposition

The aim of these experiments was to produce a graphite sample with carbonaceous material deposited onto its surface. Graphite 1-2 mm particle size samples were used in these experiments. The carbon precursors were chosen based on which C-13 material would be commercially available following standardisation of the doping experiments (Table 11). Additionally, precursors were selected based on their chemical composition in order to attain a wide variation of deposits. D-mannose was selected based on its oxygen content. The other two precursors were chosen because of their structure; myristic acid is a long chain hydrocarbon whereas naphthalene is aromatic. The amounts of carbon precursor used was; 100 mg, 50 mg, 10 mg, 5 mg, 1 mg and a 0 mg blank per 1 g of graphite. A sample size of 20

g of graphite was chosen for these doping experiments so that enough material would be available for the characterisation at different stages of the treatment process. These experiments were initially conducted using Magnox graphite due to its availability and were repeated with AGR graphite when it became available and depending on the success of the deposition which was evaluated from the samples characterisation.

Table 11 - Carbon precursor information

Carbon precursor	Formula	Amount of carbon precursor (g) /20 g of graphite						Solvent
Naphthalene	$C_{10}H_8$	2	1	0.2	0.1	0.02	0	Chloroform
Myristic acid	$C_{14}H_{28}O_2$	2	1	0.2	0.1	0.02	0	Chloroform
D-mannose	$C_6H_{12}O_6$	2	1	0.2	0.1	0.02	0	Methanol

Initially, 20 g of graphite of 1-2 mm particle size was added to a round bottomed flask which was then placed into a vacuum oven at 110°C for 1-2 hours to remove any moisture. Various amounts of carbon precursor (see Table 11) were dissolved in the appropriate solvent. The round bottom flask was removed while still hot from the vented vacuum oven and sealed with a rubber septum cap. The dissolved carbon precursor was injected through the rubber septum and onto the hot graphite sample. A rotary evaporator was used to remove the solvent and uniformly coat the graphite samples with the carbon precursor. All samples were then dried in the vacuum oven and collected.

2.3.1 Charring Stage using a Thermobalance

Converting the various carbon deposits into a carbonaceous char on the graphite surface was achieved initially using a thermobalance. ~10 mg samples from the solution deposition stage were used having been dried in a vacuum oven overnight. The temperature program used was from ambient to 700°C at 10°C.min^{-1} which was chosen based on the highest boiling point of different precursors selected. Nitrogen was selected for the charring experiments at a flow rate of 50 ml.min^{-1}.

2.3.2 Charring samples in Bulk

Using a thermobalance to char samples had its limitations due to only a small amount of sample could be used for each experiment because of the small crucible size. Consequently an apparatus was set up in order to char the doped graphite samples in bulk (Figure 10).

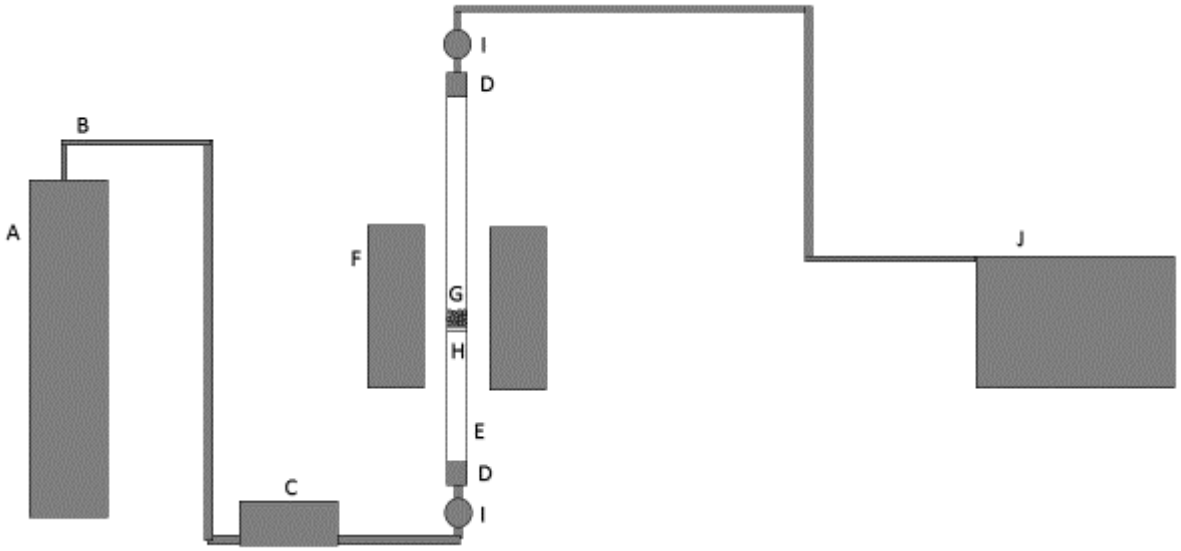

Figure 10 - Schematic of bulk charring experimental set-up, where A: Nitrogen gas cylinder, B: Tubing, C: Mass flow controller, D: Swagelok fittings, E: Quartz tube, F: Furnace, G: Doped graphite sample, H: Either glass wool or a sintered frit), I: Valve, J: Mass spectrometer.

Using a sample size ranging from 1-5 g, the doped graphite samples were placed into a quartz tube. They were held in place in the middle of the tube by either glass wool or a sintered frit (the former was used initially before the latter became available and was subsequently used for the majority of the experiments). The furnace employed was a Carbolite 1200 Deg C vertical split tube furnace with an integrated Eurotherm 2408 temperature controller. The quartz tube was positioned so that the sample was held in the middle of the furnace. Using a mass flow controller 20 $ml.min^{-1}$ of nitrogen was allowed to flow through the system for the amount of time taken to completely remove any oxygen from the system, as indicated by the mass spectrometer. Once the oxygen had been sufficiently removed from the system the valve located at the bottom of the quartz tube was closed to stop the flow of gas. The furnace was then heated to 700°C with the valve at the top of the tube remaining open for the duration of the heating program. Once the furnace reached 700°C the remaining valve was

closed and the temperature was held for 20 minutes. The samples were then allowed to cool and then collected.

2.3.3 Oxidation of Charred Samples

In order to evaluate whether the deposition and charring experiments had been successful a series of experiments using a thermobalance were performed. By oxidising the samples and observing any mass loss outside the normal range of graphite oxidation, it was possible to establish whether carbonaceous material was present on the graphite surface and had not been removed during the charring stage. These experiments were carried out using air at a flow rate of 50 $ml.min^{-1}$ and a temperature ramp from ambient to 900°C at 10°$C.min^{-1}$.

2.4 Microwave Plasma Chemical Vapour Deposition

Chemical Vapour Deposition (CVD) is a process involving the condensation of a precursor in the gas state into a solid deposit on the surface of a substrate. This usually involves the cracking of a hydrocarbon gas at a high temperature under an inert atmosphere to produce thin-films or carbon-carbon composites[84]. CVD is used extensively in the nanotechnology industry to produce thin layers of diamond and graphitic type carbonaceous deposits as well as carbon nanotubes[85]. The microwave produced plasma used to assist in the deposition process uses electrical energy to initiate homogenous reactions to produce chemically active ions and radicals. These radicals can then take part in heterogeneous reactions which in turn produce the formation of a deposit on the substrate surface. The use of plasma allows the deposition process to take place at lower temperatures compared to thermal CVD[86]. The apparatus used in this study utilises a single-mode microwave cavity. This generates a single standing wave pattern of forward and reflected waves which prevents the formation of hot and cold spots within the sample. The single-mode cavity produces a uniform heating pattern and a high electrical field strength compared to a multi-mode cavity[87-89]. A number of experiments were carried out in order to produce a carbonaceous deposit on the surface of graphite using microwave assisted CVD (Figure 11).

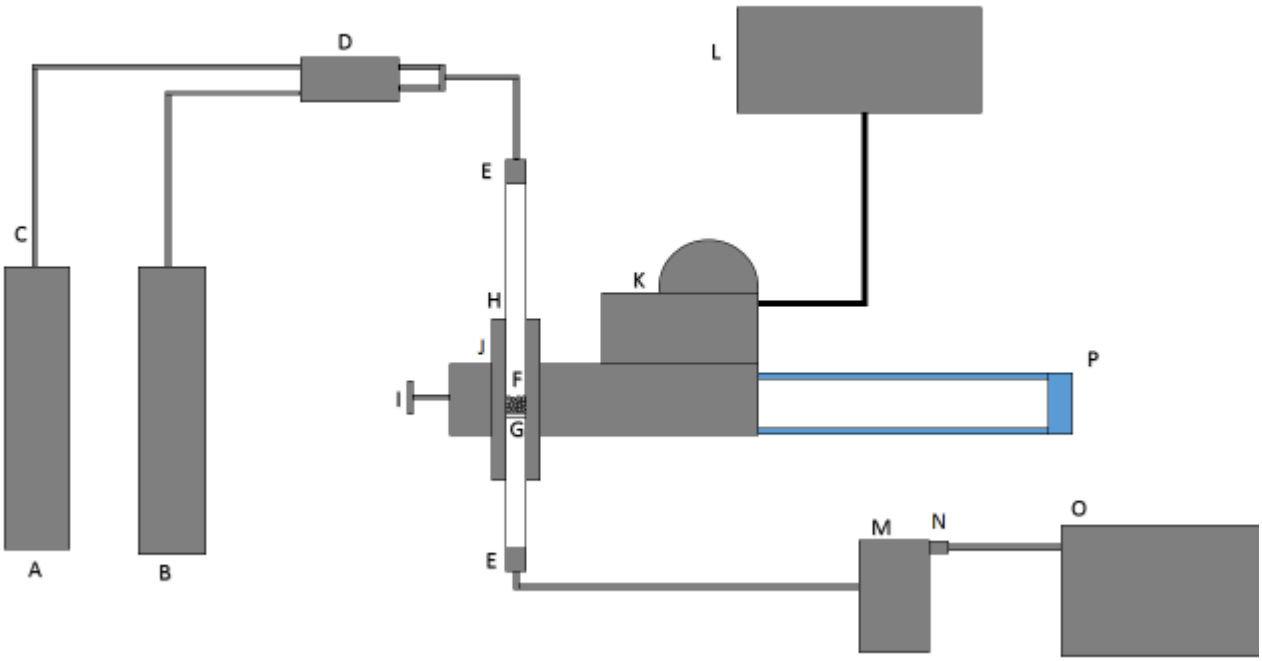

Figure 11 - Schematic for microwave plasma chemical vapour deposition experimental set up, where A: Methane gas cylinder, B: Argon gas cylinder, C: Tubing, D: Mass flow controller, E: Swagelok fittings, F: Graphite sample, G: Sintered frit, H: Quartz tube, I: Plunge tuner, J: Single-mode Microwave cavity, K: Microwave generator, L: Microwave controller, M: Vacuum pump, N: Vacuum exhaust, O: Mass Spectrometer and P: Circulation of water from a sink used as coolant

Using a sample size of 2 g, particulate graphite samples (1-2 mm) were placed into a quartz tube. They were held in place in the middle of the tube by a sintered frit. The quartz tube was used because it is microwave transparent[90] and was positioned so that the graphite samples were held in the middle of the microwave cavity and would be in the microwave field. The quartz tube was connected to a gas supply containing a mix of argon carrier gas and methane precursor gas. To achieve a 2% methane concentration mass flow controllers were used to flow 49 $ml.min^{-1}$ of argon and 1 $ml.min^{-1}$ of methane into the system. A mass spectrometer was used to indicate when oxygen had been completely removed from the system. Using a Vacuubrand PC3001 Vario vacuum pump with integrated CVC 3000 controller a pressure of 10 mbar was applied to the system. Ensuring that the tap for the water cooling was employed, the microwave controller was set to a power outage of 200 Watts and the plunge tuner was operated in order to achieve the minimum reflectance of microwaves. The plasma produced gave off a pink/purple colour and was maintained for 1 hour until the generator was switched off and the samples allowed to cool and then collected.

2.5 Thermal Treatment

The aim of these experiments was to find the optimum temperature at which the selective removal of the deposits could be achieved. In order to decontaminate graphite samples from the carbonaceous deposits present a series of isothermal experiments were carried out (Figure 12). Using a sample size of 1 g, the graphite samples with carbonaceous deposits were placed into a quartz tube. They were held in place in the middle of the tube by a sintered frit. The quartz tube was positioned so that the samples were held in the middle of the furnace. Using a mass flow controller 15 $ml.min^{-1}$ of air was allowed to flow through the system. In order to investigate whether the deposits could be removed with little oxidation to the underlying graphite, samples were thermally treated both with and without the application of a vacuum. Using a Vacuubrand PC3001 Vario vacuum pump with integrated CVC 3000 controller a pressure of 5 mbar was applied to some of the experiments. The samples were then heated by the Carbolite 1200 DegC vertical split tube furnace with an integrated Eurotherm 2408 temperature controller at temperatures between 450-800°C for a period of 5 hours, at which point the furnace and sample were allowed to cool and the samples were collected.

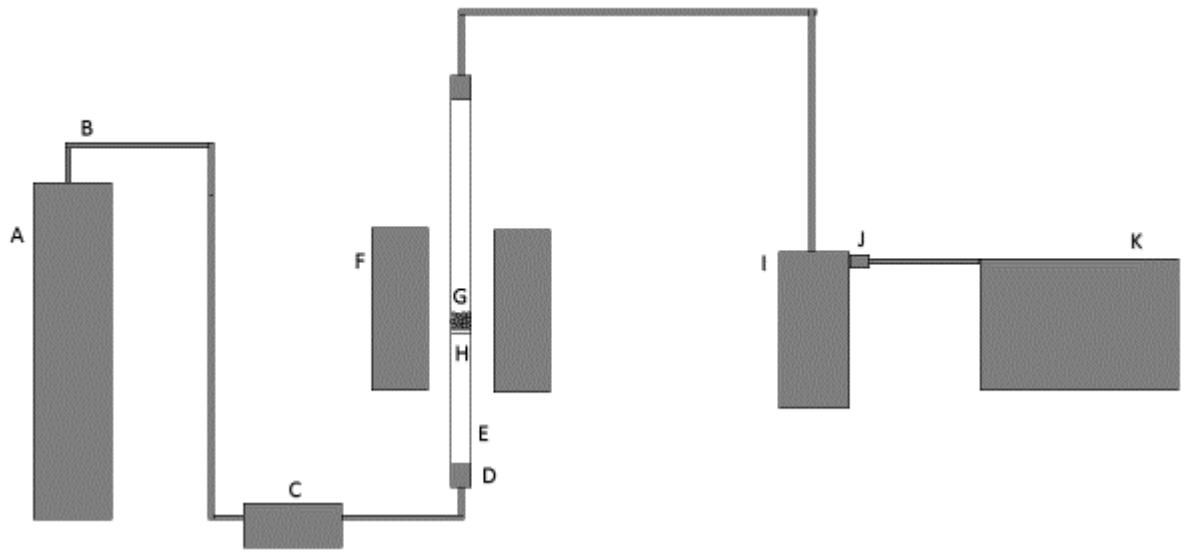

Figure 12 - Schematic for thermal treatment experimental set-up, where A: Gas Cylinder, B: Tubing, C: Mass flow controller, D: Swagelok fittings, E: Quartz Tube, F: Furnace, G: Graphite sample with carbonaceous deposit, H: Sintered frit, I: Vacuum pump, J: Vacuum exhaust and K: Mass Spectrometer

2.6 Summary

A number of different processes were involved in order to reach the stage where the removal of carbonaceous deposits from graphite could be investigated by thermal treatment (Figure 13 and Figure 14). In addition two different deposition methods were examined, solution deposition and microwave plasma assisted chemical vapour deposition. Solution deposition required an additional stage to char the carbon precursor to the graphite surface. This was unnecessary with the microwave method as deposits were formed in situ from the thermal breakdown of the gaseous precursor.

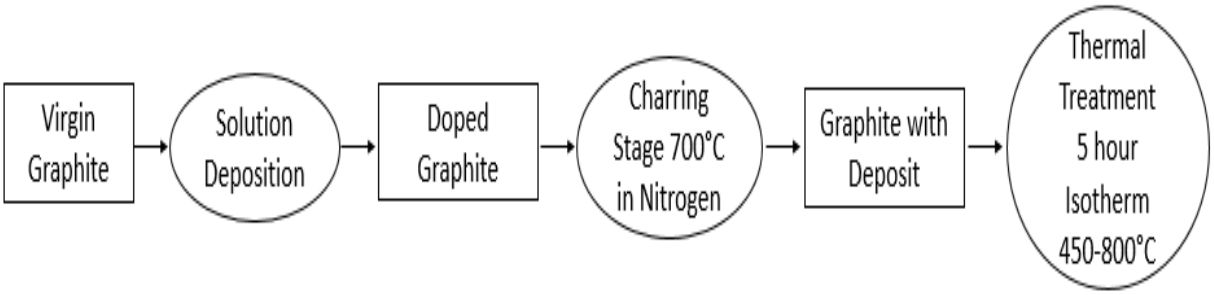

Figure 13 - Flow chart of techniques involved with solution deposited samples

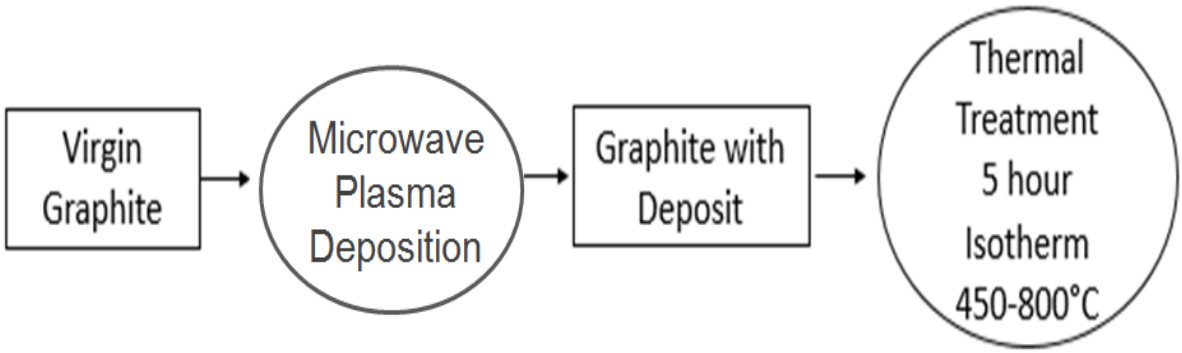

Figure 14 - Flow chart of techniques involved with microwave deposited samples

2.7 Characterisation

In order to fully understand the chemical composition and morphology of the carbonaceous deposits produced, a number of characterisation techniques were implemented. These techniques were also used to evaluate the success of each experimental stage. Comparisons can be made between the results of virgin graphite samples, samples with carbonaceous deposits present and also with samples that have been thermally treated to remove the deposits.

2.8 Scanning Electron Microscopy

Scanning Electron Microscopy (SEM) was used to characterise the surface morphology of virgin graphite samples and various carbon deposits. This analytical technique was important as it allowed the assessment of the effectiveness of the deposition techniques as well as methods used to remove the deposits.

SEM is a technique which produces a magnified image of a sample by scanning over its surface with a beam of electrons. These electrons interact with the electrons present within the sample, producing backscattered electrons, secondary electrons and x-rays, all of which can be collected by multiple detectors and processed to produce an image. The magnification of the sample is controlled by focussing the electron beam using a series of electromagnets, all occurring under vacuum[91].

The apparatus used during this project was a FEI Quanta 200 SEM. Samples were prepared for SEM by using tweezers to fix graphite particles to an adhesive carbon pad attached to an aluminium stub. These stubs were placed upon the SEM stage in line with the electron beam. Two to three graphite particles were analysed per each experiment. Samples were analysed under a high vacuum using an Everhart-Thornley secondary electron detector. All samples were analysed using SEM at x150, x300, x600, x1200, x2500, x5000 and x10,000 magnifications and using a spot size of 4.0 and a 20 KeV filament charge.

2.9 Raman Spectroscopy

Raman Spectroscopy was employed in order to demonstrate the presence of carbonaceous deposits on the graphite surface. It provides an understanding of a sample's chemical

composition and the differences between various carbonaceous materials; be it highly ordered graphitic carbon or disordered and amorphous carbon[92].

Raman spectroscopy is a technique used to characterise the vibration, rotation and bending of molecules which when excited by a laser emit scattered radiation. When a molecule is excited by radiation it is promoted to a (virtual) higher energy state (Figure 15). The molecule will return to its original energy state by releasing a photon of a certain frequency. When the photon released is the same frequency as the incident radiation its known as elastic or Rayleigh scattering. When a photon is produced which exhibits less energy than the incident radiation the molecule will relax back to a higher vibrational energy state than it was originally. This energy transition is known as Stokes Raman scattering and is one of the two variants of inelastic scattering. The other represents anti-Stokes Raman scattering which is the phenomenon where the photon produced has more energy than the incident radiation. The molecule, once it's been excited to a higher energy state, will relax back to a lower energy state than it was previously.

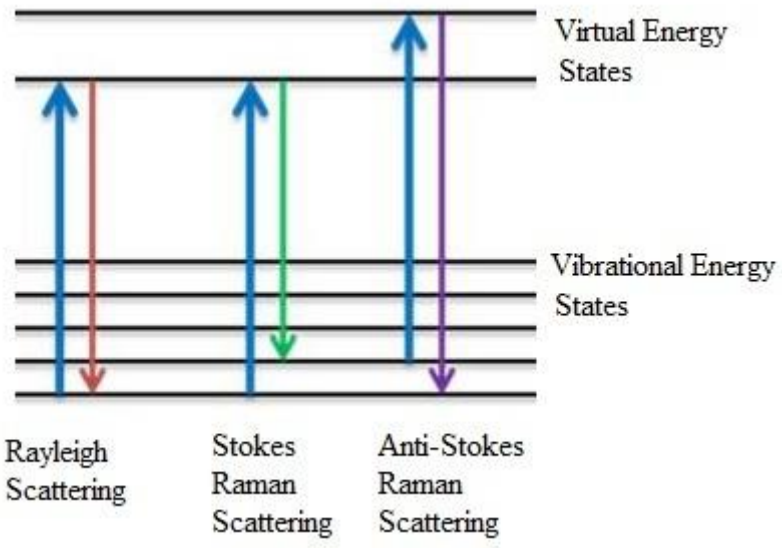

Figure 15 - Energy level diagram of Raman scattering[93]

Stokes scattering produces a more intense Raman signal due to the higher vibrational energy level and is the most common form of scattering recorded when spectra are produced. A Raman spectrum represents the shift in frequency of a produced photon from the excitation wavelength, often called the Raman Shift. It is a plot of Raman scattering intensity against wavelength and is a very useful characterisation tool[94].

Raman Spectroscopy is often coupled with microscopy providing a high magnification visualisation of the sample as well as Raman analysis. The incident radiation or laser is passed through a microscope objective and focused onto the sample (Figure 16). Confocal Microscopy has the addition of a spatial filter where the backscattered Raman signal is refocused onto a pinhole aperture. Returning to the spectrometer the filtered signal is dispersed onto a charge coupled device camera and produces a spectrum. Confocal Microscopy has the additional benefits of providing a three-dimensional image with a high spatial resolution and depth discrimination[95].

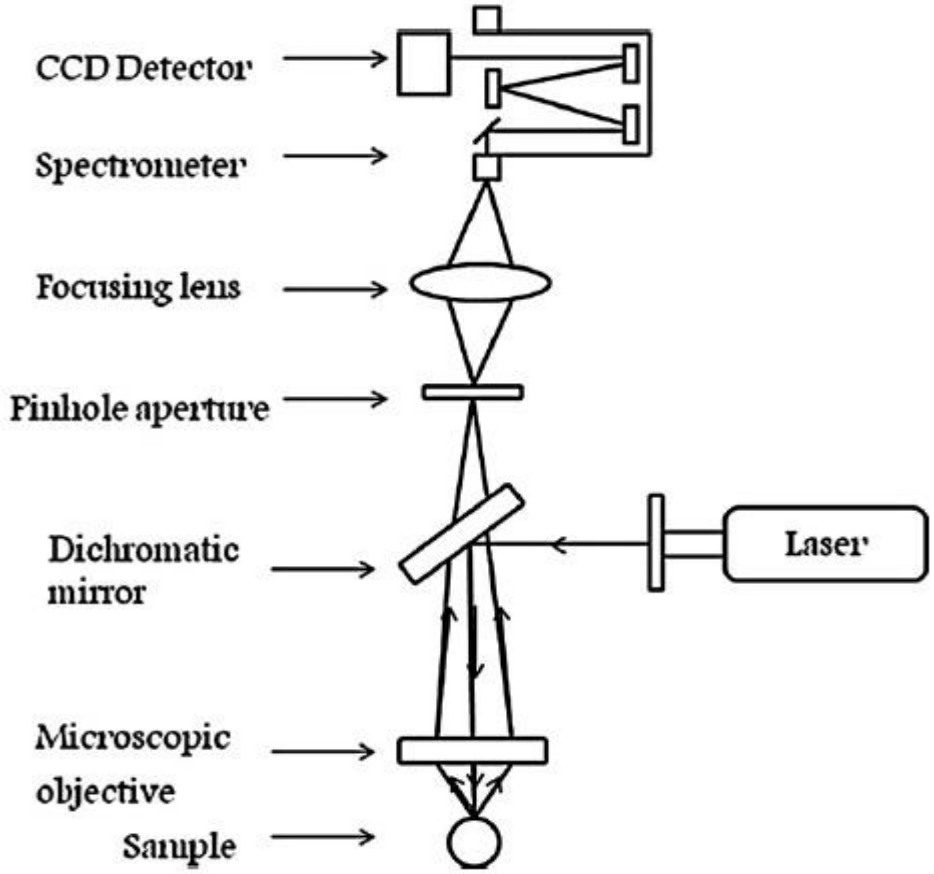

Figure 16 - Schematic of confocal Raman microscope[95]

The Raman apparatus used during this study was a Horiba Jobin Yvon LabRAM HR 800 confocal Raman microscope. As there is no sample preparation required for Raman analysis, two to three graphite particles from each experiment were positioned onto a glass slide and placed under the microscope. Samples were analysed using a 532 nm laser, x50 long working distance objective, along with a diffraction grating of 300 grooves per millimetre. The instrument was calibrated before each set of experiments using the 520.7 cm^{-1} peak of a

silicon standard. To achieve the maximum intensity possible, the hole size was set to 400 µm along with a slit of 100 µm.

2.10 Thermal Gravimetric Analysis

Thermal Gravimetric Analysis (TGA) was used in an inert atmosphere in order to produce a carbonaceous char on the surface of graphite samples which had undergone solution deposition. Furthermore, to establish the presence of carbon precursors on the graphite sample surface TGA was performed using an oxidising atmosphere and comparisons were made between the oxidation profiles of virgin graphite samples and graphite samples with deposits present. TGA uses a balance to transmit a continuous measure of a samples mass as the temperature of the sample increases uniformly. Mass changes will occur as the sample reacts with the flowing atmosphere which surrounds the sample.

The thermobalance used during this project was a Stanton Redcroft TG760 series with a platinum sample crucible. The crucible is suspended from a hang down wire attached to a balance unit with a two piece platinum stirrup and counter balance. The thermobalance is connected to a water supply so that it can cool back down to room temperature quickly after analysis. The temperature of the furnace is monitored by two thermocouples, one in contact with the furnace wall and one below the crucible measuring the sample temperature. Gas flows down from the top of the furnace past the sample crucible. A schematic of the TG760 can be seen on the next page in Figure 17[96].

A plot known as a thermal gravimetric curve which portrays mass as a function of temperature or time is the usual mode of data presentation. Mass changes will appear as steps in a TGA curve. Alternatively, results can be displayed using the first derivative of the TGA curve as a function of temperature and time. This plot is known as the Differential Thermal Gravimetric (DTG) curve and shows the rate at which the mass changes. Mass changes will appear as peaks in a DTG curve. An example of both of these plots can be seen on the next page (Figure 18) which portrays the thermal decomposition characteristics of calcium oxalate monohydrate, which is a common standard used for the calibration of thermobalances and was used periodically throughout this research. Its used because it displays a specific decomposition profile with three different steps in an inert atmosphere. The first step is dehydration at ~170°C where the sample loses water to form anhydrous calcium oxalate from

the monohydrate. Secondly, CO is given off as calcium carbonate is formed at ~500°C, and lastly at 750°C calcium carbonate decomposes releasing CO_2 and forming calcium oxide[97].

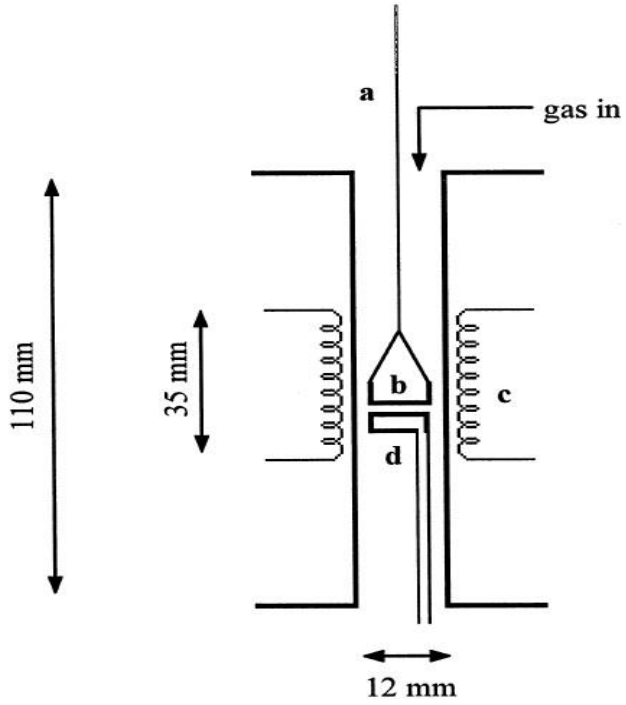

Figure 17 - Schematic of a Stanton Redcroft TG760. Key: a = hang down wire, b = crucible, c=furnace winding, d= sample thermocouple[96]

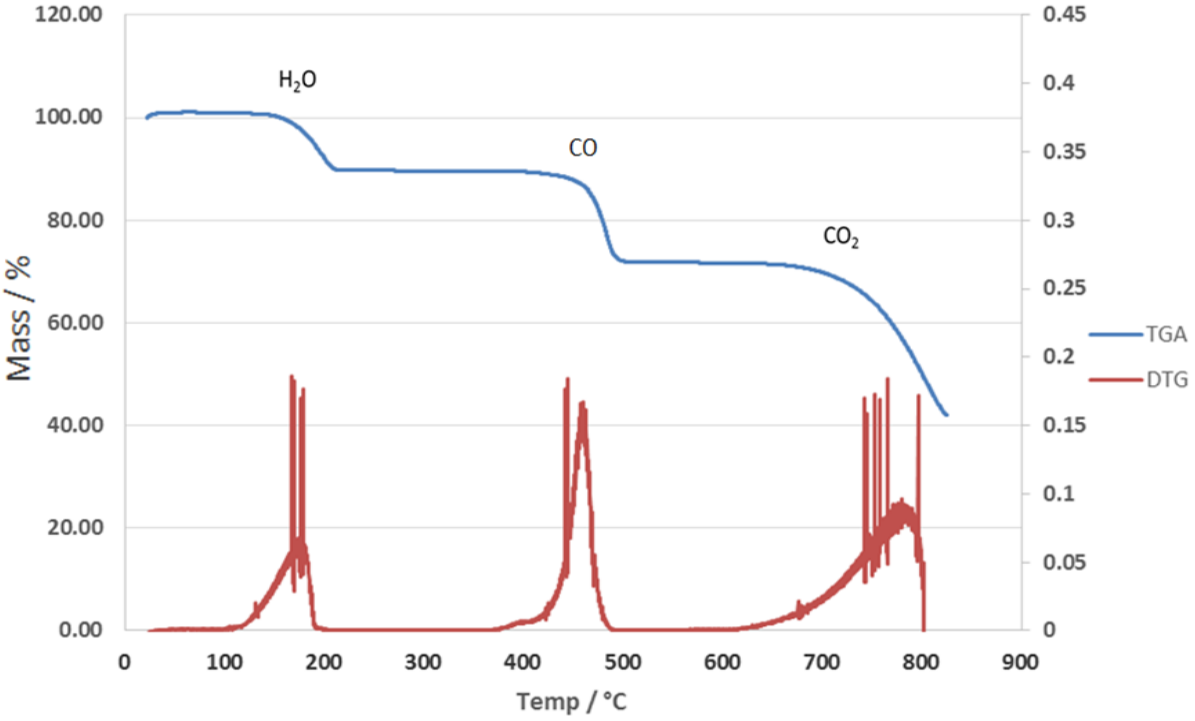

Figure 18 - Decomposition of calcium oxalate monohydrate

A well-documented phenomenon with TGA experiments is the buoyancy effect. This is where a sample appears to gain mass during a heating experiment and is caused by the fact that as the temperature changes the density of the gas flowing over the sample also changes. In addition the gas at the furnace wall will heat up quicker than the gas flowing over the sample. The hot gas at the furnace walls will rise and force cold gas at the centre of the furnace down towards the crucible giving an incorrect mass increase reading. This is also known as the convection effect. As the design of the thermobalance allows the gas to flow over the hang-down system there will be evidence of a dragging effect in the direction of the gas flow. Additionally the velocity of the gas flow will increase with temperature which will also alter the sample weight reading given by the apparatus. Fortunately data can be corrected for these effects by running a blank experiment, which uses the same temperature program and an empty crucible. This will record the extent of the buoyancy effect. Through the application of a linear polynomial function to reduce noise and by subtracting the blank buoyancy result from the measured sample result, the true mass change of the sample during the experiment can be obtained[98].

2.11 Mass Spectrometry

Mass Spectrometry was used to analyse the off gas produced during the thermal treatment of virgin graphite and graphite with various carbon deposits. This analytical technique was important as it allowed the assessment of the effectiveness of the thermal treatment by indicating the presence of C-12 and C-13 CO_2 produced.

Mass Spectrometry is a technique that uses ionization to generate charged molecules or fragments from a chemical compound. The charged species are manipulated by the application of magnetic or electric fields, which separate the molecules according to their mass. A spectrum is then produced from the detection of the separated ions. The gaseous analyte is ionized through bombardment with high energy electrons which cause extensive fragmentation, due to the electrons having a higher energy than the strength of the bonds within the sample. Since the mass spectrometer can separate ions of different mass it is a useful tool when analyzing different isotopes of the same atom, for example the differentiation between C-13 and C-12[94].

Where gas analysis was required during the course of this project a HIDEN Analytical HPR-20 QIC Mass Spectrometer was used. This instrument uses a quadrupole mass analyser which

is composed of four parallel metallic rods, two with a positive electrical potential and two with a negative electrical potential. For a given amplitude only the ions of a given mass to charge ratio will oscillate and have a stable trajectory through the quadrupole, between the rods and reach the detector. This allows the user to select certain ions and fragments they are interested in by varying the amplitude to detect the different mass to charge ratios (m/z) of different species[99]. For most of the experiments CO_2 was detected using the m/z of 44 and CO was detected using the m/z of 28. For experiments where C13 carbon precursors were used, different m/z were selected. C13 CO_2 was detected using the m/z of 45 and C13 CO was detected using the m/z of 29. The quartz inlet capillary of the mass spectrometer was connected directly to the off gas tube of the experimental set up. By using a Faraday detector in Multiple Ion Detection (MID) mode a real-time display of the gases produced during the course of the thermal treatments could be obtained.

2.12 Carbon-14 Content of Carbonaceous Deposits and Graphite

A series of experiments were carried out using irradiated graphite samples involving the TGA of Oldbury reactor graphite and the investigation of the distribution of C-14 activities present in irradiated graphite and carbonaceous deposits. This work was carried out as part of the EPSRC Industrial CASE award and was funded by the NNL. The irradiated graphite samples were handled and analysed in the active laboratories at the National Nuclear Laboratory (NNL) Preston Laboratory based at the Springfields Ltd site.

The study involved the use of TGA to oxidise graphite samples whilst collecting the CO_2 produced. The experiments were comprised of three procedures. An irradiated graphite disc was first split into three pieces. Piece 1 samples were analysed for total C-14 content by pyrolysis. Piece 2 samples underwent TGA to characterise deposit concentrations and underlying graphite and deposit oxidation behaviour. From this data, the time required for removing the deposits by oxidation could be determined. The same experimental parameters were used for the TGA of Piece 3 samples, this time treating the material for the time necessary to remove the deposit determined from Piece 2 samples. A second period of oxidation on Piece 3 samples was used to determine the C-14 content of the underlying graphite. The residue of Piece 3 then has its total C-14 content measured by pyrolysis to enable the C-14 mass balance on Piece 3 to be compared with the total C-14 measured on Piece 1. Established NNL analytical procedures were applied throughout these experiments.

2.12.1 Sample Receipt

Discs sectioned from six cores trepanned from an Oldbury Magnox reactor fuel channel were used in these experiments; they were stored at Sellafield before being delivered to Springfields. Discs from the fuel channel end of the trepanned cores were chosen because they have a higher concentration of carbonaceous deposit[41]. These discs having dimensions of ~ ø12 x 6 mm were dissected into three pieces, by cutting the disc in half and then cutting one piece in half again (Figure 19).

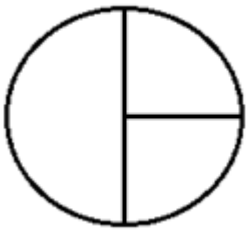

Figure 19 - Diagram of samples received

The sample preparation was undertaken prior to delivery to Springfields, by a team at Sellafield. Upon arrival at Springfields, Piece 1 samples (Table 12) were transferred to the Measurement and Analysis Team. The selected cores were from three different fuel channels with unique reactor identifiers J17A4, J17C5 and Q15C5. Using the sample Q15C5 _2/1 (3U) as an example, the 2/1 identifies the sequential core number when the channel was trepanned (core 2) and the radial position in the core (each core is sectioned into three 6mm long discs, so disc 1 is the first at the channel wall). The identifier in brackets (3U in this example) denotes whether the core is from the Upper or Lower position (Upper in this case) and from which graphite layer counting from the bottom of the core (3 in this example).

Table 12 - Sample references and weights

NNL Identity	Piece 1 Weight (g)	Piece 2 Weight (g)	Piece 3 Weight (g)	Total Weight (g)	Axial Height in core (m)
J17A4_13/1 (9U)	0.414	0.203	0.195	0.812	6.85
J17A4_8/1 (6U)	0.256	0.610	0.285	1.151	4.62
J17C5_8/1 (6U)	0.225	0.475	0.240	0.940	4.62
Q15C5_2/1 (3U)	0.206	0.399	0.220	0.825	1.98
Q15C5_3/1 (4L)	0.174	0.397	0.209	0.780	2.66
Q15C5_4/1 (4U)	0.342	0.676	0.371	1.389	2.95
Q15C5_8/1 (6U)	0.712	0.397	0.383	1.492	4.62

2.12.2 Complete Carbon-14 Content (Piece 1)

A full C-14 analysis was carried out by the Measurement and Analysis Team employing established NNL procedures to analyse the Piece 1 samples (Table 12). This was achieved by complete pyrolysis of the graphite samples in a furnace at 800°C in the presence of a platinum alumina catalyst. A 50:50 mixture of air and oxygen was utilised at a flow of 0.25 litres per minute. Any carbon present was converted to CO_2 and captured in a series of gas-bubblers containing Carbosorb. An aliquot of the trap liquor was mixed with scintillation cocktail and the C-14 activity was determined by United Kingdom Accreditation Service (UKAS) accredited liquid scintillation counting.

2.12.3 Liquid Scintillation Counting

Liquid scintillation counting is a very sensitive radiation detection system. It utilises the phenomenon that irradiated atoms will emit a radioactive particle (alpha or beta) or gamma-rays in a process known as radioactive decay. The interaction of alpha and beta particles with atoms causes ionization, the removal or addition of electrons, whilst gamma-rays cause secondary electron emissions which then ionize other atoms. Some atoms are not fully ionized by this interaction and instead possess electrons at a higher energy state. These atoms can revert back to a lower energy state (ground state) by releasing energy. The scintillation cocktail which is mixed with the liquid sample absorbs the released energy and re-emits it as flashes of light which are then quantified by the counter. The detection and counting of every

emission event would provide a truly accurate measurement of disintegrations per minute however this is not possible in most cases. Additionally, there is a significant amount of background radiation caused by cosmic radiation and naturally occurring isotopes. In order to convert the counts per minute which are measured into the number of decay events which actually occur, requires corrections for both background and efficiency[100].

2.12.4 Thermal Gravimetric Analysis (Piece 2)

TGA was carried out on the Piece 2 samples to determine the time required for removing the deposits by oxidation. A NETZSCH 449C STA TGA with an air flow of 10 $ml.min^{-1}$ was employed for all experiments. The sample was held for 2 hours at 200°C to ensure any moisture had been removed, then ramped up to 450°C and held at this temperature for 50 hours. The furnace was allowed to cool down to 200°C and held for 2 hours at this temperature before returning to ambient temperature. A nominal 200°C was maintained for two hours before and after the run to achieve stable datum points for any statistical analysis that may be carried out. The temperature program used was a standard NNL procedure. Effluent gases were passed through four gas bubblers in series to capture the Tritium (H-3) and C-14 produced (Figure 20). Drechsel bottles 1 and 2 each contained 100 ml 0.1M nitric acid for the collection of H-3. Drechsel bottles 3 and 4 each contained 100 ml of Carbosorb for the collection of C-14. Two Drechsel bottles were used for each isotope in case the scrubber solution in the first bottle became saturated. The safety case for operating the experiments required H-3 to be collected and disposed of in an appropriate manner (the solutions were not analysed). While the gases produced during the Piece 2 TGA were passed through gas bubblers, the solutions were not analysed as this information was obtained from the Piece 3 analysis.

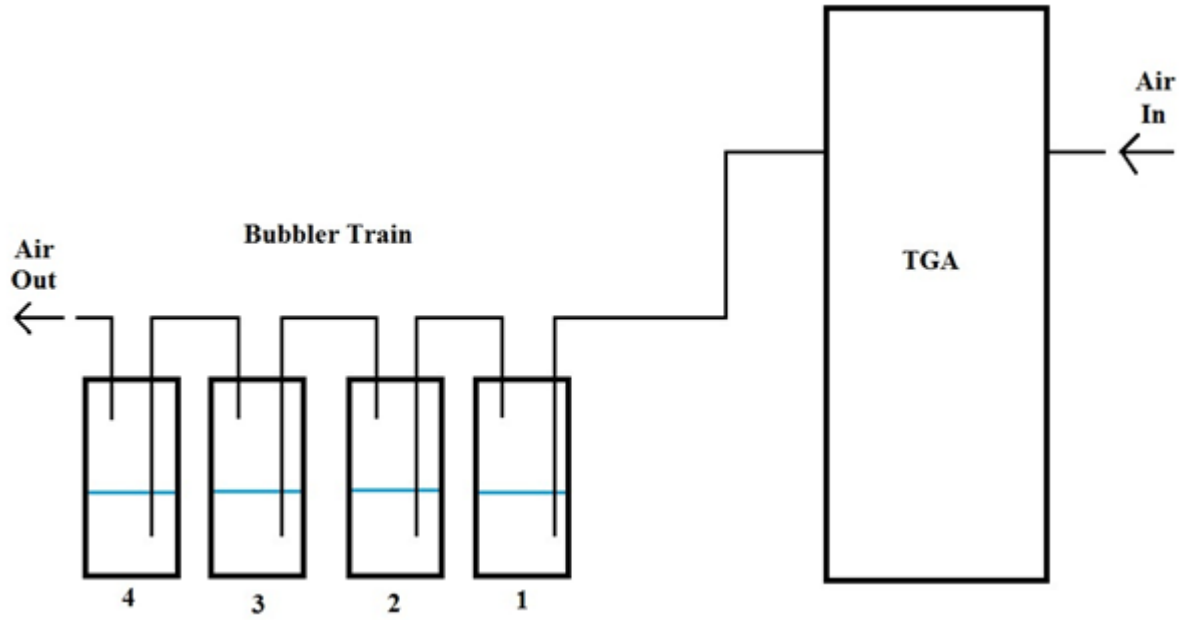

Figure 20 - Schematic of experimental set up

2.12.5 Piece 3 Analysis

The analysis of the Piece 3 samples involved several stages. Firstly the same TGA experimental parameters as the Piece 2 samples were used with the exception that the oxidation time at 450°C was based upon the estimated time for the removal of the deposit (which was determined from the Piece 2 samples). The cooling period provided adequate time to completely flush out the system before the collection of the liquor from the bottles. The bottles were replaced with fresh liquor before the oxidation of the graphite sample continued for a further ~100 hours to produce a 1-2% mass loss in the specimen (the actual duration was determined from the oxidation data generated from Piece 2).

The Carbosorb samples allocated to deposit and 1-2% underlying graphite as well as the remaining solid graphite samples was sent to the Measurement and Analysis Team for C-14 analysis. An aliquot of each of the Carbosorb gas bubbler samples was taken and the C-14 activity was obtained by liquid scintillation counting. The C-14 content of the residual solid graphite was evaluated by fully combusting the samples and trapping the CO_2 produced in Carbosorb, for measurement by liquid scintillation counting, as with the Piece 1 samples.

2.12.6 Extended Oxidation

One Piece 3 sample (J17C5_8/1 (6U) in Table 12) was progressed as above but included an extended oxidation following the removal of the deposit. This experiment was included to measure the rate of C-14 released with increasing mass loss. Once the deposit had been removed through oxidation (~2%) the temperature program was continued until another ~2% mass loss was produced, with the liquor bottles being changed at four ~0.5% increments. The C-14 content was determined as described above.

2.12.7 Quality Assurance

In order to ensure the quality of the data produced a number of quality assurance steps were put in place. The performance of the TGA apparatus was tested at the start of the project and half way through the experimental proceedings using a calcium oxalate standard. The drift in the apparatus over the period of oxidation was measured from an empty crucible 'blank' run performed after every two sample runs following the same sample temperature program. The temperature in the laboratory was logged during the experiments in the event that results would have to be corrected for lab temperature. Subsequently, it was decided that the application of this correction did not improve the data traces. An excess amount of Carbosorb was used in the gas bubblers to ensure all CO_2 produced from the experiments was collected. Carbosorb is an amine which absorbs 4.8 millimoles per ml, equivalent to 57 mg of carbon[101,102]. Each bottle containing 100 ml of Carbosorb was capable of absorbing 5.7g of carbon, more than adequate to capture all the CO_2 produced during the experiments.

3. RESULTS AND DISCUSSION

The following section will provide the results and interpretation of the various methods employed to produce and remove carbonaceous deposits as well as their subsequent characterisation. Furthermore, this section will also include the results from the secondment at the National Nuclear Laboratory which involved the analysis of carbonaceous deposits and irradiated graphite for C-14 content and its disposition throughout the sample.

3.1 Virgin Graphite Characterisation

In order to characterise carbonaceous deposits produced onto the graphite surface and samples where the deposits have been removed, the characterisation of virgin graphite samples becomes important to provide a base with which to compare.

3.1.1 Scanning Electron Microscopy

SEM analysis was carried out on a number of virgin graphite samples to ascertain the nature of the surface structure and its morphology. Initially, after size reduction, as received solid graphite samples were analysed using SEM.

The virgin graphite samples exhibited a very mixed surface morphology. There were areas which displayed a randomly oriented grain like appearance with graphite crystals aligned and of similar size (A and C in Figure 21). Additionally there were areas present which displayed rough and porous morphology (B and D in Figure 21). The large pores are caused by the escape of entrapped gases during the graphite manufacturing process. Despite different coke pitches used during their manufacturing process both virgin Magnox and AGR graphite exhibit a similar but diverse surface structure[103,104]. These SEM images will provide an important comparison when analysing samples for the presence of a carbonaceous deposit.

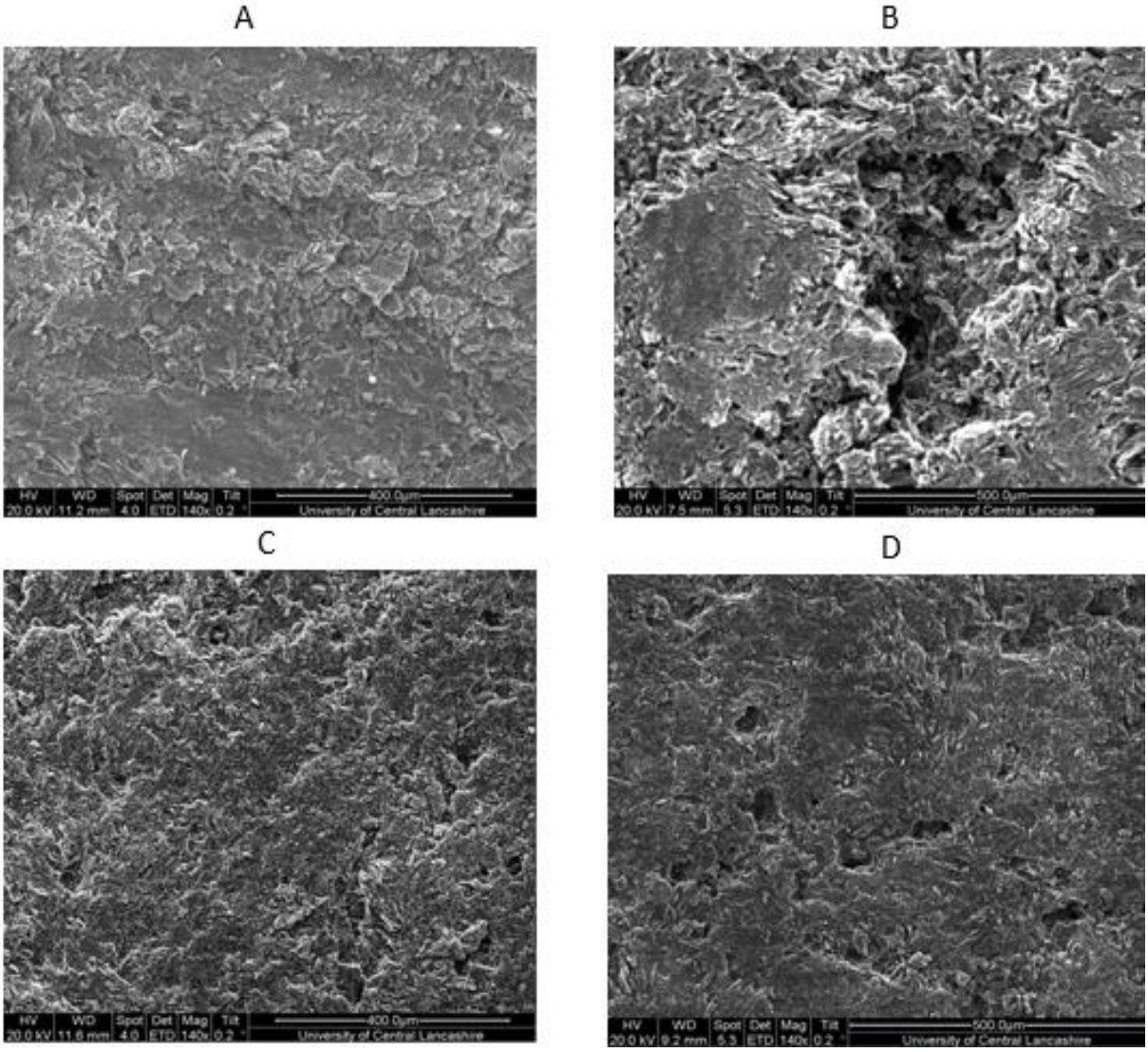

Figure 21 - SEM images of virgin graphite samples at x140 magnification; A and B- Magnox graphite, C and D- AGR graphite

3.1.2 Raman Spectroscopy

Raman spectroscopy is commonly used to analyse the bonding states within carbonaceous material. The degree of structural ordering of a sample can be ascertained, from highly ordered diamond[105], graphite[106] and graphene[107] to the more disordered amorphous carbon or soot[108].

The Raman spectra of all disordered carbon and poly-aromatic hydrocarbons[109] are dominated by two peaks known as the G and D peaks. The peak labelled G for 'Graphite' arises at ~1580 cm^{-1} and is attributed to the stretching modes of sp^2 bonded carbon. This results from the C=C (π state) in the hexagonal layers of graphite and has 2_{EG} symmetry[110] (Figure 22). The peak labelled D for 'disorder' arises at ~1350 cm^{-1} and indicates the presence of disordered carbon and arises from the A_{1G} breathing motion of the sp^2 rings.

Figure 22 - Carbon motions in the A- E_{2g} Symmetry of the G peak and B – A_{1g} D breathing mode[92]

A single crystal of graphite will only have the G peak present in its Raman spectrum however the graphite samples used in this study show the presence of a small amount of disorder (Figure 23). Also present in this spectrum is the presence of a peak at ~2700 cm^{-1} which is known as either the 2D peak or G' peak and is caused by the second order scattering of the D peak[111].

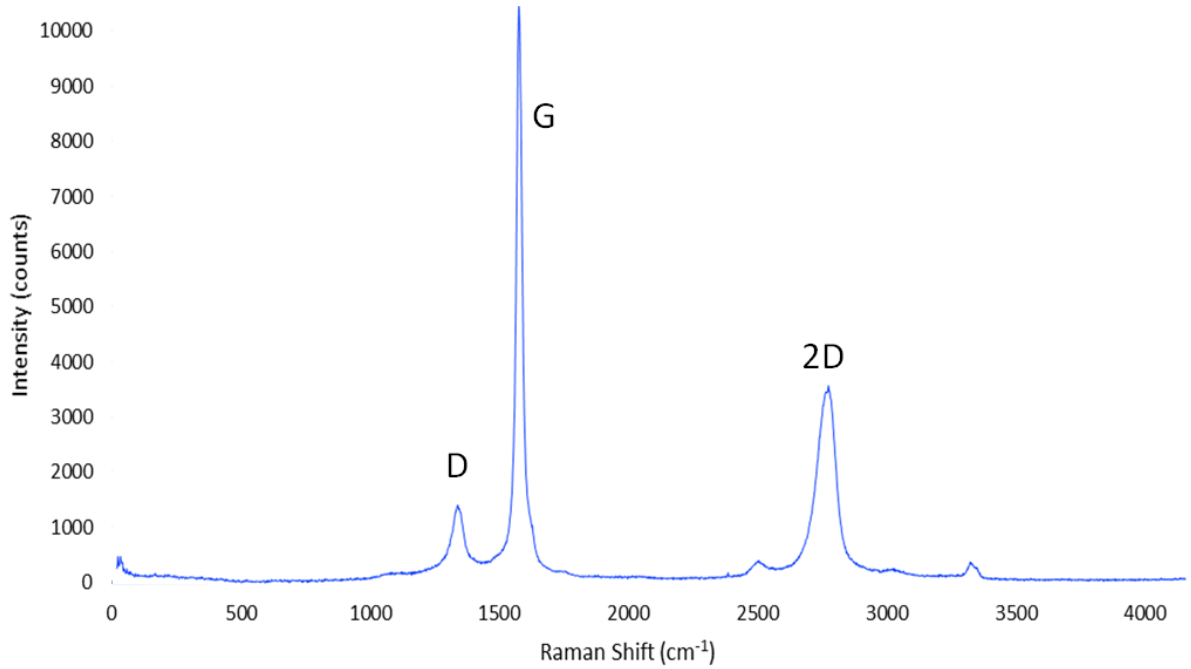

Figure 23 - Raman spectrum of virgin Magnox graphite

A comparison of the spectrum produced from both AGR and Magnox graphite shows that the graphite samples are very structurally similar (Figure 24). The characteristic G and D peaks attributed to graphite can be observed, and the intensity of the D peaks are similar indicating a similar amount of disorder is present.

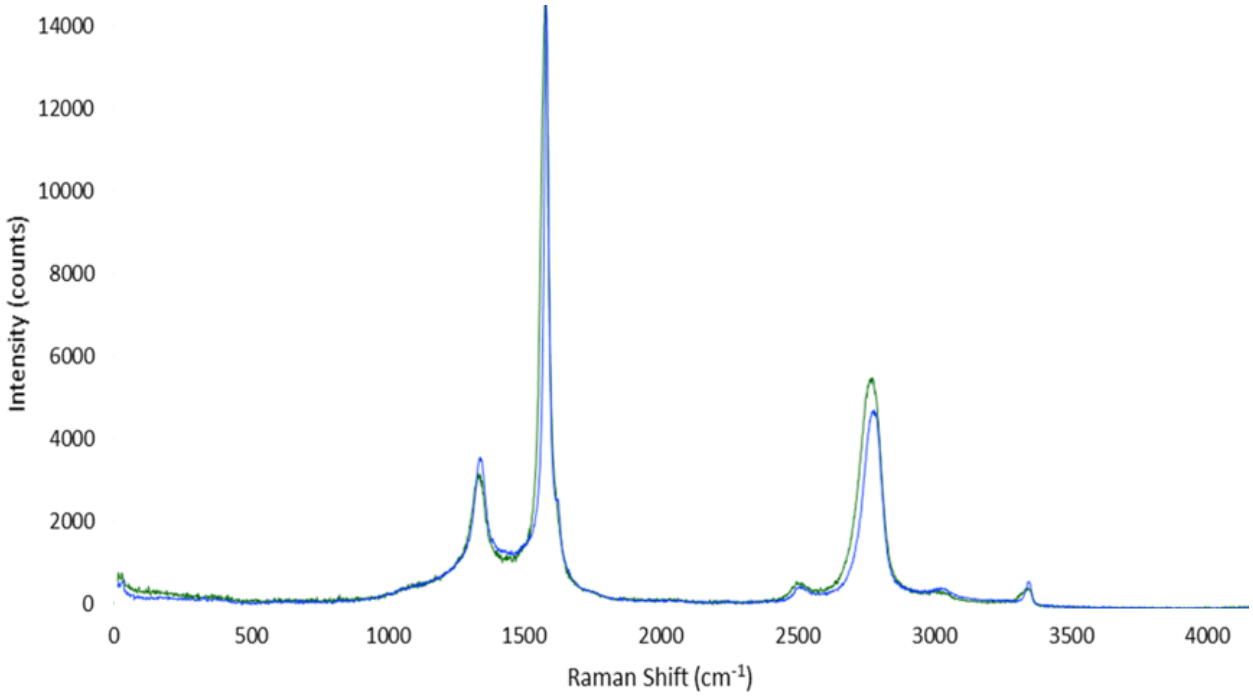

Figure 24 - Raman spectra of virgin Magnox graphite (blue) and virgin AGR graphite (green)

3.1.3 Thermal Gravimetric Analysis

The mass loss profiles of Magnox and AGR graphite (Figure 25) showed that the 1-2 mm graphite particle samples of each type of graphite have different oxidation characteristics. AGR graphite does not exhibit a mass loss until after ~800°C whereas Magnox graphite appears to oxidise at a lower temperature around ~750°C. In addition AGR graphite exhibits a mass loss of ~2% whereas Magnox graphite loses ~5% by the end of the temperature programme. These differences are due to the different coke types used during the manufacturing process. AGR graphite is formed using a pitch coke and produces a graphite sample with a slower oxidation rate compared to Magnox graphite which utilises a petroleum coke[112].

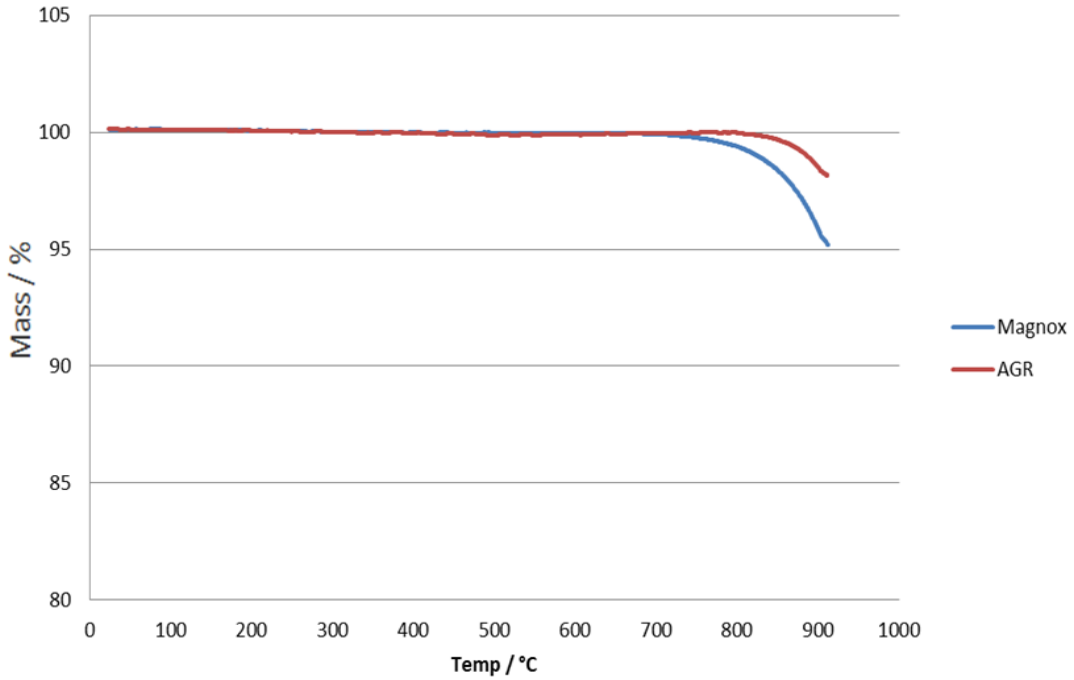

Figure 25 - TGA profile of Magnox graphite and AGR graphite

3.2 Characterisation of Carbonaceous Deposits

In order to produce a deposit which resembled the carbonaceous deposits produced on the graphite within a nuclear reactor; two experimental protocols have been investigated. The first method involved the deposition from solution of a carbon containing precursor. The precursors evaluated were limited to D-mannose, myristic acid and naphthalene. The second method investigated utilised a low pressure plasma deposition of a carbonaceous layer from a

methane/argon atmosphere. Upon producing a suitable deposit the deposition technique was repeated using a C-13 precursor. A method for the removal of the deposit was then evaluated and studied. At each stage of the deposition and removal procedures it was necessary to perform a number of different analyses in order to fully characterise the samples produced.

3.3 Solution Deposition and Charring

The solution deposition method of depositing carbon involved several different stages. The first stage involved doping the carbon precursor onto the graphite surface. The second stage was to convert the doped precursor into a carbonaceous char on the graphite surface. Two different charring methods were investigated; one using a thermobalance and the other using a bulk charring procedure.

SEM was used to compare graphite which had been doped with a carbonaceous precursor with SEM images of the carbonaceous deposits which had been charred using both the thermobalance method and the bulk charring procedure. Although samples were produced using a range of precursor amounts on the graphite surface only the maximum sample size (2 g of precursor with 20 g of graphite) were analysed initially.

Raman Spectroscopy was also used to produce a spectra from graphite doped with several carbon precursors. The spectra of the carbon precursor was also analysed for comparison purposes. This Raman analysis provided evidence of the success of the doping and charring procedures in order to evaluate which samples should be progressed to the next stage of analysis.

Initially the method used for charring the doped precursors onto the graphite surface was by using a thermobalance. The charred samples were then oxidised in the thermobalance; any mass loss that fell outside the usual temperature range where graphite oxidises confirmed the production of a carbonaceous deposit. A mass loss profile was also produced from TGA for each of the carbon precursors which were used to compare with the charring profiles. Samples which exhibited successful results were selected for charring in bulk and then particles were chosen for TGA to determine whether a char was produced successfully using this method. Numerous repeats were conducted for the TGA of doped and charred samples for comparison purposes and their results will be displayed in the following sections.

3.4 D-mannose

3.4.1 Scanning Electron Microscopy

The most successful carbon deposits formed using the solution method was using D-mannose. After the doping process the white substrate could easily be seen on the graphite surface with the naked eye. The SEM analysis confirmed that D-mannose had been successfully doped onto the graphite surface (Figure 26). The graphite surface had been completely obscured by white crystals of D-mannose.

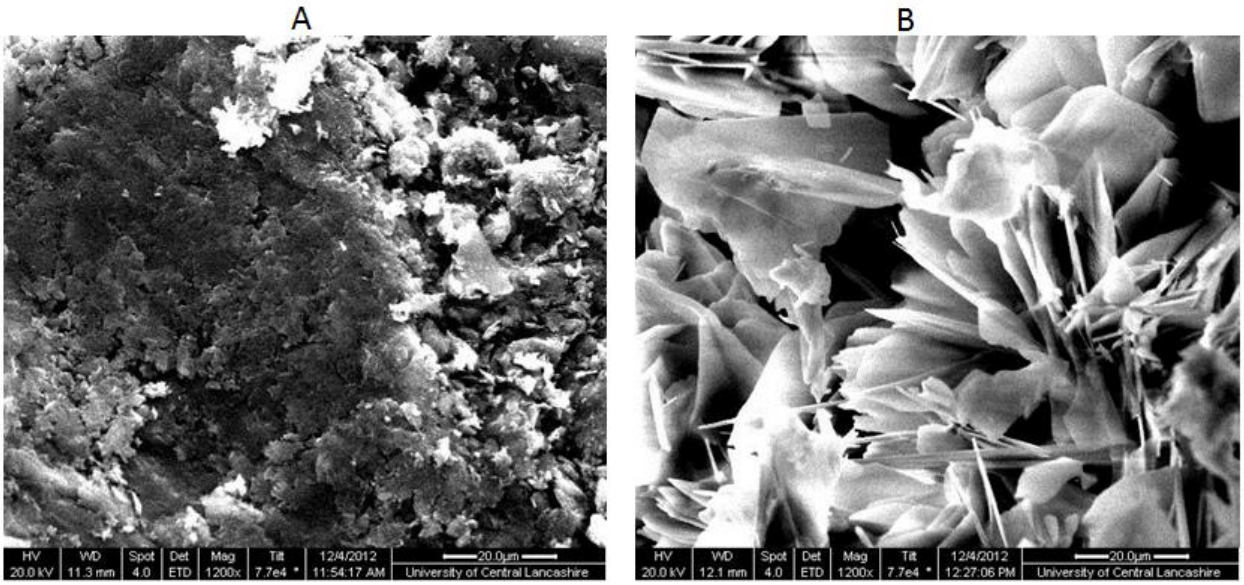

Figure 26 - SEM images at x1200 magnification of A- virgin Magnox graphite and B- Magnox graphite doped with D-mannose

After the charring stage the graphite samples no longer looked white to the naked eye but they did appear to glisten in the light. Upon SEM analysis a significant change was evident (Figure 27). In place of the large white crystals was the presence of what appeared to be a carbonaceous deposit made up of a series of bubbles or an 'irregular honeycomb arrangement'. At an increased magnification the deposit appeared to be a very thin film which covered the majority of the sample. Samples that have been charred using the bulk charring procedure produce a deposit that looks identical to that observed from charring samples using the thermobalance (Figure 28).

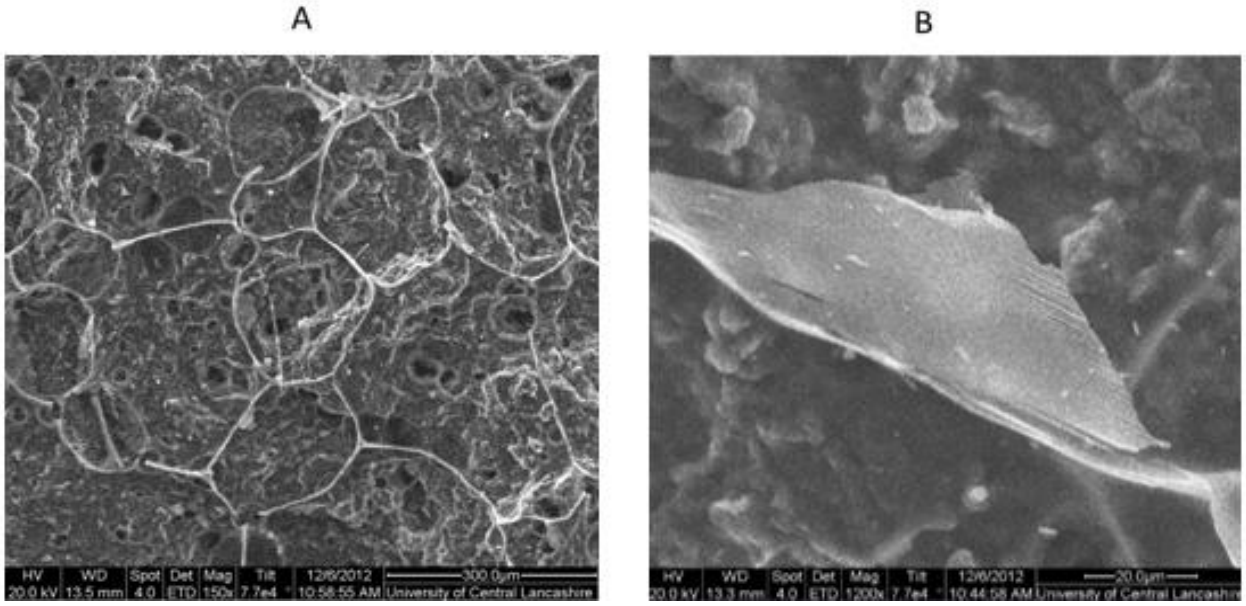

Figure 27 - SEM images of Magnox graphite with D-mannose deposits after the charring stage at A- x150 magnification and B- x1200 magnification

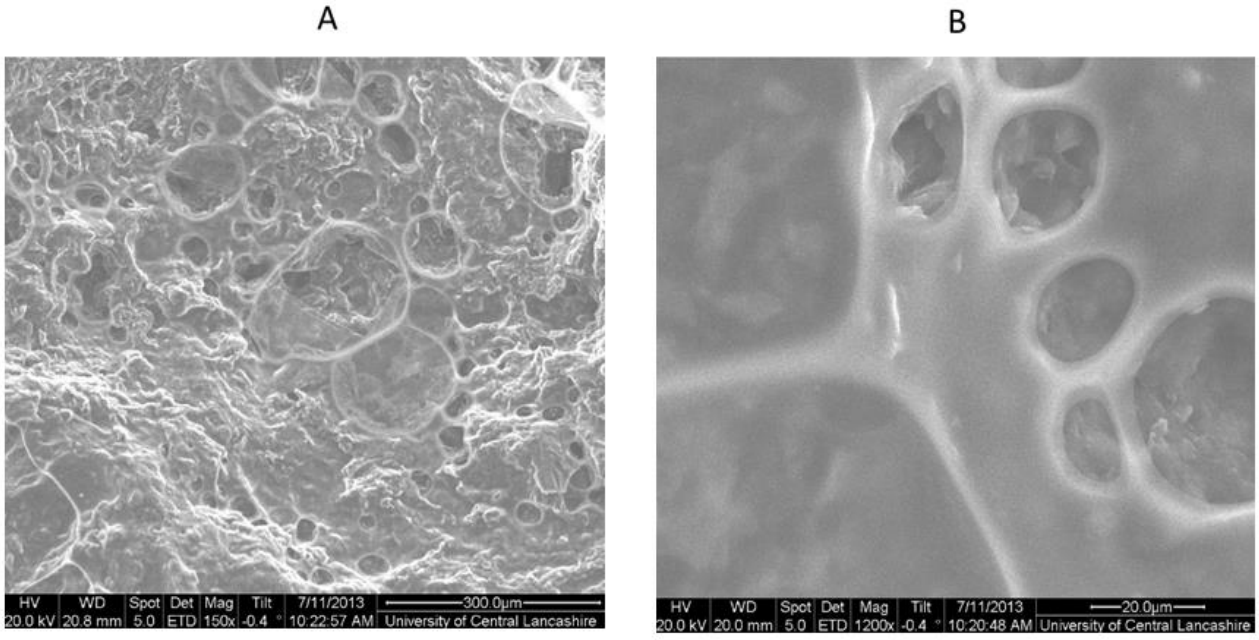

Figure 28 - SEM images of Magnox graphite with D-mannose deposits that have been charred in bulk at A- x150 magnification and B- x1200 magnification

3.4.2 Raman Spectroscopy

Compared to the characteristic three peak arrangement observed from the Raman spectrum of virgin graphite the spectrum of D-mannose was very different (Figure 29). D-mannose is a sugar monomer which is also a stereoisomer of glucose. Like most carbohydrates the spectrum produced from D-mannose exhibits a strong peak at ~3000 cm^{-1} which is attributed to the (O-H) stretching vibration[113]. The series of weak peaks between ~200-500 cm^{-1} are recognised as the deformation of the (C-C-C), (C-C-O) and (C-O) bonds in addition to the twisting motion of the (C-C) bond which make up the main skeletal vibrations of glucose, as does a stronger peak at ~523 cm^{-1}. The vibrational stretching of the (C-C) and (C-O) bonds can be attributed to peaks between ~800 cm^{-1} to ~950 cm^{-1} as can the deformation of the (C-C-H) bond. The weak peaks from ~1000 cm^{-1} to ~1500 cm^{-1} are recognised as the angle bending of the (C-O-H) bonds[114].

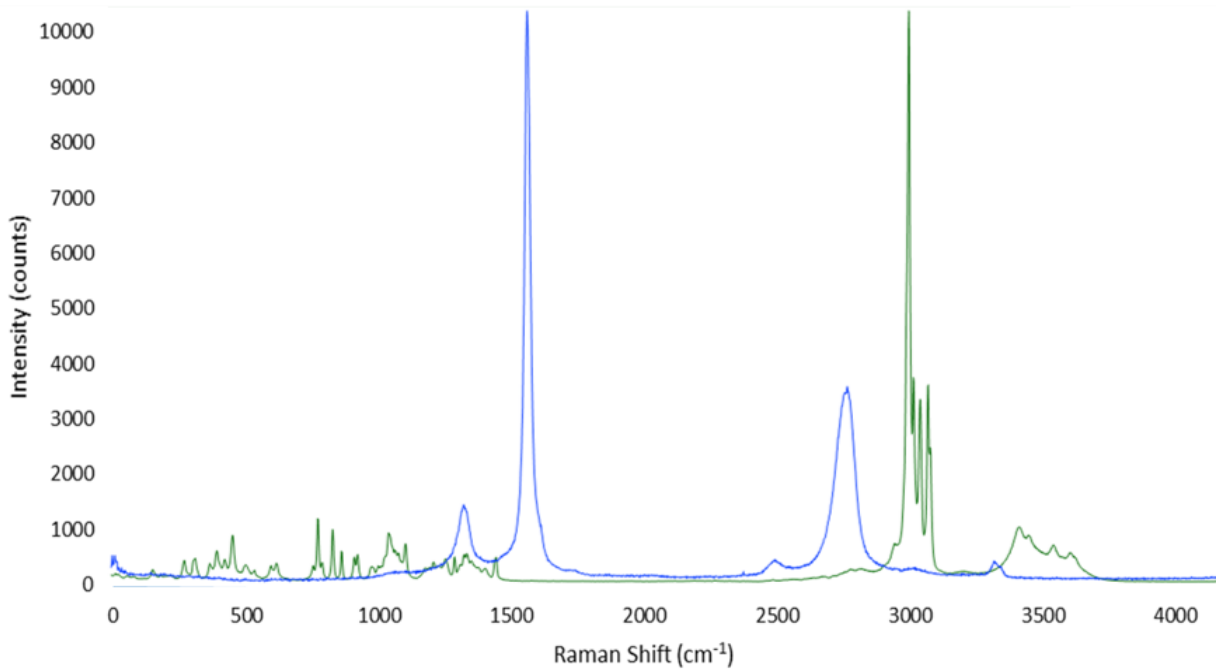

Figure 29 - Raman spectra of virgin Magnox graphite (blue) and D-mannose (green)

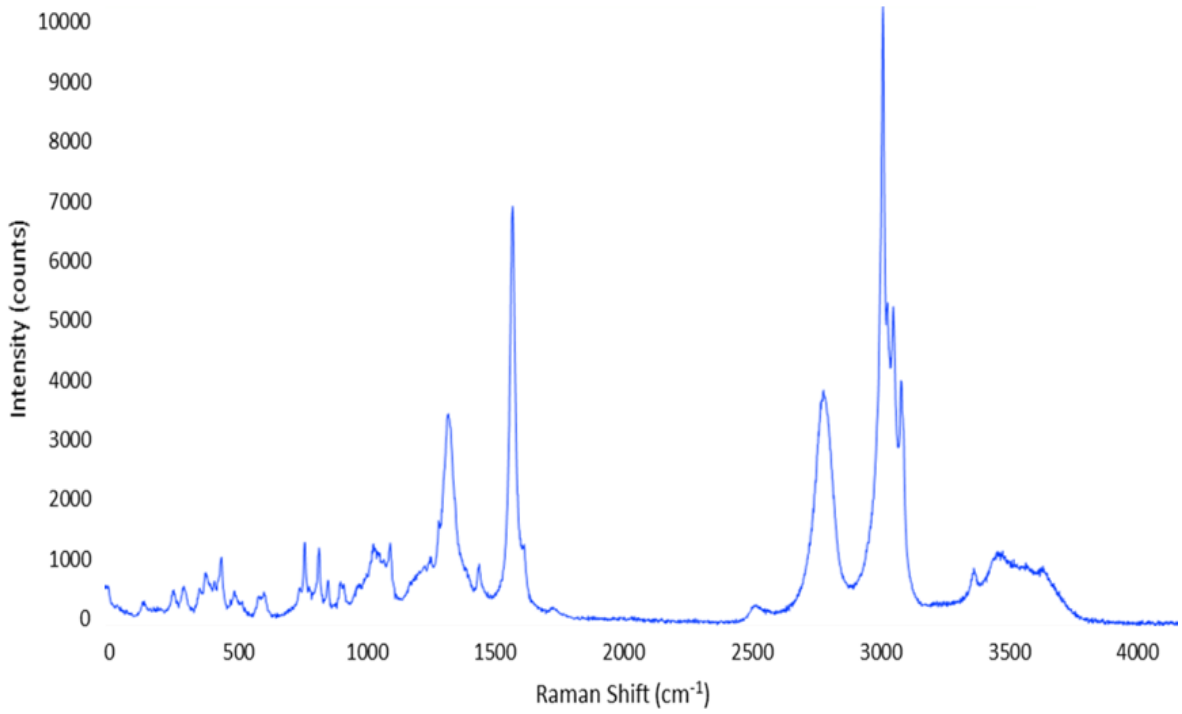

Figure 30 - Raman spectrum of Magnox graphite doped with D-mannose

When analysing a graphite sample with D-mannose doped onto the surface the spectra produced exhibited a combination of peaks from both the spectra of graphite and D-mannose (Figure 30). The strong (O-H) stretch attributed to D-mannose can be observed at ~3000 cm^{-1} as well as the G and D peaks characteristic of graphite which can be observed at ~1580 cm^{-1} and ~1350 cm^{-1} respectively. The D peak appears to be more intense compared to virgin graphite due to the fact that a layer of D-mannose is now present on the graphite surface thus increasing the amount of disorder present. The 2D peak of graphite was also present at ~2700 cm^{-1}. There were also numerous weaker peaks between ~500 cm^{-1} – 1500 cm^{-1} present which are attributed to D-mannose.

Using Raman spectroscopy the change in structure of the substrate on the graphite surface before and after the charring procedure can be determined. The spectrum of graphite with D-mannose deposits after the charring stage was notably different (Figure 31). All of the peaks attributed to the D-mannose structure have been removed. The spectrum that remains was a characteristic three peak arrangement similar to virgin graphite. However the intensity of the D peak at ~1350 cm^{-1} was much stronger than what had been observed previously with virgin graphite. This indicated the presence of a disordered amorphous carbon material was now on the graphite surface[115].

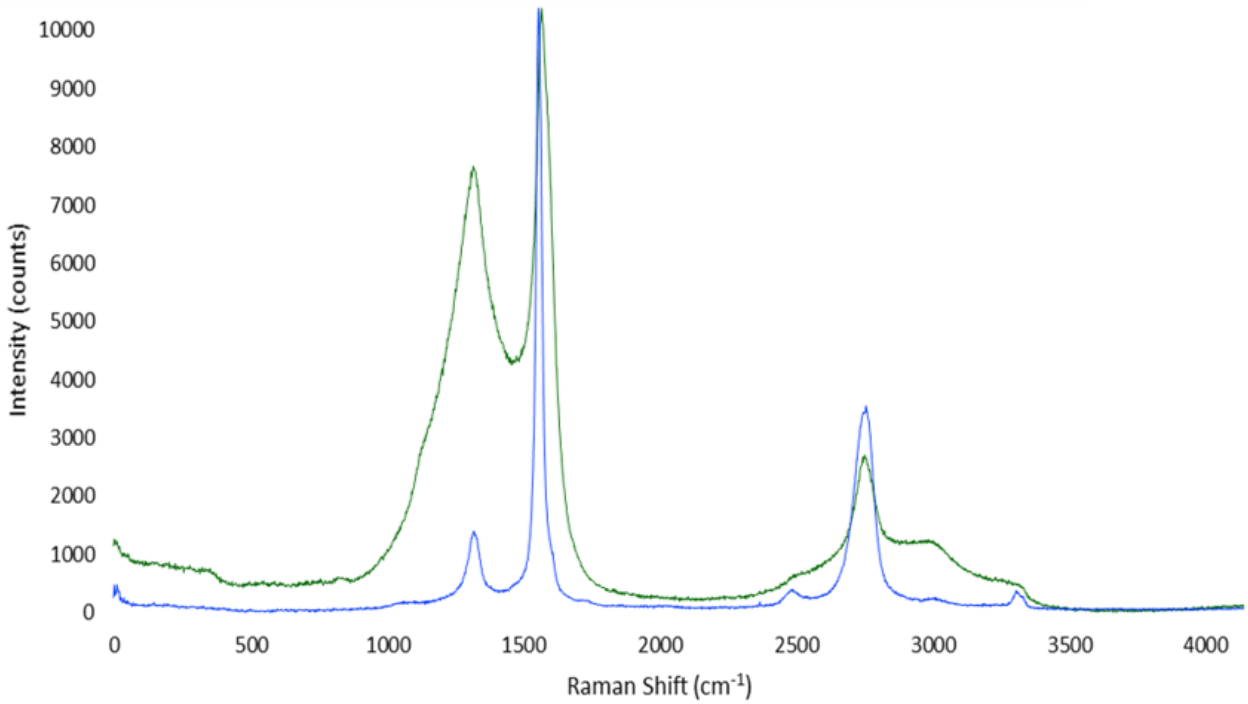

Figure 31 - Raman spectra of virgin Magnox graphite (blue) and graphite with D-mannose carbonaceous char present (green)

3.4.3 Thermal Gravimetric Analysis

The mass loss profile of D-mannose (Figure 32) displayed a degradation process made up of two stages. The sample starts to decompose at ~200°C with a dehydration reaction. This is followed by deep dehydration, cracking and deoxygenation reactions at ~300°C producing acetic acid, formic acid and heterocyclic furan derivatives[116]. By 500°C the decomposition process has stopped leaving a 20% yield of a solid formation known as humin in saccharide chemistry[117].

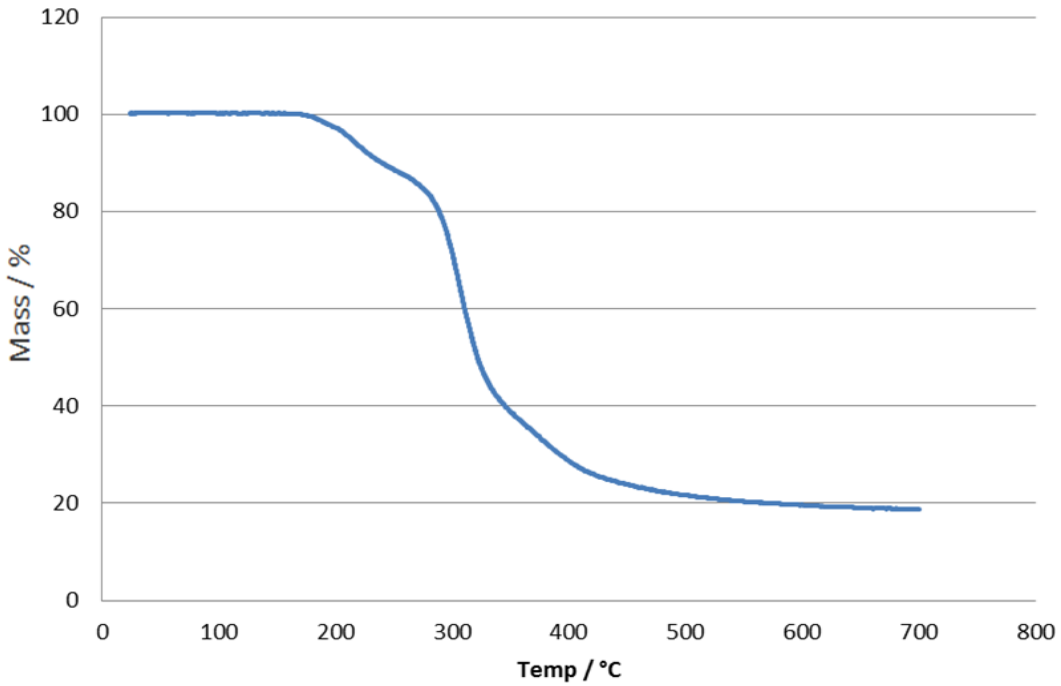

Figure 32 - TGA profile of the charring of D-mannose in nitrogen

Although graphite samples were prepared with a range of precursor amounts only the samples with the largest amount of carbon precursor were analysed initially, in order to determine the success of the doping and charring procedures. During the doping procedure 20 g of graphite were prepared with 2 g of D-mannose. During the charring procedure, which involved a temperature ramp to 700°C in nitrogen, virgin graphite samples did not exhibit a mass loss (Figure 33). This baseline was compared with two repeats of the charring of graphite samples doped with 2 g of D-mannose, which exhibited a change in mass of ~4 and ~10% with mass loss starting at ~200°C and stopping at ~400°C. The differences in mass change indicate that graphite particles have not been uniformly coated.

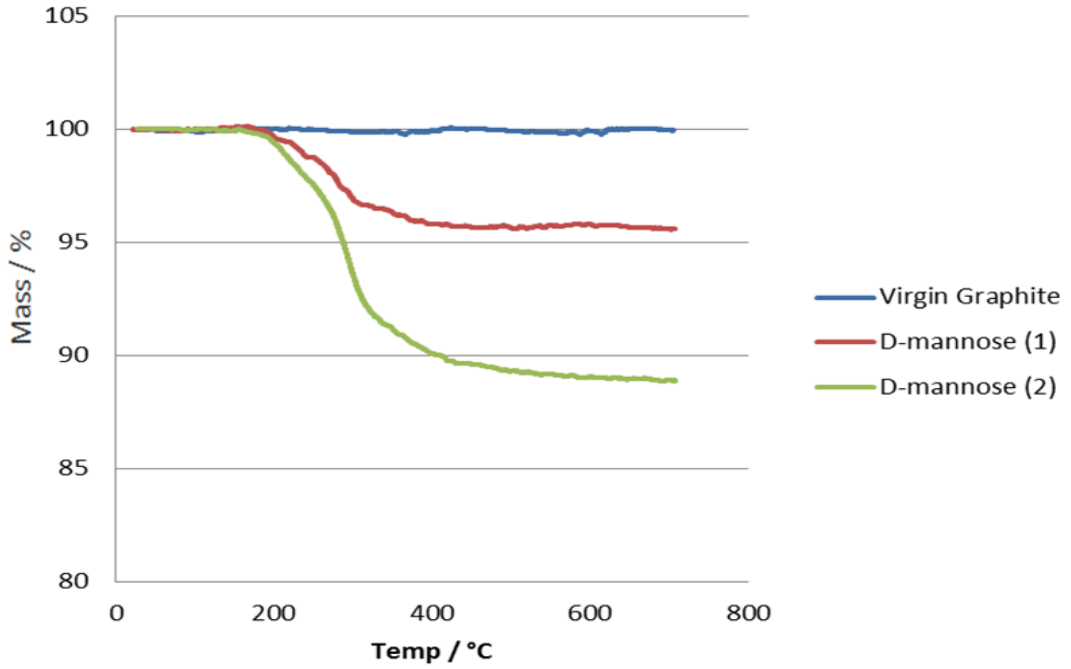

Figure 33 - TGA profile of the charring process in nitrogen of virgin graphite and two repeats of graphite doped with 2 g of D-mannose

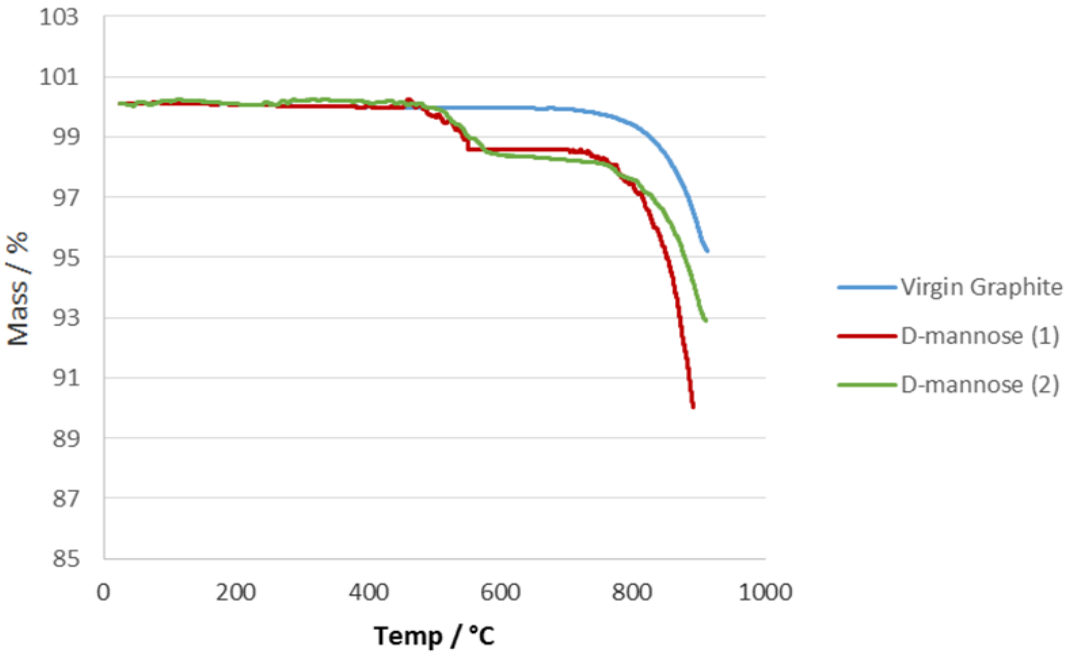

Figure 34 - TGA profile of the oxidation in air of virgin graphite and two repeats of graphite with D-mannose char

In order to assess whether any carbonaceous deposit remained on the graphite surface after the charring procedure, samples were placed into the thermobalance to undergo oxidation in air. The success of the charring stage was determined from the comparison of the oxidation profiles of virgin graphite and the charred samples. Whereas virgin graphite starts to oxidise at ~800°C (Figure 34) a mass loss of ~2% was observed between 500-600°C for graphite samples doped with 2 g of D-mannose post charring process.

As TGA provided evidence of a successful charring using 2 g of D-mannose analysis was carried out on graphite samples doped with 1 g of D-mannose to evaluate any differences in charring between varying precursor amounts.

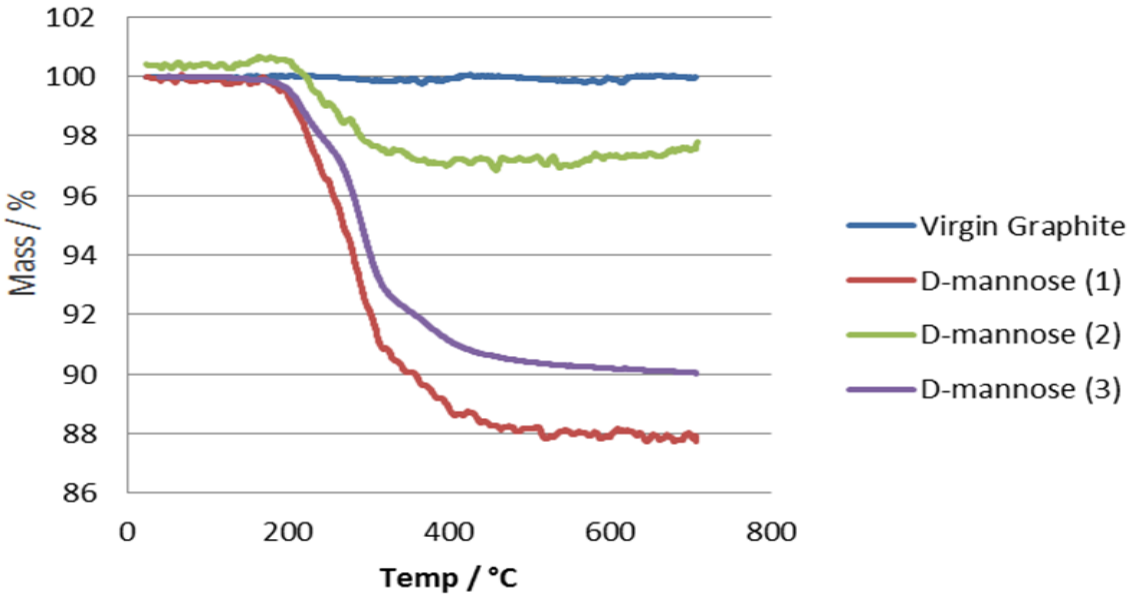

Figure 35 - TGA profile of the charring process in nitrogen of virgin graphite and three repeats of graphite doped with 1 g of D-mannose

As with the 2 g samples a range of mass loss amounts could be observed from the graphite doped with 1 g of D-mannose during the charring process (Figure 35). Mass loss commences at ~200°C and finishes by ~400°C and percentage mass losses of 3, 10 and 12% could be observed between three separate repeats of the charring procedure. These mass losses shown by graphite doped with 1 g of D-mannose fall within a similar range as graphite doped with 2 g of D-mannose. The variance in the mass losses also indicated that the graphite particles were not uniformly doped with precursor material.

Having undergone the charring process graphite samples with 1 g of D-mannose were placed into the thermobalance again but in an air atmosphere in order to assess whether a char was present by oxidising it from the graphite surface (Figure 36).

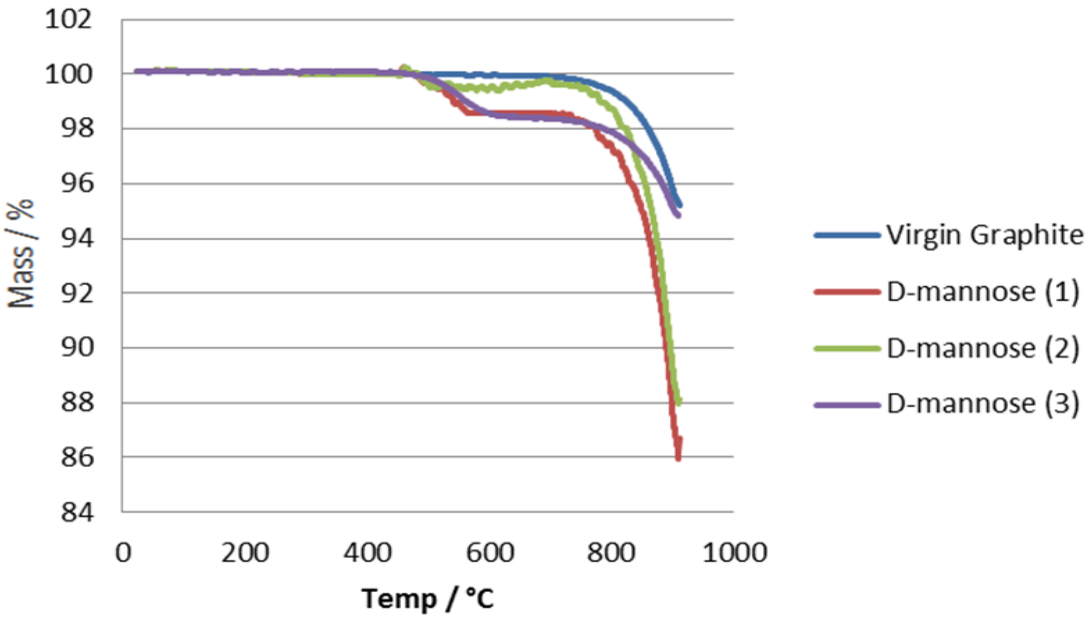

Figure 36 - TGA profile of the oxidation in air of virgin graphite and three repeats of graphite with 1 g of D-mannose char

Similar to the 2 g mannose char samples mass losses of ~1-2% could be observed between 500°C and 600°C attributed to the oxidation of the carbonaceous char present. This was followed by a mass loss at ~800°C attributed to the oxidation of graphite. There was also evidence of particles exhibiting less carbonaceous char than others which also supports the fact that the particles were not uniformly doped with precursor material.

Since it was evident that carbonaceous chars had been successfully produced using D-mannose it was selected to undergo the bulk charring process. Particles were then selected to undergo oxidation in the thermobalance to produce an oxidation profile of the bulk charred samples (Figure 37). A variance in the amount of mass loss between samples was once again observed, ranging between ~1-4%. The onset temperature for the oxidation of the chars appeared to be slightly higher at ~550°C compared with the samples charred using the thermobalance which was ~500°C. For the majority of the samples mass loss appeared to cease at ~600°C similar to previous samples. However one exception was observed whose oxidation appeared to stop at ~700°C. This may have been due to the amount of

carbonaceous char present as this was also the sample which lost the most amount of mass during oxidation.

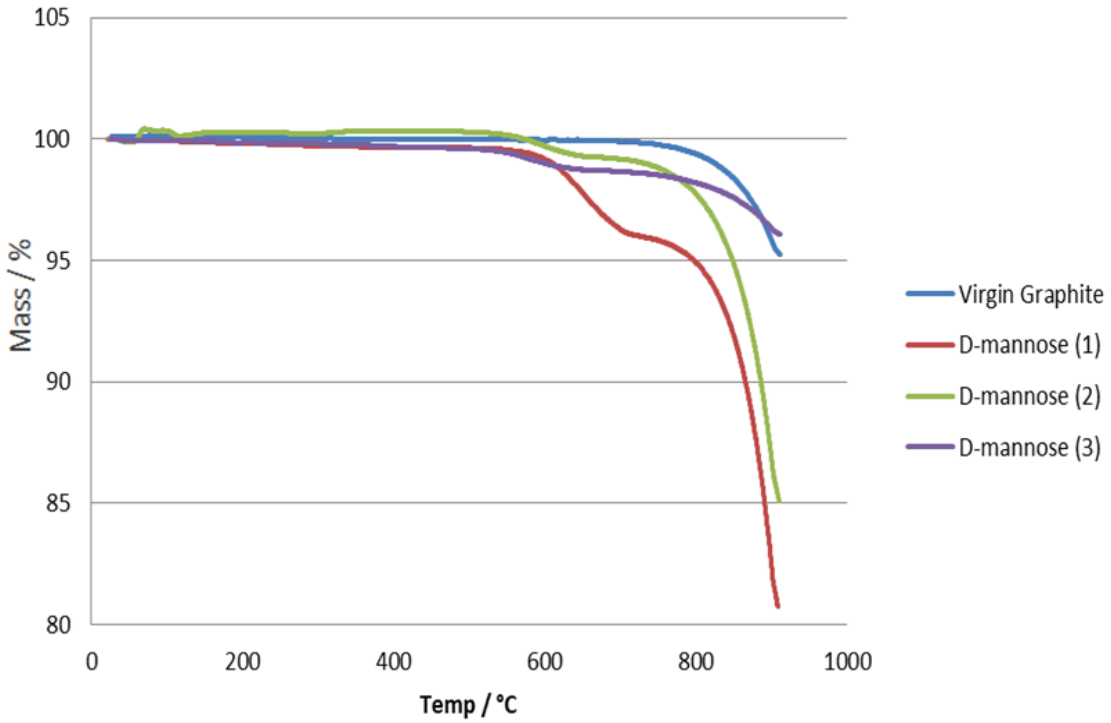

Figure 37 - TGA profile of the oxidation of virgin graphite and three repeats of graphite doped with 2 g of D-mannose which have been charred in bulk

The bulk charring procedure was also carried out on graphite samples with other amounts of carbon precursor. Graphite samples doped with 1 g of D-mannose exhibited a 0.5-1% mass loss between ~550°C and ~600°C indicating that a char deposit had been successfully produced (Figure 38).

Samples that had been prepared with 0.2 g of D-mannose were also selected for bulk charring. However the oxidation profiles showed no difference from the oxidation profile of virgin graphite (Figure 39) meaning that either all of the D-mannose material was lost during the charring stage or that the thermobalance was not sensitive enough to detect such a small amount of deposit.

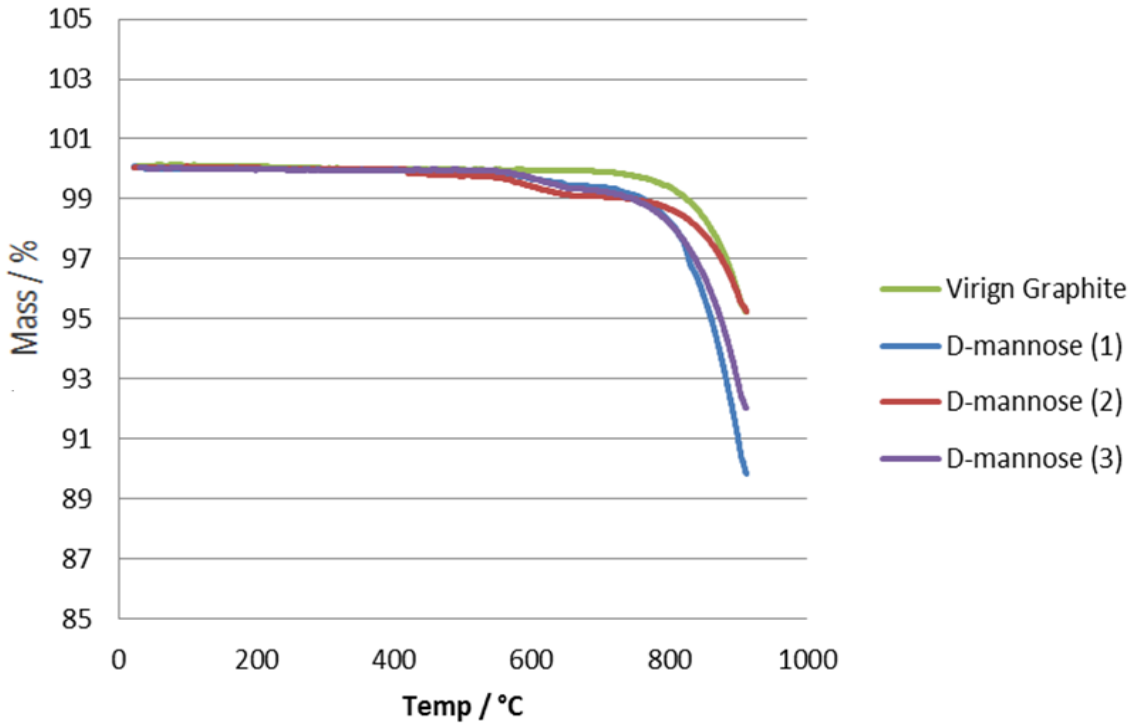

Figure 38 - TGA profile of the oxidation of virgin graphite and three repeats of graphite doped with 1 g of D-mannose which have been charred in bulk

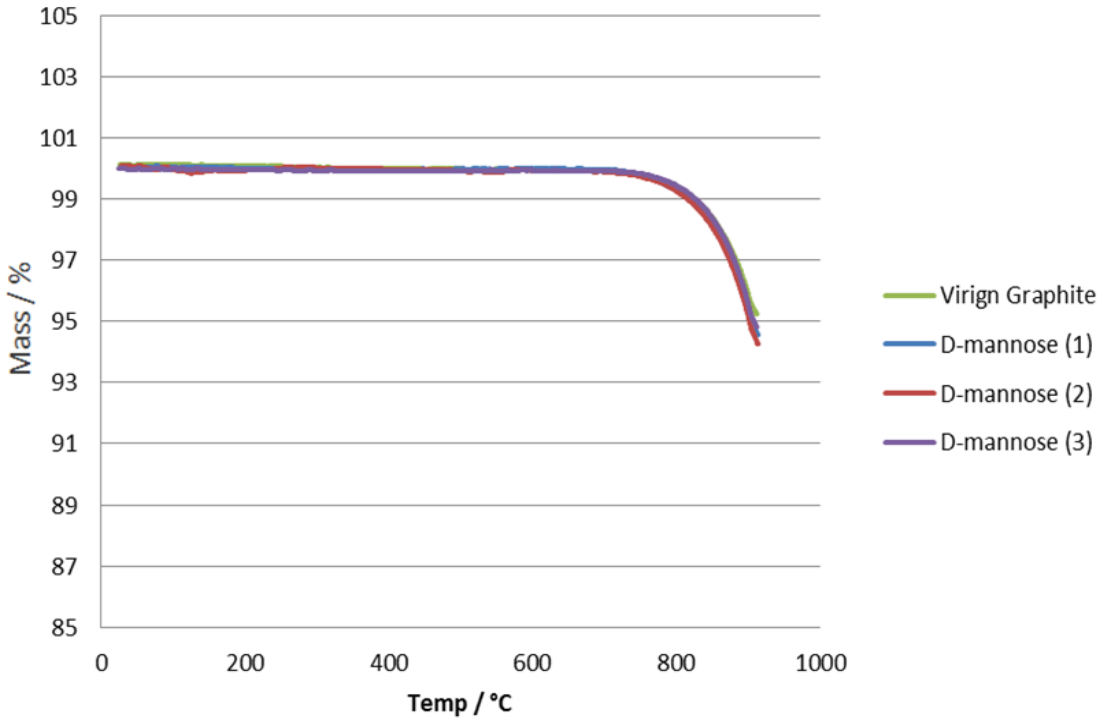

Figure 39 - TGA profile of the oxidation of virgin graphite and three repeats of graphite doped with 0.2 g of D-mannose which have been charred in bulk

3.5 Myristic Acid

3.5.1 Scanning Electron Microscopy

After the doping process using close observation graphite samples doped with myristic acid appeared to glisten in the light. Using SEM analysis a definitive change from virgin graphite could be observed (Figure 40). There were now areas on the graphite surface where there appeared to be large irregular regions of the myristic acid dopant which were darker than the graphite surface.

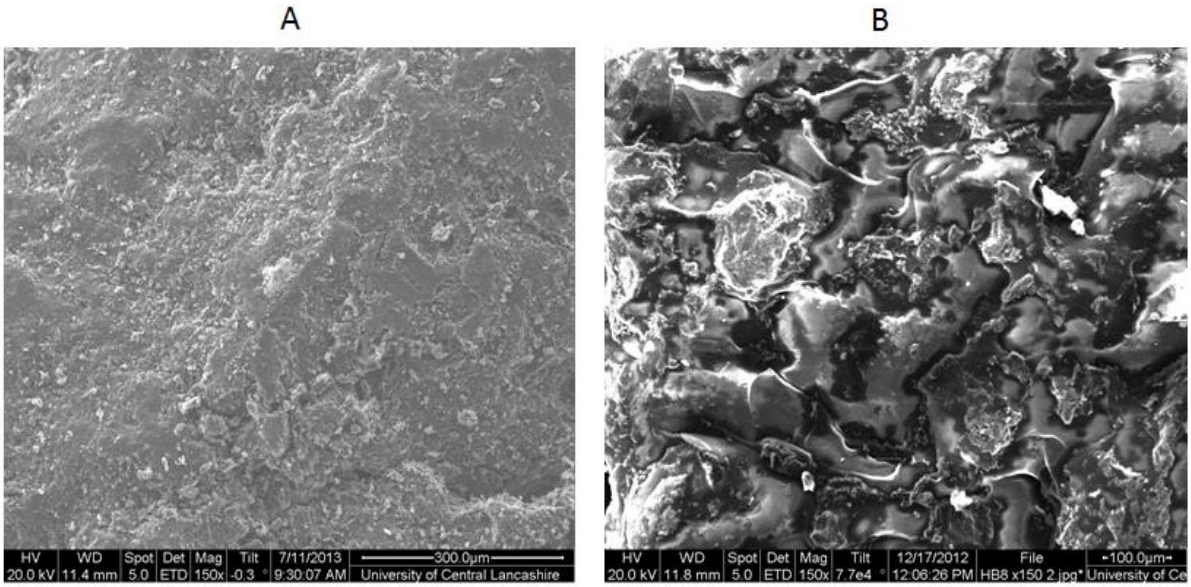

Figure 40 - SEM images at x150 magnification of A- virgin Magnox graphite and B- Magnox graphite doped with myristic acid

After the charring stage the graphite samples no longer appeared to glisten in the light. Upon SEM analysis a significant change was evident. The large dark regions were no longer present leaving a surface indistinguishable from virgin graphite (Figure 41). At an increased magnification the absence of a visible difference from virgin graphite remained. The bulk charring procedure and charring the samples using a thermobalance produced identical results. This could mean that the charring process had completely removed any trace of myristic acid from the graphite samples. However it could also mean that the chars formed were difficult to perceive using SEM and with complementary analysis; Raman Spectroscopy and TGA, a better understanding of the success of this sample deposition would be obtained.

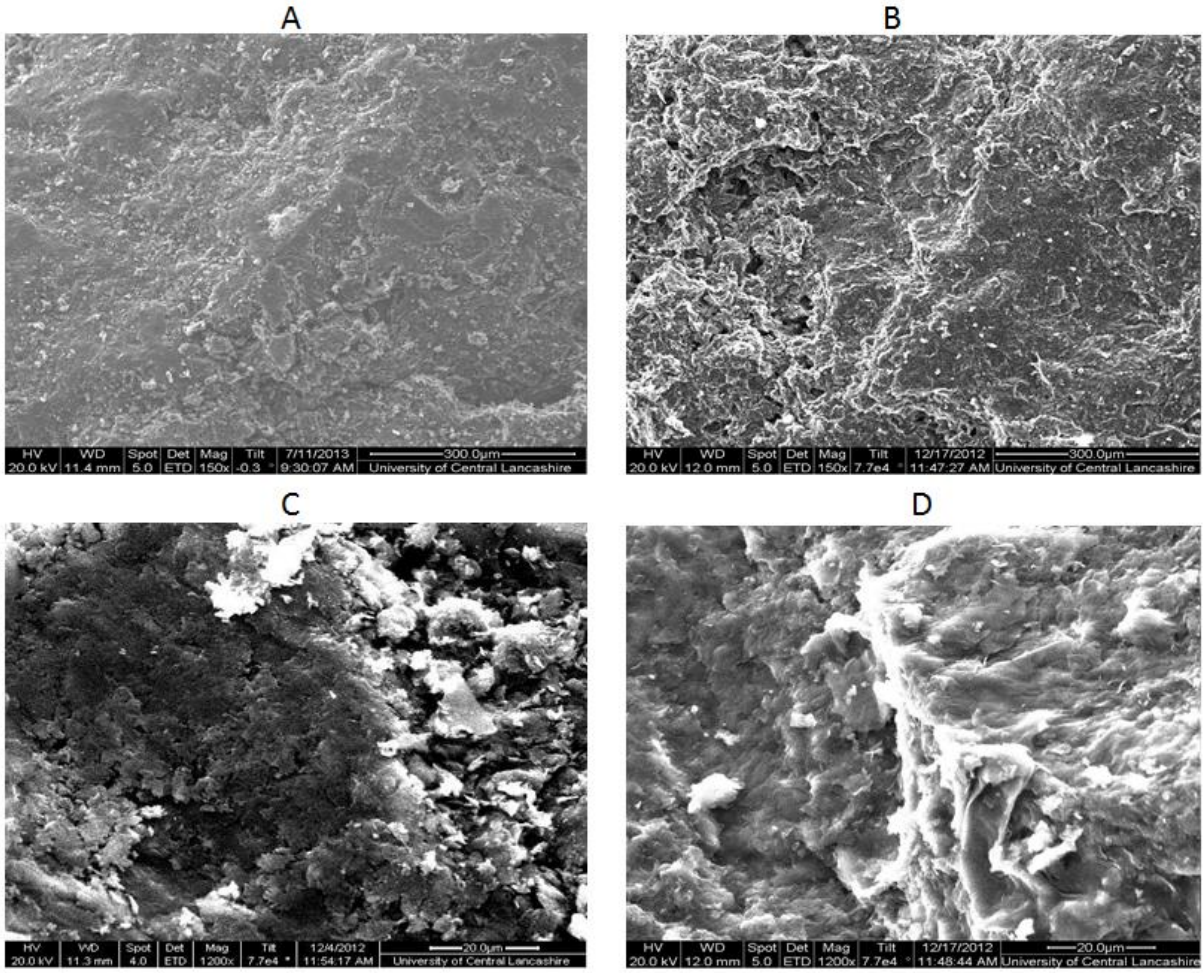

Figure 41 - SEM images of A- virgin Magnox graphite at x150 magnification, B- Magnox graphite with myristic acid deposits after the charring stage at x150 magnification, C- virgin Magnox graphite at x1200 magnification and D- Magnox graphite with myristic acid deposits after the charring stage at x1200 magnification

3.5.2 Raman Spectroscopy

The Raman spectra of fatty acids are predominantly made up of peaks arising from the vibrations of the hydrocarbon chains and were easily distinguishable from the spectrum of graphite (Figure 42). The peaks with the highest intensity were in the region between ~2800 cm^{-1} and ~3000 cm^{-1} and are attributed to the symmetric and asymmetric vibrational stretching of the (C-H) bonds. In the region of ~1400-1500 cm^{-1} the peaks are accredited to the deformation of the (H-C-H) bonds in addition to the peaks between ~1000 cm^{-1} and ~1200 cm^{-1} which are recognised as the stretching of the (C-C) bonds[118].

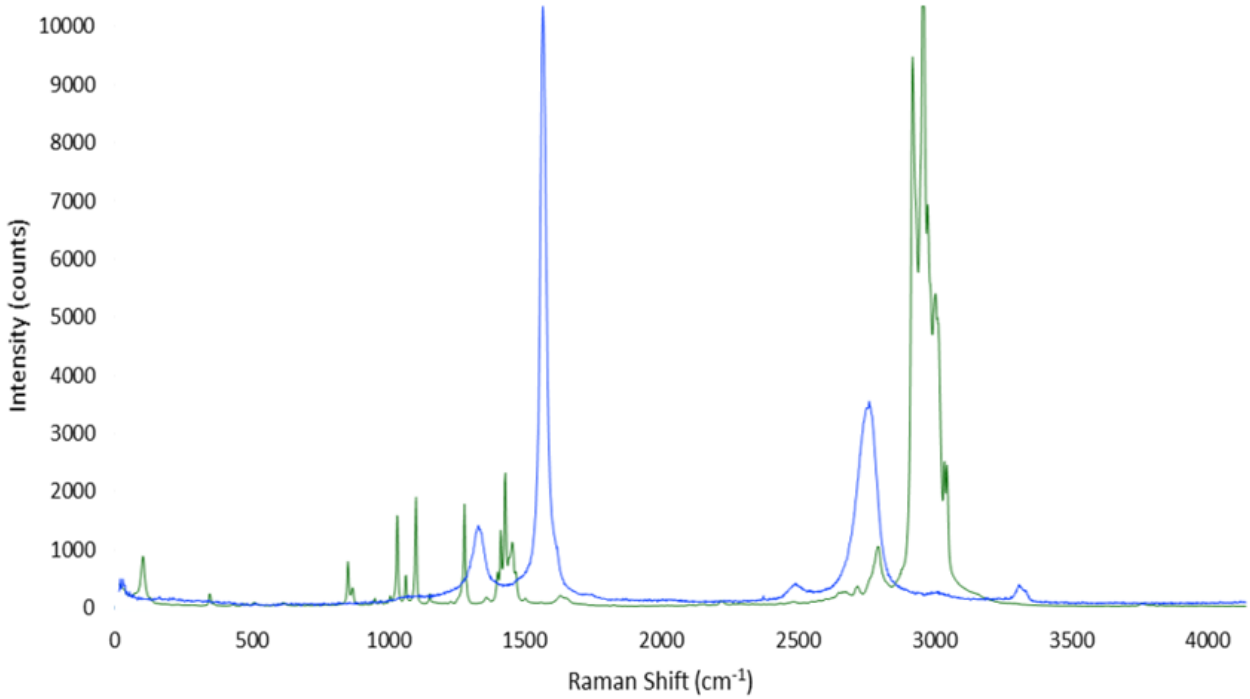

Figure 42 - Raman spectra of virgin Magnox graphite (blue) and myristic acid (green)

In contrast to the graphite samples doped with D-mannose, the Raman spectra from the graphite doped with myristic acid displayed either a spectrum consistent with graphite or a spectrum consistent with myristic acid, depending on the positioning of the laser beam on the graphite particle (Figure 43). From this there is a clear inference that the coating of the myristic acid did not cover the graphite surface as uniformly as the samples with D-mannose.

When analysing graphite samples with myristic acid doped onto the surface having undergone the charring procedure using Raman spectroscopy, a notable change was observed. There were no longer any of the peaks attributed to the spectrum of myristic acid. Only the characteristic three peaks of the graphite sample were observed (Figure 44). Unlike the charred D-mannose samples where the D peak at ~1350 cm^{-1} was a lot more intense, the charred myristic acid samples displayed a D peak with a similar intensity as virgin graphite. As the SEM images also showed no difference from virgin graphite this may indicate that myristic acid does not form a carbonaceous char on the graphite surface and instead was completely removed during the charring process.

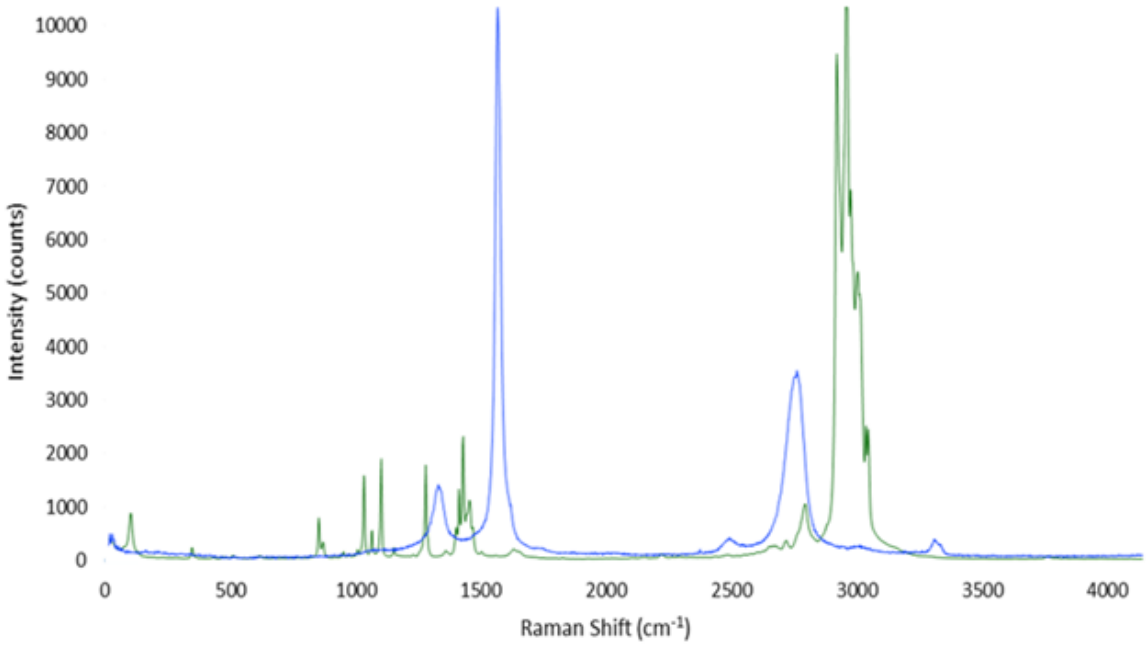

Figure 43 - Raman spectra of Magnox graphite doped with myristic acid exhibiting peaks attributed to graphite (blue) and peaks attributed to myristic acid (green)

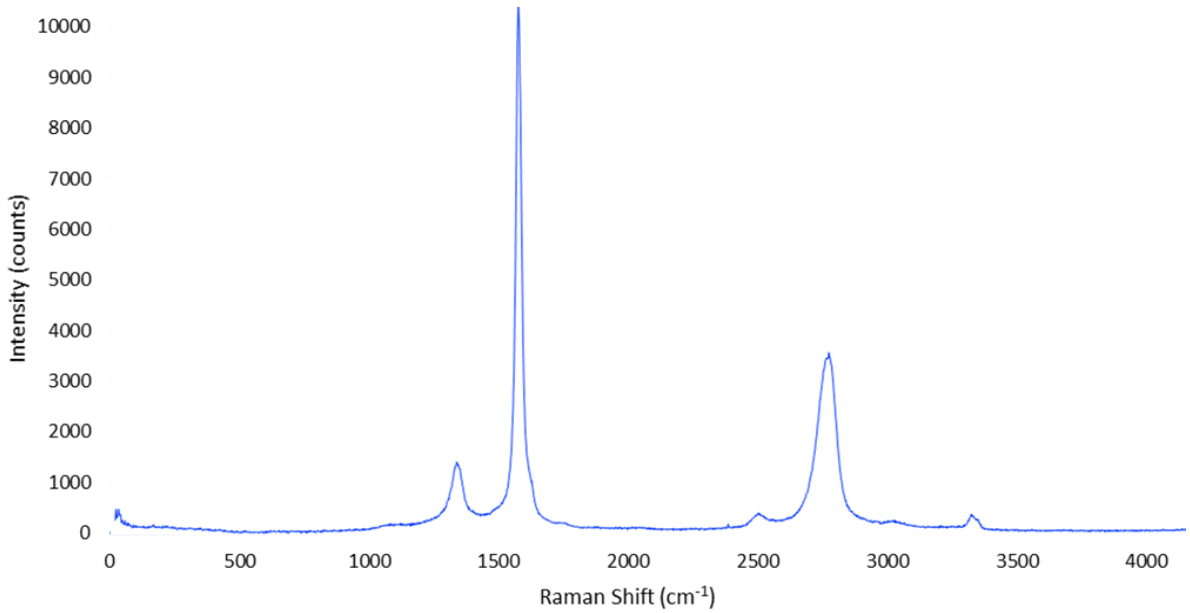

Figure 44 - Raman Spectra of graphite with myristic acid after the charring procedure

3.5.3 Thermal Gravimetric Analysis

The mass loss profile of myristic acid precursor (Figure 45) shows that the myristic acid evaporates completely and there is no remaining residue[119]. The process can be seen to commence at ~160°C with complete loss of sample being achieved by ~260°C. This mass loss profile is common for myristic acid[120] as well as other fatty acids such as stearic acid[121] in addition to various lipids[122].

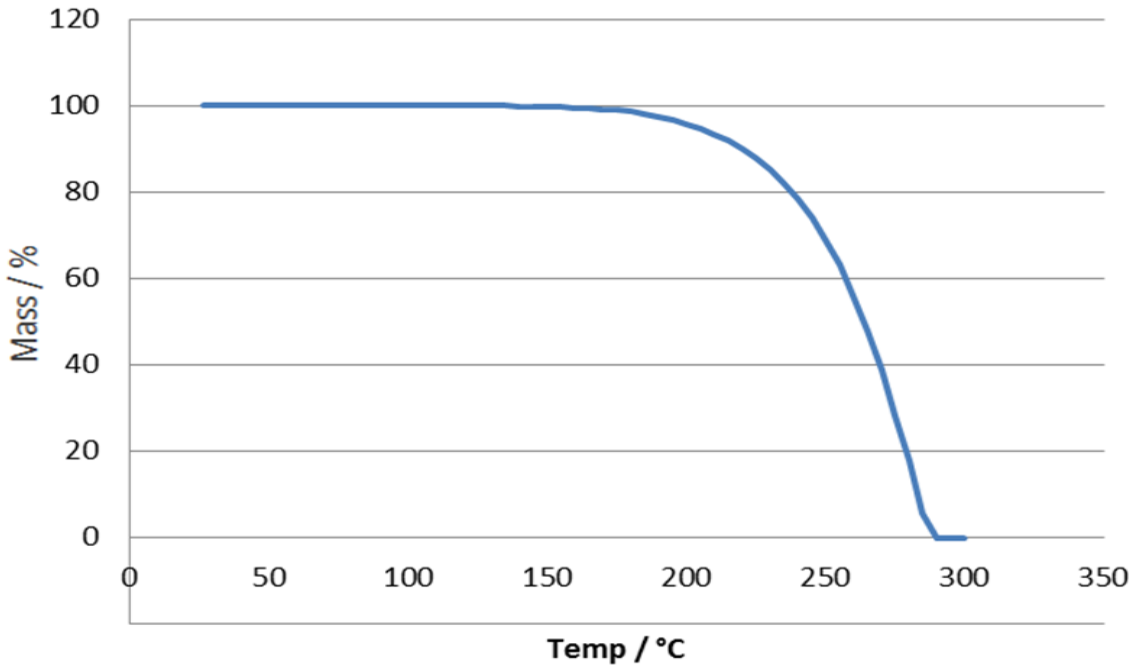

Figure 45 - TGA profile of the charring of myristic acid in nitrogen

It was hoped that doping myristic acid onto the surface of graphite would assist in the decomposition process, resulting in the formation of a deposit prior to the loss to the gas phase through evaporation. Samples with the largest amount of carbon precursor were analysed initially, in order to determine the success of the doping and charring procedures. During the doping procedure 20 g of graphite were prepared with 2 g of myristic acid. During the charring procedure virgin graphite samples did not exhibit a loss in mass. There was a significant difference between virgin graphite compared with two repeats of the charring of graphite samples doped with 2 g of myristic acid (Figure 46). Several repeats showed a mass loss of 6% starting at ~120°C and stopping at ~260°C identical to the oxidation profile of myristic acid. Encouragingly there appeared to be a high level of inter particle reproducibility, unlike the D-mannose coated particles. This indicates that while the coating

may not be uniform, individual particles appear to have been doped with very similar amounts of myristic acid.

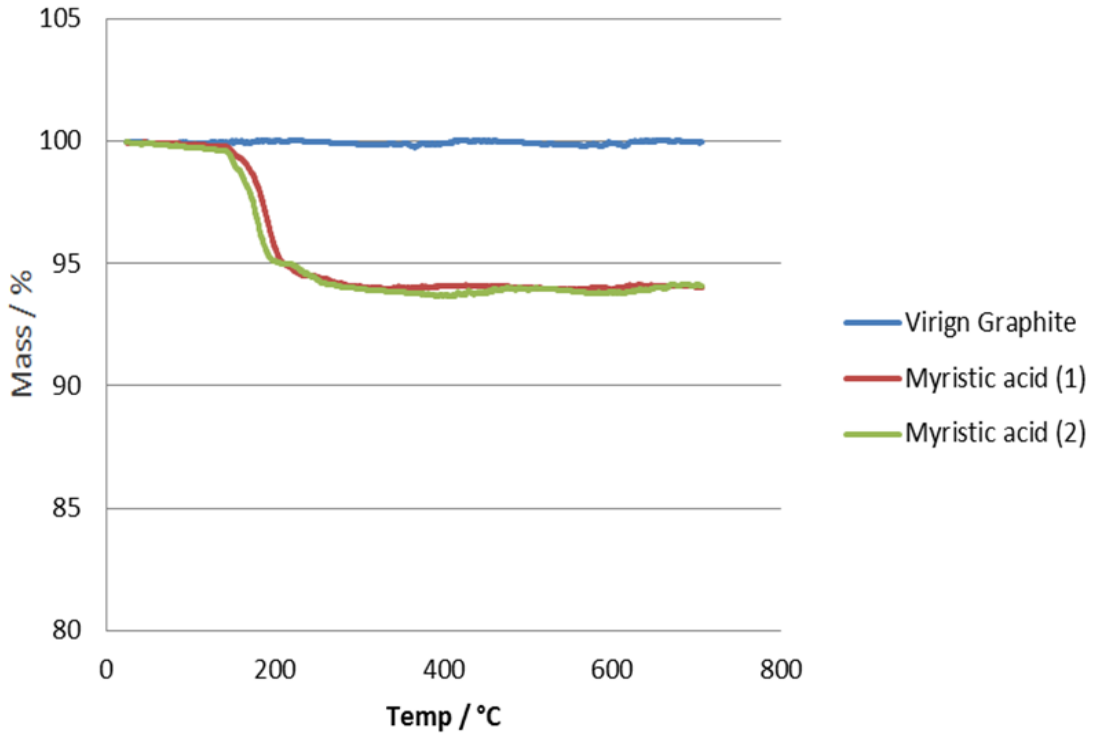

Figure 46 - TGA profile of the charring process in nitrogen of virgin graphite and two repeats of graphite doped with 2 g of myristic acid

To assess whether any carbonaceous deposit remained on the graphite surface after the charring procedure, samples were placed into the thermobalance to undergo oxidation in air. The oxidation profiles of graphite doped with 2 g of myristic acid after the charring process were identical to the profile for virgin graphite (Figure 47). The only observable mass change occurs after ~800°C, the temperature that graphite starts to oxidise at. This may indicate that all of the myristic acid material is lost during the charring process and a carbonaceous char was not formed.

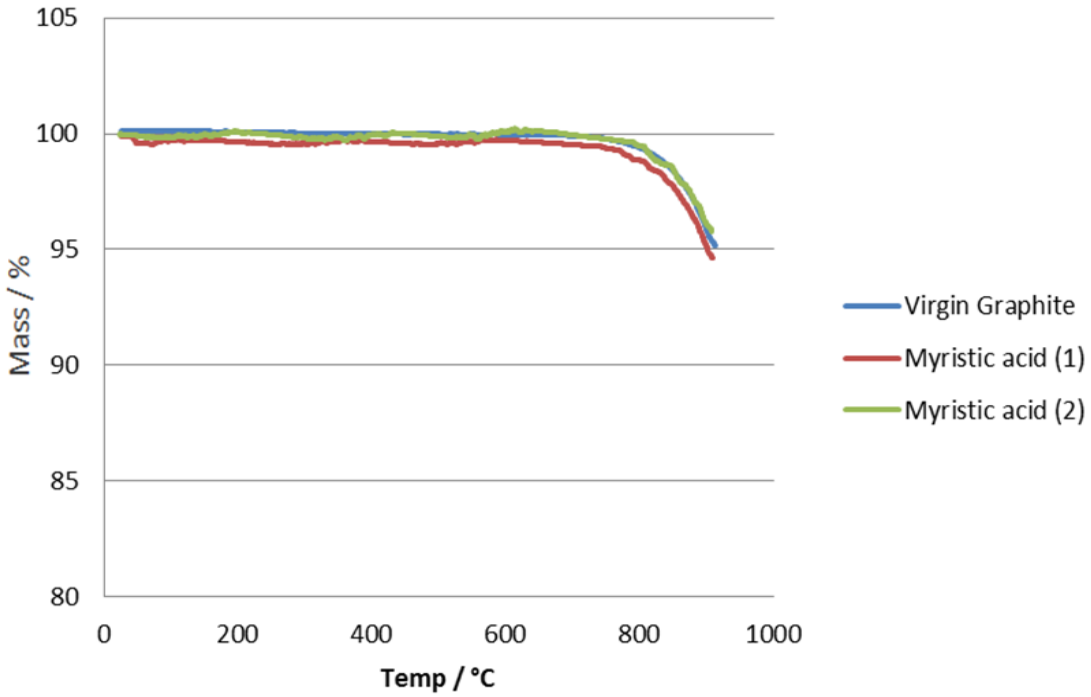

Figure 47 - TGA profile of the oxidation in air of virgin graphite and two repeats of graphite with myristic acid char

Despite the results from the thermobalance chars graphite samples doped with 2 g of myristic acid were selected to undergo charring in bulk to determine whether the unsuccessful charring was method specific. The oxidation profiles of the samples having undergone the bulk charring technique were similar to virgin graphite with mass loss occurring only after the sample had reached ~800°C (Figure 48). However they did exhibit a greater mass loss compared to virgin graphite. The differences in the mass lost by the samples could be due to the deposition and bulk charring procedure which may have altered the surface area or structure of the samples or it may be due to the variable particle size used. The results show that myristic acid does not form a carbonaceous char on the graphite surface from either charring technique used.

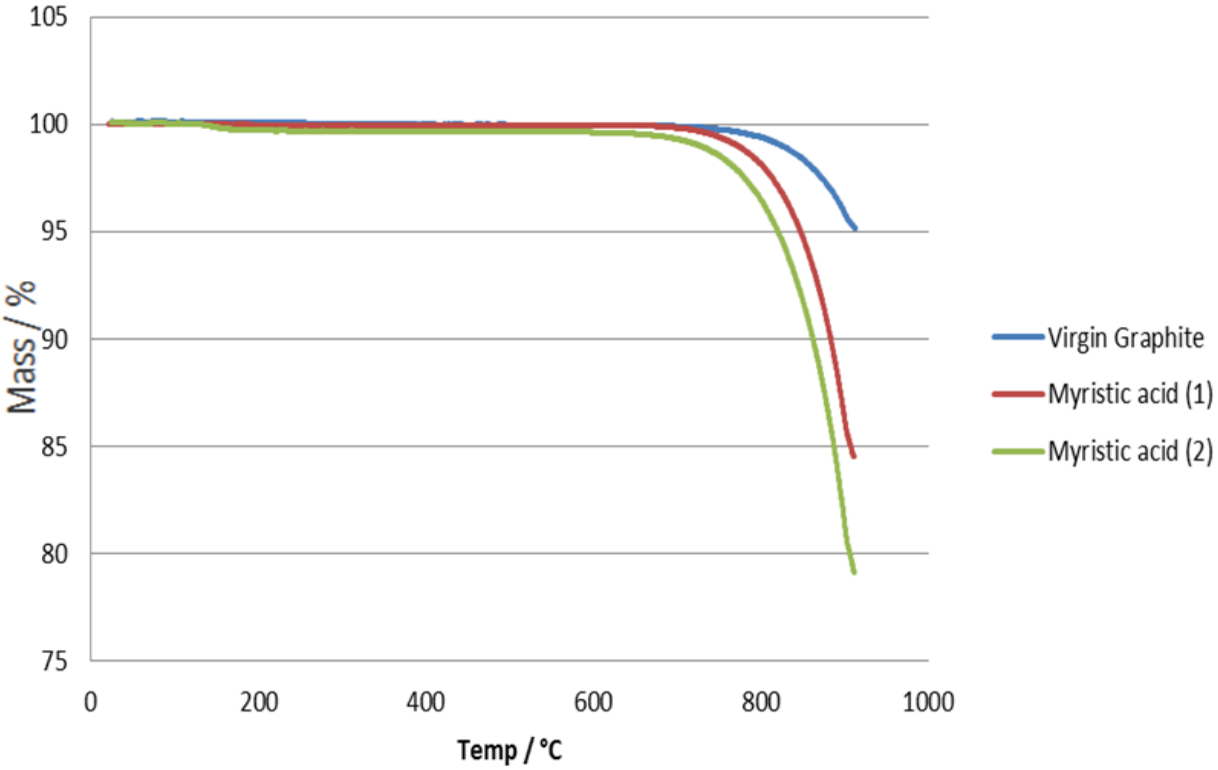

Figure 48 - TGA profile of the oxidation of virgin graphite and two repeats of graphite doped with 2 g of myristic acid which have been charred in bulk

3.6 Naphthalene

3.6.1 Scanning Electron Microscopy

After the doping process close observation of graphite doped with naphthalene showed that they appeared to glisten slightly in the light. Using SEM analysis a visible change from virgin graphite could be observed (Figure 49). Clusters of naphthalene crystals could now be observed over the entirety of the graphite surface. However they were much less abundant than the doped D-mannose samples and more difficult to observe (Figure 26).

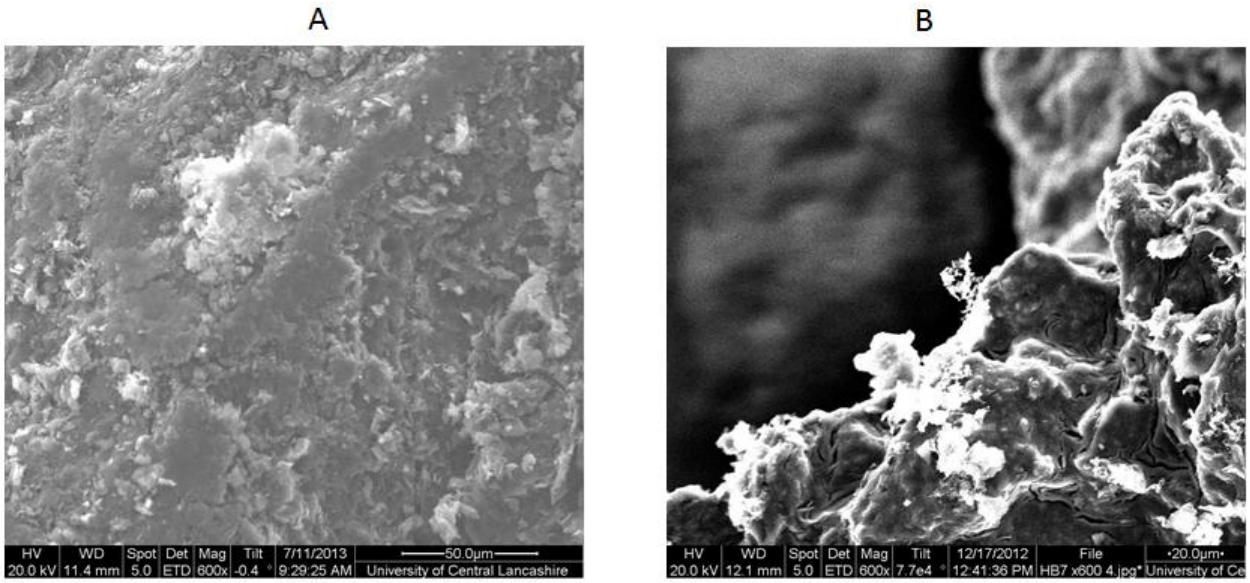

Figure 49 - SEM images at x600 magnification of A- virgin Magnox graphite and B- Magnox graphite doped with naphthalene

After the charring stage the graphite samples no longer appeared to glisten in the light. The samples were then analysed using SEM to determine if a carbonaceous deposit could be observed. However the electron micrographs (Figure 50) proved to be inconclusive as there was very little difference between the virgin graphite and the charred samples. This could mean that the charring process had completely removed any trace of naphthalene from the graphite samples. However it could also mean that the chars formed were difficult to perceive using SEM and with complementary analysis; Raman Spectroscopy and TGA, a better understanding of the success of this sample deposition would be obtained.

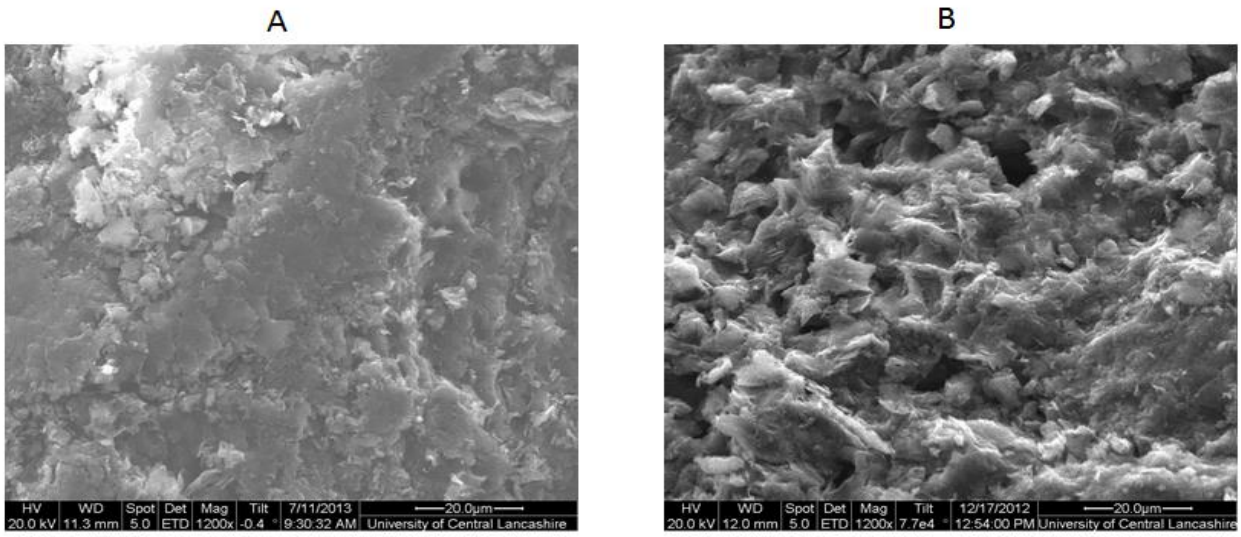

Figure 50 - SEM images at x1200 magnification of A- virgin Magnox graphite and B- Magnox graphite with naphthalene deposits after the charring stage

3.6.2 Raman Spectroscopy

Naphthalene is a polycyclic aromatic hydrocarbon whose Raman spectrum exhibits very intense peaks due to the symmetry present in the sample, and it is easily distinguishable from the spectrum of graphite (Figure 51).

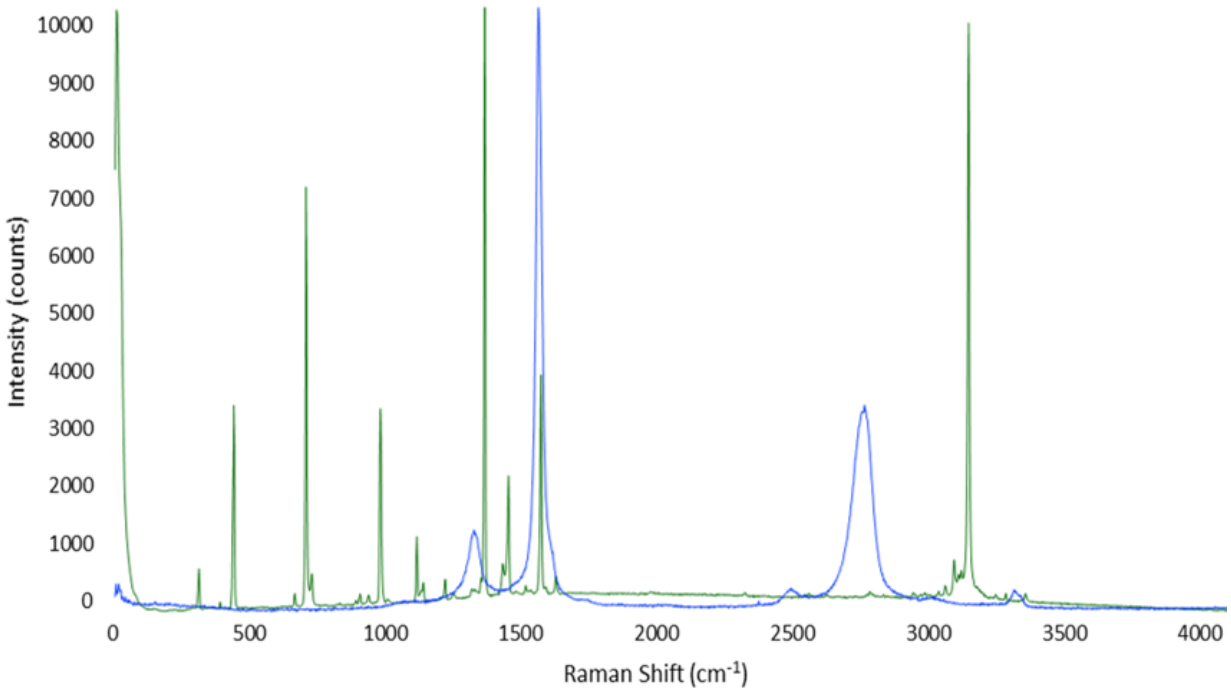

Figure 51 - Raman spectra of virgin Magnox graphite (blue) and naphthalene (green)

One of the prominent peaks at ~3000 cm^{-1} is attributed to the stretching of the (C-H) bonds. At ~1600 cm^{-1} a weak peak attributed to the stretching of the (C=C) bonds can be observed. This stretching mode also produces intense peaks at ~1400 cm^{-1} along with contributions from the bending of the C-H bonds. Numerous peaks between ~1000 cm^{-1} and ~1500 cm^{-1} are recognised as stretching of the (C-C) bonds and bending of the (C-H) bonds whereas peaks observed at ~500 cm^{-1} and ~750 cm^{-1} are accredited to the bending of the (C-C-C) bonds and the radial breathing mode respectively[123].

The Raman spectra for graphite samples with naphthalene doped onto the graphite surface exhibited either a characteristic graphite spectrum or a naphthalene spectrum (Figure 52). This was similar to the spectra observed from graphite doped with myristic acid but differed from the graphite samples doped with D-mannose because a spectrum was produced with a combination of peaks from graphite and D-mannose. By analysing the SEM images it seemed samples with naphthalene did not cover the graphite surface as uniformly as the D-mannose samples.

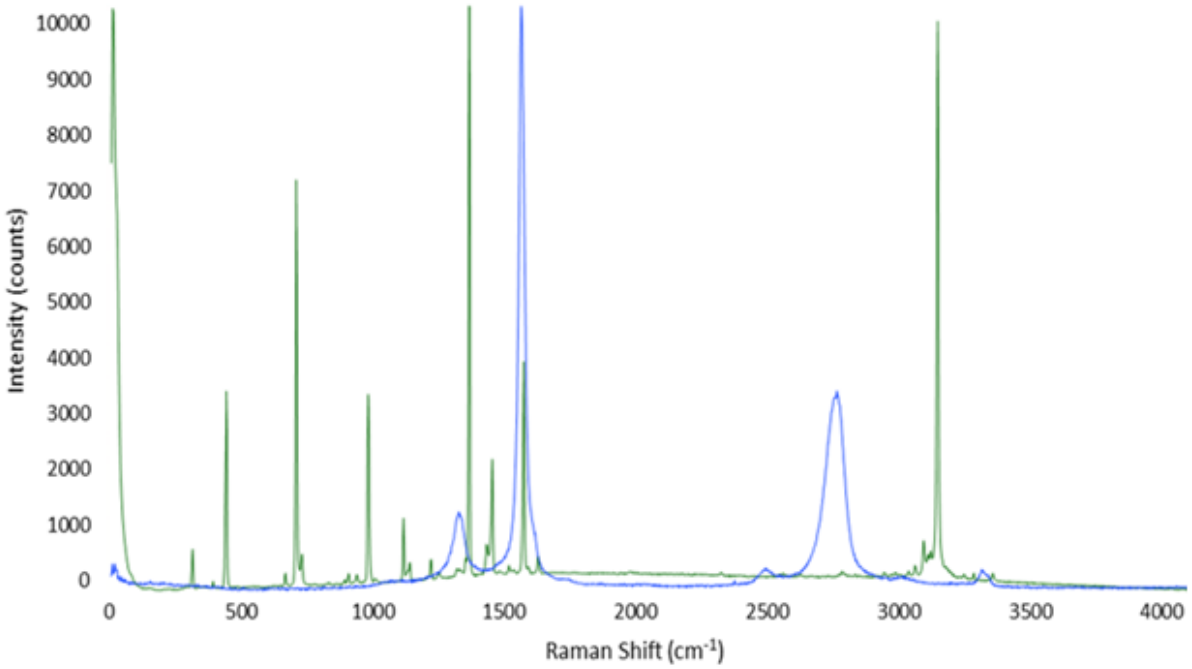

Figure 52 - Raman spectra of Magnox graphite doped with naphthalene exhibiting peaks attributed to graphite (blue) and peaks attributed to naphthalene (green)

When analysing graphite samples with naphthalene doped onto the surface having undergone the charring procedure using Raman spectroscopy, a notable change was observed. There were no longer any of the peaks attributed to the spectrum of naphthalene. Only the characteristic three peaks of the graphite sample were observed (Figure 53). Contradictory to the charred D-mannose samples but similar to the charred myristic acid samples the D peak at ~1350 cm^{-1} did not exhibit a higher intensity than virgin graphite. As the SEM images also displayed no difference from virgin graphite this may indicate that naphthalene did not form a carbonaceous char on the graphite surface and instead was completely removed during the charring process.

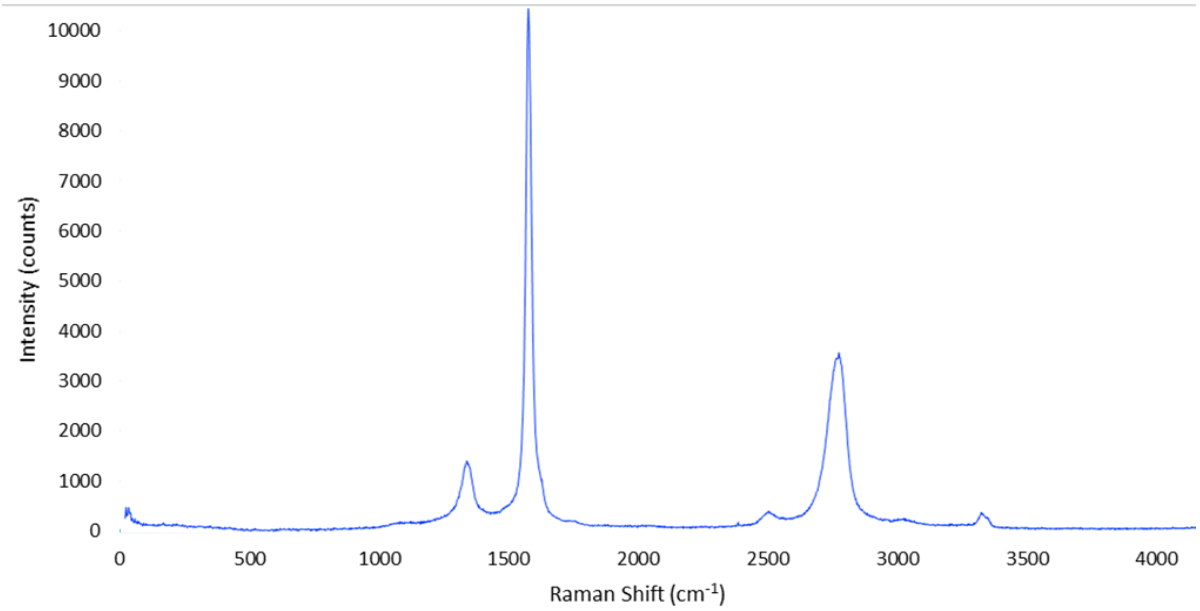

Figure 53 - Raman Spectra of graphite with naphthalene after the charring procedure

3.6.3 Thermal Gravimetric Analysis

The mass loss profile of naphthalene precursor (Figure 54) shows that naphthalene evaporates completely and there is no remaining residue. The process can be seen to commence at ~70°C with complete loss of sample being achieved by ~180°C. This mass loss profile is common for naphthalene[124].

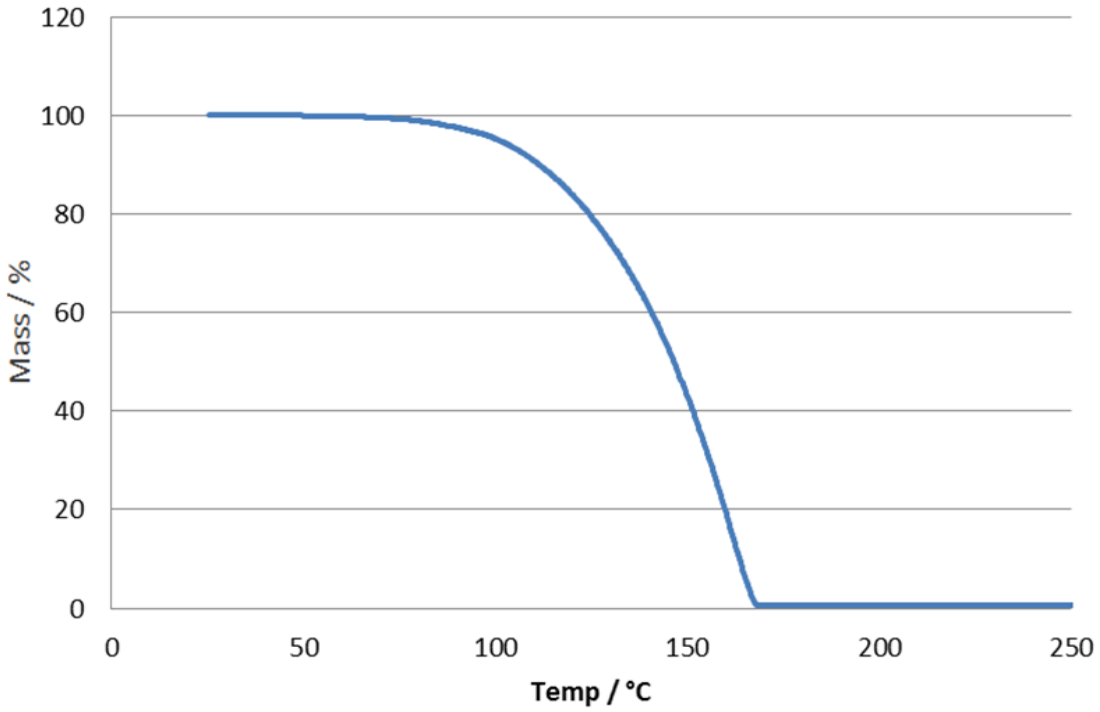

Figure 54 - TGA profile of the charring of naphthalene in nitrogen

It was hoped that doping naphthalene onto the surface of graphite would assist in the decomposition process, resulting in the formation of a deposit prior to the loss to the gas phase through evaporation. Samples with the largest amount of carbon precursor, 2 g of naphthalene, were analysed. During the charring procedure virgin graphite samples did not exhibit a mass loss. There was no significant difference between virgin graphite compared with two repeats of the charring of graphite samples doped with 2 g of naphthalene (Figure 55). This was interesting because a mass loss was observed during the charring stage of other carbon precursors used. The oxidation profiles of graphite doped with 2 g of naphthalene after the charring process were identical to the profile for virgin graphite (Figure 56). This also indicated that there was no naphthalene material on the graphite surface. The only observable change in mass occurred after ~800°C, the temperature that graphite starts to oxidise at.

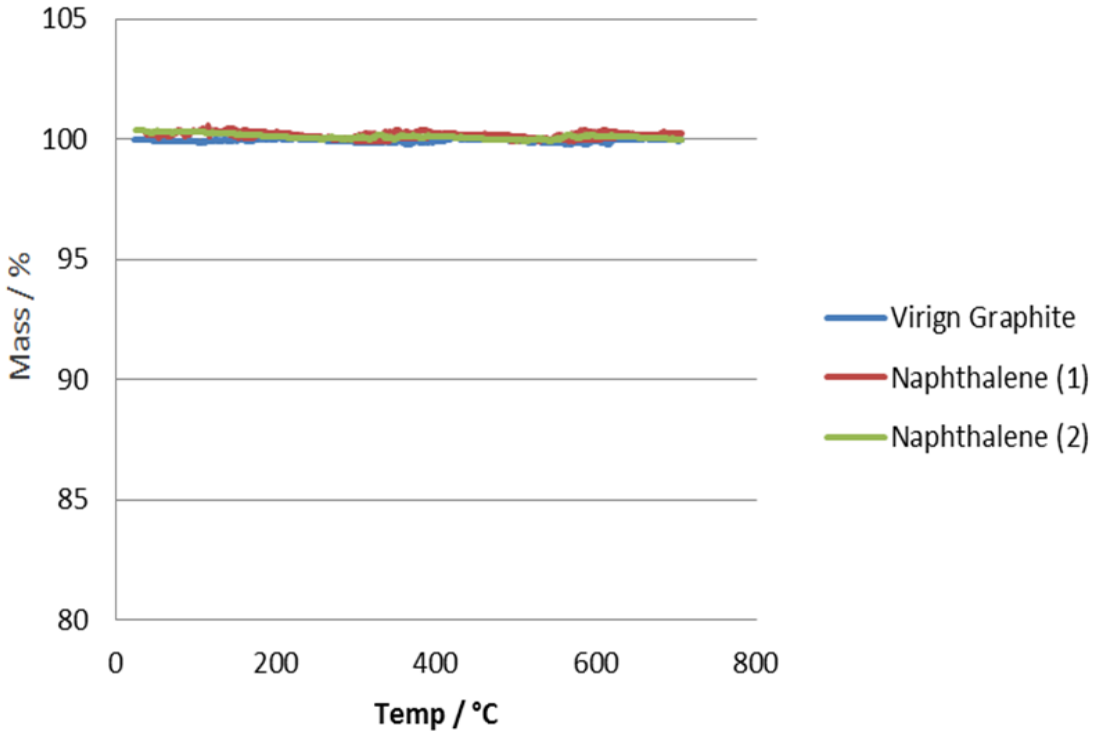

Figure 55 - TGA profile of the charring process in nitrogen of virgin graphite and two repeats of graphite doped with 2 g of naphthalene

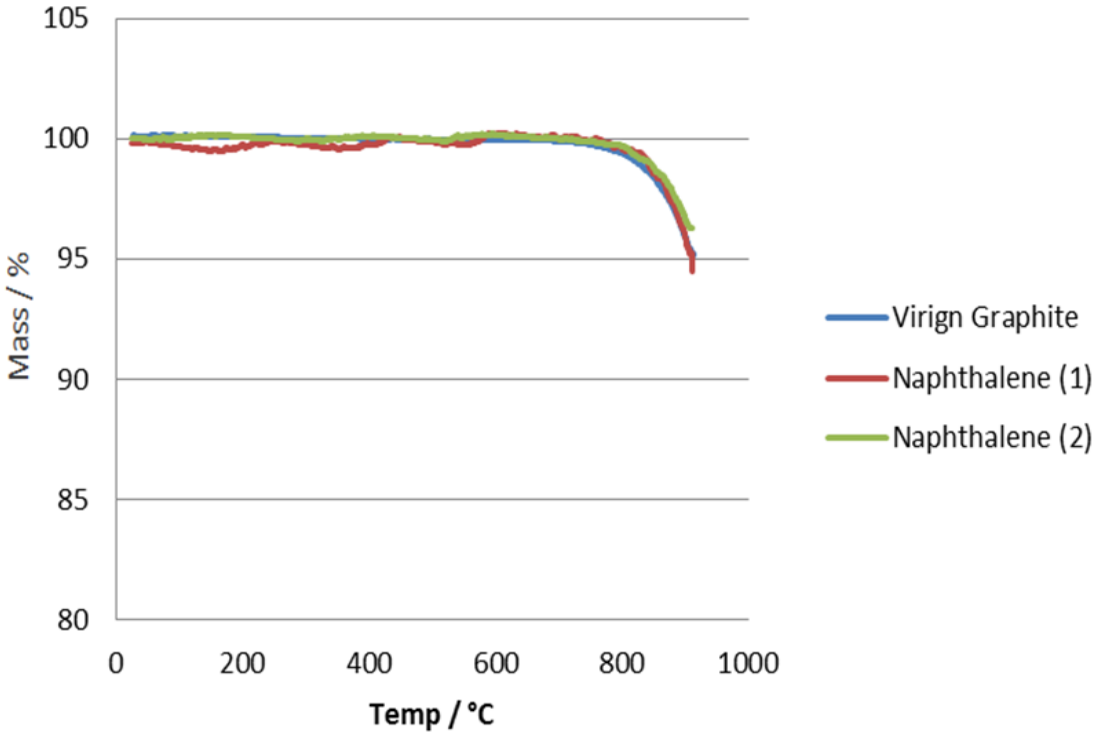

Figure 56 - TGA profile of the oxidation in air of virgin graphite and two repeats of graphite with naphthalene char

The mass loss profiles indicate that there was no naphthalene present on the graphite samples, even before the charring procedure; however SEM and Raman analysis showed that it was present. This shows that the doping process was very ineffective and either, only a certain amount of particles had naphthalene deposited onto them or perhaps there is such a minute amount of naphthalene present that the thermobalance could not detect the mass loss. Despite the results from the thermobalance chars graphite samples doped with 2 g of naphthalene were selected to undergo charring in bulk to determine whether a successful char could be formed using this method. The oxidation profiles of the samples having undergone the bulk charring technique did not show any mass loss until the temperature where graphite started to oxidise at ~800°C (Figure 57). However they did exhibit more mass loss compared to virgin graphite. The differences in the mass lost by the samples could be due to the deposition and bulk charring procedure which may have altered the surface area or structure of the samples or it may be due to the variable particle size used. The results show that naphthalene does not form a carbonaceous char on the graphite surface from either charring technique used.

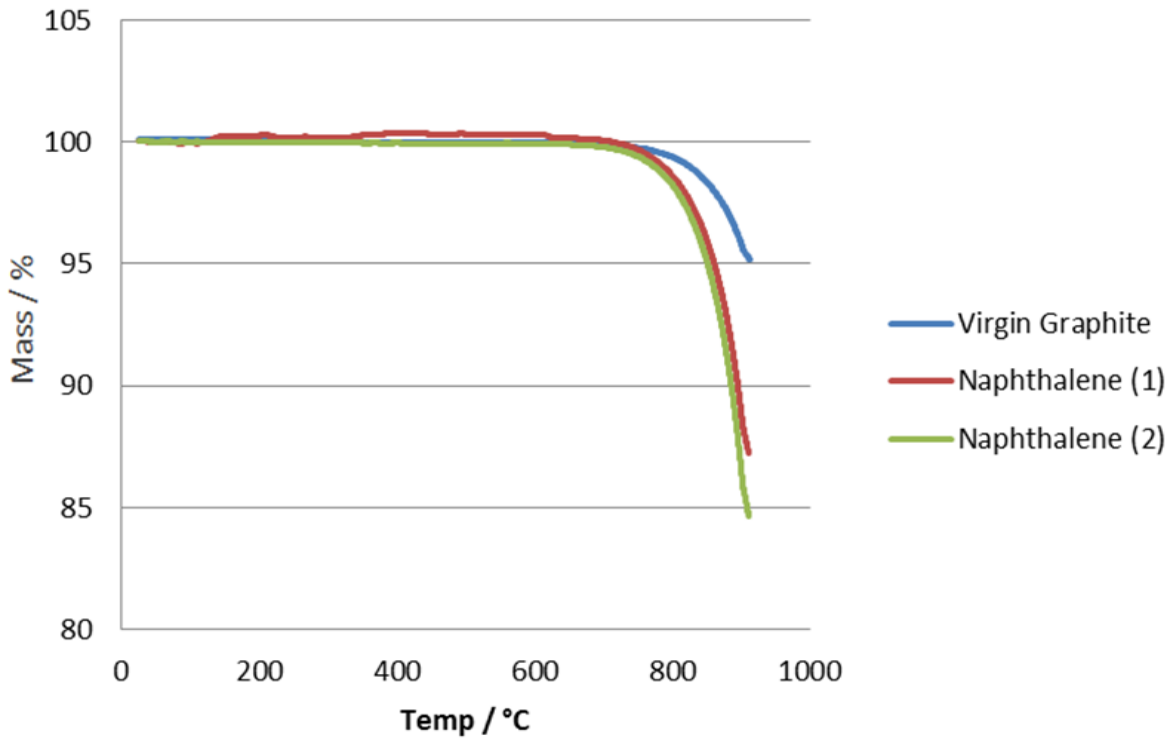

Figure 57 - TGA profile of the oxidation of virgin graphite and two repeats of graphite doped with 2 g of naphthalene which have been charred in bulk

3.7 Solution Deposition Summary

The production of carbonaceous material on the surface of graphite using the solution deposition of a carbon containing precursor was of limited success. While doping the sample with D-mannose produced a viable deposit, both myristic acid and naphthalene did not. The reason behind the lack of success can be attributed to the fact that the myristic acid and naphthalene completely evaporated before any decomposition could take place (Figure 45 and Figure 54), while the heating of D-mannose does result in a residue (Figure 32).

It was hoped that doping myristic acid and naphthalene onto the surface of graphite would assist in the decomposition process, resulting in the formation of a deposit prior to the loss to the gas phase through evaporation. Unfortunately the results in the preceding sections confirm that this did not occur and consequently only the D-mannose doped sample produced a viable deposit for the thermal treatment studies.

3.9 Microwave Plasma Deposition

The method which utilised microwave plasma to assist in the chemical vapour deposition process involved the use of only one carbon precursor which was methane. There was no requirement to char these samples as the deposits were formed in situ from the thermal breakdown of the gaseous precursor. In order to evaluate the success of this method samples were analysed using SEM, Raman spectroscopy and TGA.

3.9.1 Scanning Electron Microscopy

The differences between virgin graphite and graphite samples having undergone the microwave deposition process could be observed easily with the naked eye. Samples appeared to have black material covering the entire graphite surface which normally appeared to be a grey colour. The SEM analysis confirmed that a carbonaceous deposit had been successfully produced on the graphite surface (Figure 58).

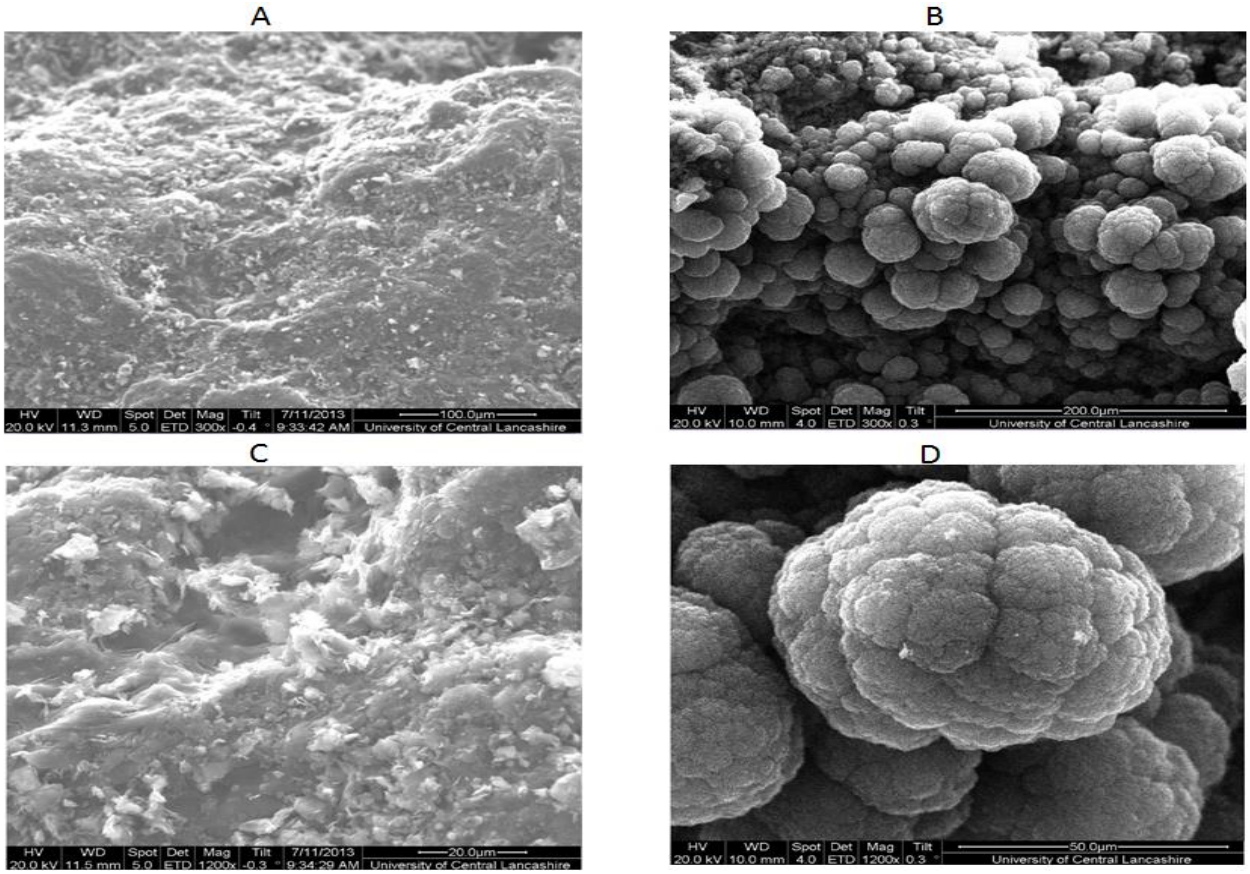

Figure 58 - SEM images of A - virgin Magnox graphite at x300 magnification, B - Magnox graphite with microwave produced deposit at x300 magnification, C - virgin Magnox graphite at x1200 magnification and D - Magnox graphite with microwave produced deposit at x1200 magnification

The graphite surface had been completely obscured by a material made up of small circular deposits with a 'cauliflower' like appearance. The morphology of these 'cauliflower' like deposits was very interesting. At higher magnifications (Figure 59) the deposits appeared to be made up of a large quantity of small fibres and not just large circular deposit particles as it appeared at lower magnifications.

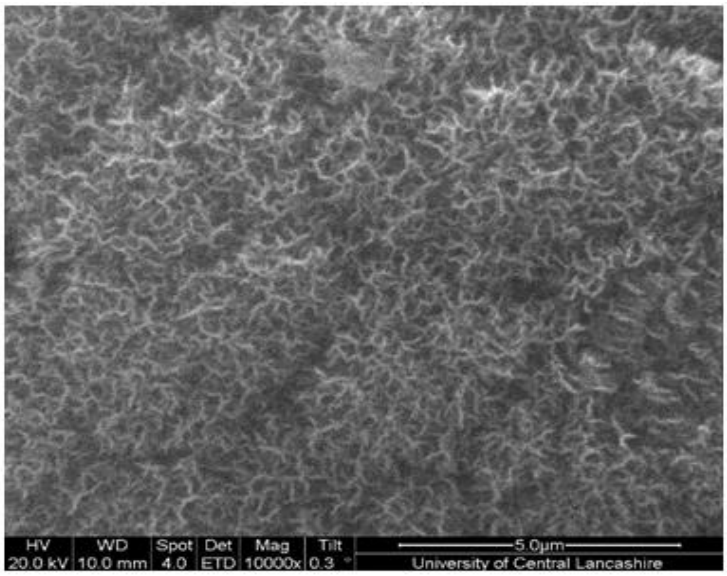

Figure 59 - SEM image of Magnox graphite with microwave produced deposit at x10,000 magnification

These 'cauliflower' like deposits have a very similar morphology to the deposits found on nuclear reactor graphite[49] (Figure 60). Similar results have also been achieved from the breakdown of natural gas to produce hydrogen, a process which produces carbonaceous deposits as a by-product[125].

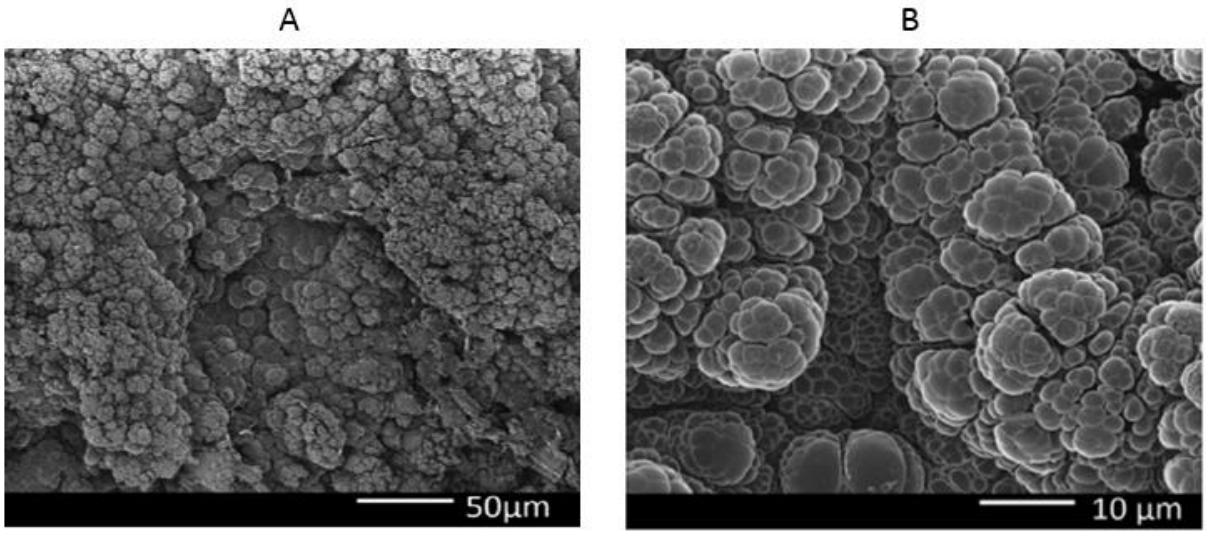

Figure 60 - FIB images of irradiated Magnox graphite with carbonaceous deposits[49]

3.9.2 Raman Spectroscopy

The following section displays the Raman spectra produced from virgin graphite samples compared with graphite samples with carbonaceous deposits formed using the microwave deposition procedure. Both samples exhibited a similar three peak arrangement however the D peak at ~1350 cm^{-1} was much higher than what had been observed previously with virgin graphite (Figure 61). This indicated the presence of a disordered amorphous carbon material on the graphite surface[115].

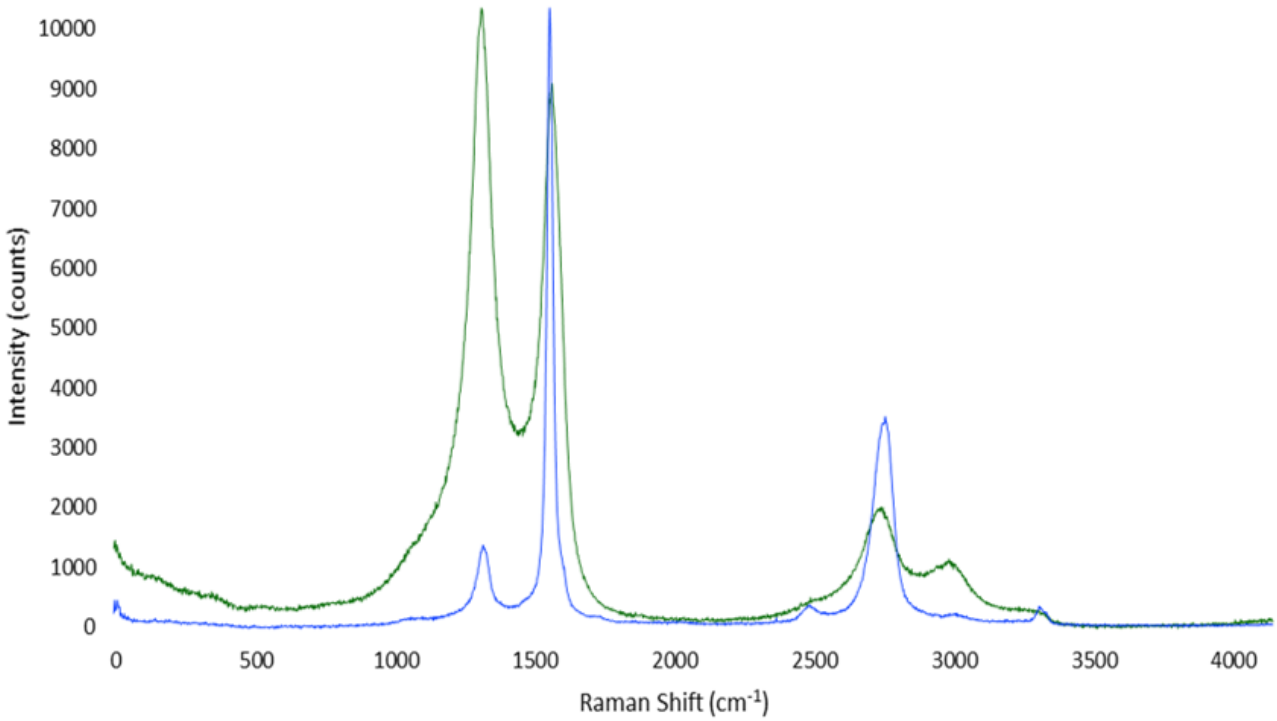

Figure 61 - Raman spectra of virgin Magnox graphite (blue) and graphite with carbonaceous deposit formed using the microwave plasma method (green)

3.9.3 Thermal Gravimetric Analysis

The mass loss profiles of virgin Magnox graphite and Magnox graphite with C-12 microwave deposits were very similar (Figure 62). So similar in fact that the data produced from TGA indicated that there was no carbonaceous deposit present at all. There was no evidence of oxidation until after ~800°C which is the same temperature that virgin Magnox graphite started to oxidise. However the data from SEM and Raman spectroscopy proved that a carbonaceous deposit was present. This data may allude to several scenarios one being that

the deposit produced using the microwave technique had a similar oxidation temperature as graphitic material. Conversely the amount of deposit present on the sample could be so small that the thermobalance was not sensitive enough to detect the change in mass which occurred during the oxidation of the deposit. Furthermore the deposits could be strongly bonded to the graphite surface and require a high temperature to break. In addition the oxidation of the deposits could be so slow that not enough time has elapsed in order for an observable amount of mass loss to occur. This last theory is substantiated by the results of the thermal analysis of deposits on irradiated graphite presented in a later section (3.21.2) which show that the removal of the deposit takes several hours to be oxidised.

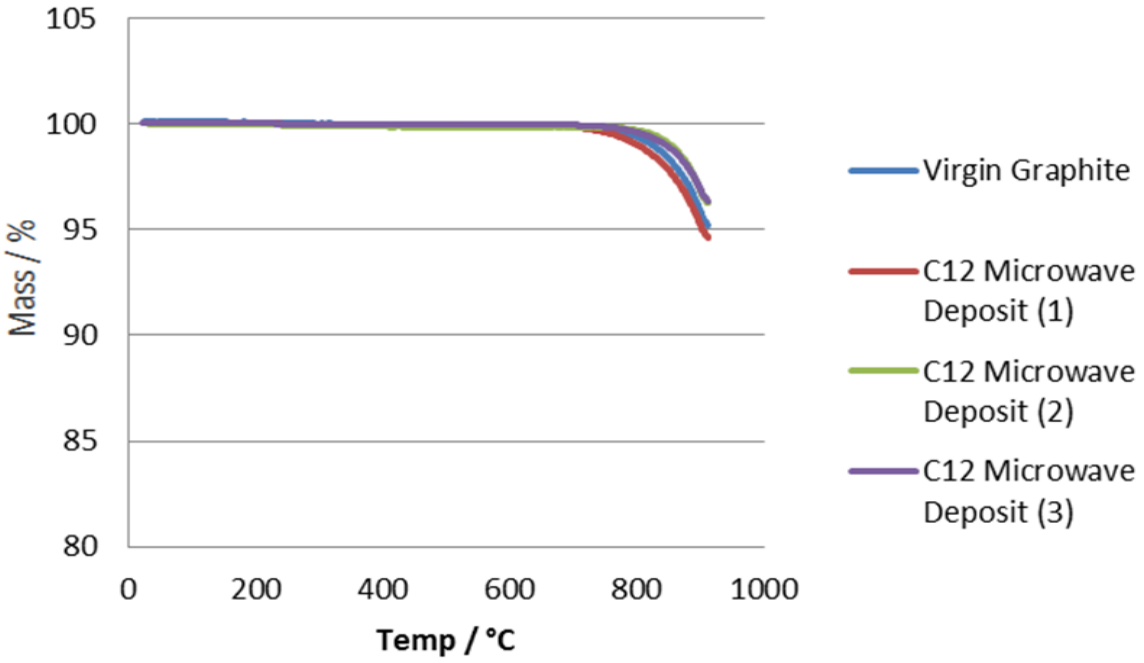

Figure 62 - TGA profile of the oxidation in air of virgin Magnox graphite and three repeats of Magnox graphite with C-12 microwave deposits

3.10 Microwave Plasma Deposition Summary

The characterisation of samples prepared using the microwave plasma assisted deposition method provided information indicating that a carbonaceous deposit had been successfully synthesised. TGA did not indicate the presence of a deposit most likely because an insufficient amount of time had elapsed in order for an observable amount of mass loss to occur. However the use of SEM and Raman spectroscopy confirmed its existence. The surface of the graphite was coated in 'cauliflower' like deposits which have a very similar morphology to the deposits found on nuclear reactor graphite[49].

The microwave deposition method was selected to prepare C-13 deposits due to the similarities of the deposits found in nuclear reactors and deposits formed using the microwave deposition method. By using C-13 labelled methane, deposits could be produced which would facilitate the study of their selective removal from graphite using mass spectrometry and Raman spectroscopy.

3.11 Characterisation of C-13 deposits

In order to determine the similarities and differences between C-12 and C-13 deposits on the graphite samples surface a number of characterisation techniques were utilised.

3.11.1 Scanning Electron Microscopy

The SEM images produced from graphite samples with C-13 deposits on the graphite surface (Figure 63) exhibited the 'cauliflower' like morphology which had been observed previously from the graphite samples with C-12 deposits (Figure 58). This was as expected as the same technique was used only with C-13 methane instead of C-12 methane.

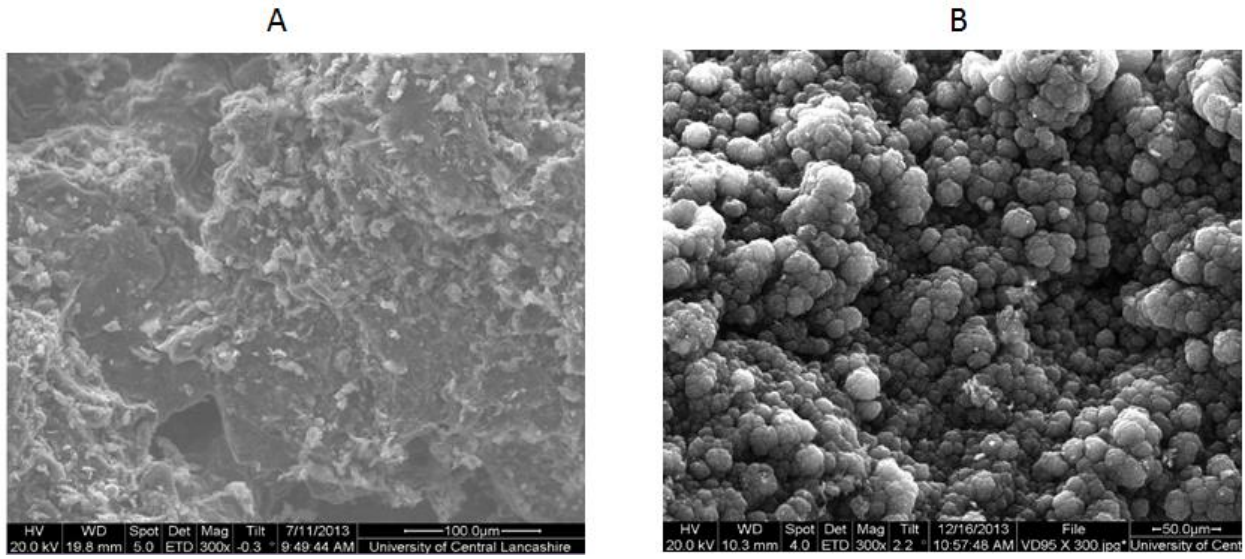

Figure 63 - SEM images at x300 magnification of A - virgin Magnox graphite and B - Magnox graphite with C-13 microwave produced deposits

3.11.2 Raman Spectroscopy

Due to the atomic mass differences between C-12 and C-13 isotopes Raman spectroscopy could be used to differentiate between them. Whilst there was no change in the Raman spectral shape, the Raman shift frequency was √12/13 times smaller with C-13 atoms than C-12. This means that there was a notable shift to the left (~50 cm^{-1}) of the Raman spectra caused by the heavier carbon atoms[126]. This shift could be used as a selective indicator as to whether or not any C-13 deposit was present on the graphite surface after the thermal treatment of the samples. The spectrum for virgin graphite portrayed the characteristic G peak arising at ~1580 cm^{-1} and the D peak arising at ~1350 cm^{-1} which was attributed to disorder (Figure 64). The spectrum for graphite with C-12 microwave deposits had a very similar spectrum to virgin graphite but the D peak had a much higher intensity. This indicated that an amorphous carbon was present with a large amount of disorder within its structure compared to the very crystalline graphite structure. The spectrum for graphite with C-13 microwave deposits showed a notable shift to the left of both the D and the G peaks from the spectrum produced from C-12 microwave deposits and also a high intensity in the D peak.

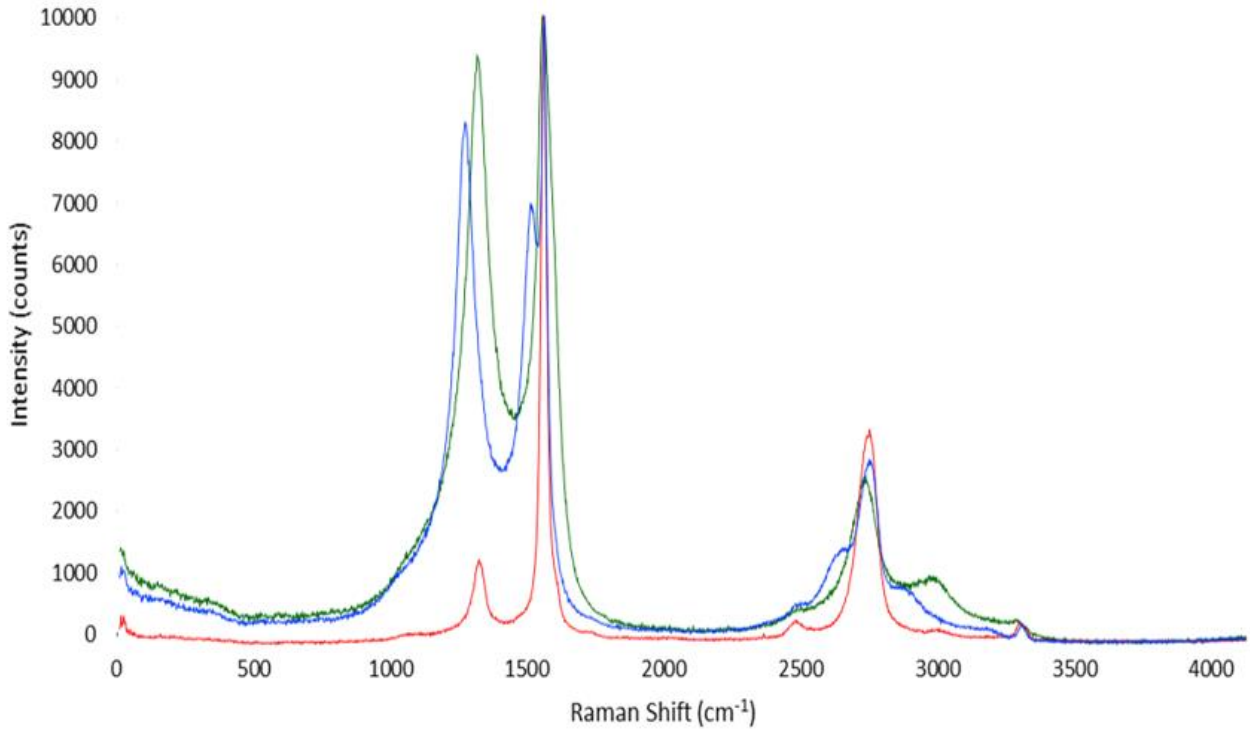

Figure 64 - Raman spectra of virgin graphite (red), graphite with C-12 microwave deposit (green) and graphite with C-13 microwave deposit (blue)

3.11.3 Thermal Gravimetric Analysis

The mass loss profiles of virgin Magnox graphite and Magnox graphite with C-13 microwave deposits were very similar (Figure 65). There was no evidence of oxidation until after ~800°C which was the same temperature that virgin graphite started to oxidise. These results were similar to that produced from graphite with C-12 microwave deposits (Figure 62). The oxidation of the deposits could be so slow that not enough time has elapsed in order for an observable amount of mass loss to occur. This is substantiated by the results of the thermal analysis of deposits on irradiated graphite presented in a later section (3.21.2) which show that the removal of the deposit takes several hours to be oxidised.

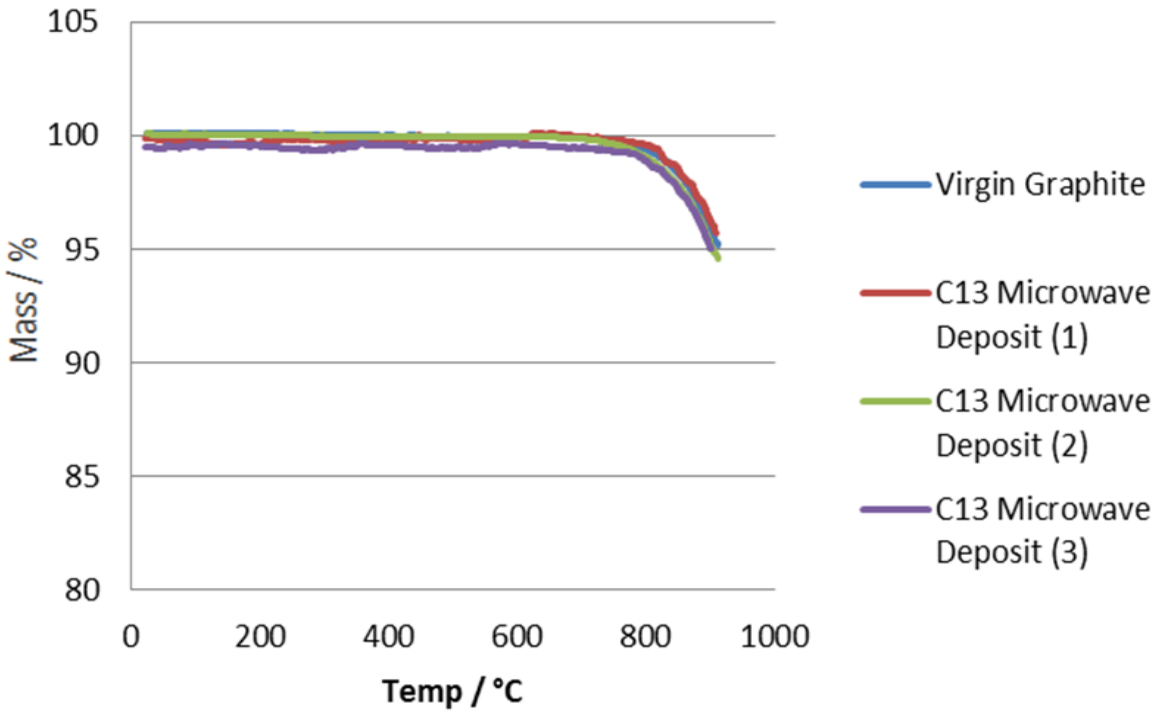

Figure 65 - TGA profile of the oxidation in air of virgin Magnox graphite and three repeats of Magnox graphite with C-13 microwave deposits

3.12 Thermal Treatment

Graphite samples with and without carbonaceous deposits were oxidised at both 10 mbar and 1 atmosphere pressure for 5 hours over a temperature range of 450-800°C with the system previously described in section 2.5. Interpretation of the evolved gas analysis (mass spectrometry), Raman spectroscopy and scanning electron microscopy images were used to demonstrate whether the deposits could be selectively removed from the graphite surface without oxidising a significant amount of the underlying graphite. Samples selected to undergo thermal treatment were the D-mannose deposits, the C-12 microwave deposits and the C-13 microwave deposits.

3.13 Virgin Graphite with a vacuum

The thermal treatment of both virgin Magnox and AGR graphite was conducted in order to provide a comparison to graphite samples with carbonaceous deposits present and also to determine whether there were any differences in the thermal treatment of Magnox or AGR graphite.

3.13.1 Mass Spectrometry and mass loss

The percentage mass loss of each of the virgin graphite samples during the thermal treatment with a vacuum at a variety of temperatures exhibited a notable trend (Figure 66). As the temperature increased so did the percentage mass loss which is consistent with an increased rate of oxidation. At the lower temperatures of 450°C and 600°C samples exhibited the least amounts of mass loss <2%. At the higher temperatures of 700°C and 800°C Magnox graphite had a much higher mass lost compared to AGR graphite. Magnox graphite exhibited a mass loss of ~19% at 700°C compared to AGR graphite which only lost ~5%. At 800°C AGR graphite only lost ~16% compared to Magnox graphite which lost ~50%.

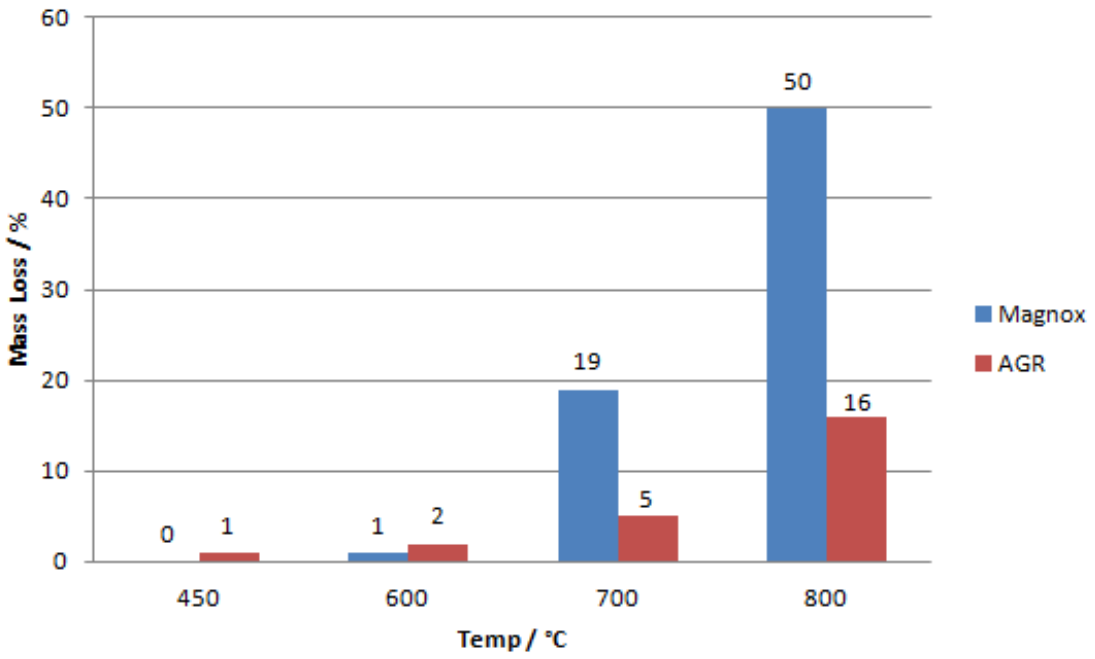

Figure 66 - Comparison of the percentage mass loss of both Magnox and AGR graphite during thermal treatment at various temperatures with a vacuum

The variances between the rates of oxidation of Magnox and AGR graphite are due to the different coke types used during the manufacturing process. AGR graphite is formed using a pitch coke and produces a graphite sample with a slower oxidation rate compared to Magnox graphite which utilises a petroleum coke. The TGA profiles of both virgin graphite samples also showed this to be the case (Figure 25).

The data from the mass spectrometer confirmed the trend observed with the mass loss data by exhibiting an increase in CO_2 production during thermal treatment at higher temperatures compared with the lower temperatures. This was the same for both Magnox graphite (Figure 67) and AGR graphite (Figure 68). There was no CO_2 production at 450°C and 600°C for both types of graphite. Their mass losses were so small that they may be due to the loss of minute amounts of graphite dust loosely adhered to the graphite surface. This dust was most likely to have been lost during sample preparation. CO was also produced during these experiments but several orders of magnitude lower than CO_2 so the majority of the mass loss is attributed to CO_2.

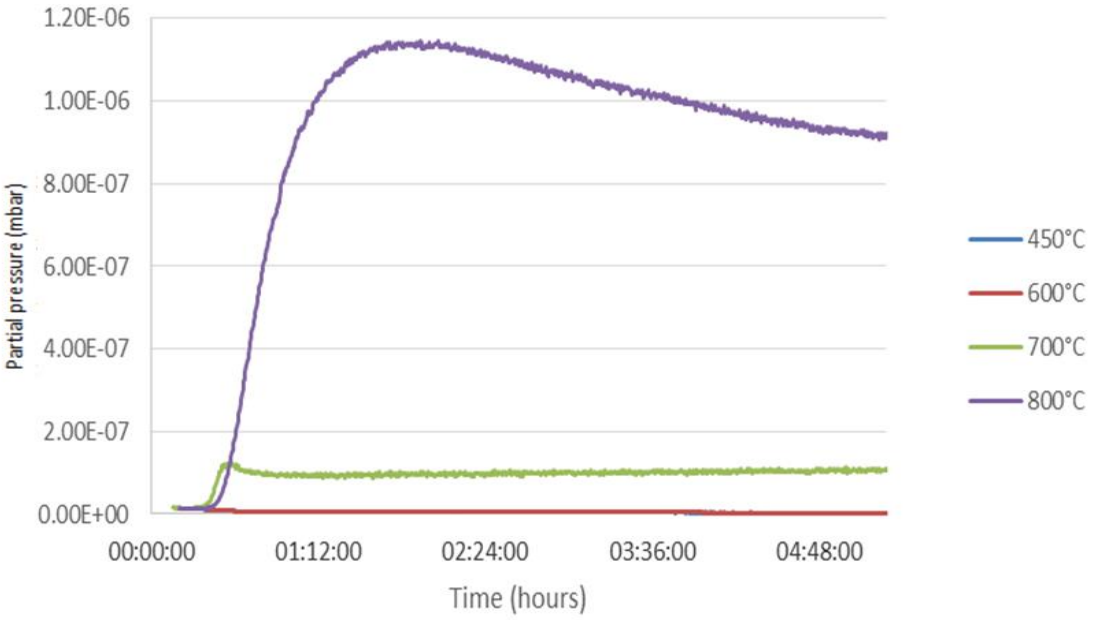

Figure 67 - Mass spectrometry data of CO_2 produced from Magnox graphite during thermal treatment with a vacuum at various temperatures

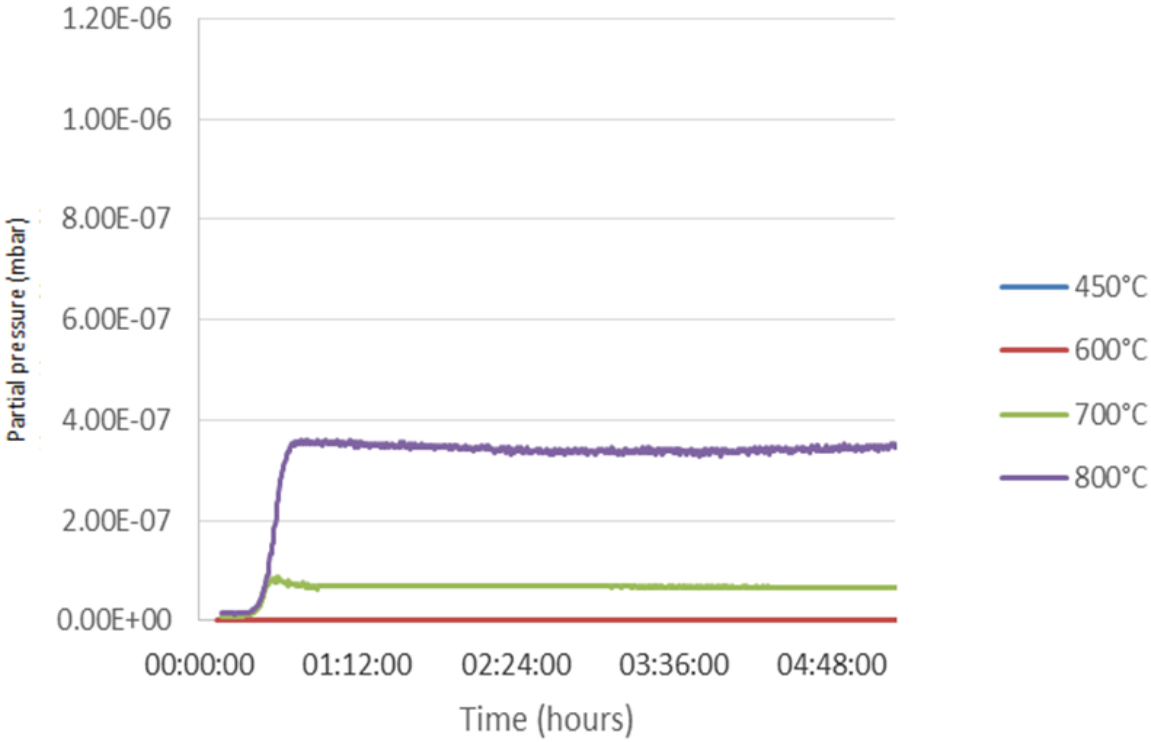

Figure 68 - Mass spectrometry data of CO_2 produced from AGR graphite during thermal treatment with a vacuum at various temperatures

The oxidation of graphite takes place through a series of adsorption and desorption routes. First oxygen diffuses to the surface of graphite or into the open pore volume where chemisorption occurs resulting in the simultaneous breaking of C-C bonds and formation of C-O bonds. The oxygen atoms that are bonded to the graphite surface form intermediate oxide complexes depending on the stability and reactivity of the active site to which they are attached. Lastly CO and CO_2 is desorbed from the surface of graphite resulting in a mass loss. The rate of graphite oxidation depends on a number of variables such as flow rate, oxygen partial pressure, temperature, gas pressure in addition to the volume porosity of the graphite and surface area of active sites or surface defects[83].

There are a number of chemical reactions which can take place during the oxidation of graphite (Figure 69). Reaction 1 is the dominant process in the gasification of graphite so it is interesting that the mass spectrometer only detects CO levels several orders of magnitude lower than CO_2. This may be due to the fact that there is sufficient oxygen in the system to combust CO (Reaction 4). This reaction takes place entirely in the gas phase and is thermodynamically favourable at higher temperatures[127,128].

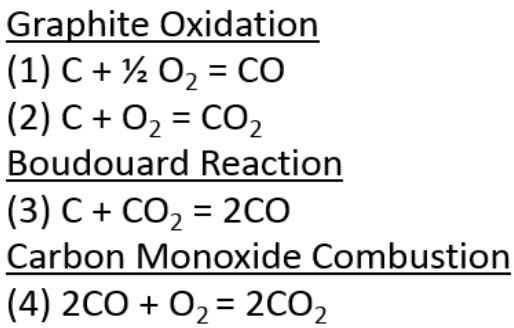

Figure 69 - Oxidation of graphite reactions[127,128]

Studies have shown that the oxidation rate of graphite is controlled by different processes at different temperatures. Below 500°C the reaction rate is controlled by the chemical reactivity of the species involved. At higher temperatures (between 600°C and 900°C) the chemical reactivity is so high that the reaction rate is now controlled by the amount of diffusion in the graphite pores which in turn is effected by density, impurity level and the graphite microstructure[129,130].

3.13.2 Scanning Electron Microscopy

In order to determine the physical change which occurs to the graphite surface during the thermal treatment various characterisation techniques were utilised for both Magnox and AGR graphite. SEM was used to visualise any changes in the samples surface morphology. At the lower thermal treatment temperatures of 450°C and 600°C the surface of the Magnox graphite samples did not look any different to virgin Magnox graphite (Figure 70). However at the higher temperatures, especially 800°C, there was a noticeable difference in the surface morphology. As well as an increase of cracks and holes the rest of the surface appeared much rougher than virgin graphite and the samples having undergone the thermal treatments at the lower temperatures. This difference was due to the amount of oxidation that had taken place during the thermal treatment. Any imperfections in the surface morphology would be increased during oxidation because an irregular surface has a high surface area which increases reaction rate.

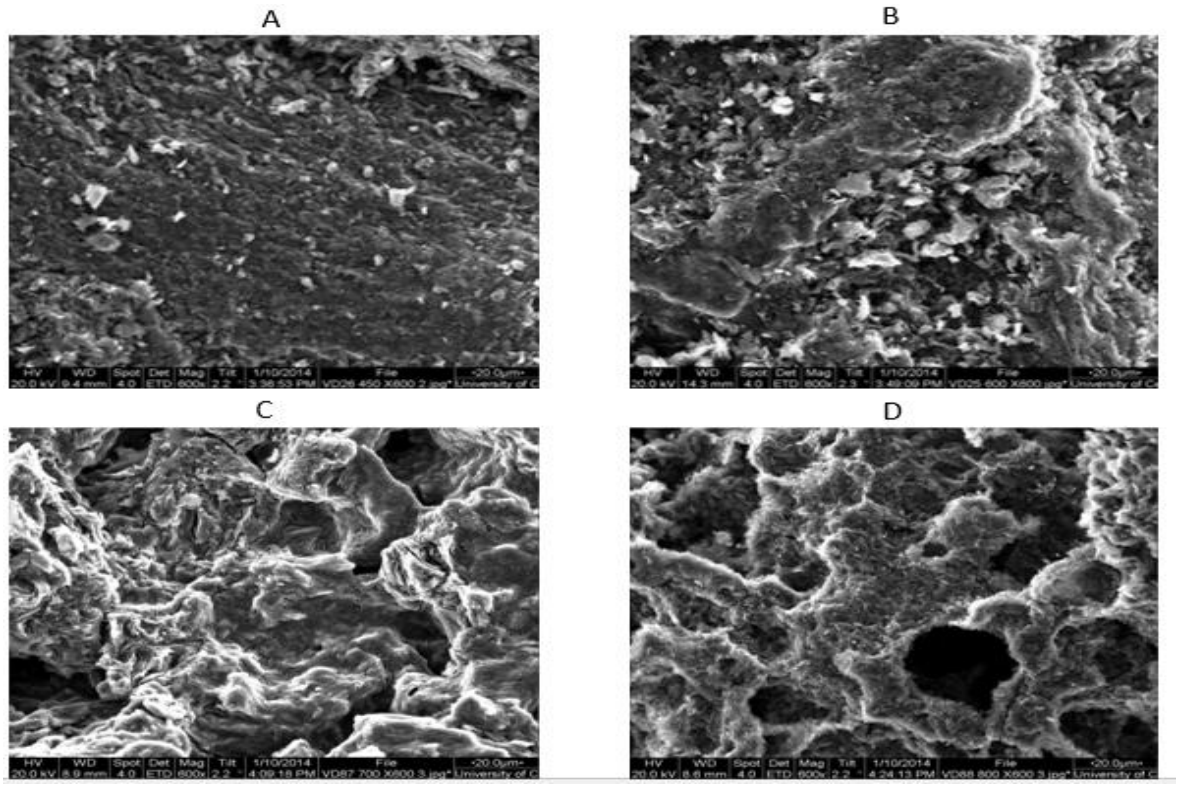

Figure 70 - SEM images at x600 magnification of A - Magnox graphite after thermal treatment with a vacuum at 450°C, B - 600°C, C - 700°C, D - 800°C

The SEM images produced for AGR graphite having undergone the thermal treatment process with a vacuum at various temperatures (Figure 71) followed the same trend which has been discussed previously. At the higher temperatures of 700°C and 800°C the graphite

samples had started to oxidise and a change in the graphite surface was evident. At the lower temperatures of 450°C and 600°C the surface was similar to that of virgin graphite indicating that little or no oxidation had taken place. This was confirmed by the mass loss and mass spectrometer data which shows minimal change in mass and no CO_2 or CO detected. The SEM images produced for AGR graphite (Figure 71) showed a very similar morphology at each of the temperatures as Magnox graphite (Figure 70).

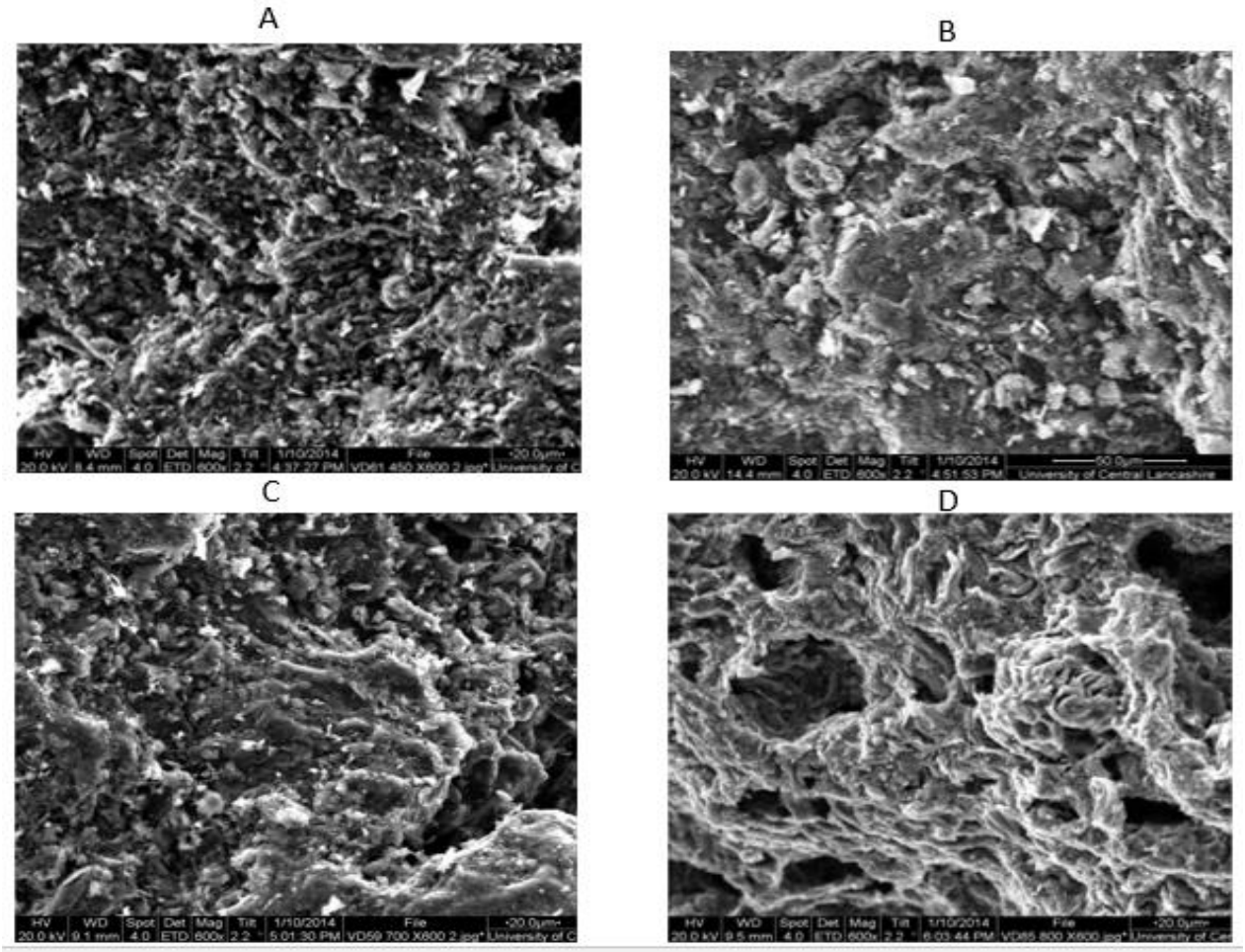

Figure 71 - SEM images at x600 magnification of A - AGR graphite after thermal treatment with a vacuum at 450°C, B - 600°C, C - 700°C, D - 800°C

3.13.3 Raman Spectroscopy

Magnox graphite samples that had been thermally treated exhibited the same characteristic Raman spectra as virgin graphite (Figure 72). The G band arising at ~1580 cm^{-1} and the D band arising at 1350 cm^{-1} could be observed as well as the 2D peak at ~2700 cm^{-1}. However a slight difference could be observed from the spectra produced from graphite samples which had been thermally treated with a vacuum. The slight increase in the D peak indicated that

there had been a change in the amount of disorder present on the graphite surface. This could mean that as the graphite surface starts to oxidise it causes an increase in the amount of defects/disorder present and thus a change in the Raman spectra produced.

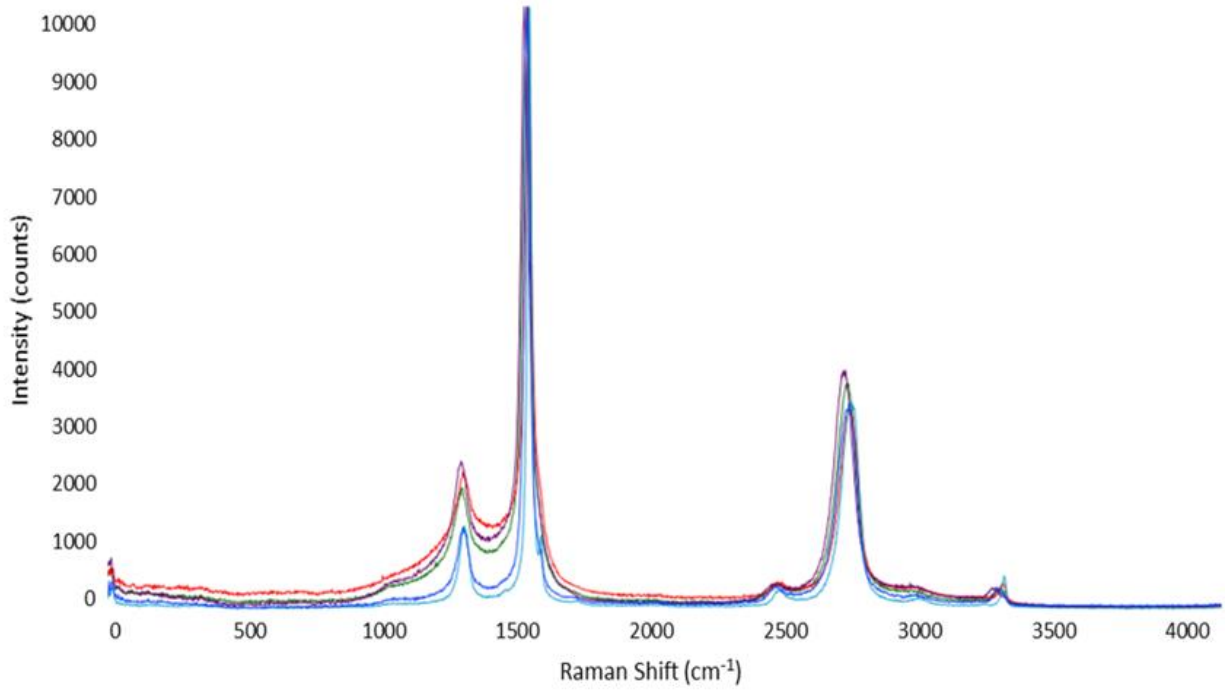

Figure 72 - Raman spectra of virgin Magnox graphite (dark blue), Magnox graphite after thermal treatment with a vacuum at 450°C (green), 600°C (red), 700°C (purple), 800°C (light blue)

The Raman analysis of the thermally treated AGR graphite samples exhibited the same increase in disorder but to a higher extent compared to Magnox graphite (Figure 73). This was surprising because Magnox graphite displayed a higher amount of oxidation compared to AGR graphite. Perhaps the amount of disorder was lower with Magnox graphite because the high amount of oxidation had removed the imperfections on the graphite surface leaving a smoother more crystalline graphite surface. However the differences could also be due to sample variation of the different graphite particles.

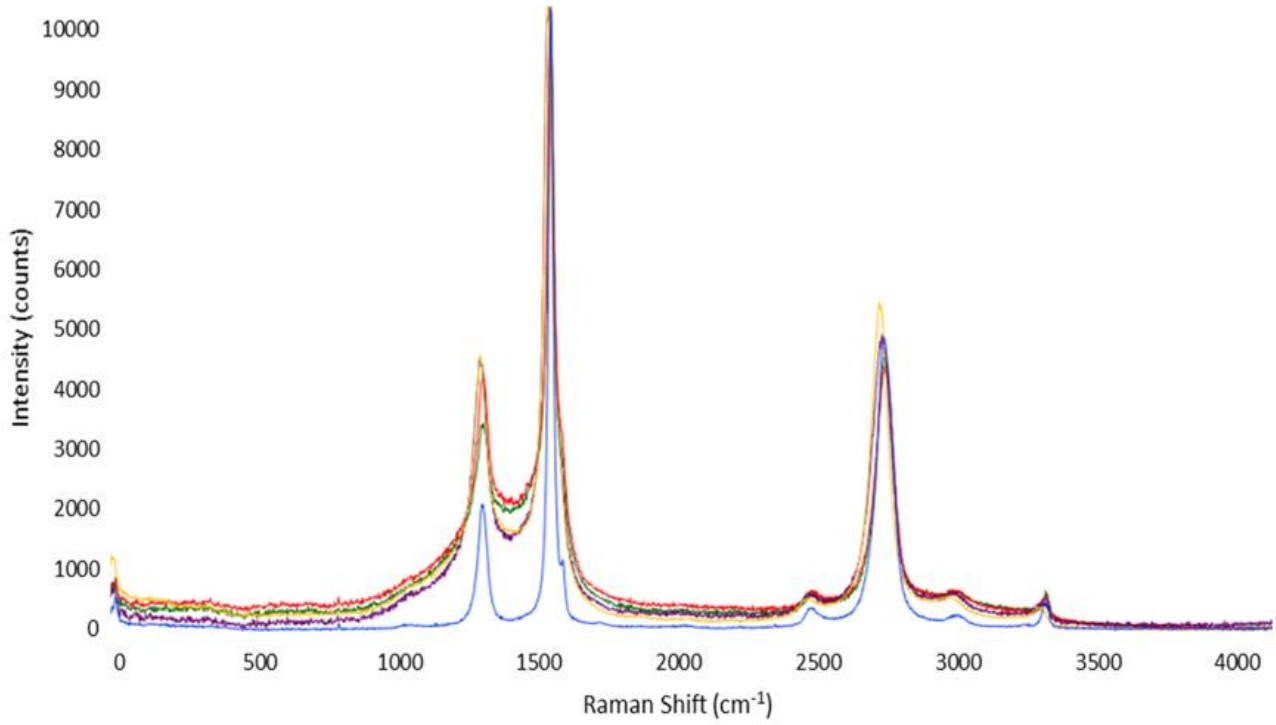

Figure 73 - Raman spectra of virgin AGR graphite (dark blue), AGR graphite after thermal treatment with a vacuum at 450°C (green), 600°C (red), 700°C (purple), 800°C (yellow)

3.14 Virgin Graphite without a vacuum

The following section will provide information on the oxidation of both virgin Magnox and AGR graphite during thermal treatment without the application of a vacuum.

3.14.1 Mass Spectrometry and mass loss

The percentage mass loss of each of the virgin graphite samples during the thermal treatment without a vacuum at a variety of temperatures exhibited a notable trend (Figure 74). As the temperature increased so did the percentage mass loss, which is consistent with an increased rate of oxidation. Magnox graphite appears to exhibit a greater mass loss at every temperature compared to AGR graphite which is similar to the thermal treatment results with a vacuum.

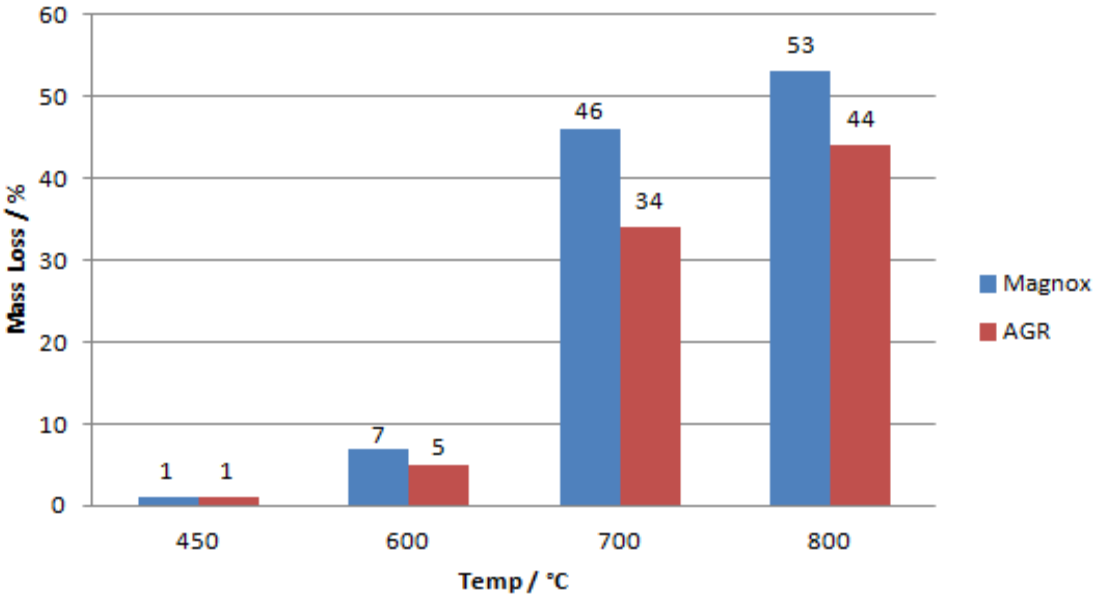

Figure 74 - Comparison of the percentage mass loss of both Magnox and AGR graphite during thermal treatment at various temperatures without a vacuum

The data from the mass spectrometer confirmed the trend observed with the mass loss data by exhibiting an increase in CO_2 production during thermal treatment at higher temperatures compared with the lower temperatures. This was the same for both Magnox graphite (Figure 75) and AGR graphite (Figure 76). The data also confirms that the rate of oxidation of Magnox graphite is higher than AGR graphite. CO was also produced during these experiments but several orders of magnitude lower than CO_2 so the majority of the mass loss is attributed to CO_2.

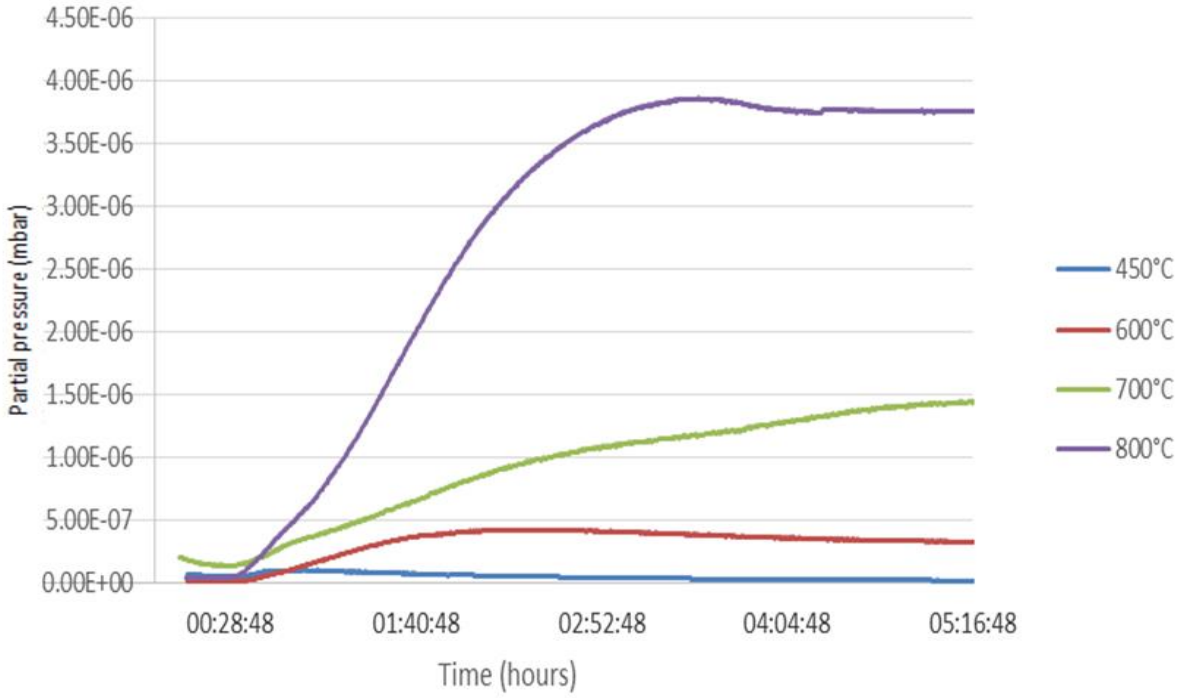

Figure 75 - Mass spectrometry data of CO_2 produced from Magnox graphite during thermal treatment without a vacuum at various temperatures

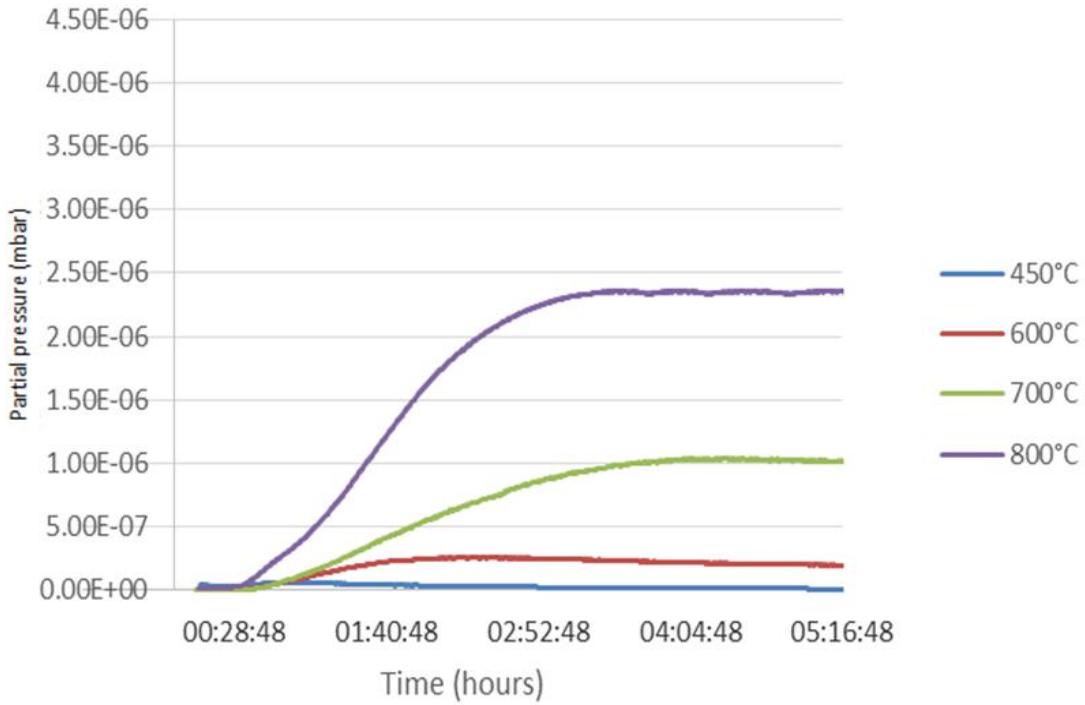

Figure 76 - Mass spectrometry data of CO_2 produced from AGR graphite during thermal treatment without a vacuum at various temperatures

3.14.2 Scanning Electron Microscopy

During the thermal treatment without the use of a vacuum the rate of oxidation was higher at all the temperatures investigated compared to the thermal treatment with a vacuum, which is as expected. SEM was used to visualise any changes in the samples surface morphology. From the interpretation of the evolved gas analysis and the TGA data it appears that Magnox graphite samples are more reactive than the AGR graphite samples. The SEM images produced for both Magnox (Figure 77) and AGR graphite (Figure 78) confirms this. At the lower temperature of 450°C both types of graphite show that little oxidation has occurred and exhibit a surface morphology similar to that of virgin graphite (Figure 21). Magnox graphite samples which have been thermally treated at the higher temperatures from 600-800°C (B-D in Figure 77) exhibit a rough and irregular surface morphology with a number of cracks which indicates that a significant amount of oxidation has occurred. Comparatively whilst AGR graphite samples having undergone thermal treatment at the same temperatures exhibit a rough irregular surface (B-D in Figure 78) the amount of oxidation appears much less compared to Magnox graphite samples. This again was expected as AGR graphite samples have a much slower rate of oxidation.

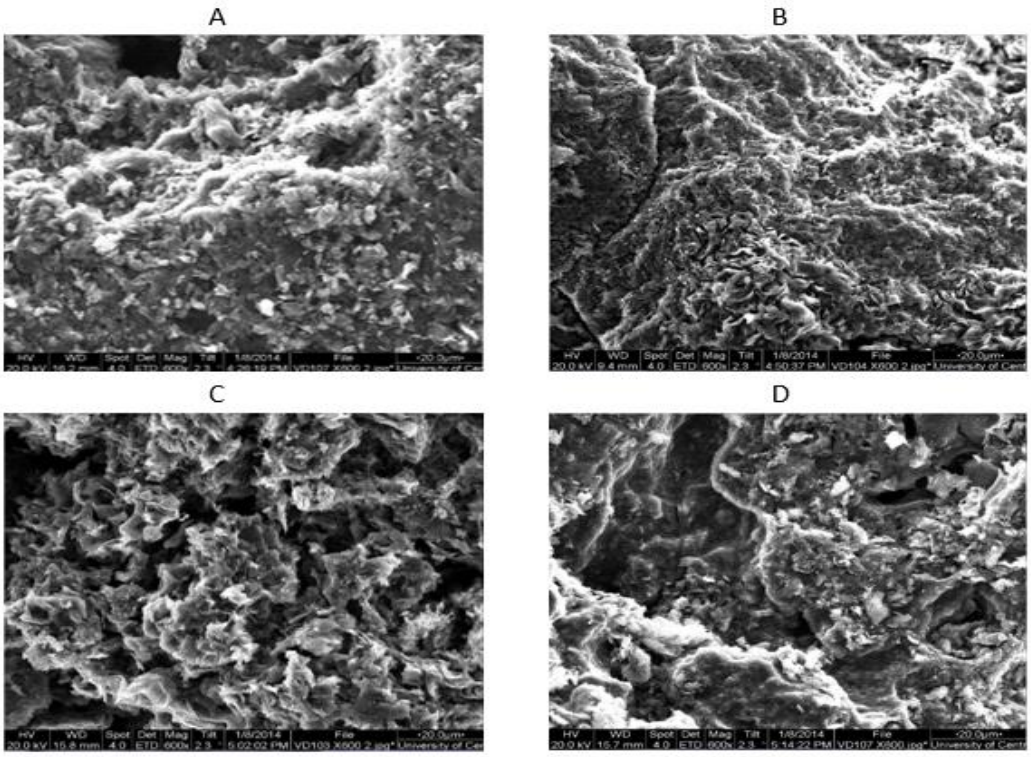

Figure 77 - SEM images at x600 magnification of Magnox graphite after thermal treatment without a vacuum at A - 450°C, B - 600°C, C - 700°C, D - 800°C

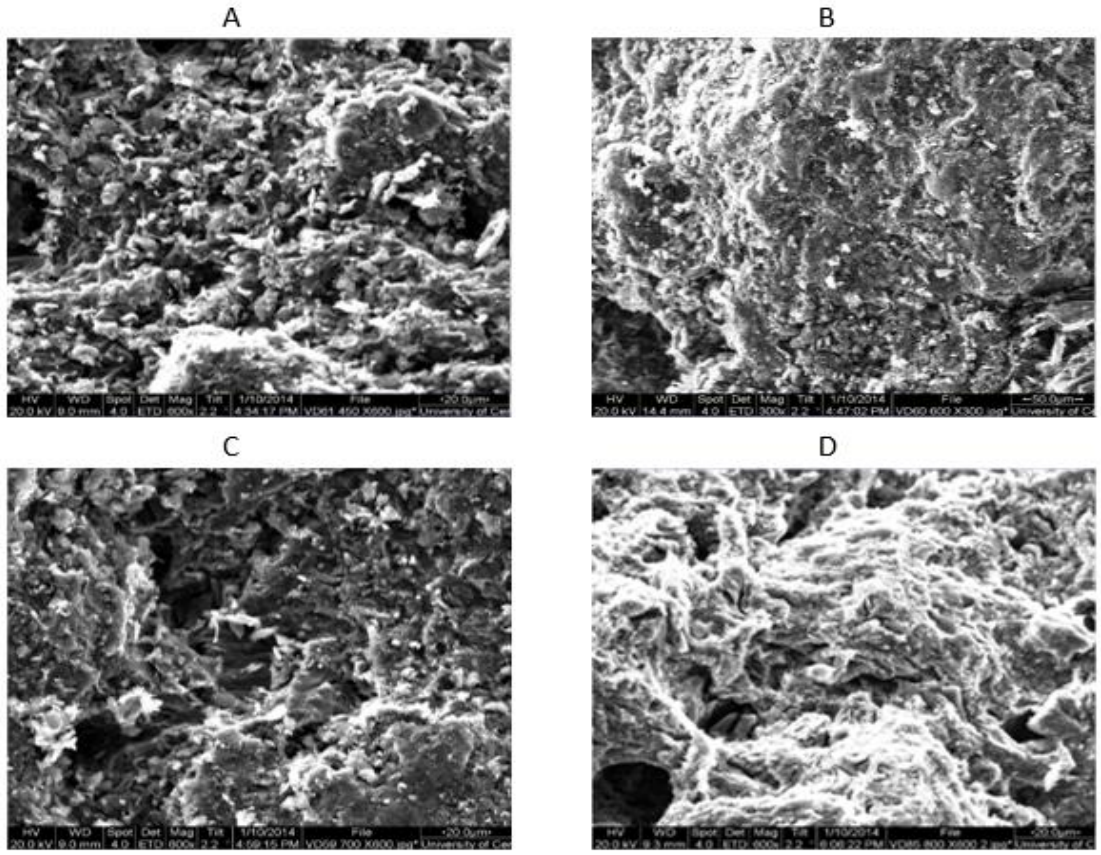

Figure 78 - SEM images at x600 magnification of AGR graphite after thermal treatment without a vacuum at A - 450°C, B - 600°C, C - 700°C, D - 800°C

3.14.3 Raman Spectroscopy

Magnox graphite samples that had been thermally treated exhibited the same characteristic Raman spectra as virgin graphite (Figure 79). The G band arising at ~1580 cm^{-1} and the D band arising at 1350 cm^{-1} could be observed as well as the 2D peak at ~2700 cm^{-1}. The intensity of the D peak is very similar to that exhibited by virgin graphite for Magnox graphite thermally treated at all temperatures. This differs from the Raman spectra of samples thermally treated with a vacuum as a slight increase in the D peak had arisen (Figure 72). It was hypothesised that as the graphite surface starts to oxidise it causes an increase in the amount of defects/disorder present and thus a change in the Raman spectra produced. However samples thermally treated without a vacuum have undergone more oxidation and so should also show an increase in the D peak even more so than samples oxidised with a vacuum, but this is not the case. Perhaps as oxidation occurs there is an initial increase in the D peak and as oxidation continues the intensity in the D peak returns to a similar level to virgin graphite.

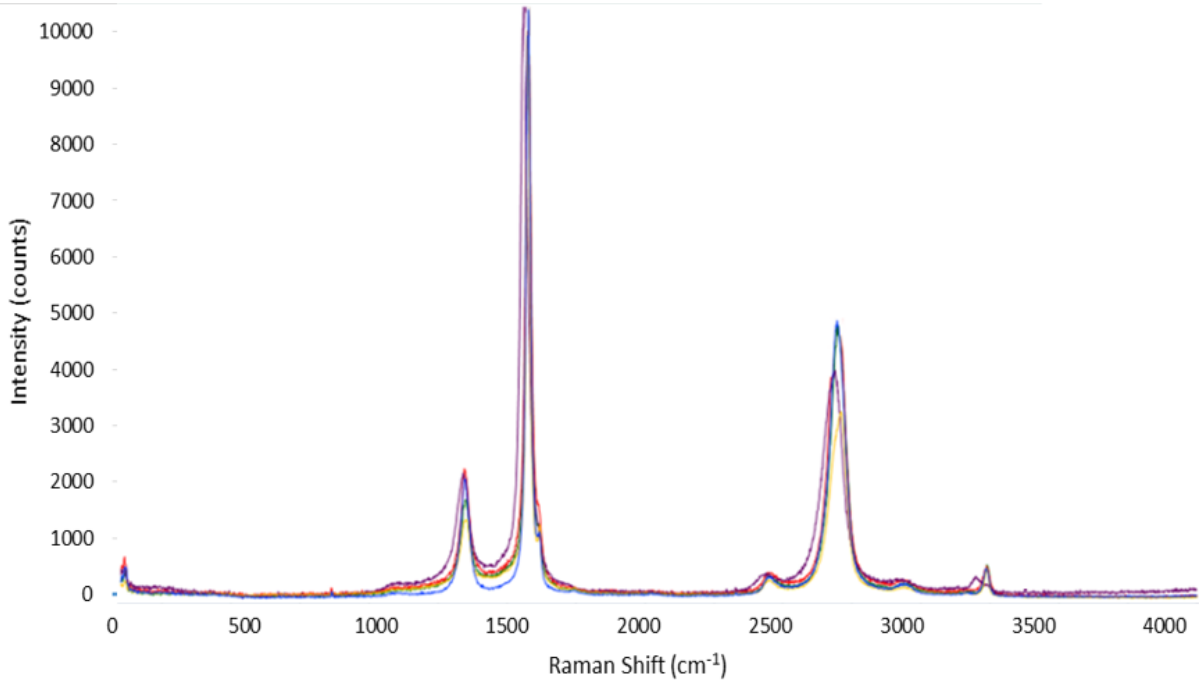

Figure 79 - Raman spectra of virgin Magnox graphite (blue), Magnox graphite after thermal treatment without a vacuum at 450°C (green), 600°C (red), 700°C (purple), 800°C (yellow)

The Raman analysis of the thermally treated AGR graphite samples without a vacuum exhibited a slight increase in disorder (Figure 80). This is comparable to the thermal treatment of AGR graphite with a vacuum which also showed an increase in the D peak (Figure 73) despite less oxidation taking place compared to Magnox graphite. This may indicate that there is still a degree of disorder present in AGR graphite because insufficient oxidation has occurred to remove it. However the differences could also be due to sample variation of the different graphite particles.

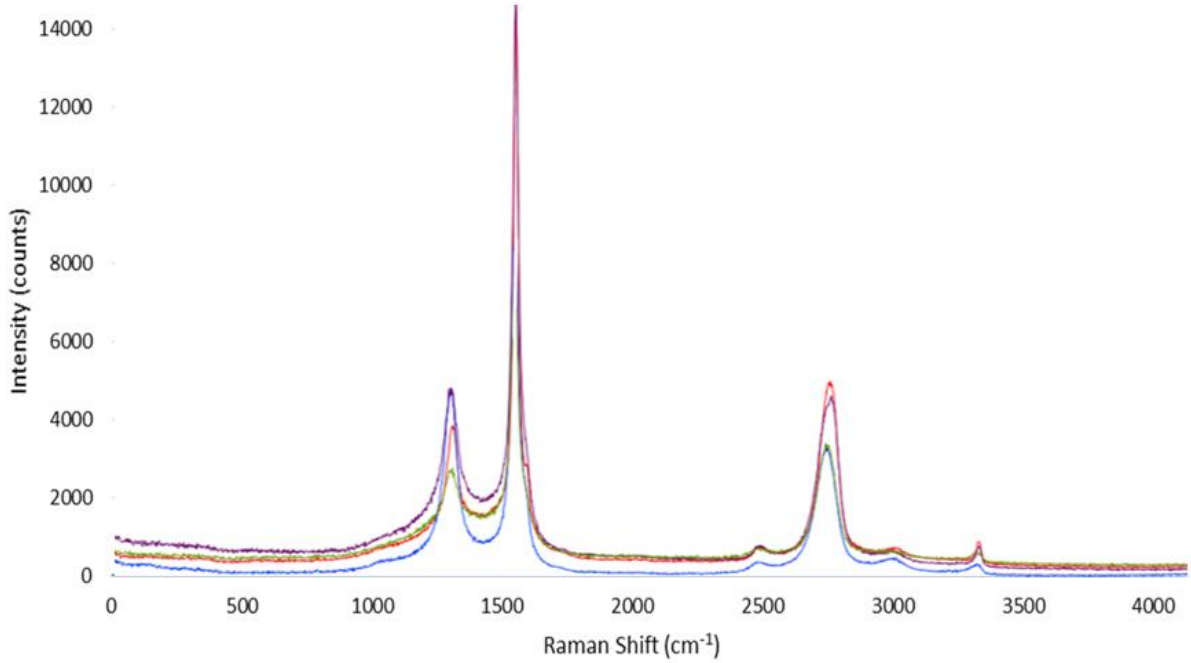

Figure 80 - Raman spectra of virgin AGR graphite (blue), AGR graphite after thermal treatment without a vacuum at 450°C (green), 600°C (red), 700°C (purple), 800°C (yellow)

3.15 D-mannose deposit with a vacuum

The following section will provide information on the removal of D-mannose deposits from the surface of both Magnox and AGR graphite during the thermal treatment at various temperatures with a vacuum applied.

3.15.1 Mass spectrometry and mass loss

The percentage mass loss of both Magnox and AGR graphite samples with a D-mannose deposit during the thermal treatment with a vacuum at a variety of temperatures (Figure 81) exhibited a similar trend to that observed with virgin graphite (Figure 66). Again as the temperature increased so did the percentage mass loss, and so the amount of oxidation that was occurring. The thermal treatment at 450°C and 600°C exhibited the least amounts of mass loss <1.5%. Once again at the higher temperatures of 700°C and 800°C it was the Magnox graphite samples which displayed a higher amount of mass lost compared to the AGR graphite samples. Magnox graphite with D-mannose deposits exhibited a mass loss of ~15% at 700°C compared to AGR graphite with D-mannose deposits which only lost ~2%. At 800°C Magnox graphite with D-mannose deposits lost ~47% compared to AGR graphite with D-mannose deposits which only lost ~18%. Magnox graphite samples with D-mannose

deposits followed the same trend as virgin Magnox graphite and also exhibited similar mass losses.

However although AGR graphite with D-mannose deposits followed the same trend as virgin AGR graphite, the samples with D-mannose deposit displayed less mass lost at 700°C compared to the mass losses of virgin AGR graphite. At 700°C virgin AGR graphite lost ~5% compared to the mass losses of ~2% displayed by AGR graphite with D-mannose deposits. This difference was most likely due to sample variation as it was unlikely that the presence of a deposit would make the sample more thermally stable. Also at the higher temperature of 800°C this difference was not evident as virgin AGR graphite lost ~16% compared to the mass loss of ~18% displayed by AGR graphite with D-mannose deposits.

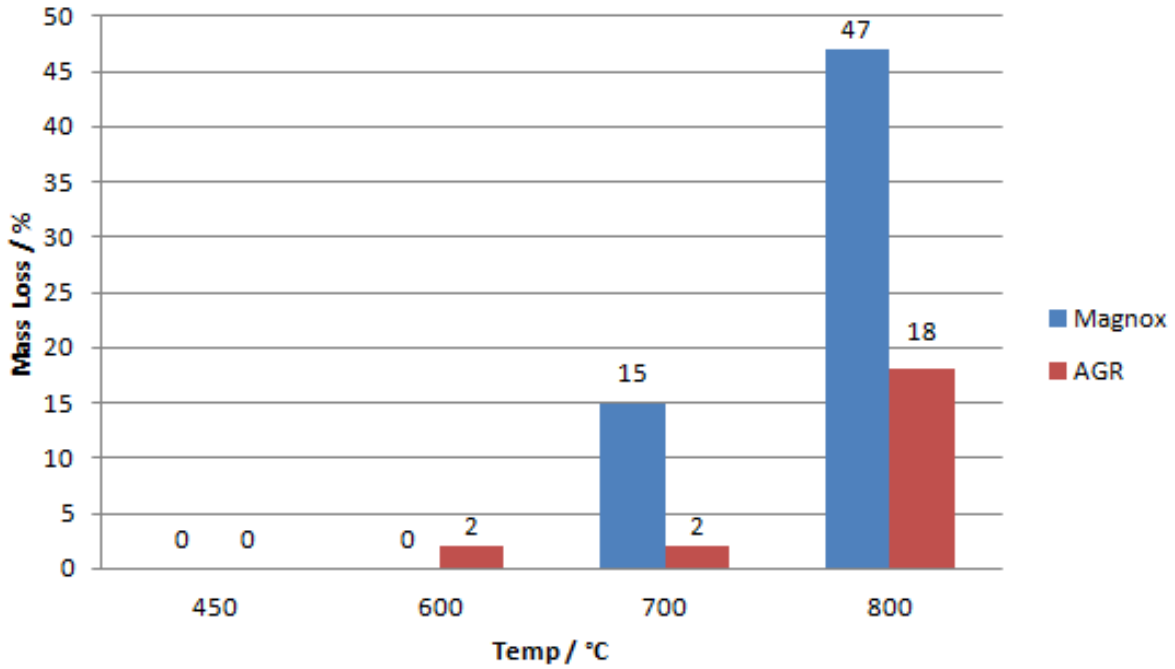

Figure 81 - Comparison of the percentage mass loss of both Magnox and AGR graphite with D-mannose deposit during thermal treatment at various temperatures with a vacuum

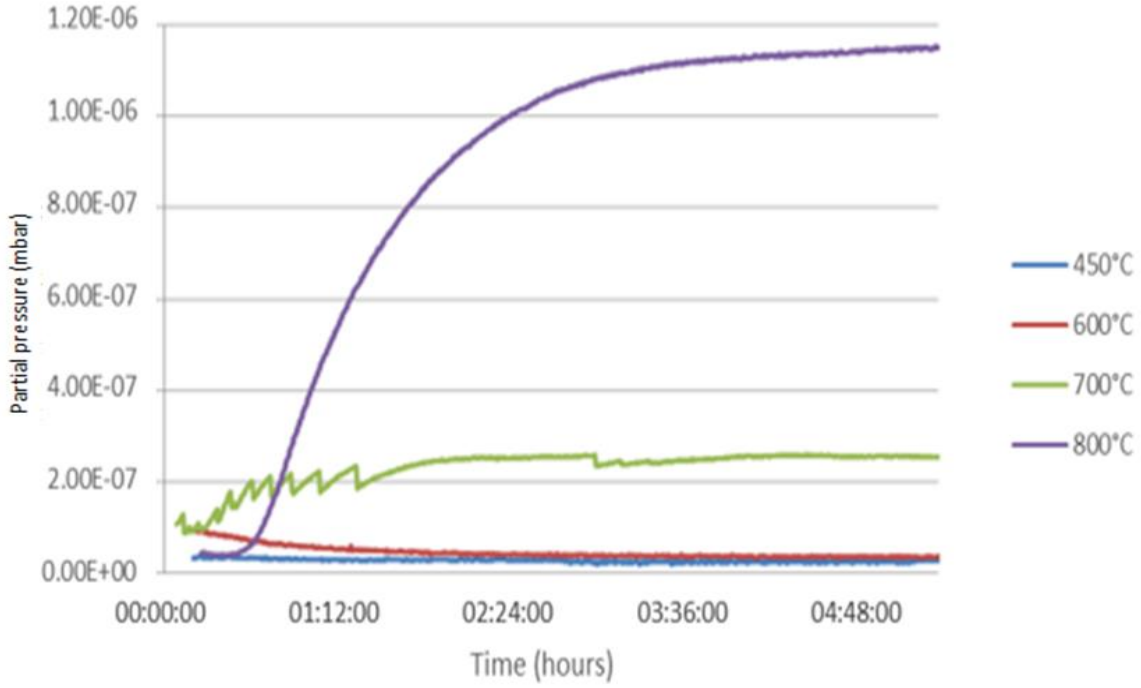

Figure 82 - Mass spectrometry data of CO_2 produced from Magnox graphite with D-mannose deposit during thermal treatment with a vacuum at various temperatures

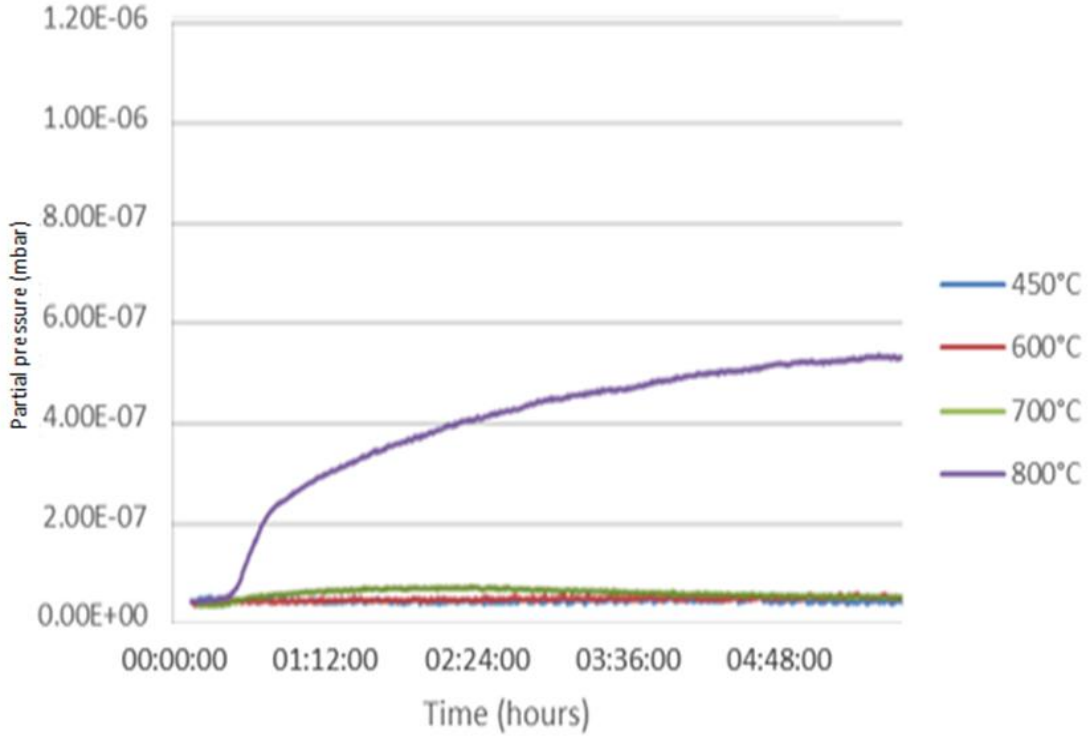

Figure 83 - Mass spectrometry data of CO_2 produced from AGR graphite with D-mannose deposit during thermal treatment with a vacuum at various temperatures

The data from the mass spectrometer confirmed the trend observed with the mass loss data by exhibiting an increase in CO_2 production during the thermal treatment at higher temperatures compared with the lower temperatures. This was the same for both Magnox graphite (Figure 82) and AGR graphite (Figure 83). CO was also produced during these experiments but several orders of magnitude lower than CO_2 so the majority of the mass loss was attributed to CO_2. There was no CO_2 production at 450°C and 600°C for both types of graphite. There was a big difference in the amount of CO_2 produced at 800°C from both types of graphite with D-mannose deposits as well as 700°C to a lesser extent. The spectra produced from Magnox graphite with D-mannose deposits thermally treated at 700°C has an unusually noisy trace compared to the rest of the data. This could be due to a drift in pressure in the mass spectrometer system.

3.15.2 Scanning Electron Microscopy

By using SEM to analyse graphite samples with a D-mannose deposit having undergone the thermal treatment process, the effectiveness of the deposit removal technique could be evaluated. Similar to the thermal treatment of virgin graphite samples with a vacuum applied, no oxidation appeared to have taken place at the lower temperatures of 450°C and 600°C. The D-mannose deposit could still be observed on the surfaces of graphite samples which had been thermally treated at these temperatures (Figure 84). However at the higher temperatures of 700°C and 800°C there was a significant change in the samples surface morphology. Not only had the D-mannose deposit been completely removed but there was also evidence that the underlying graphite had started to oxidise. The SEM images showed that the surface was very rough with numerous cracks and imperfections across the entire graphite surface.

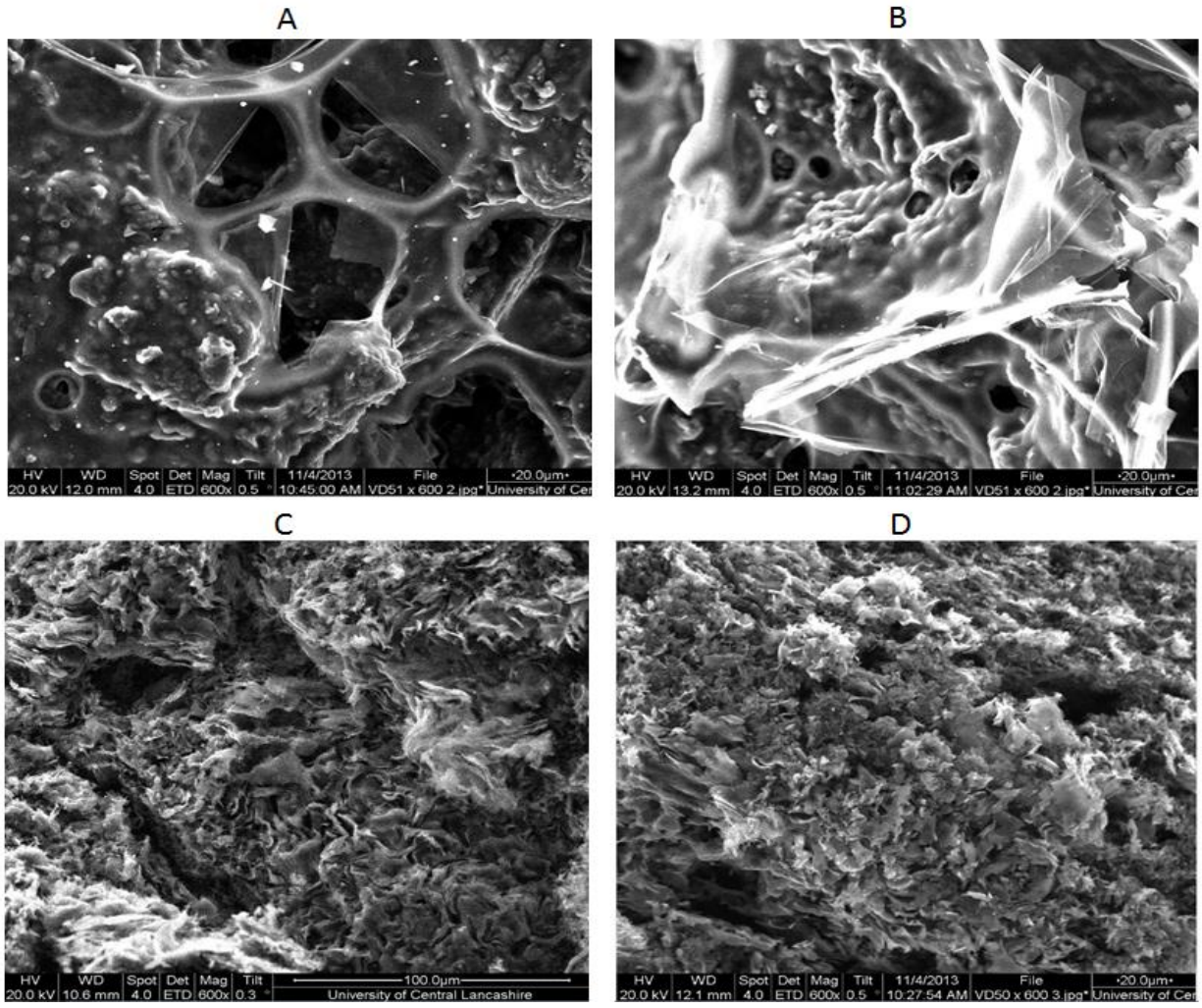

Figure 84 - SEM images at x600 magnification of Magnox graphite with a D-mannose deposit having undergone thermal treatment with a vacuum at A - 450°C, B – 600°C, C – 700°C and D – 800°C

The SEM images produced for AGR graphite with D-mannose deposits having undergone the thermal treatment process with a vacuum at various temperatures (Figure 85) followed the same trend which has been discussed previously. At the lower temperatures of 450°C and 600°C no oxidation appeared to have taken place and the presence of the D-mannose deposit was clearly visible on the graphite surface. Although at 600°C the deposit was less clearly visible in the SEM images there was no indication of oxidation from the mass spectrometry data. At the higher temperatures of 700°C and 800°C the D-mannose deposits had been completely removed with the underlying graphite beginning to oxidise as well with a significant change in the graphite surface evident. However there was significantly more evidence of oxidation on the surface of the Magnox graphite samples where the graphite surface appeared rougher with more imperfections compared to the AGR graphite. This was in corroboration with the mass spectrometry and mass loss data.

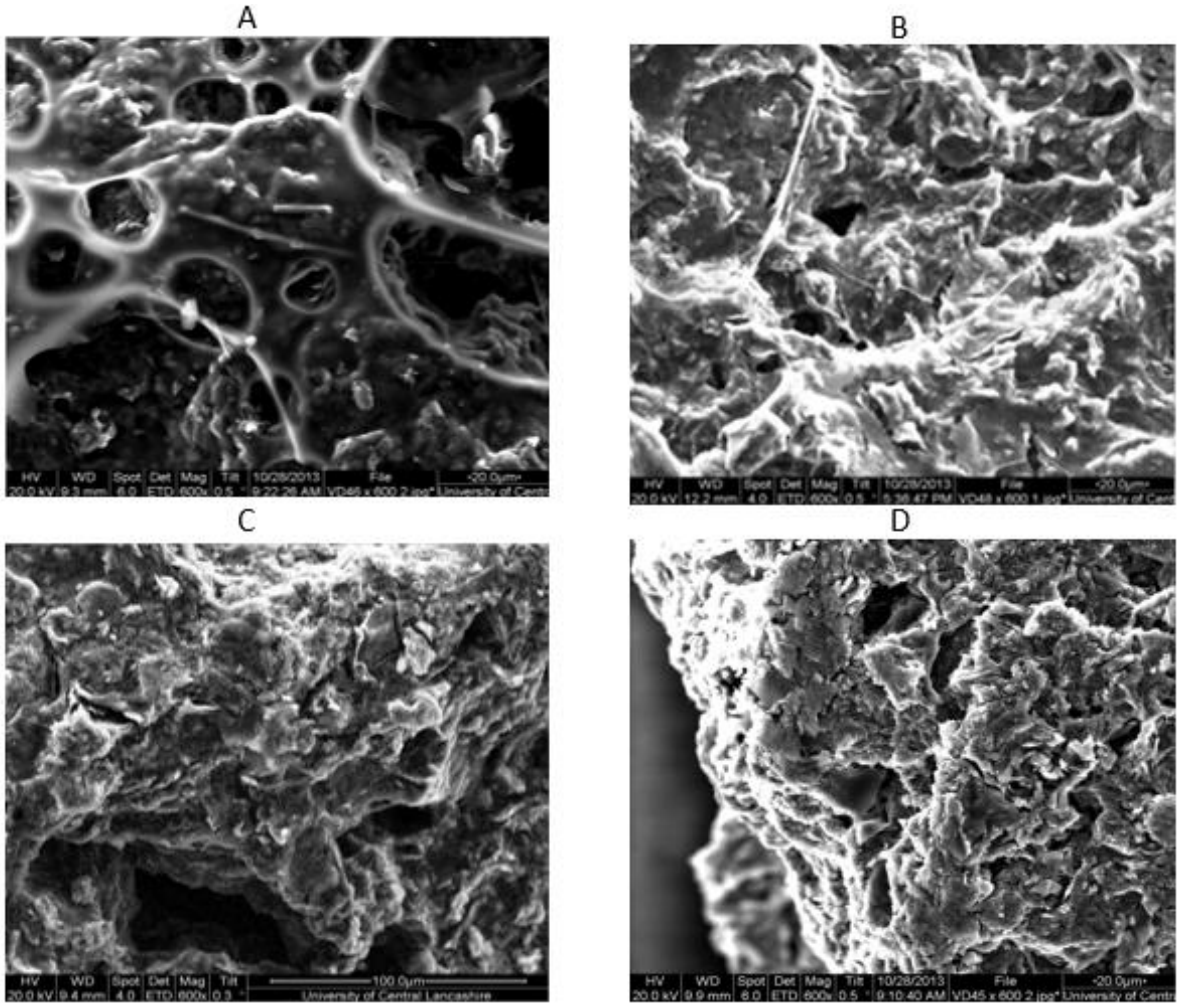

Figure 85 - SEM images at x600 magnification of AGR graphite with a D-mannose deposit having undergone thermal treatment with a vacuum at A - 450°C, B – 600°C, C – 700°C and D – 800°C

3.15.3 Raman Spectroscopy

Raman Spectroscopy was used in order to determine the removal of a deposit from the graphite surface. Several spectra were produced for both Magnox and AGR graphite samples with a D-mannose deposit present having undergone thermal treatment with a vacuum applied at various temperatures. All samples exhibited the characteristic G and D peaks at ~1580 cm^{-1} and 1350 cm^{-1} respectively. The Raman spectra for all of the Magnox samples with D-mannose deposits showed a range of intensities in the D peak which indicated the presence of disordered carbon material or carbon deposits (Figure 86). The spectra for virgin graphite showed very little disorder present in the highly crystalline material indicated by a low intensity in the D peak. Graphite with the D-mannose deposit on the surface showed a high intensity in the D peak. Samples which had undergone thermal treatment with a vacuum

at the lower temperatures of 450°C and 600°C displayed a D peak with a similar high intensity as the sample with D-mannose deposit which had not gone through the thermal treatment procedure. This confirmed the results from the SEM and mass spectrometer which showed that the D-mannose deposits were still present on the graphite surfaces at these temperatures. The 2D peak at ~2700 cm^{-1} has also changed from a sharp peak to a short broad peak in the same area with the samples treated at the lower temperatures. The samples that had undergone treatment at 700°C and 800°C showed a decrease in the D peak indicating that the deposits had been removed. The intensity of the D peak of the Magnox graphite sample thermally treated with a vacuum at 800°C was approaching the same intensity of virgin Magnox graphite.

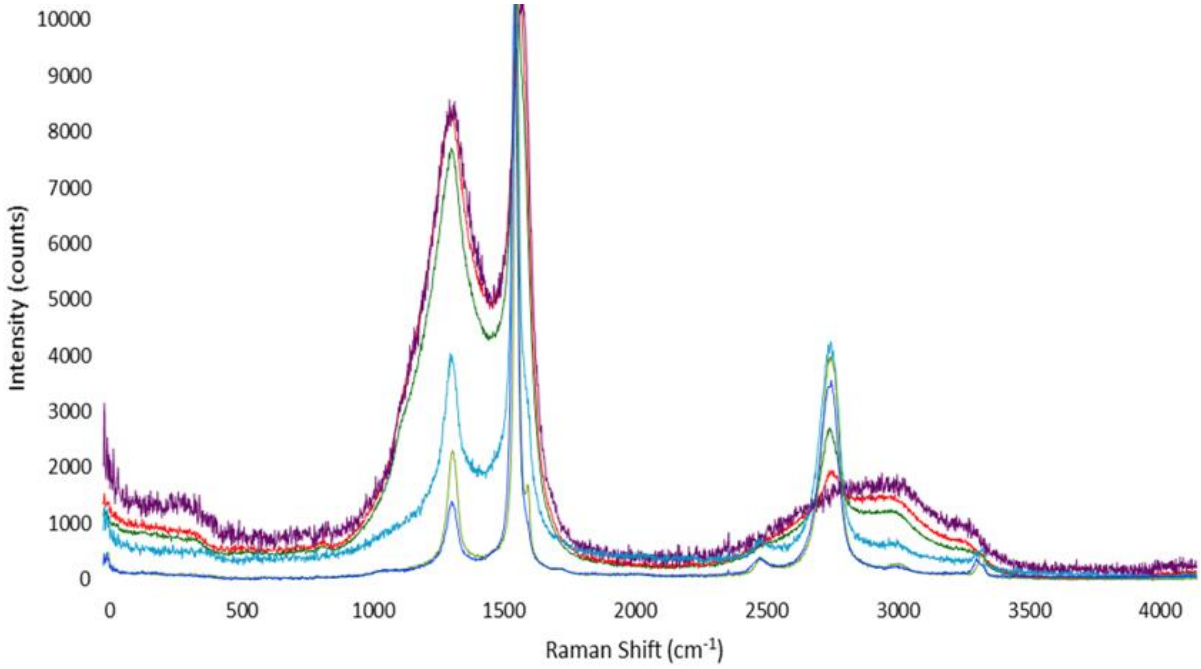

Figure 86 - Raman spectra of virgin Magnox graphite (dark blue), Magnox graphite with D-mannose deposit (dark green), Magnox graphite with D-mannose deposit after thermal treatment with a vacuum at 450°C (red), 600°C (purple), 700°C (light blue), 800°C (light green)

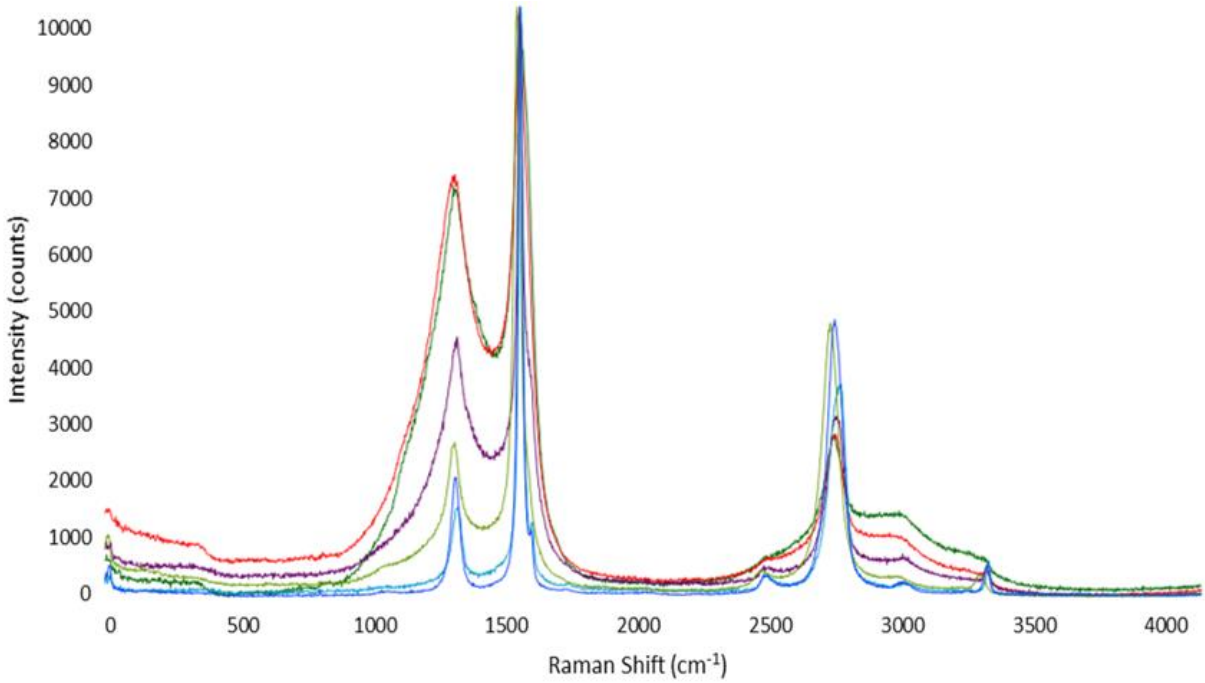

Figure 87 - Raman spectra of virgin AGR graphite (dark blue), AGR graphite with D-mannose deposit (dark green), AGR graphite with D-mannose deposit after thermal treatment with a vacuum at 450°C (red), 600°C (purple), 700°C (light blue), 800°C (light green)

The same trend could be observed from the Raman spectra produced from the AGR graphite samples with a D-mannose deposit which had been thermally treated at various temperatures with a vacuum (Figure 87). The samples treated at 450°C had an identical D peak intensity as the AGR graphite sample with D-mannose deposit without thermal treatment, which was similar to the Magnox data. However the sample treated at 600°C displayed a lower D peak intensity than the samples treated at 450°C. This difference was not observed with the Magnox data and may indicate that the deposit had started to oxidise at 600°C. Although no oxidation or significant mass change was observed during the treatment the SEM showed an alteration in the appearance of the deposit indicating that perhaps oxidation had started. The D peak intensities of samples treated at 700°C and 800°C were approaching the same intensity of virgin AGR graphite which indicated that the deposit had been removed.

In summary there is evidence that the deposit formed from the deposition of D-mannose can be removed by a thermal treatment with a vacuum at a temperature lower than that at which significant bulk graphite oxidation occurs. This is supported by both Raman and SEM analysis. The results indicate that the deposit formed on the AGR graphite is perhaps more reactive from the SEM images and Raman spectroscopy however, this is not substantiated from the evolved gas analysis.

3.16 D-mannose deposit without a vacuum

The following section will provide information on the removal of D-mannose deposits from the surface of Magnox graphite during the thermal treatment at various temperatures without the application of a vacuum.

3.16.1 Scanning Electron Microscopy

During the thermal treatments without the use of a vacuum oxidation will occur at lower temperatures compared to the thermal treatment with a vacuum. This is because the partial pressure of oxygen is higher and so will react with the carbon surface more readily compared to when a vacuum is applied and the partial pressure of oxygen is lower. The SEM images produced for samples during these experiments confirms this statement as the deposits had been completely removed from samples treated at all four temperatures even the lower temperature of 450°C (Figure 88). At each temperature the SEM images showed that the D-mannose deposit had been removed leaving behind a rough irregular surface which indicated that the underlying graphite had started to oxidise.

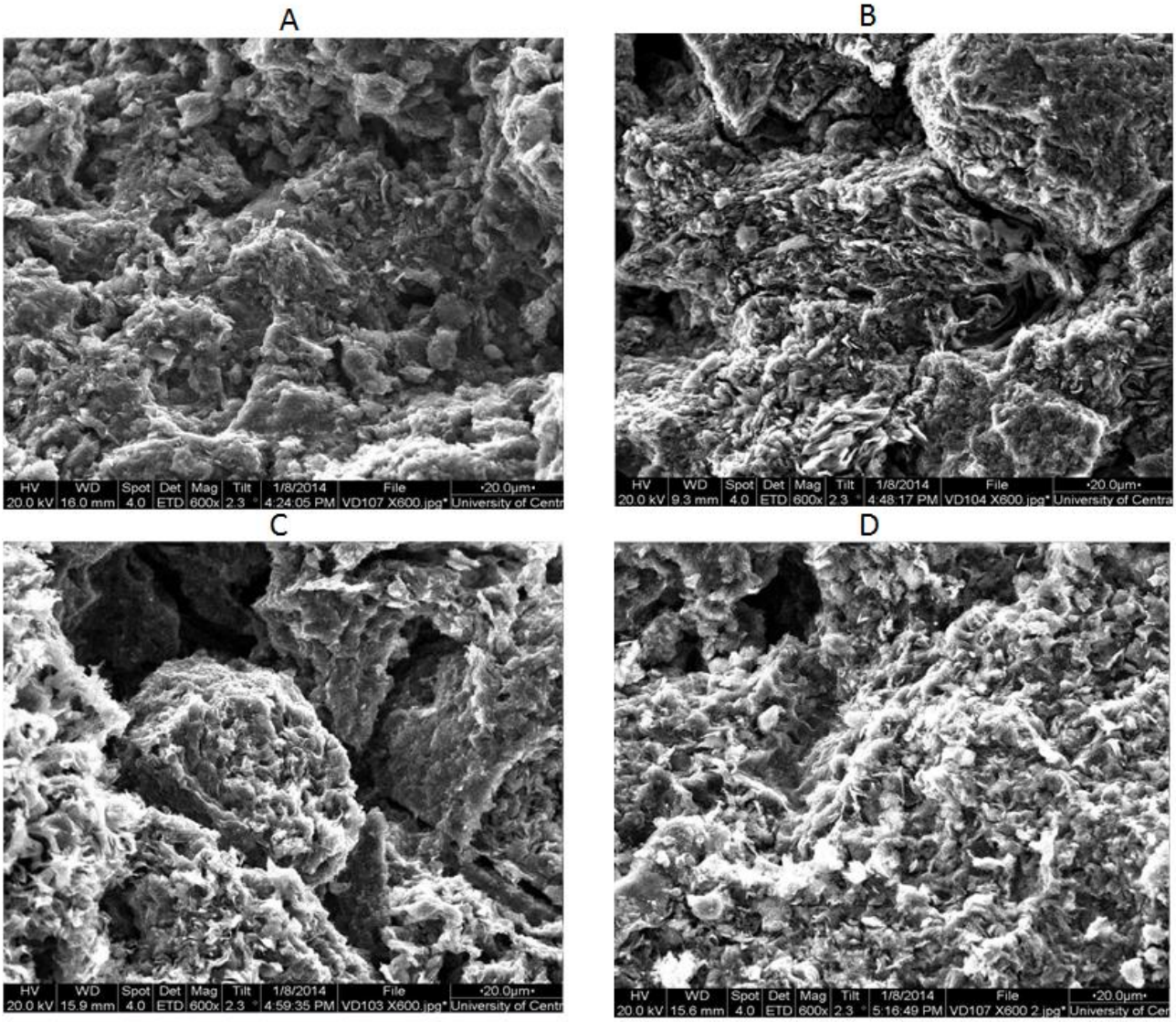

Figure 88 - SEM images at x600 magnification of Magnox graphite with a D-mannose deposit having undergone thermal treatment without a vacuum at A - 450°C, B – 600°C, C – 700°C and D – 800°C

3.16.2 Mass spectrometry and mass loss

The percentage mass lost during these experiments exhibited a similar trend to that observed with the mass lost by samples thermally treated with a vacuum, in that the percentage mass loss increased with increasing temperature. Similar mass losses were observed from the thermally treated samples at the higher temperatures of 700°C and 800°C which both lost ~55% (Figure 89).

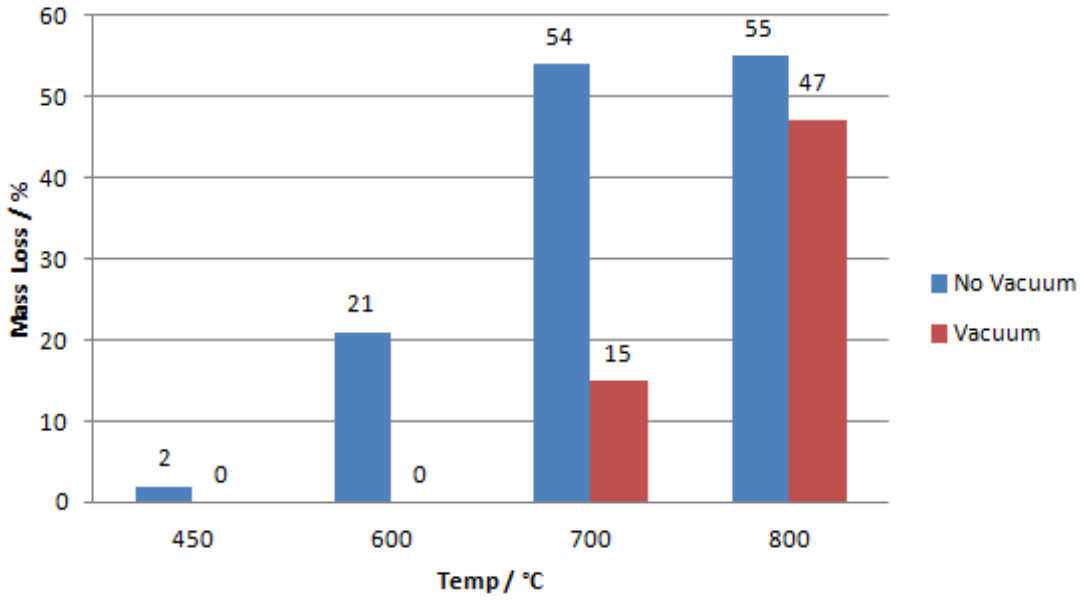

Figure 89 - Comparison of the percentage mass loss of Magnox graphite with D-mannose deposit during thermal treatment at various temperatures with and without a vacuum

Although higher, the mass lost by the treated sample at 800°C without a vacuum (~55%) was fairly similar to the mass lost by the sample treated at this temperature with a vacuum (~47%). At 700°C the mass lost had increased from ~15% with a vacuum to ~54% without a vacuum. Furthermore the mass losses at the lower temperatures of 450°C and 600°C increased from negligible amounts with a vacuum to ~2% and ~21% respectively.

The data produced from the mass spectrometer showed a steady increase in the amount of CO_2 produced as the temperature of the treatment increases (Figure 90). It was difficult to observe whether any CO_2 had been produced from the mass spectrometer data for the sample treated at 450°C. However the SEM images showed that the deposits had been completely removed from the graphite surface. Therefore the mass spectrometer data for the data at 450°C was expanded (Figure 91). It was now observed that CO_2 had been produced during the thermal treatment at 450°C just on a smaller scale than the rest of the isothermal experiments. This data displayed an initial peak and then decline of CO_2 produced suggesting that the deposit was oxidised first with minimal oxidation to the graphite underneath.

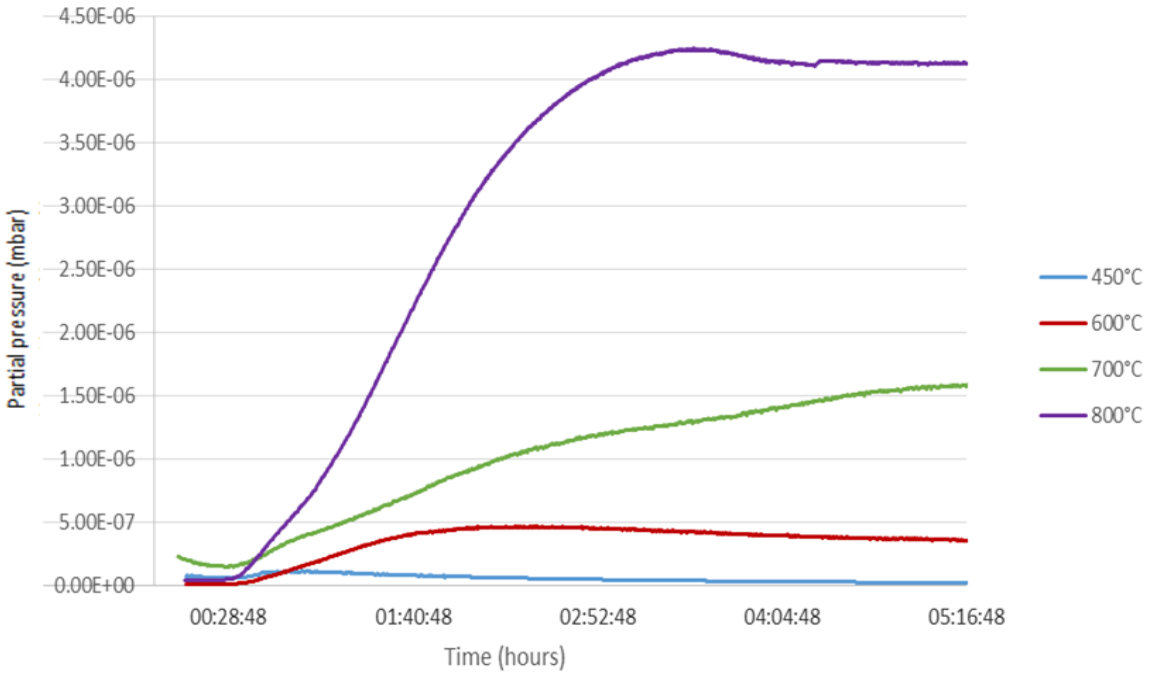

Figure 90 - Mass spectrometry data of CO_2 produced from Magnox graphite with D-mannose deposit during thermal treatment without a vacuum at various temperatures

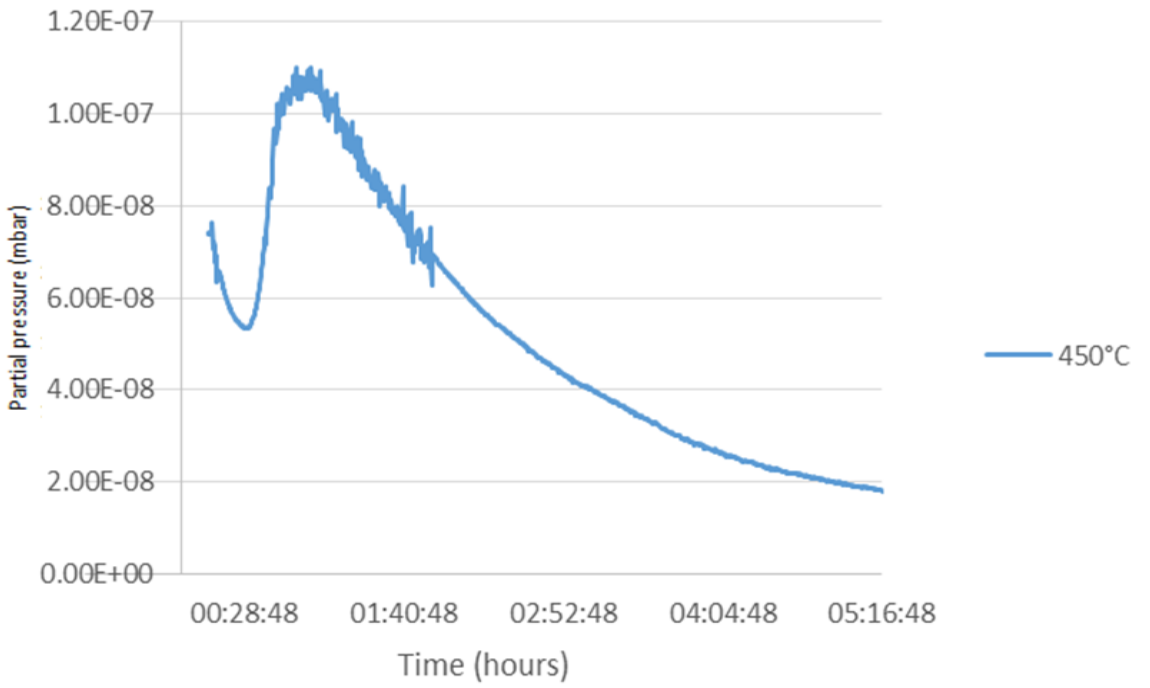

Figure 91 - Mass spectrometry data of CO_2 produced from Magnox graphite with D-mannose deposit during thermal treatment without a vacuum at 450°C

3.16.3 Raman Spectroscopy

Raman Spectroscopy was used in order to determine the removal of a deposit from the graphite surface. Several spectra were produced for Magnox graphite samples with a D-mannose deposit present having undergone thermal treatment without the application of a vacuum at various temperatures. All samples exhibited the characteristic G and D peaks at ~1580 cm^{-1} and 1350 cm^{-1} respectively. The Raman spectra for all of the samples with D-mannose deposits showed a range of intensities in the D peak which indicated the presence of disordered carbon material or carbon deposits (Figure 92).

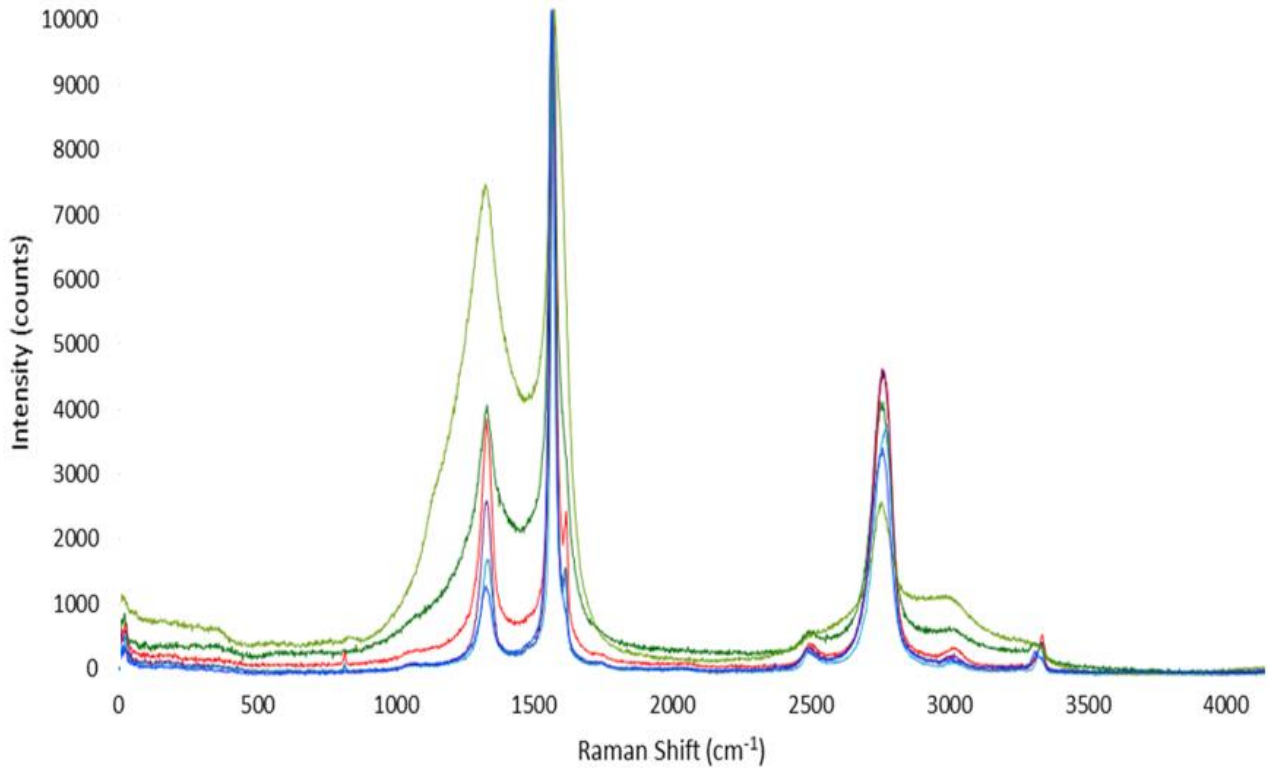

Figure 92 - Raman spectra of virgin Magnox graphite (dark blue), Magnox graphite with D-mannose deposit (light green), Magnox graphite with D-mannose deposit after thermal treatment without a vacuum at 450°C (dark green), 600°C (red), 700°C (purple), 800°C (light blue)

The spectra for virgin graphite displayed a D peak with the lowest intensity indicating that there was very little disorder present in the highly crystalline graphitic material. Graphite with the D-mannose deposit on the surface showed the highest intensity in the D peak. All thermally treated samples without a vacuum showed a lower D peak intensity compared to the D peak of a sample that had not been thermally treated. This differed from the data produced from samples treated with a vacuum as deposits were still present after treatment at 450°C and 600°C and so the D peak intensity was the same as a sample that had not been thermally treated. The 2D peak at ~2700 cm^{-1} was present as a sharp peak for all of the samples. While SEM and mass spectrometer data confirmed that the deposits had been removed the intensity of the D peak for samples treated at 450°C and 600°C was higher than the intensity of the D peak of virgin Magnox graphite, although was less than the D peak of D-mannose deposits without thermal treatment. This may be due to the fact that the surface of the graphite sample had been completely altered through oxidation and there had been an increase in disorder. However the samples treated at the higher temperatures where the graphite surface had been significantly changed through oxidation, exhibited a lower intensity in the D peak similar to that of virgin graphite.

In summary all samples thermally treated without a vacuum exhibited higher reactivity and mass lost compared to the samples treated with a vacuum due to an increased partial pressure of oxygen. Furthermore there is a larger range in reactivity exhibited from samples treated with a vacuum compared to samples treated without. Samples thermally treated at 700°C and 800°C without a vacuum have very similar mass losses and reactivity. This indicates that these parameters are approaching the maximum oxidation rate capable with this apparatus.

3.17 C-12 Microwave deposits with a vacuum

The following section will provide information on the removal of C-12 microwave deposits from the surface of both Magnox and AGR graphite during the thermal treatment at various temperatures with a vacuum applied.

3.17.1 Mass spectrometry and mass loss

The percentage mass loss of both Magnox and AGR graphite samples with C-12 microwave deposits during the thermal treatment with a vacuum at a variety of temperatures (Figure 93) exhibited a similar trend to that observed with virgin graphite, in that as the temperature increased so did the amount of oxidation and so the percentage mass loss.

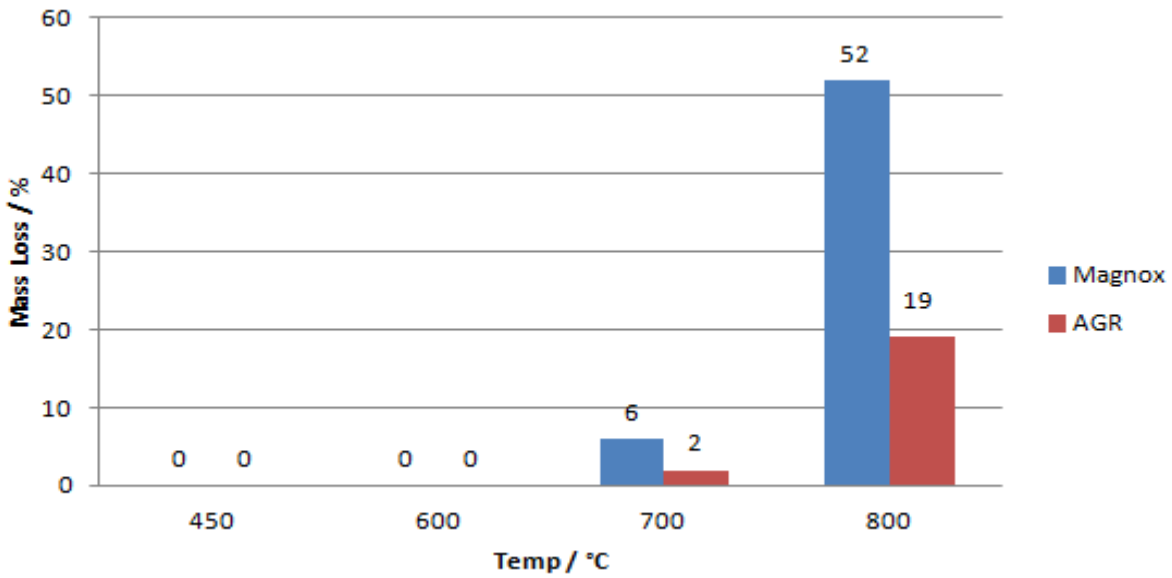

Figure 93 - Comparison of the percentage mass loss of both Magnox and AGR graphite with C-12 microwave deposit during thermal treatment at various temperatures with a vacuum

There was no evidence of oxidation from samples which had been thermally treated at 450°C and 600°C as there was negligible mass lost from the samples. Similar to the results from the thermal treatment of virgin graphite and graphite with D-mannose deposits, at the higher temperatures of 700°C and 800°C the Magnox graphite samples displayed a higher amount of mass loss compared to the AGR graphite samples. Magnox graphite samples with C-12 microwave deposits exhibited a mass loss of ~6% at 700°C compared to AGR graphite with C-12 microwave deposits which only lost ~2%. At 800°C Magnox graphite with C-12 microwave deposits lost ~52% compared to AGR graphite with C-12 microwave deposits

which only lost ~19%. In most cases Magnox graphite samples with C-12 microwave deposits displayed similar mass losses to both virgin Magnox graphite (Figure 66) and Magnox graphite with D-mannose deposits (Figure 81). However the thermal treatment of Magnox graphite with C-12 microwave deposits at 700°C generated a mass loss of only ~6%. This was very low compared to the ~19% lost by virgin Magnox and ~15% lost by Magnox graphite with D-mannose deposits. Perhaps the deposits produced using the microwave plasma technique produced a deposit which was strongly bonded and more thermally stable than the samples with the D-mannose deposit even though it appeared to have a higher surface area which would make it more reactive. The deposits produced using a microwave plasma show a similar slow oxidation rate as that exhibited by deposits found on reactor graphite presented in later sections (3.21.2). However the differences could also be due to the variance in size of the particles which make up the samples which were thermally treated.

Regarding the AGR graphite samples the thermal treatment of samples with C-12 microwave deposits produced similar mass losses to both the samples with D-mannose deposits and the virgin AGR material. The thermal treatment at 800°C of AGR graphite with C-12 microwave deposits produced a mass loss of ~19% which was similar to the ~18% mass loss observed from AGR graphite with D-mannose deposits and the ~16% lost by virgin AGR graphite. At 700°C AGR samples with C-12 microwave deposits exhibited a loss of ~2% slightly less than the ~5% lost by virgin AGR graphite.

The data from the mass spectrometer confirmed the trend observed with the mass loss data by exhibiting an increase in CO_2 production during the thermal treatment at higher temperatures compared with the lower temperatures. This was the same for both Magnox graphite (Figure 94) and AGR graphite (Figure 95). CO was also produced during these experiments but several orders of magnitude lower than CO_2 so the majority of the mass loss was attributed to CO_2. Although there was negligible mass lost from the samples which underwent thermal treatment at 450°C and 600°C there was a very small CO_2 peak produced at the start of each experiment. This was most likely caused by oxidation of loosely held material or partial oxidation of the deposit however samples showed very little change in mass. The thermal treatment at 700°C of graphite with C-12 microwave deposits produced a similar mass loss and CO_2 production with both AGR and Magnox graphite.

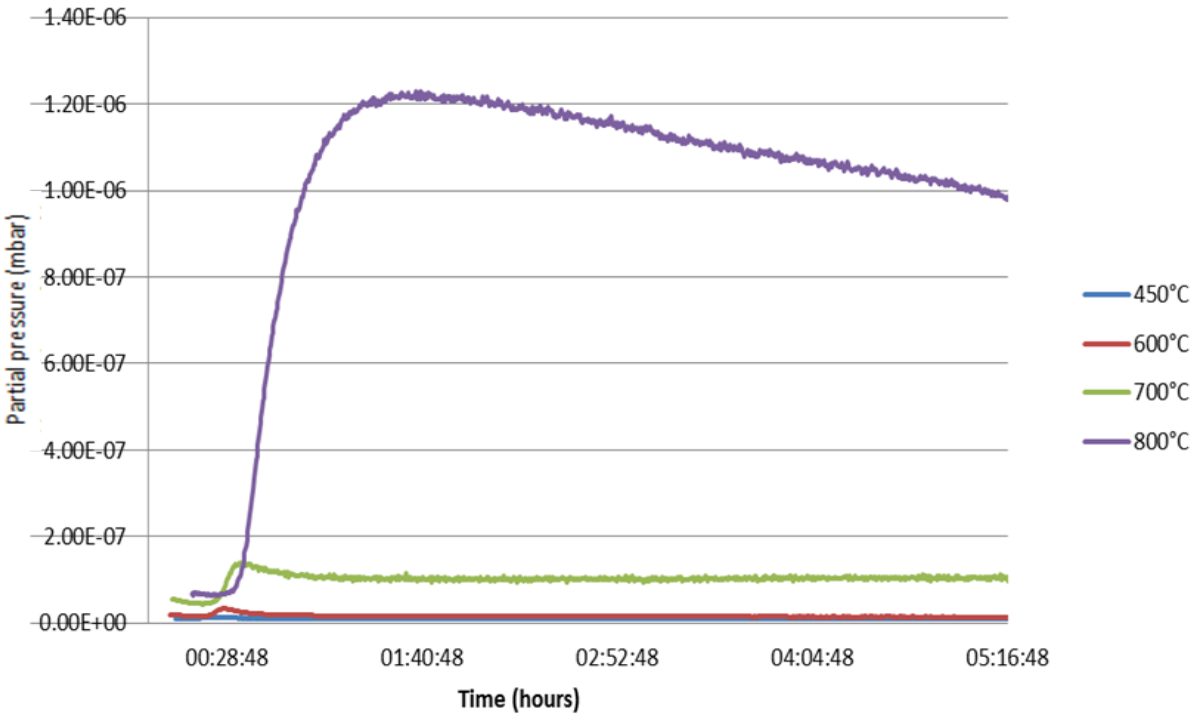

Figure 94 - Mass spectrometry data of CO_2 produced from Magnox graphite with C-12 microwave deposits during thermal treatment with a vacuum at various temperatures

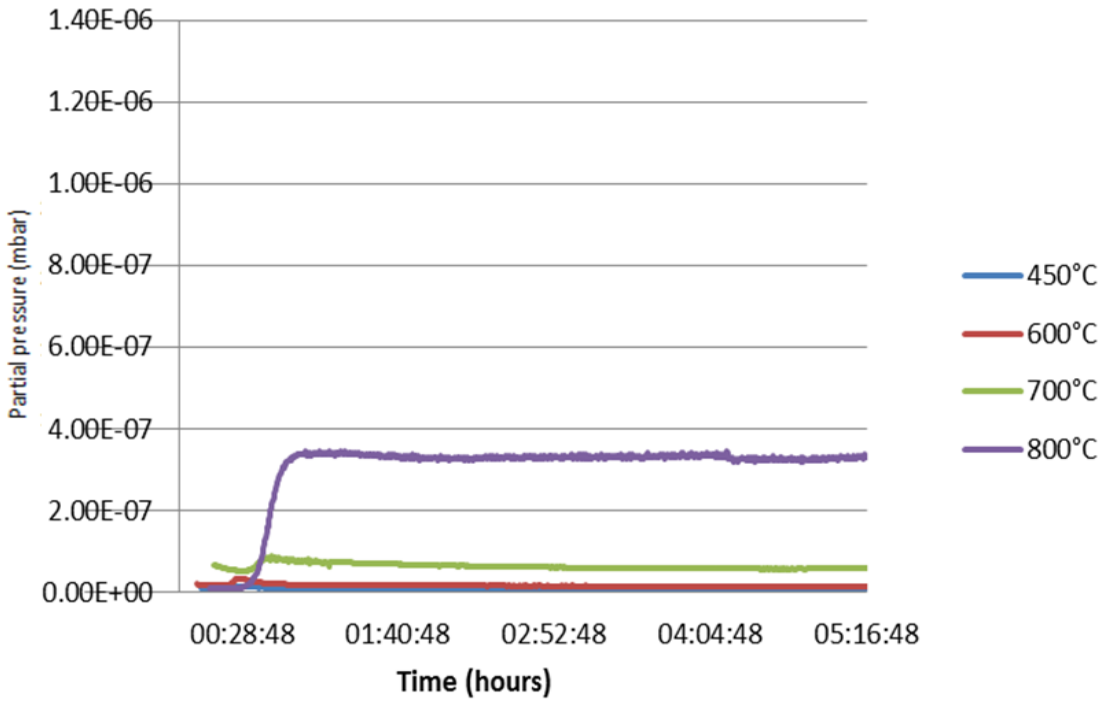

Figure 95 - Mass spectrometry data of CO_2 produced from AGR graphite with C-12 microwave deposits during thermal treatment with a vacuum at various temperatures

3.17.2 Scanning Electron Microscopy

SEM was used to analyse graphite samples with a C-12 microwave deposit which had undergone thermal treatment. This was carried out in order to determine the effectiveness of the technique for deposit removal. Graphite samples with C-12 microwave deposits do not exhibit signs of oxidation taking place at the lower temperatures of 450°C and 600°C (Figure 96). The 'cauliflower' like morphology of the C-12 microwave deposits could still be observed on the surfaces of graphite samples which had been thermally treated at these temperatures. These results are similar to the results from the thermal treatment with a vacuum applied of virgin graphite samples and graphite with D-mannose deposits which showed little evidence of oxidation occurring. However at the higher temperatures of 700°C and 800°C there was a significant change in the samples surface morphology. Not only had the C-12 microwave deposit been completely removed but there was also evidence that the underlying graphite had started to oxidise. The SEM images showed that the surface was very rough with numerous cracks and imperfections across the entire graphite surface.

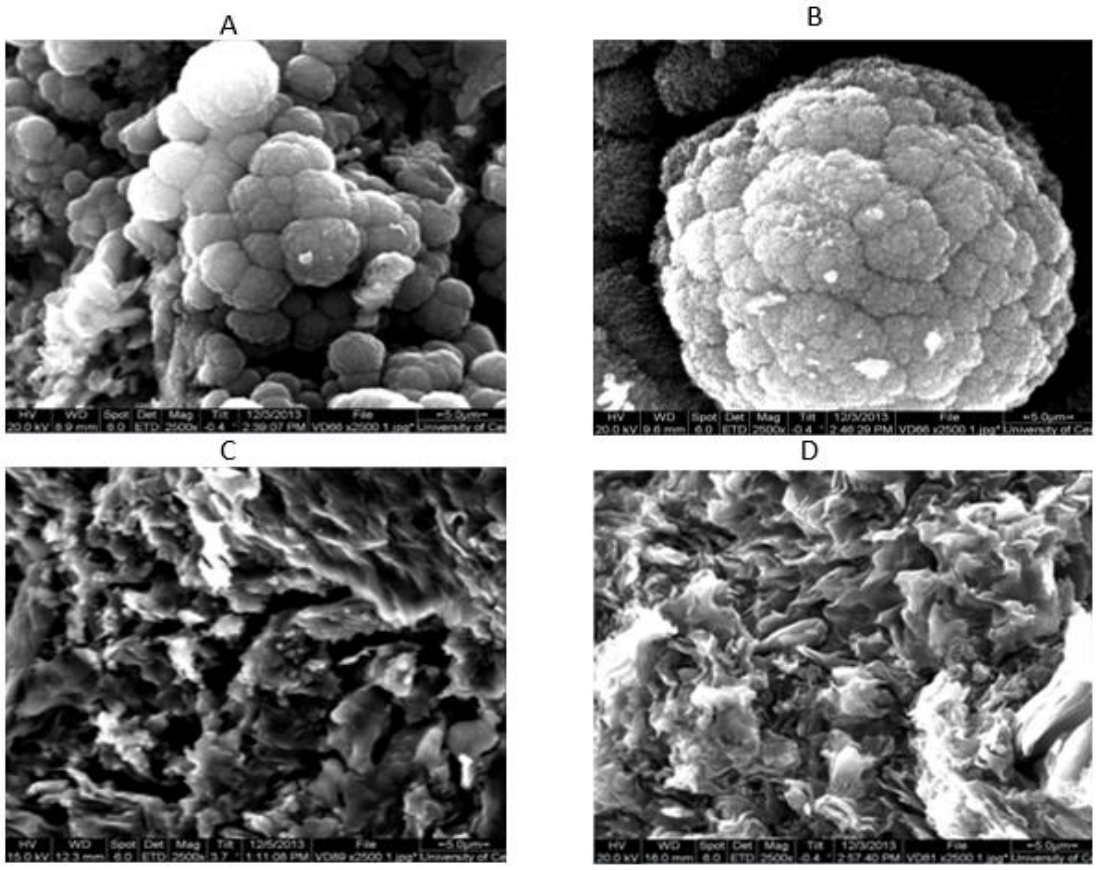

Figure 96 - SEM images at x2500 magnification of Magnox graphite with a C-12 microwave deposit having undergone thermal treatment with a vacuum at A - 450°C, B – 600°C, C – 700°C and D – 800°C

The SEM images produced for AGR graphite with C-12 microwave deposits having undergone the thermal treatment process with a vacuum at various temperatures (Figure 97) followed the same trend which has been discussed previously. At the lower temperatures of 450°C and 600°C no oxidation had taken place and the presence of the 'cauliflower' like deposit was clearly visible on the graphite surface. At the higher temperatures of 700°C and 800°C the C-12 microwave deposits have been completely removed and a change in the graphite surface is evident suggesting that the underlying graphite had started to oxidise. However there was significantly more evidence of oxidation on the surface of the Magnox graphite samples which exhibited a rough surface with numerous cracks compared to the AGR graphite. This was in corroboration with the mass spectrometry and mass loss data.

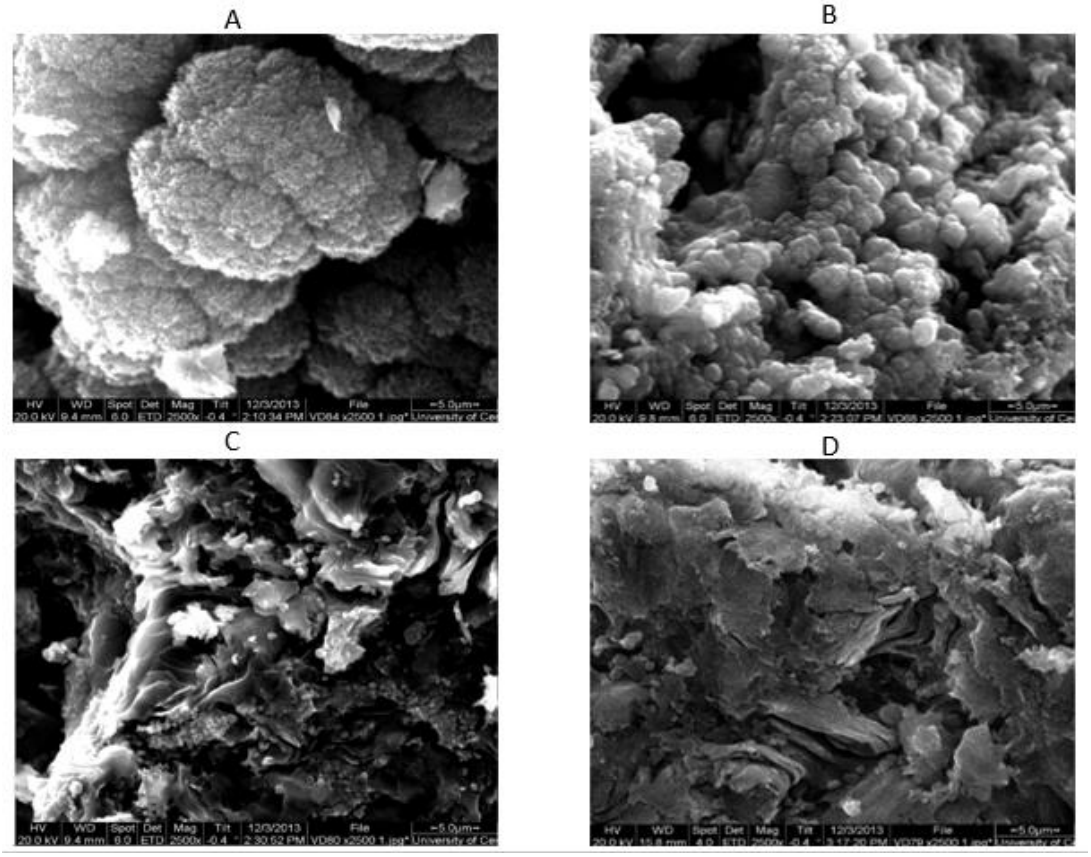

Figure 97 - SEM images at x2500 magnification of AGR graphite with a C-12 microwave deposit having undergone thermal treatment with a vacuum at A - 450°C, B – 600°C, C – 700°C and D – 800°C

3.17.3 Raman Spectroscopy

Raman Spectroscopy was used in order to determine the removal of a deposit from the graphite surface. Several spectra were produced for both Magnox and AGR graphite samples

with a C-12 microwave deposit present having undergone thermal treatment with a vacuum applied at various temperatures. All samples exhibited the characteristic G and D peaks at ~1580 cm^{-1} and 1350 cm^{-1} respectively. The Raman spectra for all of the Magnox samples with C-12 microwave deposits showed a range of intensities in the D peak which indicated the presence of disordered carbon material or carbon deposits (Figure 98). The spectra for virgin graphite showed very little disorder present in the highly crystalline material indicated by a low intensity in the D peak. Graphite samples with the C-12 microwave deposits which have not been thermally treated exhibited a much higher intensity in the D peak and were equal to the intensity of the samples which had been thermally treated with a vacuum at the lower temperatures of 450°C and 600°C. This confirms the results from the SEM and mass spectrometer which showed that the C-12 microwave deposits were still present on the graphite surfaces at these temperatures. The samples that have undergone thermal treatment at 700°C and 800°C showed a decrease in the intensity of the D peak which was approaching the same intensity as virgin Magnox graphite indicating the carbonaceous deposits had been successfully removed.

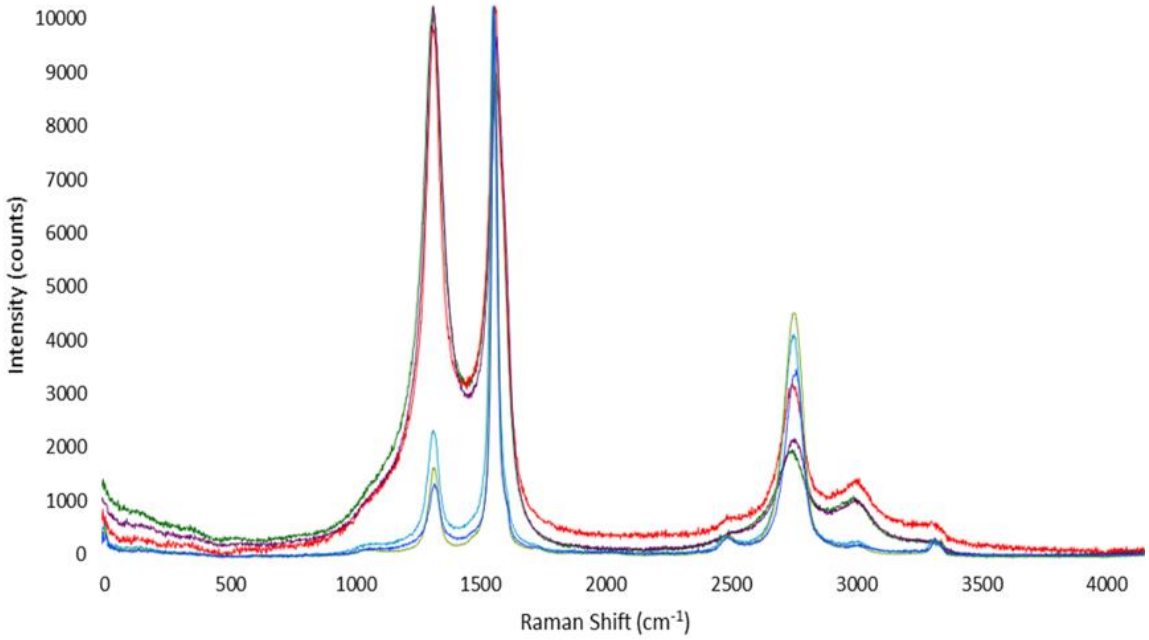

Figure 98 - Raman spectra of virgin Magnox graphite (dark blue), Magnox graphite with C-12 microwave deposit (dark green), Magnox graphite with C-12 microwave deposit after thermal treatment with a vacuum at 450°C (red), 600°C (purple), 700°C (light blue), 800°C (light green)

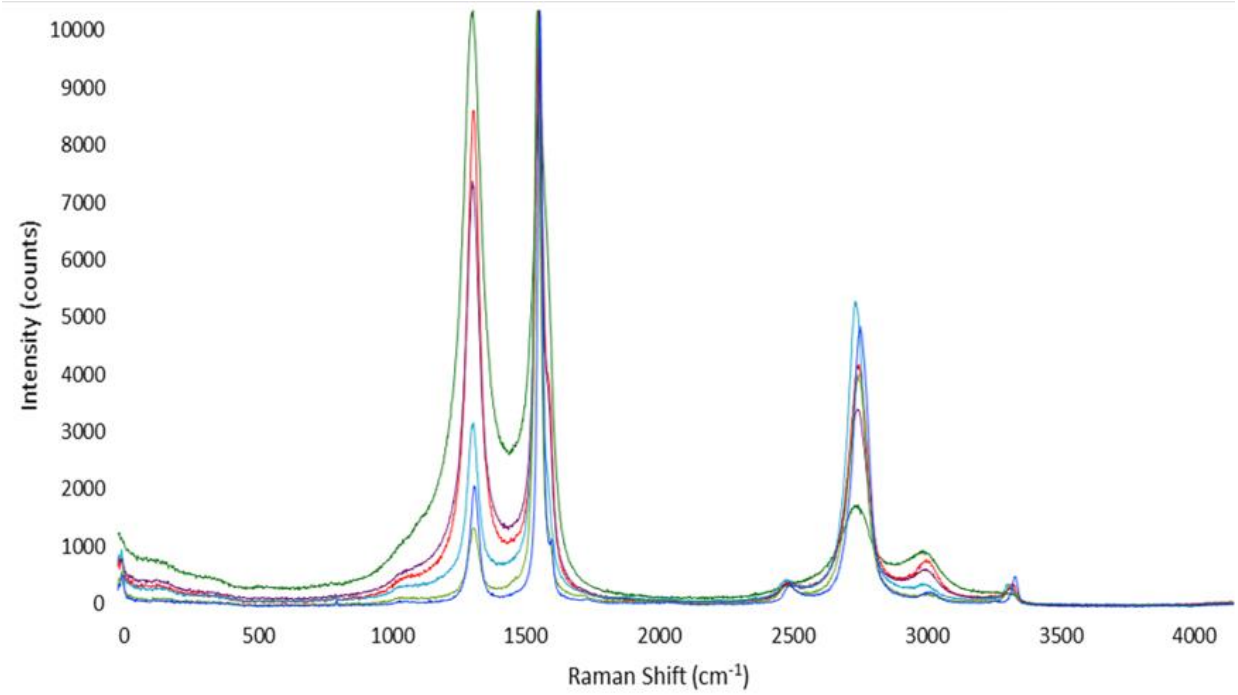

Figure 99 - Raman spectra of virgin AGR graphite (dark blue), AGR graphite with C-12 microwave deposit (dark green), AGR graphite with C-12 microwave deposit after thermal treatment with a vacuum at 450°C (red), 600°C (purple), 700°C (light blue), 800°C (light green)

A similar trend could be observed from the Raman spectra produced from the AGR graphite samples with C-12 microwave deposits which had been thermally treated at various temperatures with a vacuum (Figure 99). However the samples treated at 450°C and 600°C displayed a lower D peak intensity than the samples which had not been thermally treated. This difference was not observed with the Magnox data and indicated that the deposit had started to oxidise at these lower temperatures. While the SEM images did not show a significant change in the deposit the mass spectrometer data did display a minute amount of CO_2 produced at the start of each experiment. Perhaps this was due to the partial oxidation of the deposit which oxidised at a lower temperature from the rest of the deposit and was the reason for the difference in the Raman spectra. Although there was no reason why this change would not be present in the Magnox data so may just be due to sample variation. The samples that have undergone thermal treatment at 700°C and 800°C showed a decrease in the intensity of the D peak which was approaching the same intensity as virgin AGR graphite indicating the carbonaceous deposits had been successfully removed. This statement was confirmed by the SEM images which showed only an oxidised graphite surface with no presence of the ‘cauliflowers’ which make up the C-12 microwave deposit.

3.18 C-12 Microwave deposits without a vacuum

The following section will provide information on the removal of C-12 microwave deposits from the surface of Magnox graphite during the thermal treatment at various temperatures without the application of a vacuum.

3.18.1 Mass spectrometry and mass loss

The percentage mass lost during these experiments exhibited a similar trend to that observed with the mass lost by samples thermally treated with a vacuum, in that the percentage mass loss increased with increasing temperature. However there was always a greater amount of mass lost from samples treated without a vacuum then with one (Figure 100).

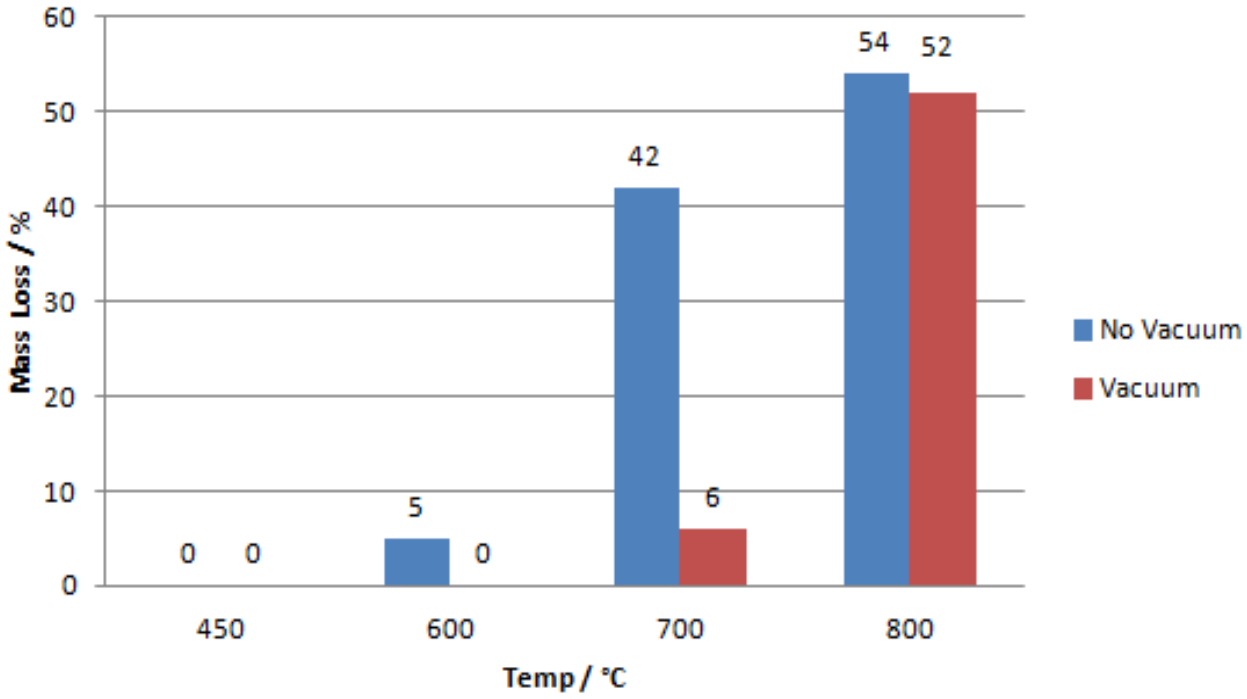

Figure 100 - Comparison of the percentage mass loss of Magnox graphite with C-12 microwave deposit during thermal treatment at various temperatures with and without a vacuum

Although higher, the mass lost by the thermally treated sample at 800°C without a vacuum (~54%) was fairly similar to the mass lost by the sample treated at this temperature with a vacuum (~52%). At 700°C the mass lost had increased from ~6% with a vacuum to ~42% without a vacuum. Whilst the mass lost at the lower temperature of 450°C without a vacuum remained as negligible as the mass lost at this temperature with a vacuum, at 600°C there was an increase of ~5% mass lost by the sample treated without a vacuum compared the negligible amount lost during treatment with a vacuum.

Also all samples thermally treated without a vacuum exhibited a higher mass lost compared to the samples treated with a vacuum due to an increased partial pressure of oxygen and a faster rate of reaction. Similar to the results of the thermally treated graphite with D-mannose deposits, samples thermally treated at 700°C and 800°C without a vacuum have a very similar amount of mass loss. This indicates that under these conditions the rate of oxidation is approaching a maximum and the experiments are likely under oxygen limiting conditions.

The data produced from the mass spectrometer showed a steady increase in the amount of CO_2 produced as the temperature of the treatment increased (Figure 101). The mass spectrometer trace at 800°C seems to show two different oxidation profiles. This may indicate that the deposit has been removed after 3 hours and the CO_2 produced after this time is attributed to the underlying graphite. This should be repeated to confirm as it could also be due to the possible drift in pressure of the mass spectrometer. At the higher temperatures of 700°C and 800°C the amount of CO_2 detected appeared to be more gradually produced over the period of the isotherm rather than a steady rate of production which was observed from the mass spectrometer data with the application of a vacuum (Figure 94). This comparison indicated that conducting the thermal treatment with a vacuum applied to the system controlled the reaction rate, because there is less oxygen present in the system then less carbon is able to react with it to form CO_2 and so less underlying graphite is oxidised. This would be beneficial to a decontamination process which would remove carbon deposits from reactor graphite, providing the deposits were richer in C-14 than the underlying graphite.

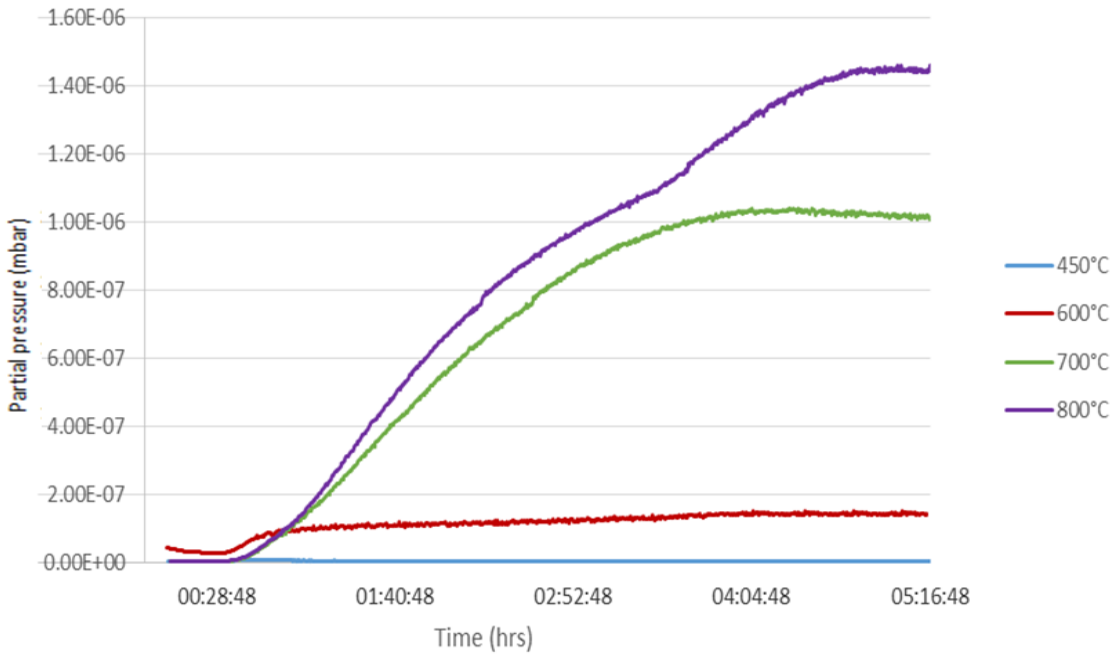

Figure 101 - Mass spectrometry data of CO_2 produced from Magnox graphite with C-12 microwave deposit during thermal treatment without a vacuum at various temperatures

3.18.2 Scanning Electron Microscopy

During the experiments without the use of a vacuum oxidation will occur at lower temperatures compared to the thermal treatment with a vacuum as there is more oxygen readily available to react with the carbon surface. The SEM images produced from Magnox graphite samples with C-12 microwave deposits which have been thermally treated at various temperatures without the use of a vacuum show this to be the case (Figure 102).

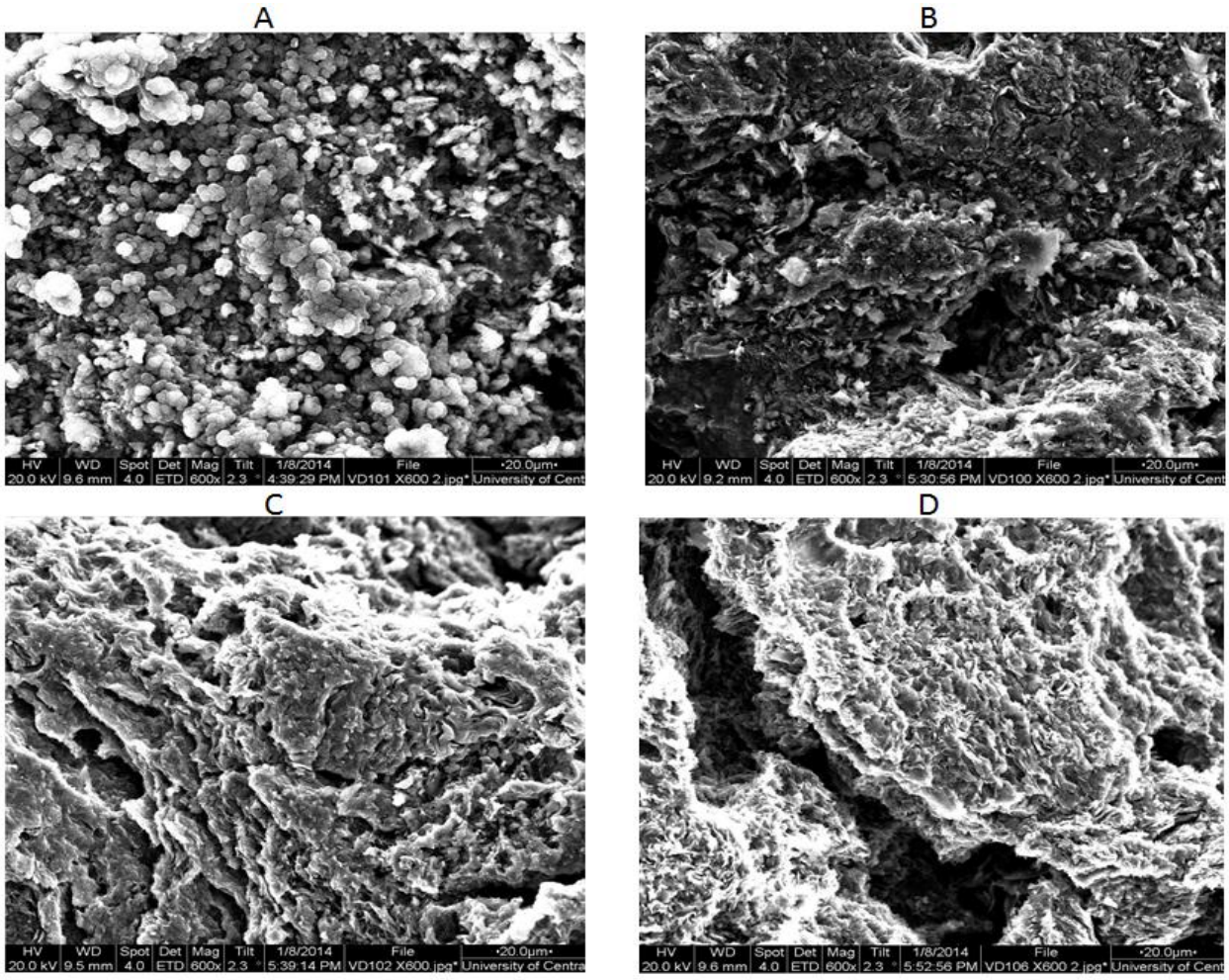

Figure 102 - SEM images at x600 magnification of Magnox graphite with a C-12 microwave deposit having undergone thermal treatment without a vacuum at A - 450°C, B – 600°C, C – 700°C and D – 800°C

Although the 'cauliflower' like morphology of the C-12 microwave deposits can still be observed on the surfaces of graphite samples treated at 450°C they have been completely removed during the treatment at 600°C. This differed from the results produced from samples with C-12 microwave deposits treated at 600°C with a vacuum, as the deposit remained on the surface after this treatment. At the higher temperatures the C-12 microwave deposits have been completely removed and the remaining graphite surface appears rough and cracked indicating that it had also started to oxidise during the process.

3.18.3 Raman Spectroscopy

Raman Spectroscopy was used in order to determine the removal of a deposit from the graphite surface. Several spectra were produced for Magnox graphite samples with a C-12 microwave deposit present having undergone thermal treatment without the application of a

vacuum at various temperatures. All samples exhibit the characteristic G and D peaks at ~1580 cm^{-1} and 1350 cm^{-1} respectively (Figure 103).

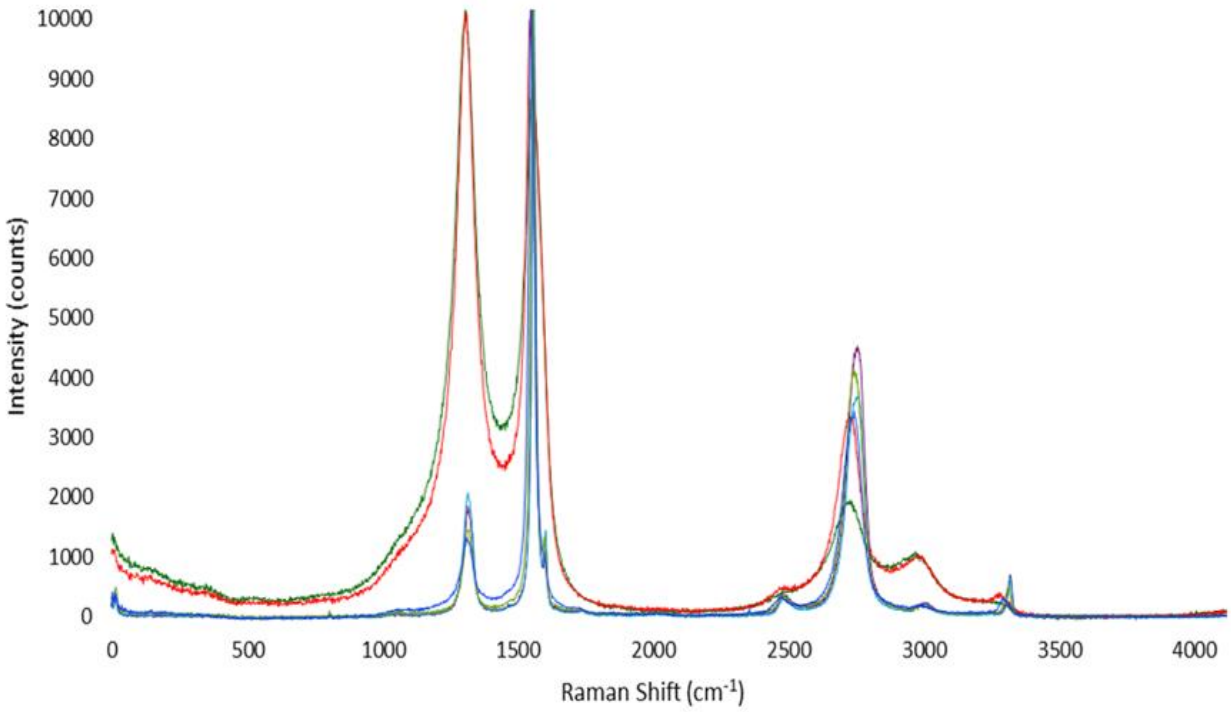

Figure 103 - Raman spectra of virgin Magnox graphite (dark blue), Magnox graphite with C-12 microwave deposit (dark green), Magnox graphite with C-12 microwave deposit after thermal treatment without a vacuum at 450°C (red), 600°C (purple), 700°C (light blue), 800°C (light green)

The spectra for virgin graphite displayed a D peak with the lowest intensity indicating that there was very little disorder present in the highly crystalline graphitic material. Graphite with the C-12 microwave deposit on the surface showed the highest intensity in the D peak which indicated the presence of disordered carbon present on the sample. The intensity of the D peak displayed by the sample which was thermally treated at 450°C was equal to that produced from a sample which had not been treated thermally, which shows that the deposit had not been altered during the treatment at this temperature. The SEM images produced from this sample also confirmed that the deposits had not been removed after treatment at 450°C. The 2D peak at ~2700 cm^{-1} was present as a sharp peak for all of the samples. The intensity of the D peak for the samples treated without a vacuum at 600°C, 700°C and 800°C were approaching the same intensity as that produced from virgin graphite. This along with the SEM images and mass spectrometer data showed that the C-12 microwave deposits have been successfully removed during treatment at these temperatures without the use of a vacuum.

3.19 C-13 Microwave deposits with a vacuum

The following section will provide information on the removal of C-13 microwave deposits from the surface of both Magnox and AGR graphite during the thermal treatment at various temperatures with a vacuum applied.

3.19.1 Scanning Electron Microscopy

By using SEM to analyse graphite samples with C-13 microwave deposits having undergone the thermal treatment process, the effectiveness of the deposit removal technique could be evaluated. The 'cauliflower' like morphology of the C-13 microwave deposits could still be observed on the surfaces of graphite samples which had been thermally treated at 450°C and 600°C (Figure 104). Much like the thermal treatment with a vacuum applied to graphite with C-12 microwave deposits no oxidation had taken place at these lower temperatures (Figure 96). However at the higher temperatures of 700°C and 800°C there was a significant change in the samples surface morphology. Not only has the C-13 microwave deposit been completely removed but there was also evidence that the underlying graphite had started to oxidise. The SEM images show that the surface was very rough with numerous cracks and imperfections across the entire graphite surface.

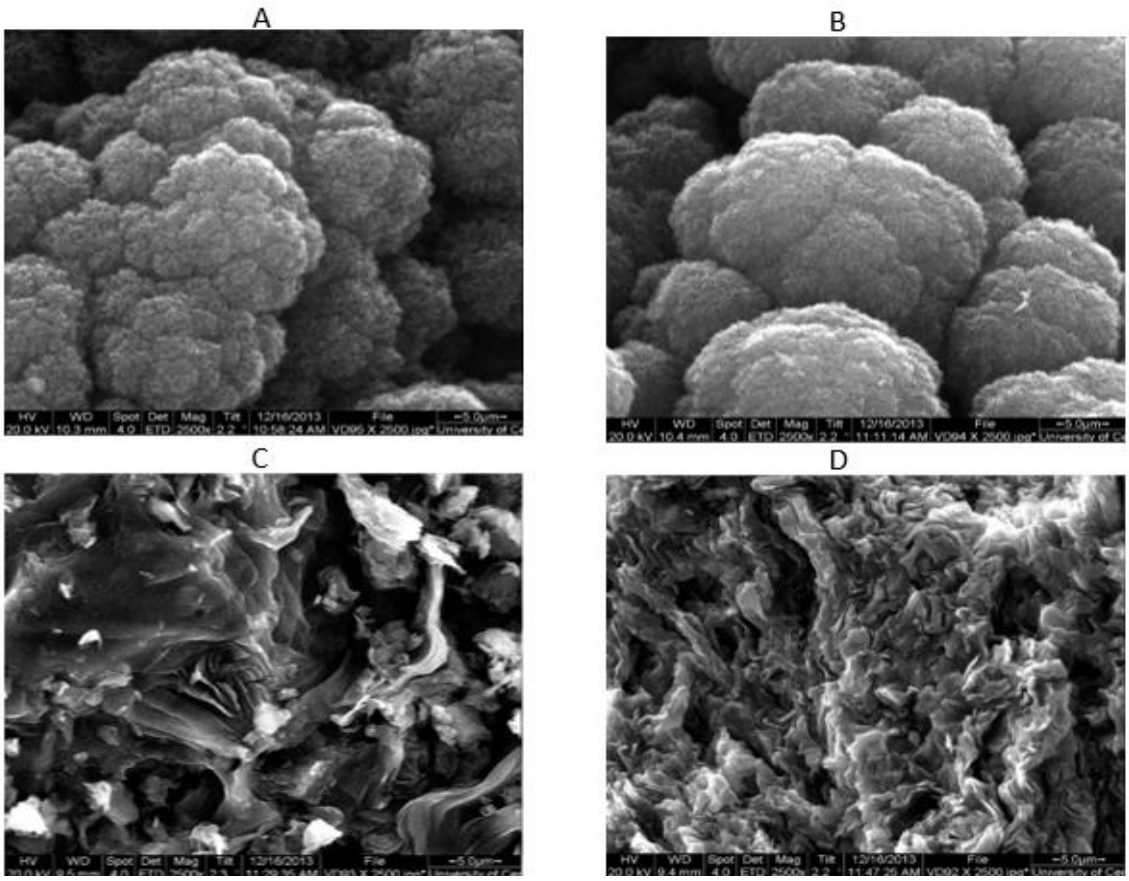

Figure 104 - SEM images at x2500 magnification of Magnox graphite with a C-13 microwave deposit having undergone thermal treatment with a vacuum at A - 450°C, B – 600°C, C – 700°C and D – 800°C

Upon initial analysis at x2500 the SEM images produced for AGR graphite with C-13 microwave deposits having undergone the thermal treatment process with a vacuum at various temperatures, (Figure 105) it appeared that the samples did not display the same trend which has been discussed previously. At the higher temperatures of 700°C and 800°C the C-13 microwave deposits may not have been completely removed as there appeared to be small circular material on the graphite surface. Whether this was the remnants of the partially oxidised deposits or a variation of the underlying graphite oxidation it was difficult to ascertain from SEM images alone. The use of mass spectrometry and Raman spectroscopy would provide additional information to aid in the interpretation of these results. At the lower temperatures of 450°C and 600°C the presence of the 'cauliflower' like deposit was clearly visible on the graphite surface however at x2500 magnification the deposit appeared to have undergone some degradation. There was also significantly less evidence of oxidation of the graphite surface. The Magnox sample showed a considerably rougher surface with more cracks than is present on AGR graphite surface.

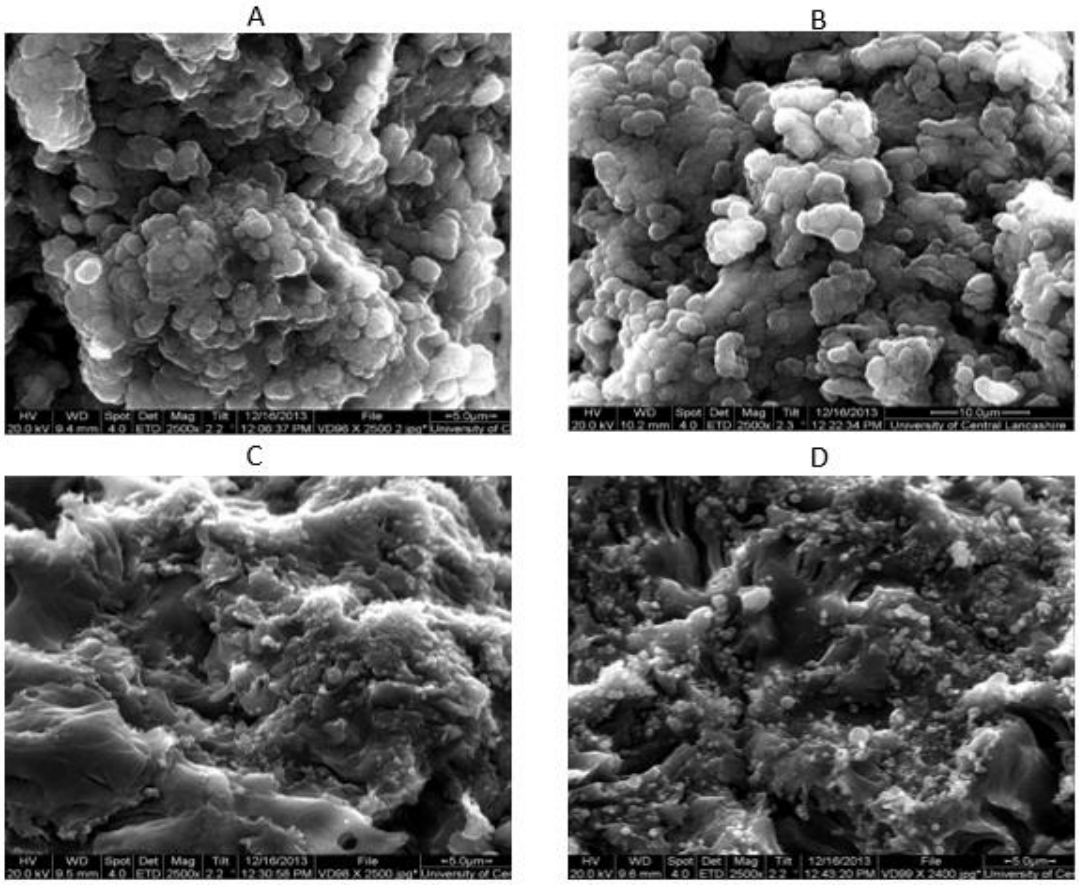

Figure 105 - SEM images at x2500 magnification of AGR graphite with a C-13 microwave deposit having undergone thermal treatment with a vacuum at A - 450°C, B – 600°C, C – 700°C and D – 800°C

More accurate conclusions could be drawn from the SEM images of the samples at the higher magnification of x10,000 (Figure 106). The C-13 samples treated at 450°C and 600°C displayed a deposit morphology similar to that observed previously with the thermal treatment of the C-12 deposited samples. Whilst at a lower magnification there appeared to be some degradation of the deposit this was not evident at higher magnifications. However it could be argued that the fact that analysis at higher magnifications was required means that some oxidation had taken place. The thermal treatments at 700°C and 800°C still exhibited small circular material on the graphite surface, which may be either oxidation of the underlying graphite or the remnants of the partially oxidised deposits. Interestingly some studies have observed this same phenomenon present on the surface of oxidised graphite and the spherical material present on the surface has been attributed to binding and filler material present in the graphite structure[128]. It is unusual that this AGR graphite sample is the only sample which displayed this phenomenon.

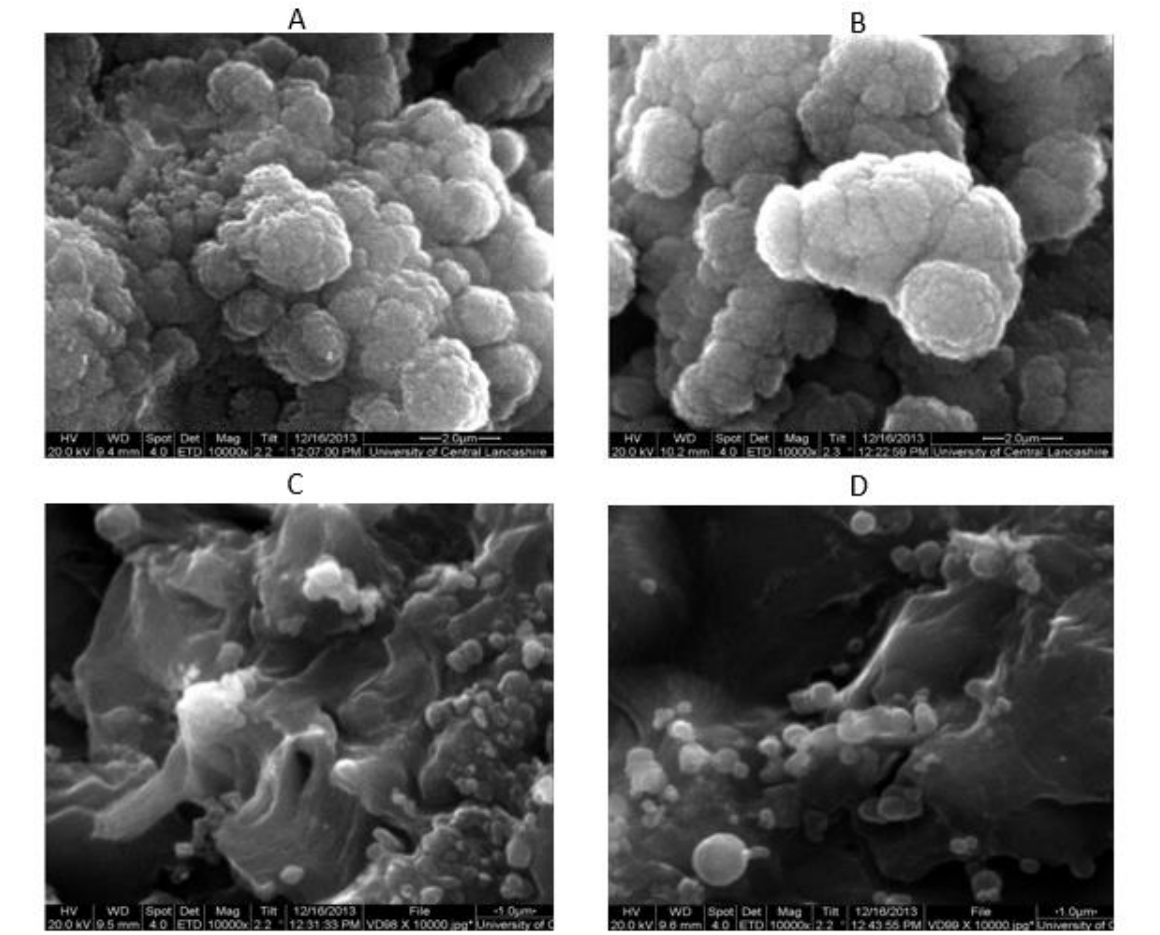

Figure 106 - SEM images at x10,000 magnification of AGR graphite with a C-13 microwave deposit having undergone thermal treatment with a vacuum at A - 450°C, B – 600°C, C – 700°C and D – 800°C

3.19.2 Mass spectrometry and mass loss

The percentage mass loss of both Magnox and AGR graphite samples with C-13 microwave deposits during the thermal treatment with a vacuum at a variety of temperatures (Figure 107) exhibited a similar trend and mass loss as discussed previously. As the temperature increased so did the amount of oxidation and so the percentage mass loss. The percentage mass loss by these samples was very similar to that observed with both types of graphite with C-12 microwave deposits.

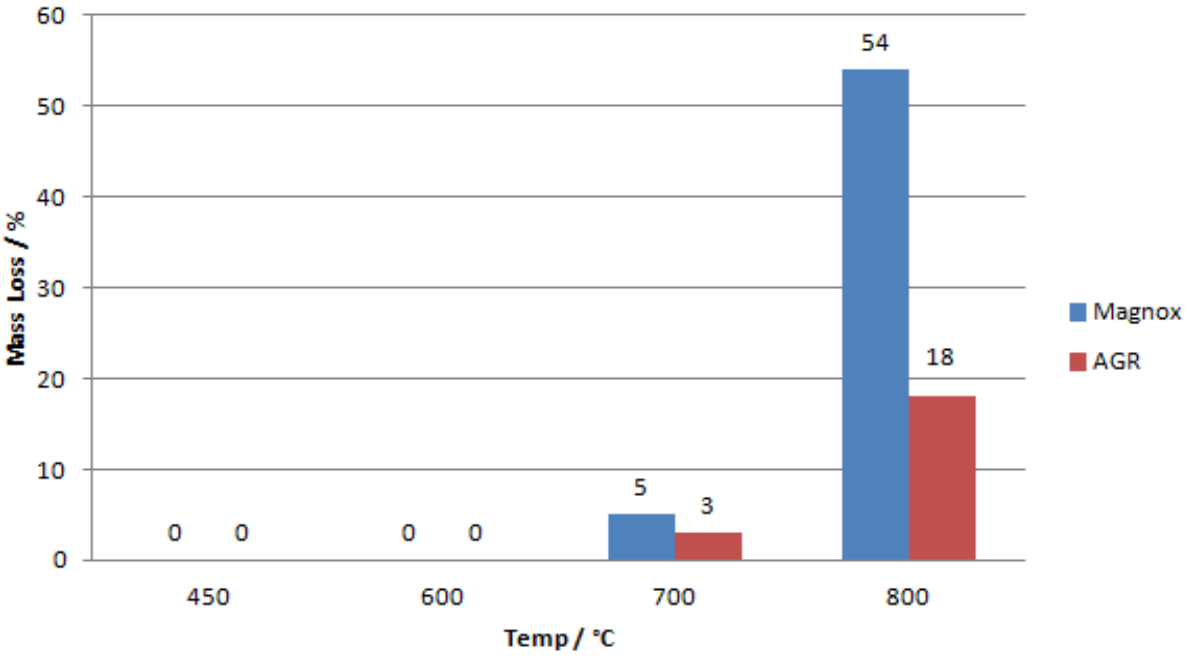

Figure 107 - Comparison of the percentage mass loss of both Magnox and AGR graphite with C-13 microwave deposit during thermal treatment at various temperatures with a vacuum

Similar to the thermal treatments of other samples with a vacuum at the lower temperatures of 450°C and 600°C there was no evidence of oxidation, as only a negligible amount of mass had been lost. In addition the treatments at the higher temperatures of 700°C and 800°C displayed a higher amount of mass lost from the Magnox graphite samples compared to the AGR graphite samples. Magnox graphite samples with C-13 microwave deposits exhibited a mass loss of ~5% at 700°C compared to AGR graphite with C-13 microwave deposits which only lost ~3%. At 800°C Magnox graphite with C-13 microwave deposits lost ~54% compared to AGR graphite with C-13 microwave deposits which only lost ~18%. These mass losses for both Magnox and AGR graphite were very close to those produced from graphite with C-12 microwave deposits (Figure 93) which in turn were unusual as they were a lot less than those produced from virgin graphite and graphite with D-mannose deposits. Perhaps the deposits produced using the microwave plasma technique produced a sample which was more thermally stable than virgin samples and the samples with the D-mannose deposit.

The data from the mass spectrometer confirmed the trend observed with the mass loss data by exhibiting an increase in C-12 CO_2 production during the thermal treatment at higher temperatures compared with the lower temperatures. This was the same for both Magnox graphite (Figure 108) and AGR graphite (Figure 110). CO was also produced during these

experiments but several orders of magnitude lower than CO_2 so the majority of the mass loss was attributed to C-12 CO_2. The thermal treatment at 700°C of graphite with C-13 microwave deposits produced a similar mass loss and C-12 CO_2 production with both AGR and Magnox graphite.

The mass spectrometer data produced for C-13 CO_2 followed the same trend of an increase in production at higher temperatures. However the spectral profile did not mimic the corresponding C-12 CO_2 trace in that there is a rapid evolution of C-13 CO_2 over the first hour after which the rate subsides. This was the same for both Magnox graphite (Figure 109) and AGR graphite (Figure 111). These results indicated that the C-13 deposits were oxidised within the first two hours of the experiments. Even though there was a small C-13 CO_2 peak observed at the start of the treatments at 600°C and to a much lesser extent at 450°C, post reaction analysis using SEM indicated that there was still deposit remaining on the surface of the graphite samples. The fact that the C-13 CO_2 produces a peak in the mass spectrum trace but the deposits have not been fully removed indicates that the deposit is non-uniform in terms of its reactivity. This heterogeneity in the simulated deposit is also seen in deposits formed on irradiated graphite which has been removed from nuclear reactors[44]. This is further substantiated by the findings reported in section 3.21.2 of this thesis.

Additionally, AGR graphite samples with C-13 deposits produces significantly less C-13 CO_2 during thermal treatment compared to the Magnox samples with C-13 deposit. As AGR graphite has a slower oxidation rate compared to Magnox graphite, this indicates that the reactivity of the graphite substrate has an effect on the amount of deposit produced onto the graphite samples surface.

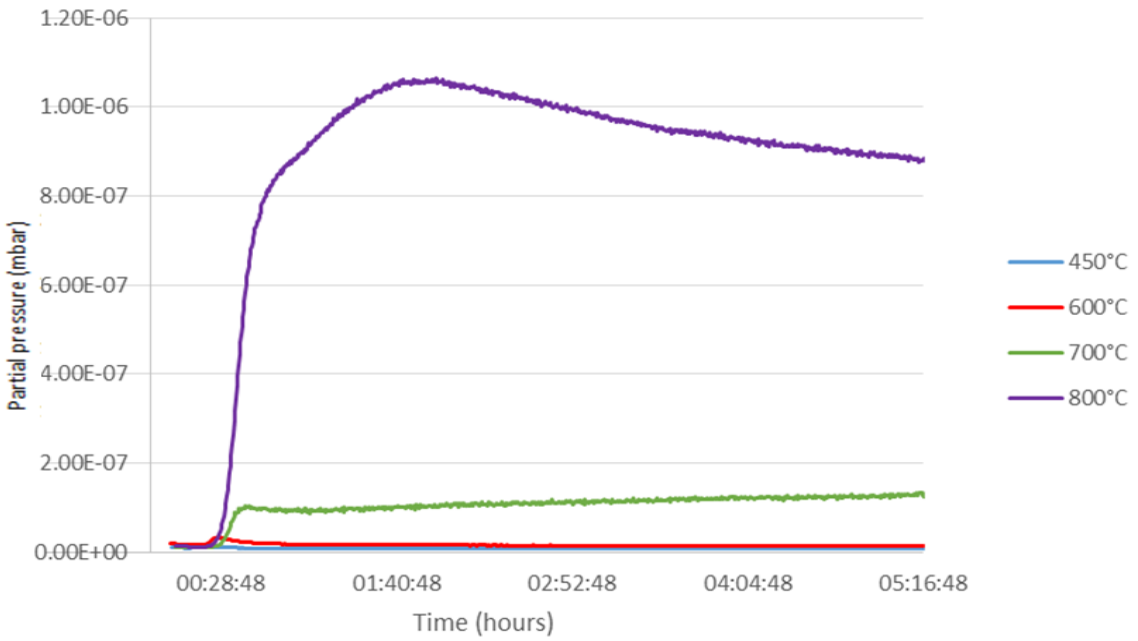

Figure 108 - Mass spectrometry data of C-12 CO_2 produced from Magnox graphite with C-13 microwave deposits during thermal treatment with a vacuum at various temperatures

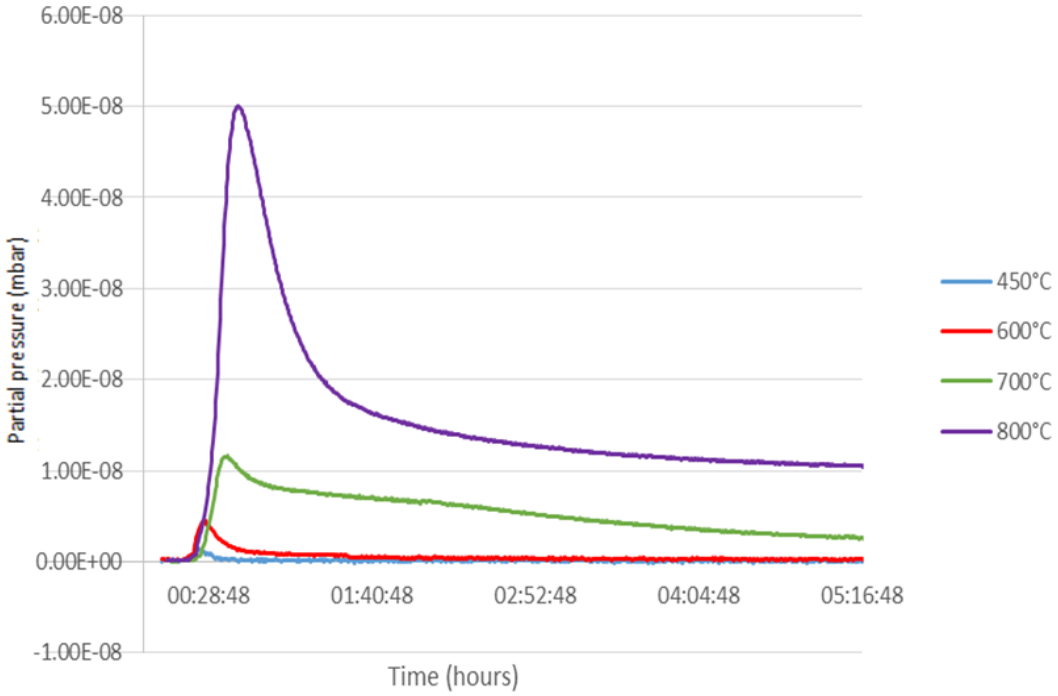

Figure 109 - Mass spectrometry data of C-13 CO_2 produced from Magnox graphite with C-13 microwave deposits during thermal treatment with a vacuum at various temperatures

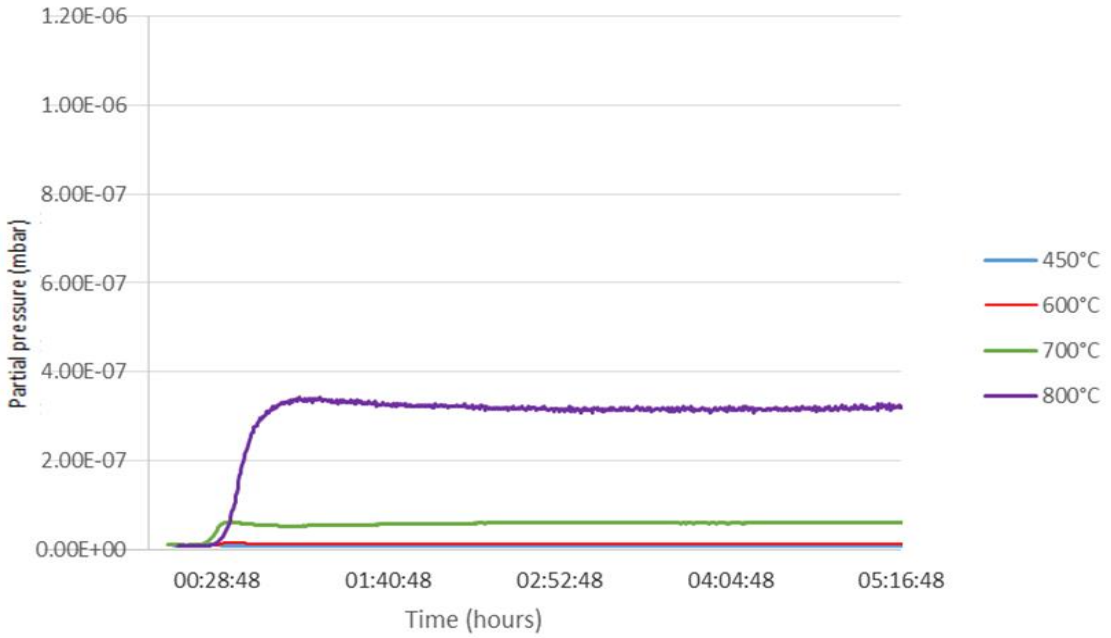

Figure 110 - Mass spectrometry data of C-12 CO_2 produced from AGR graphite with C-13 microwave deposits during thermal treatment with a vacuum at various temperatures

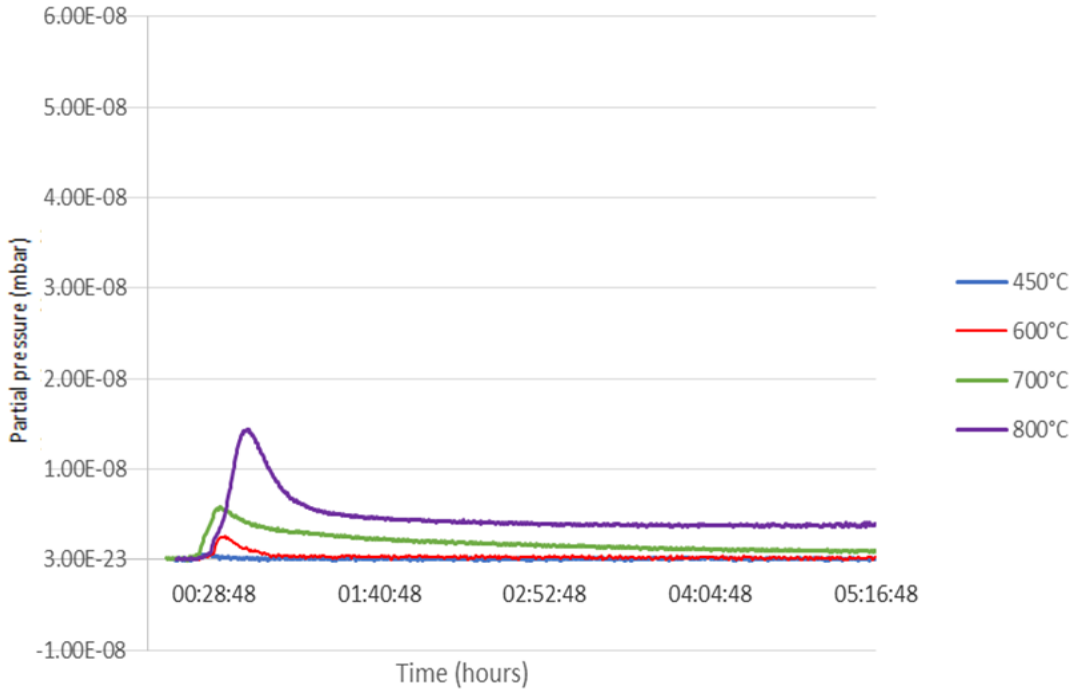

Figure 111 - Mass spectrometry data of C-13 CO_2 produced from AGR graphite with C-13 microwave deposits during thermal treatment with a vacuum at various temperatures

3.19.3 Raman Spectroscopy

Raman Spectroscopy was used in order to determine the removal of a deposit from the graphite surface. Several spectra were produced for both Magnox and AGR graphite samples with a C-13 microwave deposit present having undergone thermal treatment with a vacuum applied at various temperatures. All samples exhibited the characteristic G and D peaks with samples with C-13 present exhibiting the characteristic shift to the left of these peaks caused by the presence of a heavier isotope (Figure 112).

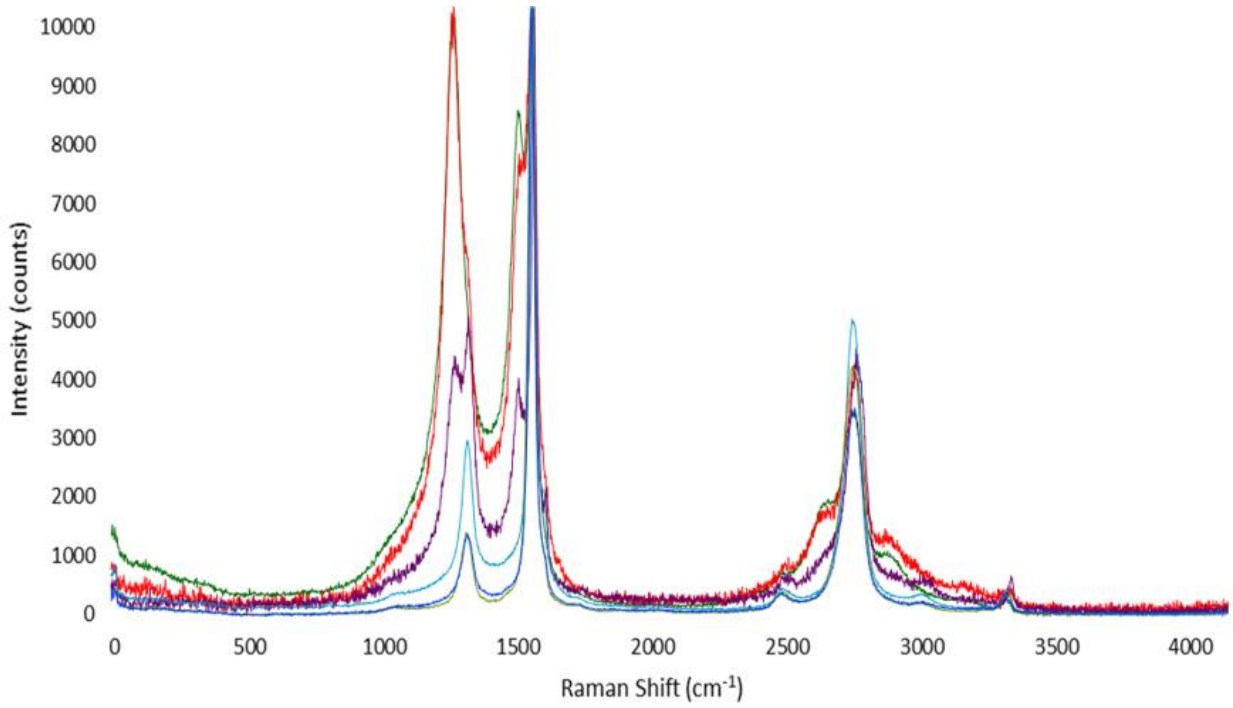

Figure 112 - Raman spectra of virgin Magnox graphite (dark blue), Magnox graphite with C-13 microwave deposit (dark green), Magnox graphite with C-13 microwave deposit after thermal treatment with a vacuum at 450°C (red), 600°C (purple), 700°C (light blue), 800°C (light green)

Not only is the shift to the left indicative of the presence of a C-13 carbonaceous deposit but also the intensity of the D peak which had been observed from previous experiments. The Magnox graphite sample with C-13 microwave deposits which had not been thermally treated exhibited the highest intensity in the D peak, whereas the spectrum for virgin graphite displayed the lowest intensity in the D peak due to having very little disorder in its structure. The sample which had been thermally treated at 450°C showed no change in the D peak intensity from that produced from a non-thermally treated sample indicating that the deposit had undergone little change at this temperature. After thermal treatment at 600°C the presence of the C-13 deposit could still be observed but at a much lower intensity than the

sample treated at 450°C. Interestingly the presence of a C-12 D peak could also be observed in this samples spectrum. This suggests that as the C-13 deposit was formed the process involved a change in the amount of disorder of the graphite surface, and as the C-13 deposit was then removed the now disordered graphite underneath could be observed. The samples that had undergone thermal treatment at 700°C and 800°C showed a decrease in the intensity of the D peak which was approaching the same intensity as virgin Magnox graphite and the spectral shift was no longer present indicating that the C-13 carbonaceous deposits had been successfully removed.

A very similar set of data was produced from the analysis of AGR graphite with C-13 microwave deposits by Raman spectroscopy (Figure 113). The graphite sample with C-13 deposits which had not been thermally treated exhibited the highest intensity in the D peak, this was also equal in intensity to the sample thermally treated at 450°C indicating that no oxidation had taken place at this temperature. However unlike the spectra produced from the Magnox sample whose D peak intensity was reduced at 600°C, the AGR sample with C-13 microwave deposits treated at 600°C displayed a D peak intensity equal to that produced from both a sample treated at 450°C and a sample which had not been treated at all. This data was corroborated by the SEM images which showed the 'cauliflower' like morphology of the deposits still present on the graphite surface after treatment at these temperatures. The samples that had undergone thermal treatment at 700°C and 800°C showed a decrease in the intensity of the D peak which was approaching the same intensity as virgin AGR graphite and the spectral shift was no longer present indicating that the C-13 carbonaceous deposits had been successfully removed.

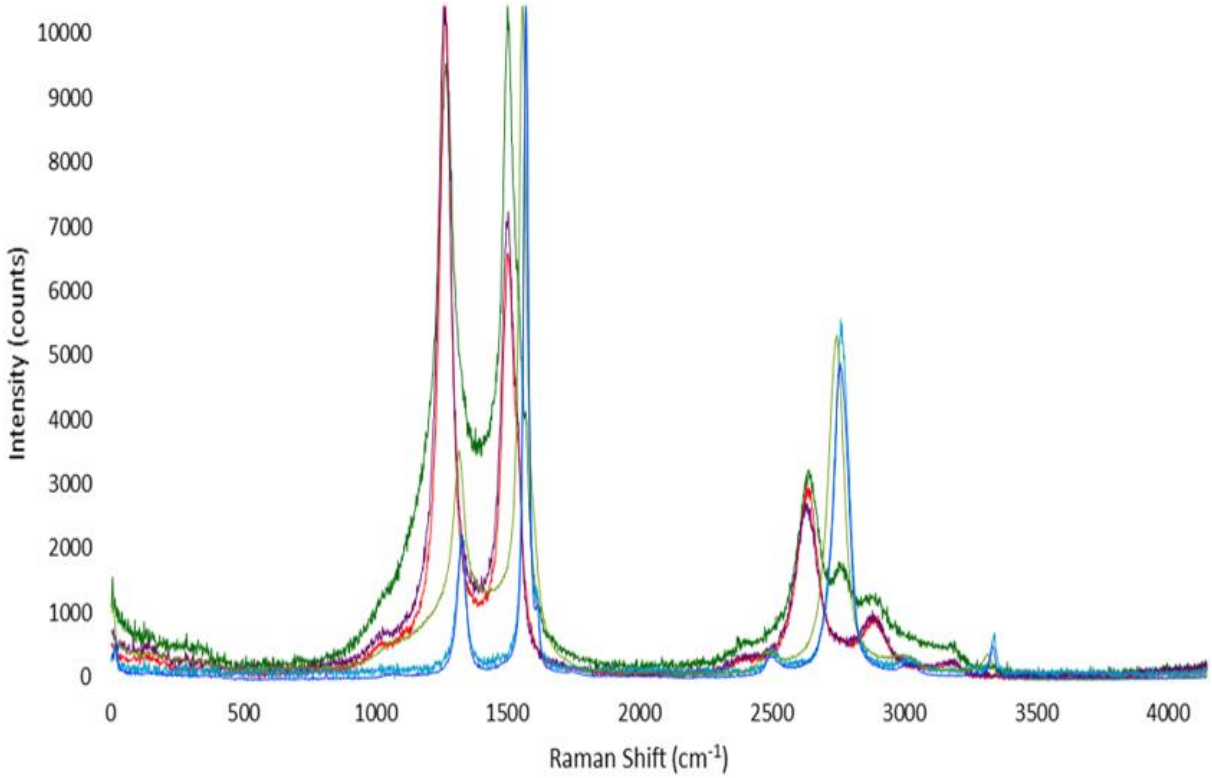

Figure 113 - Raman spectra of virgin AGR graphite (dark blue), AGR graphite with C-13 microwave deposit (dark green), AGR graphite with C-13 microwave deposit after thermal treatment with a vacuum at 450°C (red), 600°C (purple), 700°C (light green), 800°C (light blue)

A combination of the data from the Raman spectroscopy and the evolved gas analysis provides a useful insight into the mechanism of deposit formation from a microwave plasma and its subsequent oxidation. Careful observation of the C-12 CO_2 traces from both Magnox and AGR graphite (Figure 108 and Figure 110 respectively) show a small peak in the C-12 CO_2 signal associated with the loss of deposit. This indicates that some of the C-12 from the virgin graphite is incorporated into the predominately C-13 deposit. This is substantiated by the Raman spectra which show that when the deposit is removed there is still an increased C-12 D peak (Figure 112, 600°C) which indicates that during the formation of the deposit the microwave plasma causes disordering of the graphite surface; this would be necessary for the inclusion of C-12 into the deposit. Once the deposit has been removed the disordered graphite surface oxidises in such a manner as to react with the disordered material preferentially until a material is produced which has a similar amount of disorder to virgin graphite (Figure 112, 800°C).

3.20 Selective Thermal Treatment

The data for the removal of deposits presented in sections 3.17- 3.19 clearly show that very little deposit was removed in the temperature range 450-600°C while the deposit is very quickly lost in the temperature range 700-800°C. Therefore it was decided to undertake a further series of experiments in the temperature range 500-650°C. This series of experiments was limited to Magnox graphite samples with C-13 microwave deposits.

3.20.1 Scanning Electron Microscopy

By using SEM to analyse graphite samples with C-13 microwave deposits having undergone the thermal treatment process, the effectiveness of the deposit removal technique with and without a vacuum could be evaluated. With regards to samples treated with a vacuum the 'cauliflower' like morphology of the C-13 microwave deposits could still be observed on the surfaces of all of the graphite samples which had been thermally treated using the new temperatures ranging from 500-650°C (Figure 114). This indicated that an insignificant amount of oxidation had taken place if any due to a slow oxidation rate. Based on previous analysis the C-13 deposits must only start to oxidise above 650°C as they have been completely removed by 700°C.

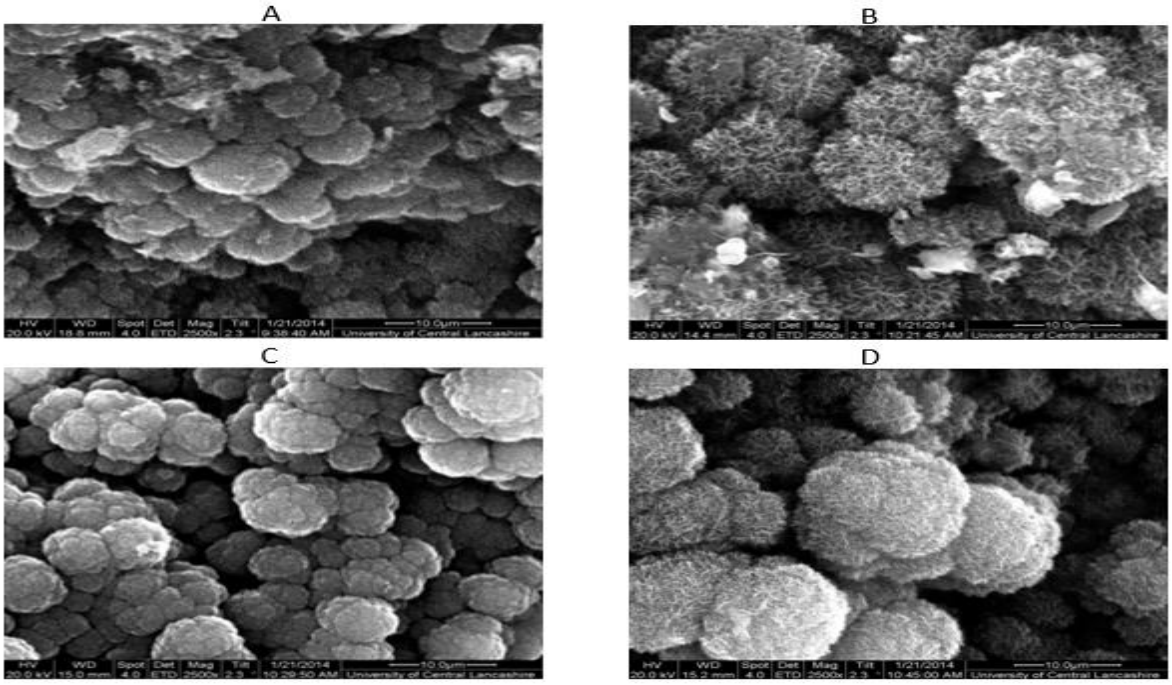

Figure 114 - SEM images at x2500 magnification of Magnox graphite with a C-13 microwave deposit having undergone thermal treatment with a vacuum at A - 500°C, B – 550°C, C – 600°C and D – 650°C

When thermally treated without the application of a vacuum, oxidation will occur at a lower temperature. The ‘cauliflower’ like morphology of the C-13 microwave deposits could still be observed on the surfaces of graphite samples treated at 500°C (Figure 115). The images produced for samples treated at 550°C demonstrate that the deposits were starting to oxidise as the morphology had changed. The deposits had been completely removed during the treatments at 600°C and 650°C. Samples treated at the higher temperatures also displayed a rough and cracked surface morphology indicating that the graphite had started to oxidise.

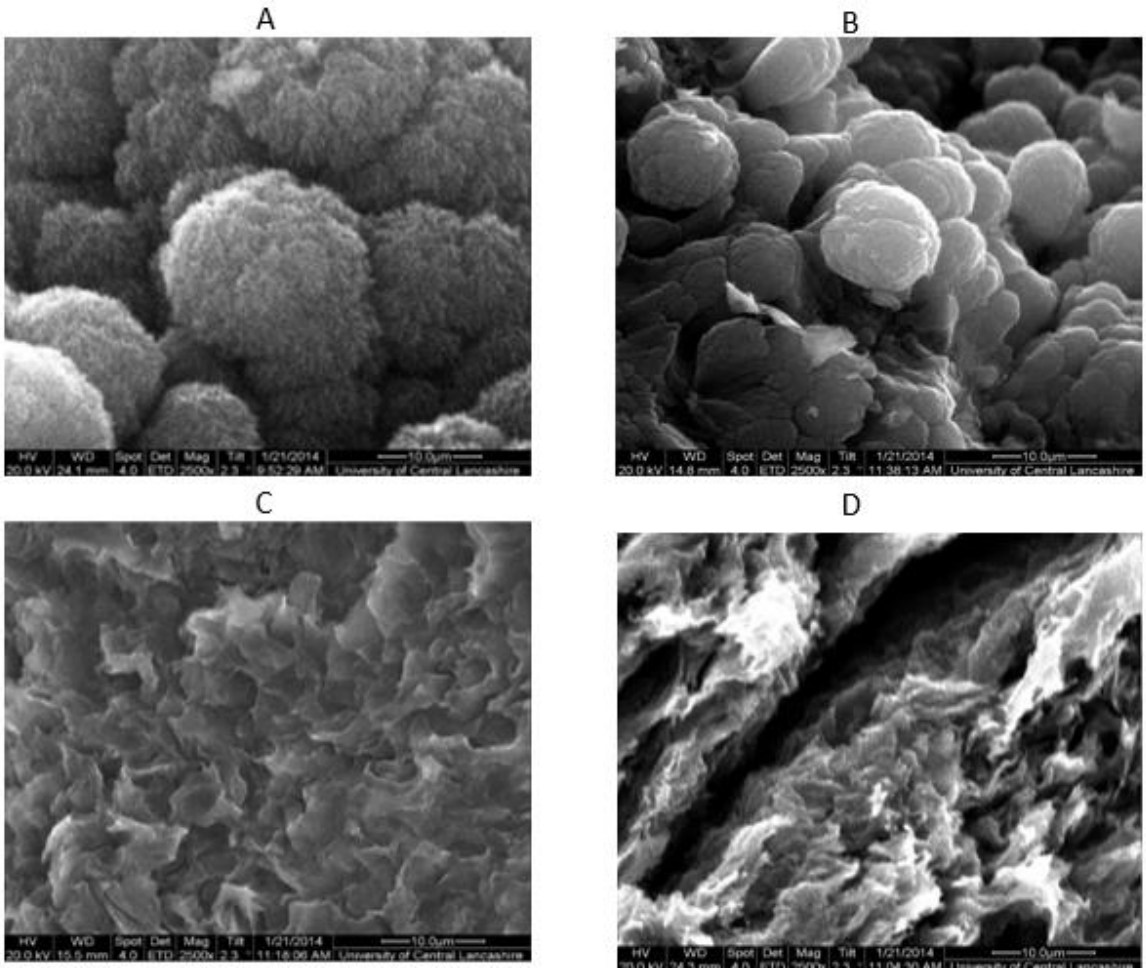

Figure 115 - SEM images at x2500 magnification of Magnox graphite with a C-13 microwave deposit having undergone thermal treatment without a vacuum at A - 500°C, B – 550°C, C – 600°C and D – 650°C

3.20.2 Mass spectrometry and mass loss

The percentage mass loss of Magnox graphite with C-13 microwave deposits during thermal treatment with and without the application of a vacuum displayed a similar trend as discussed previously where, as the temperature increased so did the amount of oxidation and thus the amount of mass lost by the sample. There was always a greater amount of mass lost from the samples thermally treated without a vacuum than with one (Figure 116). This is because the partial pressure of oxygen is higher without the application of a vacuum. At 650°C the mass lost had increased from ~2% with a vacuum applied to ~20% without the use of a vacuum. Whilst the mass lost at the lower temperature of 500°C without a vacuum remained as negligible as the mass lost at this temperature with a vacuum, at 550°C there was an increase to ~1% mass loss by a sample treated without a vacuum compared with the negligible amount lost during treatment with a vacuum. The mass lost by the sample treated at 600°C increased from ~1% with a vacuum applied to ~4% without a vacuum.

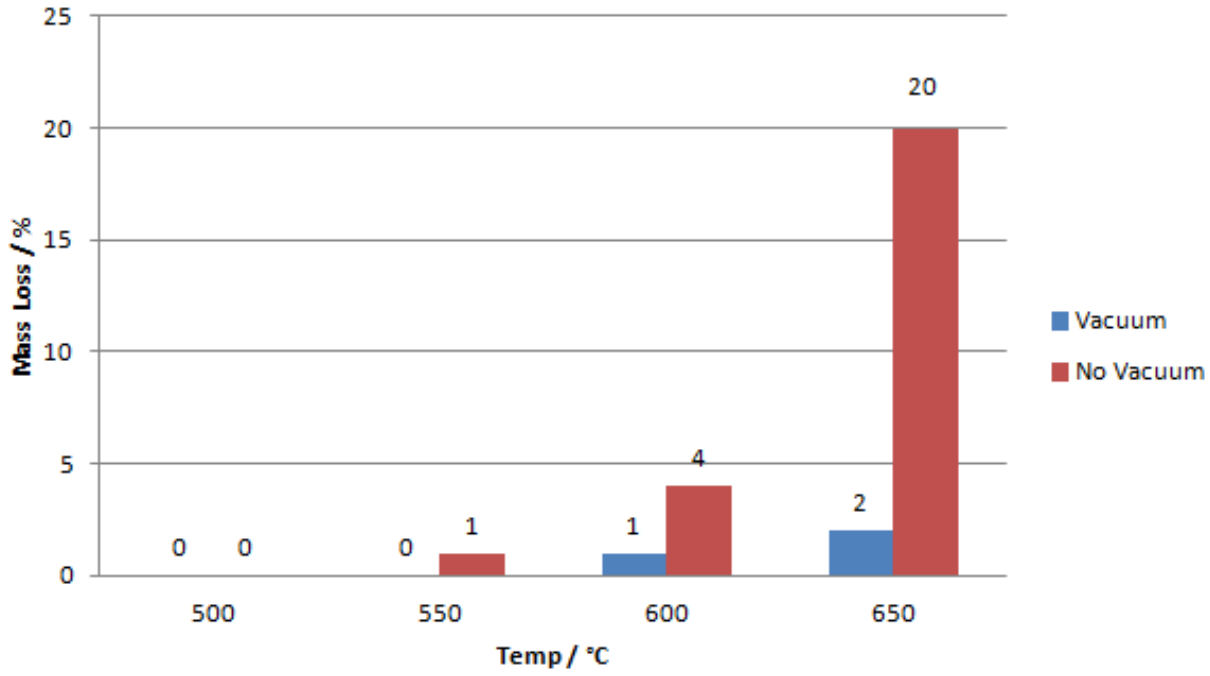

Figure 116 - Comparison of the percentage mass loss of Magnox graphite with C-13 microwave deposit during thermal treatment at various temperatures with and without a vacuum

The average rate of reaction can be determined by simply dividing the mass loss by the duration of experiment (300 minutes) (Table 13). A simplified rate equation can be proposed which includes the partial pressure of oxygen.

$$Rate = k \times [PO_2]^n$$

Between the vacuum condition of 5 mbar and atmospheric pressure the partial pressure of oxygen varies between $1x10^{-3}$ mbar and 0.2 mbar i.e. a factor of 200. Throughout this series of experiments it can be seen that the difference in rate between vacuum and atmospheric pressure is approximately 10 (Figure 116). Therefore it can be shown that the partial pressure of oxygen must be raised to the power of 0.5 in the simplified rate equation shown above. This is confirmed by the low to intermediate temperature data in Figure 89 and Figure 100 and confirms that the high temperature atmospheric pressure experiments are likely to have been performed under oxygen limiting conditions.

Table 13 - Reactivity and mass loss of Magnox graphite with C-13 microwave deposits during thermal treatment with and without a vacuum

Sample	Average Rate ($mg.min^{-1}$)	Mass lost (mg)
500°C with Vac	0.002	1
550°C with Vac	0.004	1
600°C with Vac	0.02	5
650°C with Vac	0.05	15
500°C without Vac	0.01	4
550°C without Vac	0.04	13
600°C without Vac	0.1	41
650°C without Vac	0.7	196

The data from the mass spectrometer confirmed the trend observed with the mass loss data by exhibiting an increase in C-12 CO_2 production during the thermal treatment at higher temperatures compared with the lower temperatures. This was the same for thermal treatment with a vacuum (Figure 117) and without (Figure 119).

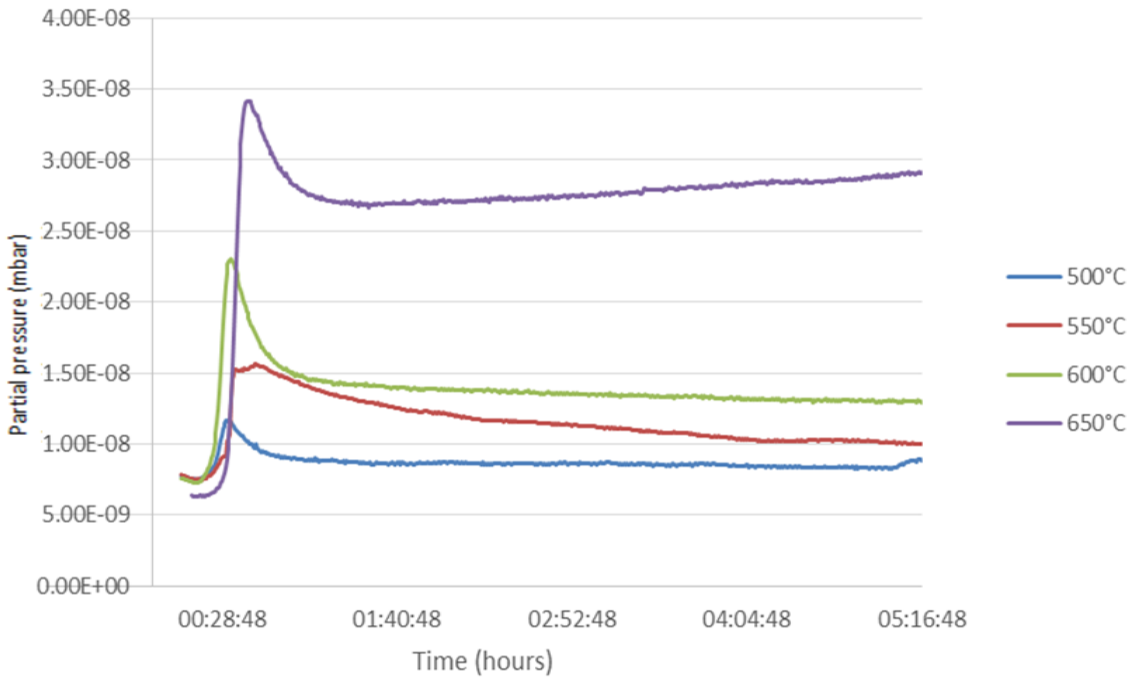

Figure 117 - Mass spectrometry data of C-12 CO_2 produced from Magnox graphite with C-13 microwave deposits during thermal treatment with a vacuum at various temperatures

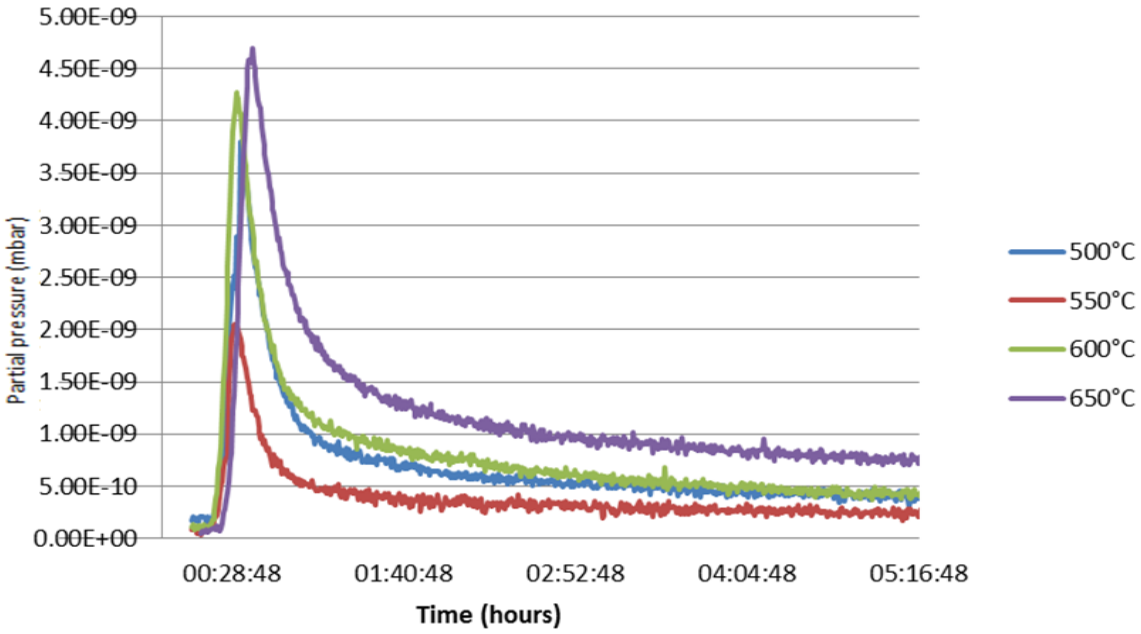

Figure 118 - Mass spectrometry data of C-13 CO_2 produced from Magnox graphite with C-13 microwave deposits during thermal treatment with a vacuum at various temperatures

CO was also produced during these experiments but several orders of magnitude lower than CO_2 so the majority of the mass loss was attributed to CO_2. Samples treated with a vacuum exhibited a peak in C-12 CO_2 at the start of the experiments which then decreased in proportion corresponding to the treatment temperature. The higher the temperature the less of a decrease in CO_2 after the initial peak. Samples treated without a vacuum at the higher temperatures of 600°C and 650°C displayed a more gradual production of C-12 CO_2 over the period of the isotherm rather than a steady rate of production which was observed from the mass spectrometer data with the application of a vacuum. This comparison indicated that conducting the thermal treatment with a vacuum applied to the system controlled the reaction rate, because there was less oxygen present in the system then less carbon is able to react with it to form CO_2. Although there was negligible mass lost from the samples which underwent thermal treatment at 500°C there was a very small CO_2 peak produced at the start of each experiment both with and without a vacuum. This could be caused by areas of more reactive deposit oxidising quickly or loosely held material although there was very little mass lost from the sample.

The mass spectrometer data produced for C-13 CO_2 followed the same trend of an increase in production at higher temperatures both with and without a vacuum. However the spectra produced were very different from that displayed by C-12 CO_2. At the start of each thermal treatment there was a sharp peak which then decreased over the course of the experiment. This sharp peak was more prominent in the data with a vacuum applied (Figure 118) although it was also present in the data without a vacuum (Figure 120) although much broader with a more gradual decrease in the peak. The fact that the thermal treatment with a vacuum produced a peak which was sharper suggested it was the superior technique with which to remove deposits. However the SEM analysis showed that the deposits had not been removed during the thermal treatment. This meant that the peak was caused by the partial oxidation of deposit. Furthermore the thermal treatment at 600°C and 650°C without a vacuum produced a C-13 CO_2 peak in the mass spectra which was almost an order of magnitude higher than that produced from the same treatment with a vacuum. The SEM images for these samples also showed that the deposits had been completely removed.

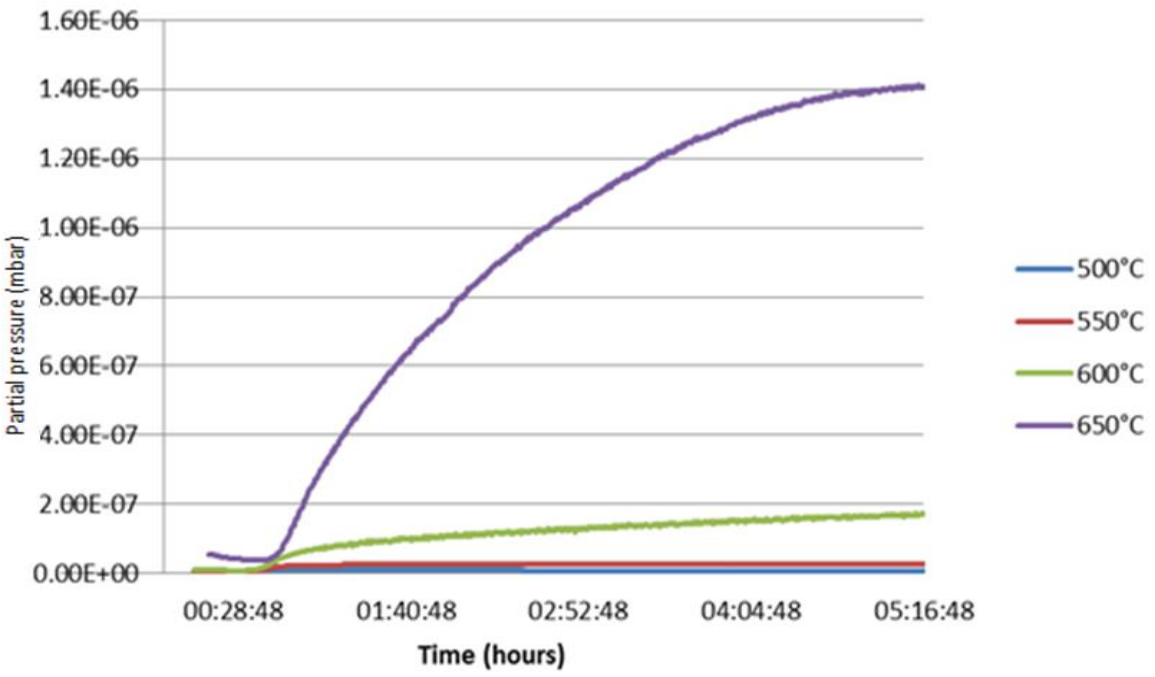

Figure 119 - Mass spectrometry data of C-12 CO_2 produced from Magnox graphite with C-13 microwave deposits during thermal treatment without a vacuum at various temperatures

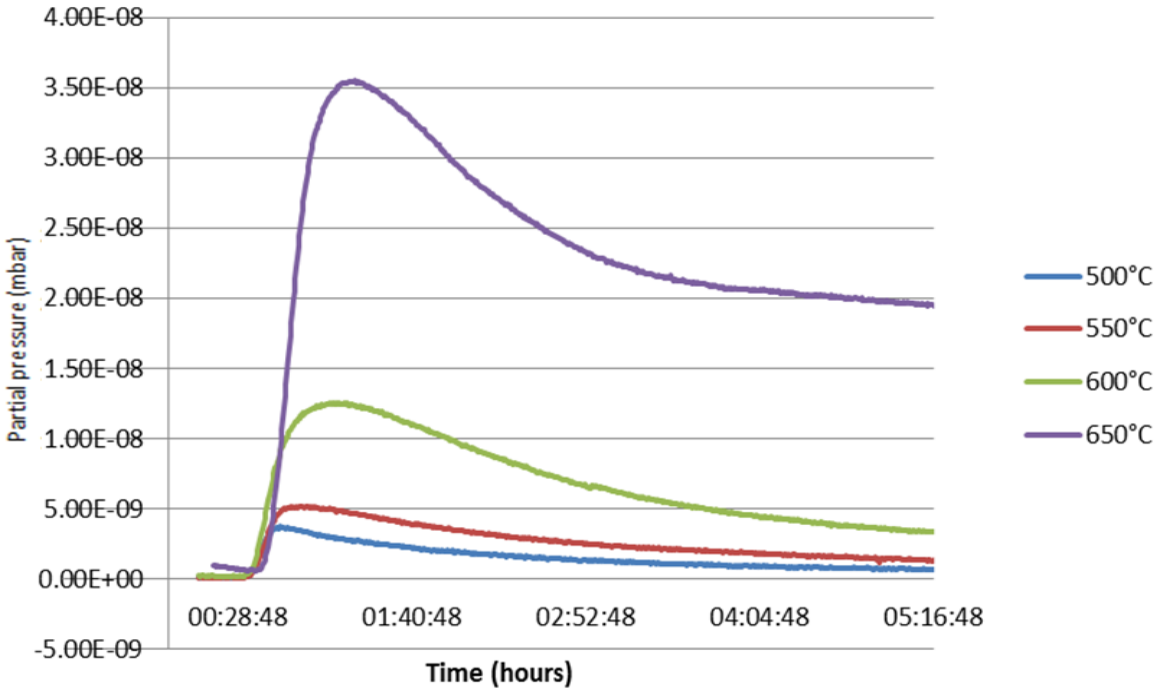

Figure 120 - Mass spectrometry data of C-13 CO_2 produced from Magnox graphite with C-13 microwave deposits during thermal treatment without a vacuum at various temperatures

The mass spectral data can be used to determine the relative efficiencies for the selective removal of the deposit. Initial experiments performed using the microbalance had shown a difference between the oxidation behaviour of virgin AGR and Magnox graphite. When the mass spectral data is compared (Figure 121) it can be seen that while at 700°C there is very little difference in the oxidation behaviour, at 800°C the AGR graphite very quickly attains a maximum rate which is much lower than the maximum rate of oxidation of Magnox graphite which is attained over a longer period of time. This observation is consistent throughout all of the experiments through the programme of work.

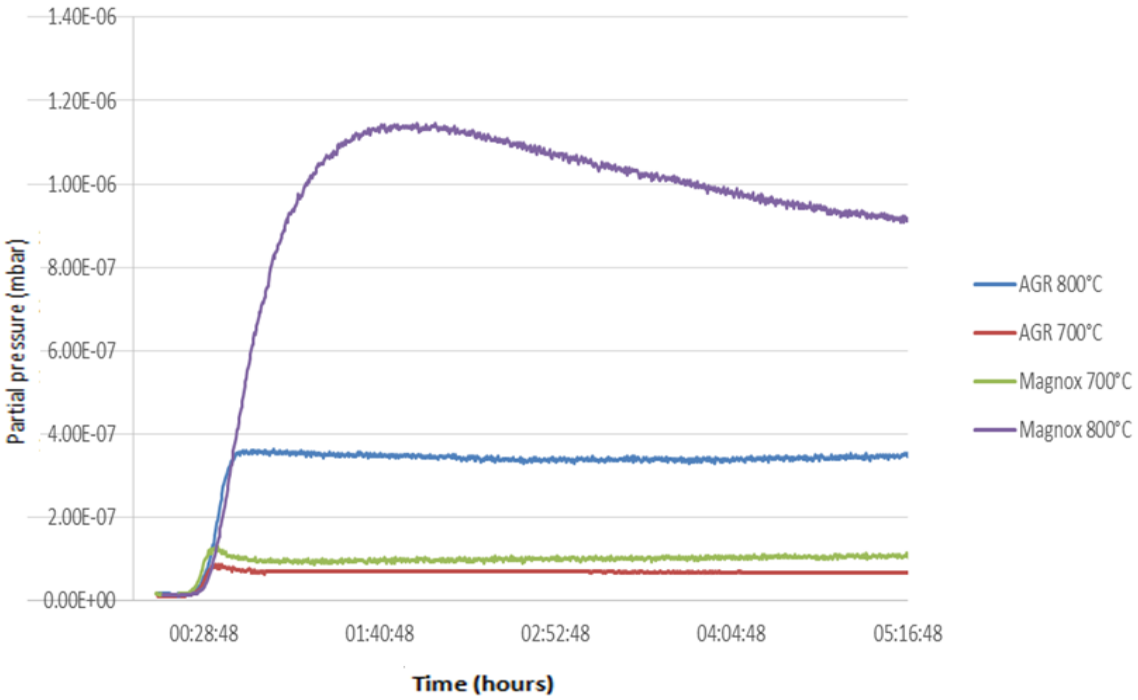

Figure 121 - Mass spectrometry data of CO_2 produced from both Virgin Magnox and AGR graphite during thermal treatment with a vacuum at 700°C and 800°C

The ultimate aim of the project has been to determine if a carbonaceous deposit can be selectively removed from a surface of graphite and if the application of a vacuum can assist with this process. In order to achieve a quantitative measure for this process the ratio of C-12 CO_2:C-13 CO_2 at the maximum rate of C-13 CO_2 evolution has been recorded for each temperature under both vacuum and atmospheric pressure (Table 14 and Table 15). If this data is plotted then it can be seen that the data points sit on a smooth curve which appears to be a log linear relationship between the selectivity and the total rate (C-13 CO_2 + C-12 CO_2) (Figure 122). This is confirmed by plotting the selectivity against the Ln of the rate of CO_2 evolution (Figure 123). This data provides strong evidence that using a vacuum does not

influence the selectivity of the removal of the carbonaceous deposit. However this is not to say that a thermal treatment could not be developed which gave a measure of selective deposit removal. The selectivity for the removal is solely a function of the rate of the process and subsequently the temperature of the process. Using such a process it would be possible to achieve a maximum selectivity of 3:1 C-12 CO_2: C-13 CO_2.

Table 14 - Ratios and the maximum rates of CO_2 production with a vacuum

Temp (°C)	C12 CO_2	C13 CO_2	C12/C13 Ratio
500	1.13E-08	3.80E-09	2.97
550	9.13E-09	2.04E-09	4.48
600	2.26E-08	4.21E-09	5.37
650	3.29E-08	4.69E-09	7.01

Table 15 - Ratios and the maximum rates of CO_2 production without a vacuum

Temp (°C)	C12 CO_2	C13 CO_2	C12/C13 Ratio
500	1.05E-08	3.70E-09	2.84
550	2.24E-08	5.12E-09	4.38
600	7.71E-08	1.24E-08	6.22
650	4.57E-07	3.53E-08	12.95

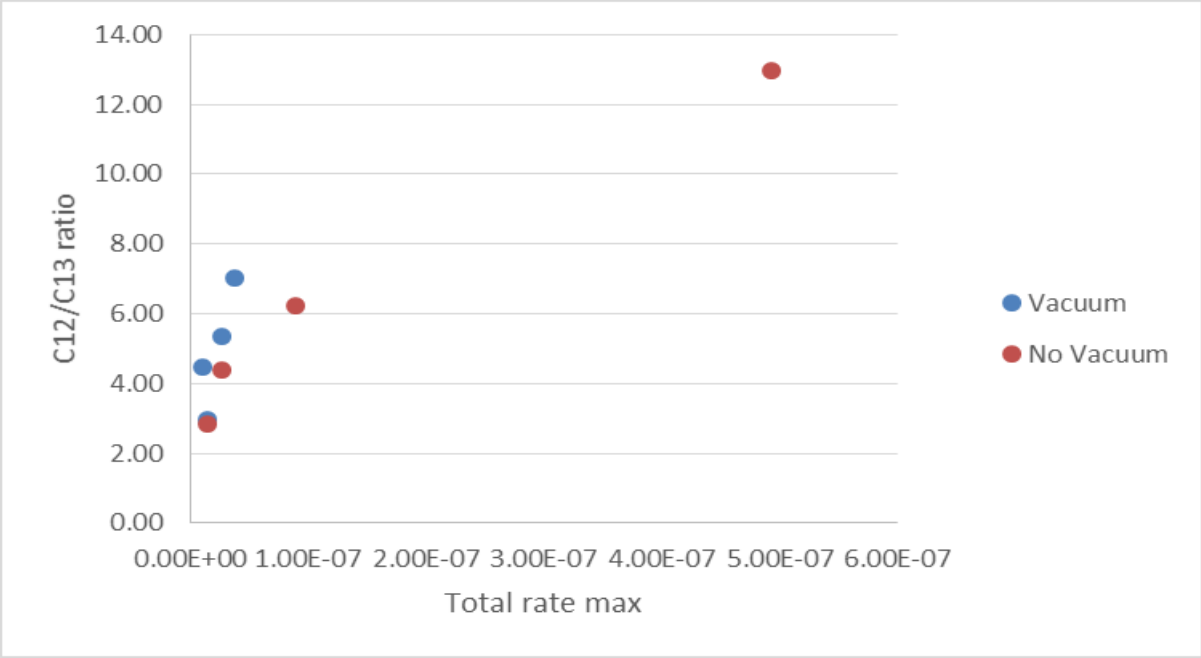

Figure 122 - Plot showing relationship between the selectivity and the total rate of CO_2 production during thermal treatment with and without a vacuum

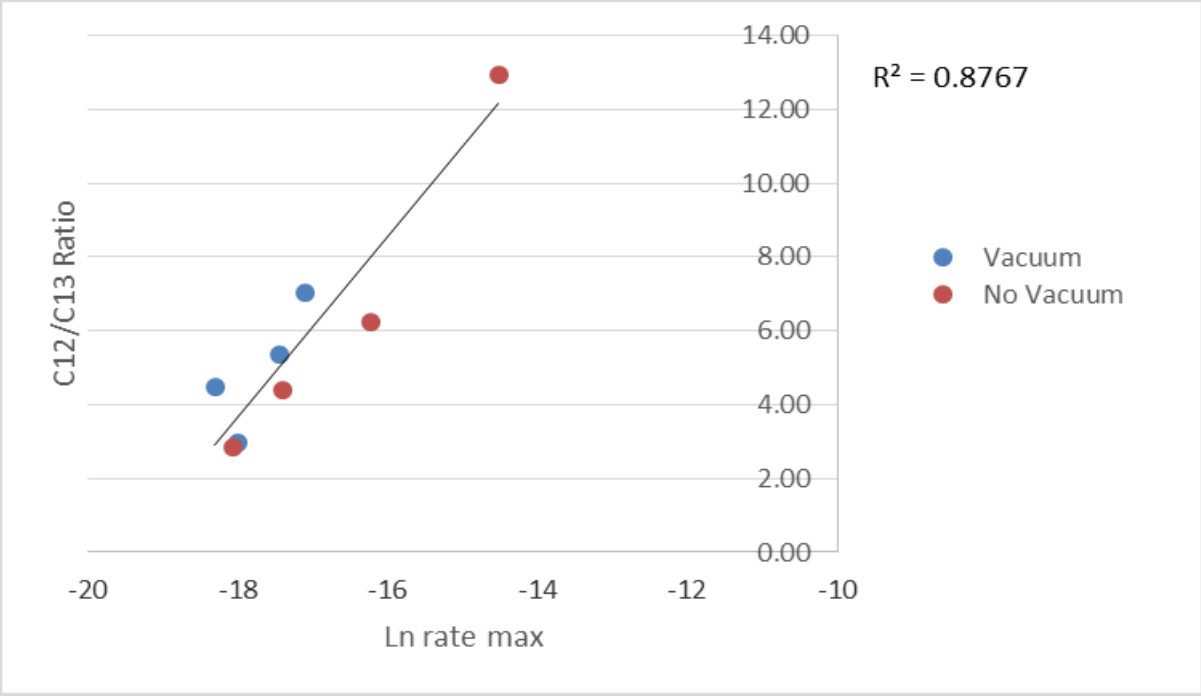

Figure 123 - Plot showing relationship between the selectivity and the Ln of the total rate of CO_2 production during thermal treatment with and without a vacuum

3.20.3 Raman Spectroscopy

Raman Spectroscopy was used in order to determine the removal of a deposit from the graphite surface. Several spectra were produced for Magnox graphite samples with a C-13 microwave deposit having undergone thermal treatment at various temperatures with and without a vacuum applied. All samples exhibited the characteristic G and D peaks with samples with C-13 present exhibiting the characteristic shift to the left of these peaks caused by the presence of a heavier isotope. Not only was the shift indicative of the presence of a C-13 carbonaceous deposit but also the intensity of the D peak which had been observed from previous experiments. The Magnox graphite sample with C-13 microwave deposits which had not been thermally treated exhibited the highest intensity in the D peak, whereas the spectrum for virgin graphite displayed the lowest intensity in the D peak due to having very little disorder in its structure.

The samples which had been thermally treated with a vacuum exhibited a D peak with the same intensity as a sample which had not been thermally treated (Figure 124). This meant that the deposits present on the graphite surface had not been altered during the thermal treatment with a vacuum. This data was corroborated by the SEM images produced for these samples which all provided evidence that the deposit was still present by displaying the ‘cauliflower’ like morphology of the microwave produced deposit on the graphite surface.

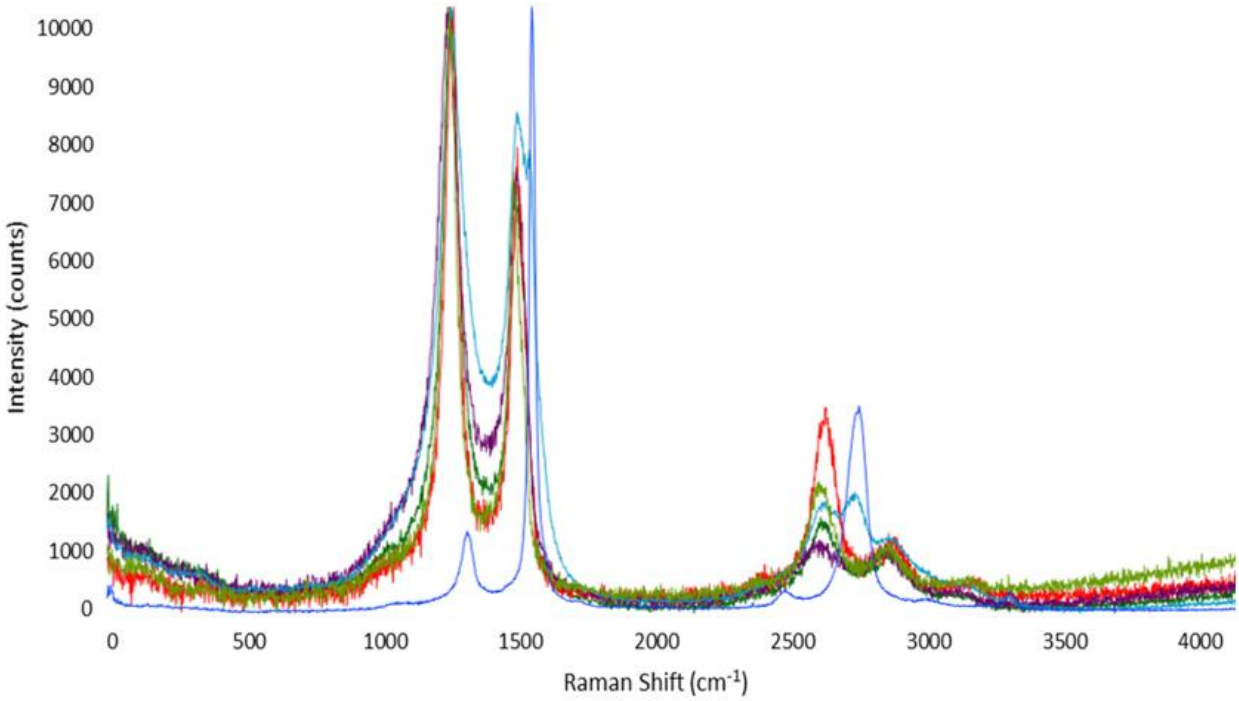

Figure 124 - Raman spectra of virgin Magnox graphite (dark blue), Magnox graphite with C-13 microwave deposit (dark green), Magnox graphite with C-13 microwave deposit after thermal treatment with a vacuum at 500°C (red), 550°C (purple), 600°C (light green), 650°C (light blue)

There was a wide variety in the intensity of the D peaks observed from the Magnox graphite samples with C-13 microwave deposits which were thermally treated without the application of a vacuum (Figure 125). The graphite sample with C-13 deposits which had not been thermally treated exhibited the highest intensity in the D peak. Samples which were thermally treated at 500°C and 550°C displayed a D peak intensity which was equal to that displayed by a non-thermally treated sample indicating the deposits were still present after treatment at these temperatures. This statement was corroborated by the SEM images which showed that the 'cauliflower' like deposit was still present. Interestingly the spectrum produced from the treatment at 550°C displayed the shifted G peak caused by the presence of C-13 as well as the ordinary G peak at ~1580 cm^{-1}. This indicated that some of the C-13 deposit had been oxidised to reveal the underlying graphite beneath. The samples that had undergone thermal treatment at 600°C and 650°C showed a decrease in the intensity of the D peak which was approaching the same intensity as virgin Magnox graphite and the spectral shift was no longer present indicating that the C-13 carbonaceous deposits had been successfully removed. This data confirmed the trends observed from the SEM images and mass spectrometer data.

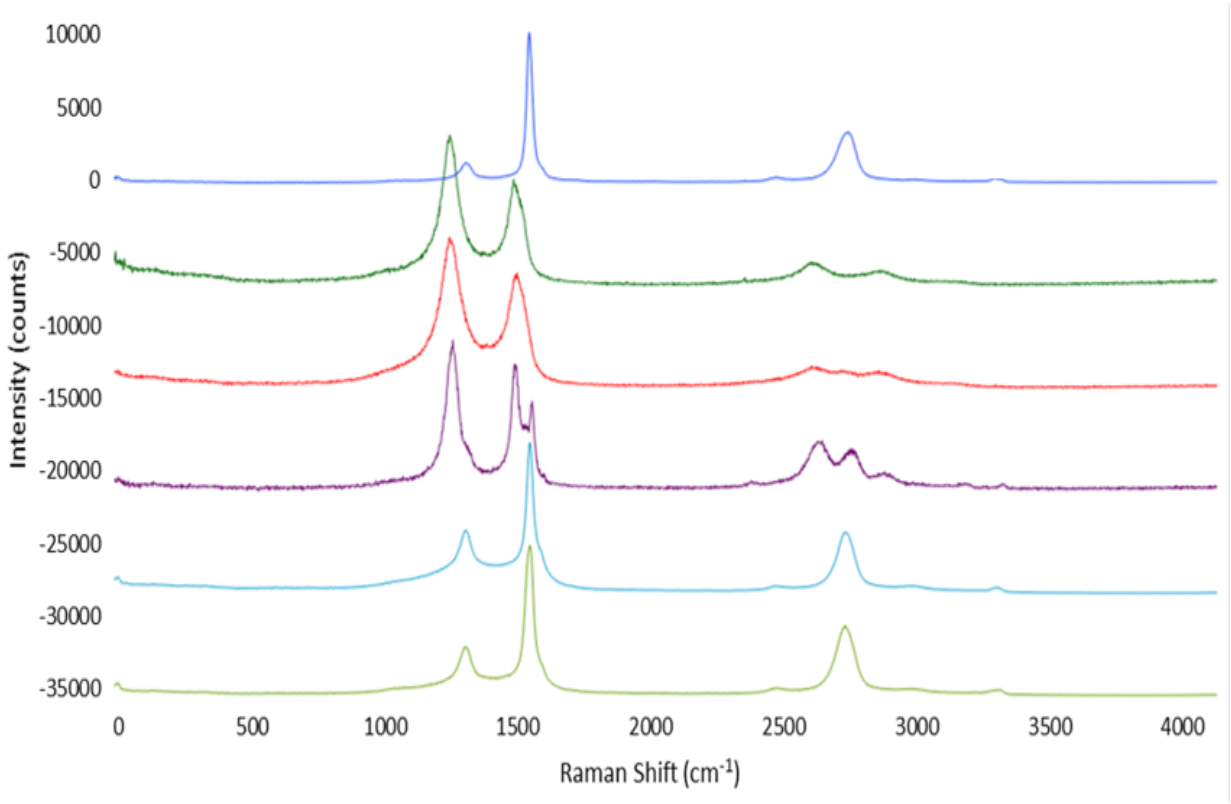

Figure 125 - Raman spectra of virgin Magnox graphite (dark blue), Magnox graphite with C-13 microwave deposit (dark green), Magnox graphite with C-13 microwave deposit after thermal treatment without a vacuum at 500°C (red), 550°C (purple), 600°C (light blue), 650°C (light green)

3.21 Carbon-14 Content of Carbonaceous Deposits and Graphite

This section provides the results and interpretation of the TGA of Oldbury reactor graphite and the partition of C-14 activities between irradiated graphite and carbonaceous deposits. As these results contain information on radioactivity it should be noted that units of radioactivity measure are Becquerels (Bq) which are defined as the activity of a quantity of radioactive material, in this case C-14, in which one nucleus decays per second. The results presented in the following sections will be quoted in Bq/g which is the specific activity of a given isotope per unit mass.

3.21.1 Complete C-14 content (Piece 1)

C-14 was positively identified in all of the Piece 1 graphite samples. Activity of C-14 has been quoted in Bq/g (Table 16 and Figure 126) and it ranges between 1.50E+05 Bq/g and 7.29E+05 Bq/g. As expected the activity of the Q15C5 samples decreases as their axial height in the core increases. The lower position samples from graphite layer 4 shows a factor 2 higher activity compared to the upper position sample. As will be seen in the TGA analysis below, there is a factor 2 difference in deposit concentration for these two samples which may explain the difference in activity. It is unlikely that C-14 precursor impurity levels would vary to this extent within a brick. Sample J17A4_13/1 (9U) has been removed from the highest axial height in the core and exhibits the lowest amount of activity at 1.50E+05 Bq/g.

Table 16 - Piece 1 C-14 analysis

NNL Identity	Piece 1 weight (g)	C-14 Activity (Bq/g)	Axial Height in core (m)
J17A4_13/1 (9U)	0.414	1.50E+05	6.85
J17A4_8/1 (6U)	0.256	2.98E+05	4.62
J17C5_8/1 (6U)	0.225	3.50E+05	4.62
Q15C5_2/1 (3U)	0.206	7.29E+05	1.98
Q15C5_3/1 (4L)	0.174	5.78E+05	2.66
Q15C5_4/1 (4U)	0.342	2.46E+05	2.95
Q15C5_8/1 (6U)	0.712	1.59E+05	4.62

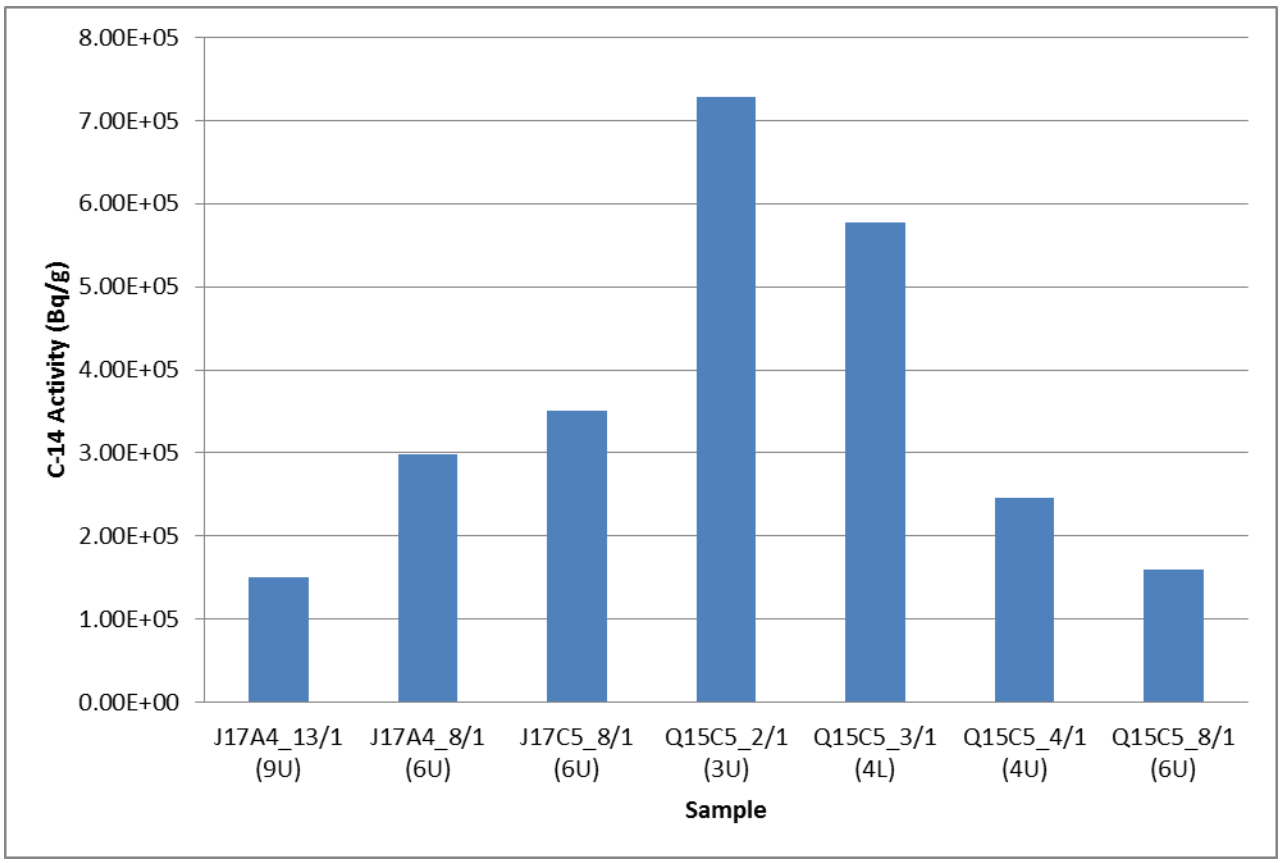

Figure 126 - C-14 activity for Piece 1 samples

3.21.2 Piece 2 Thermal Gravimetric Analysis

Piece 2 samples were subjected to TGA to determine the time required for removing the deposits by oxidation (Figure 127). Sample J17A4_8/1 exhibited an unusual profile and so was rejected from any further analysis. The other profiles show that the deposit present has a much faster oxidation rate than the underlying graphite, as expected; all samples lost ~1-3%. The time required for the removal of deposits ranged from 13-28 hours (Table 17).

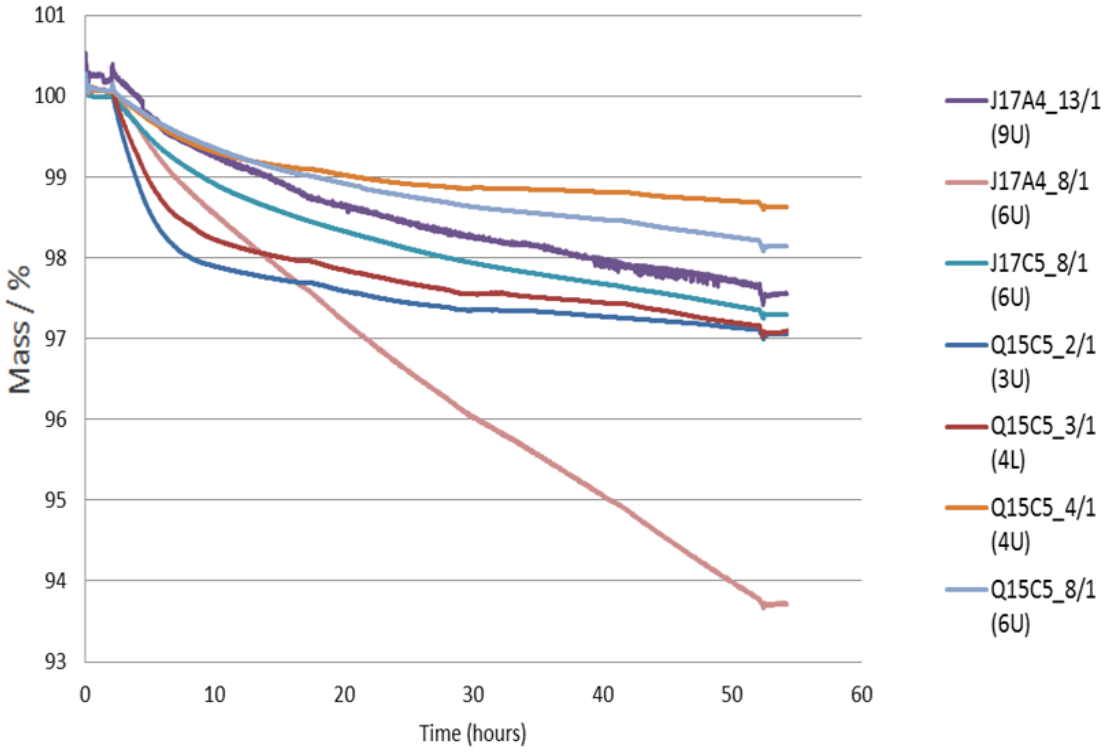

Figure 127 - TGA profiles of the Piece 2 samples

Table 17 - Deposit oxidation times

NNL Identity	Deposit oxidation time (hours)
J17A4_13/1 (9U)	28
J17C5_8/1 (6U)	28
Q15C5_2/1 (3U)	13
Q15C5_3/1 (4L)	16
Q15C5_4/1 (4U)	26
Q15C5_8/1 (6U)	28

3.21.3 Mathmatica Analysis

Using a standard model the application of Mathmatica software, which adds a non-linear plot to TGA data[131], was used to calculate the deposit concentration (μg of deposit per g of graphite), deposit reactivity (g of deposit per g of sample per hour) and graphite reactivity (μg of graphite per g of sample per hour) (Table 18).

Table 18 - Concentration and reactivity data of piece 2 samples

NNL Identity	Deposit concentration ($\mu g\ g^{-1}$)	Deposit reactivity ($g\ g^{-1}\ h^{-1}$)	Graphite reactivity ($\mu g\ g^{-1}\ h^{-1}$)	Axial Height in core (m)
J17A4_13/1 (9U)	13224	0.167	300.0	6.85
J17C5_8/1 (6U)	14350	0.183	290.3	4.62
Q15C5_2/1 (3U)	24699	0.361	129.4	1.98
Q15C5_3/1 (4L)	20759	0.297	191.8	2.66
Q15C5_4/1 (4U)	10144	0.175	89.6	2.95
Q15C5_8/1 (6U)	9990	0.166	203.5	4.62

Deposit concentrations range from 9990-24699 μg/g. The Q15C5 samples exhibit a trend of deposit concentration decreasing with increasing axial height up the core, as expected. This trend in deposit concentration is the same shown by historical Oldbury graphite samples[132]. Furthermore, the results from Piece 1 C-14 activity portray the same trend: as axial height increases the C-14 activity decreases. Samples J17A4_13/1 (9U) and J17C5_8/1 (6U) have very similar deposit concentrations. Although the former sample is from the highest location in the core, the samples originate from different channels.

3.21.4 Piece 3 Gas bubbler C-14 Content

Each Piece 3 sample has four allocated bubbler activities as well as the C-14 content of the residual graphite. The oxidation times have been set in order to capture principally C-14 from the deposits in the first stage and principally C-14 from the graphite in the second stage. However the allocation of C-14 between deposit and graphite may require some correction. Two gas bubblers were nominally allocated to the C-14 of the deposit (but will include some activity from oxidised graphite) and from now on will be noted D1 and D2. Two further bubblers were nominally allocated to the underlying graphite (but may include C-14 from any remaining deposit) and will now be known as G1 and G2. Activity has been quoted in Bq (Table 19) and is the activity based on the total volume of the sample (100 ml per bubbler). C-14 was positively identified in 14 of the 20 gas bubbler samples analysed. In order to display the results in terms of C-14 activity in the deposit compared to underlying graphite the activities from D1 and D2 have been combined as have G1 and G2 (Figure 128). Less than values are quoted when a result falls below the level that can be determined as an exact activity. The Minimum Detectable Activity (MDA) is a function of the background (or blank) counts and is based on a multiple (4.65) of the standard deviation of the counts (i.e. 4.65σb). The MDA formulas are based on the Currie paper[133] and documented in an American National Standard[134]. The less than values have been removed from any comparisons made and are only present in the second bubbler in the train which is not unusual.

Table 19 - Piece 3 gas bubbler activities

NNL Identity	C-14 Activity D1 (Bq)	C-14 Activity D2 (Bq)	C-14 Activity G1 (Bq)	C-14 Activity G2 (Bq)
J17A4_13/1 (9U)	5.51E+03	2.14E+00	1.63E+03	2.57E+00
Q15C5_2/1 (3U)	4.23E+04	<1.4E+00	8.88E+02	< 1.4E+00
Q15C5_3/1 (4L)	2.80E+04	<1.4E+00	6.40E+02	< 3.8E+00
Q15C5_4/1 (4U)	1.35E+04	2.27E+00	7.36E+02	< 3.7E+00
Q15C5_8/1 (6U)	1.01E+04	3.66E+00	1.44E+03	< 3.7E+00

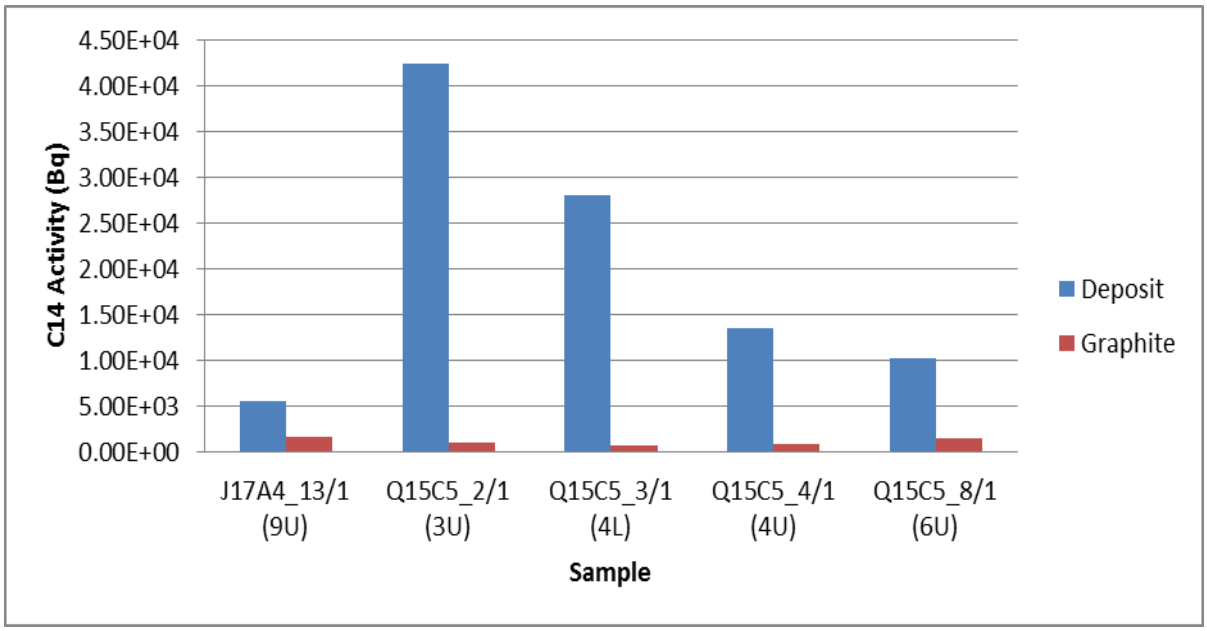

Figure 128 - Piece 3 combined gas bubbler activities

Similar to the Piece 1 C-14 activities the J17A4 sample has the lowest activity compared to the other samples. Again the Q15C5 samples C-14 activity decreases as axial height in the core increases. The gas bubbler data shows that there is a higher activity of C-14 released from the deposits than there is from ~1-2% of the underlying graphite. However these results do not take into account the activity present in the remaining solid graphite samples.

3.21.5 Piece 3 C-14 Content of Residual Graphite

C-14 was positively identified in all of the Piece 3 residual graphite samples. Activity has been quoted in Bq/g (Table 20 and Figure 129). There is again a significant amount of variation between the samples. The activities ranged from 5.57E+04 Bq to 8.83E+04 Bq. Deviating from the trend is the J17A4 sample which does not exhibit the lowest activity, even though it comes from the highest position in the core, although it does come from a different channel.

Table 20 - Piece 3 C-14 content of residual graphite

NNL Identity	Weight (g)	C-14 Activity (Bq/g)	Axial Height in core (m)
J17A4_13/1 (9U)	0.190	8.03E+04	6.85
Q15C5_2/1 (3U)	0.211	6.03E+04	1.98
Q15C5_3/1 (4L)	0.205	5.57E+04	2.66
Q15C5_4/1 (4U)	0.363	6.71E+04	2.95
Q15C5_8/1 (6U)	0.368	8.83E+04	4.62

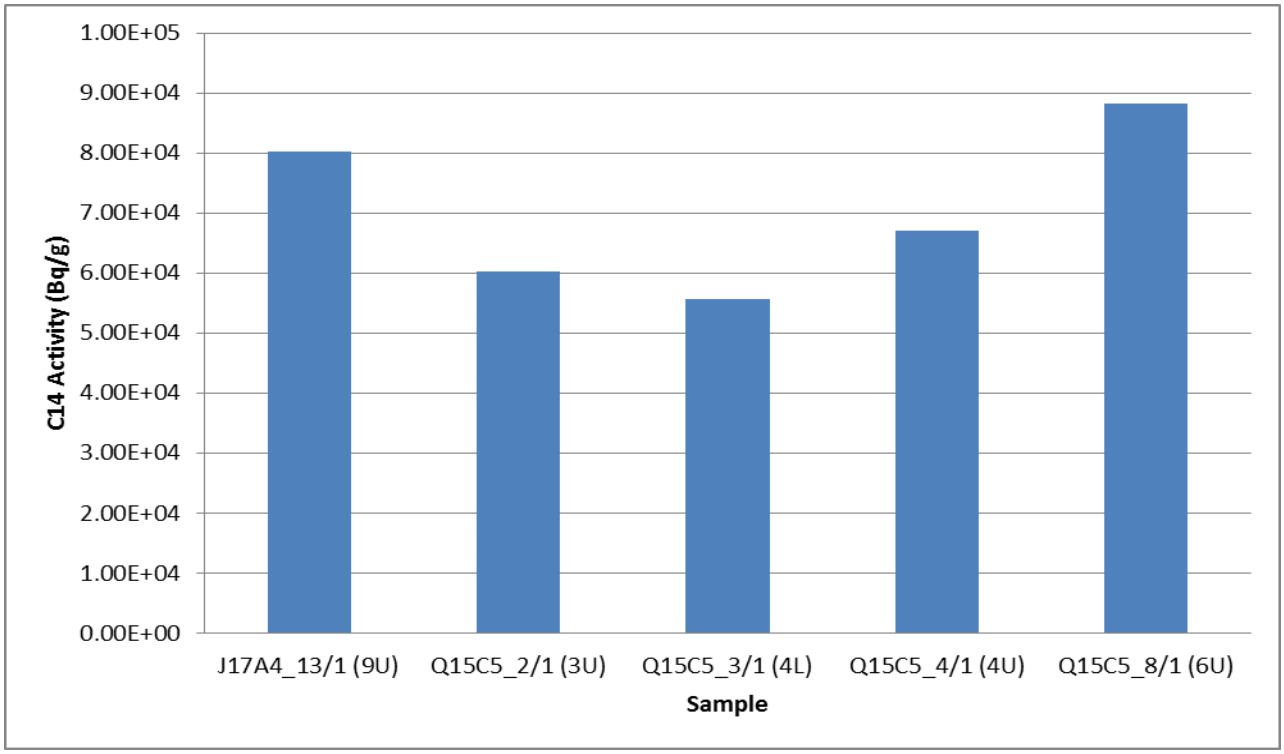

Figure 129 - C-14 content of residual graphite Piece 3 samples

3.21.6 Mass Balance

A mass balance calculation was performed for each sample in order to compare activities from Piece 1 solid samples with the combined activities of the Piece 3 bubbler and graphite solid samples (Figure 130). Unfortunately, the mass balances ranged from 77-33%. This may be due to the fact that the level of deposit is not uniform throughout the whole disc sample or was lost during machining into three pieces. It may be coincidental that the discrepancy increases with increasing total C-14 activity.

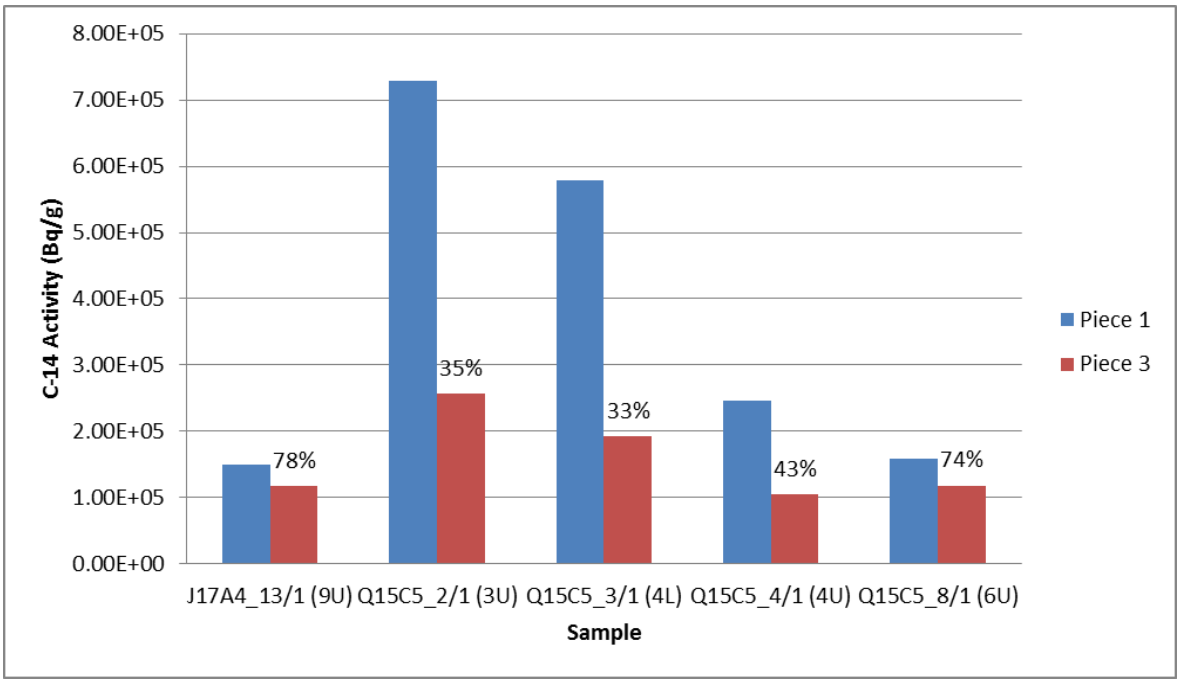

Figure 130 - Mass balance of Piece 1 samples compared to the combined activity of Piece 3 samples from the gas bubblers and residual graphite

3.21.7 Extended Oxidation

This experiment was included to measure the rate of C-14 released with increasing mass loss. After the deposit was removed (~2% mass loss), oxidation was continued until ~4% mass loss with the Drechsel bottles being changed at four ~0.5% mass loss increments. Sample J17C5_8/1 (6U) in Table 12 was chosen for this analysis. There were 10 Carbosorb gas bubblers associated with this experiment, two for each oxidation step. For illustrative purposes the data from both bubblers in one step have been combined (Table 21). There is significantly higher C-14 content in the bubblers attributed to the deposit than in the remaining bubblers combined (Figure 131). As mass loss increases the C-14 activity continues to decrease.

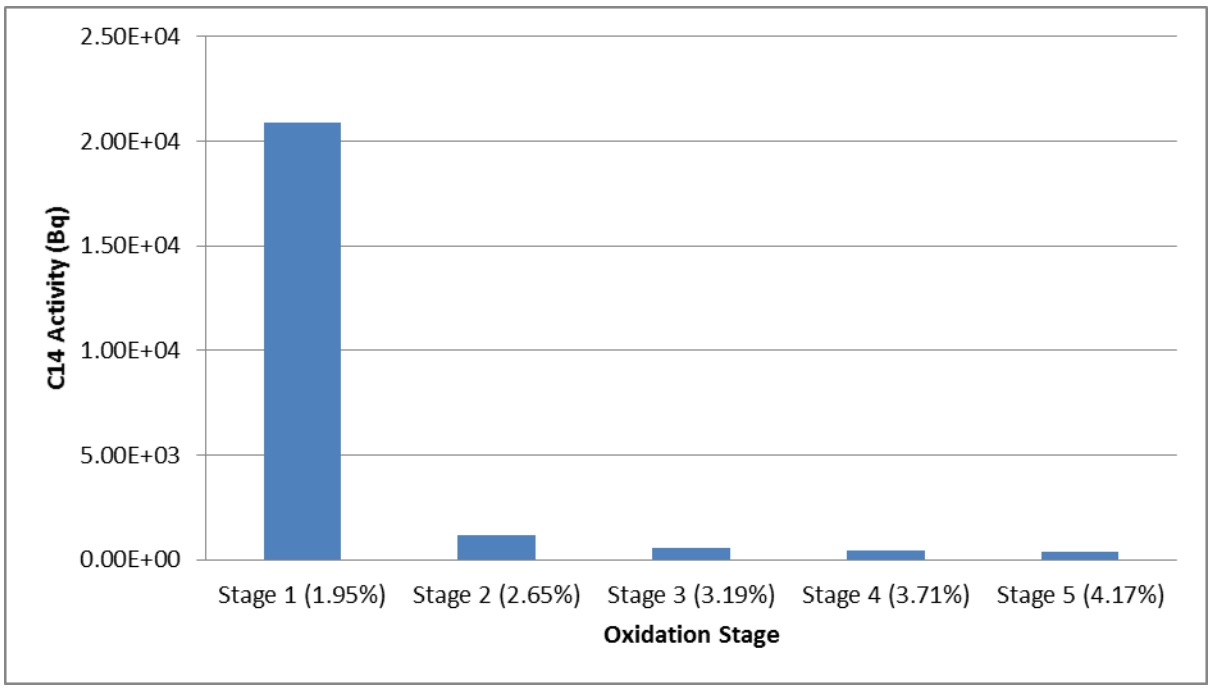

Figure 131 - C-14 activity with increasing mass loss (values in brackets show cumulative mass loss)

Table 21 - C-14 activity with increasing mass loss

Sample Name	C-14 Activity Bubbler 1 (Bq)	C-14 Activity Bubbler 2 (Bq)	Combined Activity (Bq)
Deposit	2.09E+04	1.63E+00	2.09E+04
Step 2	1.19E+03	1.47E+00	1.19E+03
Step 3	5.80E+02	2.50E+00	5.83E+02
Step 4	4.46E+02	1.80E+00	4.48E+02
Step 5	3.64E+02	2.12E+00	3.66E+02

3.21.8 C-14 Correction

In order to accurately interpret the allocation of C-14 activity between deposit and graphite it was necessary to perform a correction to the activity data from the gas bubblers. This is because the activity attributed to the deposit may contain activity from oxidised graphite and vice versa.

The specific activity of graphite used in the calculation was from the residual graphite remaining after TGA of Piece 3 samples. The specific activity of C-14 of the deposits had to be calculated by combining the TGA profiles of deposit and underlying graphite to extrapolate the mass of deposit and graphite lost. By multiplying the mass of graphite lost by the specific activity of graphite the amount of C-14 activity attributed to graphite was obtained. Subtraction of this value from the total C-14 activity detected in the gas bubbler (nominally attributed to the deposit) provides a more accurate C-14 activity attributed to the deposit (Bq). Dividing this value by the extrapolated mass of deposit calculated, provides the specific activity of C-14 from the deposit (Bq/g) (Table 22).

Table 22 - Corrected C-14 activity data

NNL Identity	Deposit C-14 Activity (Bq/g)	Graphite C-14 activity (Bq/g)
J17A4_13/1 (9U)	1.92E+06	8.03E+04
J17C5_8/1 (6U)	7.42E+06	7.14E+04
Q15C5_2/1 (3U)	9.78E+06	6.03E+04
Q15C5_3/1 (4L)	9.29E+06	5.57E+04
Q15C5_4/1 (4U)	4.67E+06	6.71E+04
Q15C5_8/1 (6U)	3.05E+06	8.83E+04

Specific activity of the deposit followed the same trend as previous data showing an increase in activity as axial height in the core increases. The average specific C-14 activity of graphite is 7.05E+04 Bq/g. Comparing this figure with the average specific C-14 activity of deposit which is 6.02E+06 Bq/g reveals an increase by of a factor of 85. These trends were not seen in the specific activity of the graphite, which is broadly similar for all samples.

3.21.9 Significance of C-14 Levels in Deposits

The analysis presented in the previous section, showing significantly higher C-14 specific activity in deposits compared to that for the underlying graphite, must be put into perspective in terms of C-14 activity across a whole fuel brick. Deposits are found principally on external brick surfaces in the fuel channels and within the graphite pores within a few millimetres of these external brick surfaces. A very approximate estimate of the total C-14 activity in deposits and in the underlying graphite can be made.

The mass of a fuel brick (average of an octagonal and square brick) is 89 kg taking no account of mass loss by radiolytic oxidation. Using the brick from which specimen Q15C5_2/1 (3U) was taken as an example, the total C-14 activity of the graphite will be 5.37E+09 Bq based upon the residual activity in Table 20. Assuming a uniform deposit cover, the deposit mass for the whole brick can be estimated from the ratio of the areas of the entire fuel channel surface to that of specimen Q15C5_2/1 (3U) and the mass of deposit on the specimen calculated in the analysis of the oxidation data in section 3.21.8.

The total mass of deposit is estimated to be ~50 g and so the total C-14 activity on the brick using the specific activity from Table 22 is 4.38E+08 Bq. Therefore the C-14 from deposit accounts for ~8% of the total C-14 activity in the brick. It is possible that this is an under-estimate: bricks with interstitial channel cut-outs are known to have deposits on interstitial channel surfaces (at a lower concentration). There may also be deposits on other outer brick geometric surfaces where there is no face to face contact between bricks, but there are no data for this. The brick selected here for analysis lies ~2 m from the bottom of the core. Studies have shown that potential C-14 contribution from carbonaceous deposit will vary with axial position[132].

While some form of oxidation treatment to remove deposits would reduce the C-14 activity of core components, any benefits for final disposal of the graphite cannot be quantified from the limited analysis presented here.

4. CONCLUSIONS

The scope of the work involved during this project involved working with both irradiated graphite samples and also attempting to simulate the carbonaceous deposits present on reactor graphite on virgin graphite material. The aim of the latter research was to develop a thermal treatment technique which would selectively remove the carbonaceous deposits whilst oxidising as little underlying graphite as possible.

4.1 Production of Carbonaceous Deposits

Two methods were investigated in order to produce carbonaceous deposits which could simulate those present on reactor graphite. Unfortunately the objective underlying the solution deposition technique of producing a large range of carbonaceous deposits using a number of structurally and chemically different carbon precursors was relatively unsuccessful in that only one of the carbon precursors (D-mannose) produced a successful deposit. This was most likely due to the fact that D-mannose is thermally stable at higher temperatures compared to the other precursors investigated. The deposit formed using D-mannose produced what might be best described as a glassy deposit. This deposit did not appear to be structurally similar to the deposits normally observed on reactor graphite, however care must be taken as there are limited studies on ex-reactor materials and these can be subject to significant differences. The D-mannose deposit also displayed different thermal characteristics from the deposits on the Oldbury graphite studied during this project. Therefore this technique was discarded as a means of producing simulant C-13 deposits.

Fortunately the second deposition technique investigated which utilised a microwave plasma and methane as a precursor produced a deposit morphologically similar to deposits found on reactor graphite. Additionally the microwave plasma produced deposit also exhibited broadly similar thermal characteristics; displaying oxidation at temperatures significantly lower than the graphite substrate.

4.2 Thermal Treatment

Thermal treatments have been demonstrated as an effective technique to decontaminate C-14 from a large volume of irradiated graphite during the incineration of GLEEP reactor graphite. However the temperatures involved in this process to date make its commercial viability questionable.

The data presented in Section 3.21.9 indicates that a 89 kg brick of graphite will contain approximately 50 g of deposit. Assuming a selectivity of 3:1 substrate removal to deposit removal (Section 3.20.2) this means that selective removal of the deposit would result in the treatment of an 89 kg brick producing a waste containing 200 g of carbon or 733 g of CO_2. This represents a significant volume reduction when considering storage within a deep geological repository. However counter to this is the fact that the deposit only contains 8% of the total C-14, hence the selective removal of the deposit would not make a significant reduction to the C-14 content of the waste stream which would be necessary for shallow burial, in current low level waste facilities.

The use of reduced pressure to improve the selectivity of the deposit removal was investigated. However, these studies confirmed that there were no benefits from using reduced pressure and that the selectivity is related to the rate of the oxidation process.

The combination of SEM and Raman spectroscopy in combination with evolved gas analysis proved to be a powerful technique for characterising carbonaceous deposits on the graphite surface and for the study of their subsequent selective oxidation.

4.3 Irradiated Graphite Research

The amount of deposit present on reactor graphite samples varies and appears to correspond with axial height in the reactor core, as previously observed in all Magnox cores. These deposits also have variable oxidation rates which may indicate the presence of catalytic impurities.

A significantly higher C-14 specific activity in the deposit was observed compared with that of the graphite. From the very limited data obtained from this study, the deposit specific activity showed a decrease with increasing axial height in the core whereas the graphite specific activity was broadly constant.

The variable (and in some cases poor) mass balances indicate that the level of deposit may not be uniform throughout the whole disc sample which were cut into three pieces.

The data from the extended oxidation experiment shows that the C-14 activity decreases significantly with increasing mass loss. The trend in C-14 activity after this first oxidation stage indicated the presence of some residual deposit in the second oxidation stage.

The average of the C-14 specific activities calculated for deposit and graphite indicate a significant difference, with the average C-14 activity of deposit higher than the average C-14 activity of graphite by a factor of 85.

Using a specimen taken from brick 3 as an example, the contribution from the deposit to the total C-14 activity of the whole fuel brick has been estimated to be ~8%. This contribution will vary with axial position within the core. While some form of oxidation treatment to remove deposits would reduce the C-14 activity of core components, any benefits for final disposal of the graphite cannot be quantified from the limited analysis presented here. As the deposit only contains ~8% of the total C-14 inventory for graphite; the assumption must be that the remainder is dispersed more uniformly through the brick. If the bulk of the C-14 is distributed through the brick then its origin is most likely from nitrogen trapped within the pore structure during its initial manufacture.

4.4 Sources of Error

Although great care was taken to ensure the accuracy of the results presented in this thesis during the course of the project there were numerous sources of error which increase the uncertainty of the results. The thermal treatment experiments were a 5 hour isotherm and due to the number of samples and different variables such as temperature and atmosphere, time restraints meant that no repeat analysis could be carried out. However TGA, SEM and Raman analysis were carried out on 2-3 graphite particles from each experiment to try and provide more comprehensive characterisation.

Apart from the work carried out using irradiated graphite samples, the graphite used for most of the experiments were prepared to have a particle size of 1-2 mm. This was achieved using a hydraulic press, pliers, hammers and a series of sieves. Due to the method of preparation and sample hardness there was a degree of variation from particle to particle. In addition it's difficult to ascertain the uniformity of the carbon deposition methods over the graphite particles.

The mass spectrometer used during the project had an internal pressure which had to be manually set before the experiments. As the isotherms lasted several hours there may have been a slight drift in pressure during the time of the experiments. In addition the evolved gases from the thermal treatments were detected using certain mass to charge fragments attributed to certain gases. However there may be a degree of uncertainty with certain traces, for example the m/z used for the detection of CO was 28 which is the same m/z which would be used for any N_2 present. The gases used for all of the experiments were a high purity see (Table 23) to ensure the accuracy of the results.

Table 23 – Purity of the gases used during the production of carbonaceous deposits

Gas	Chemical Purity (%)
Argon	99.998
Nitrogen	99.9
C-12 Methane	99.995
C-13 Methane (98.5% isotopic enrichment)	99.9

5. FUTURE WORK

From the analysis carried out during this project it appeared that the application of a vacuum to the thermal treatment of graphite was not beneficial to the selective removal of the carbonaceous deposits. However, additional work could be carried out in order to investigate this area further. Through coupling SEM with a catalyst stage, images could be taken during the thermal treatment to provide a better understanding of the oxidation process. Furthermore carrying out TGA with a vacuum applied and in combination with mass spectrometry would provide an improved understanding of the decontamination process. Although the thermobalance used in this study may not have been sensitive enough to detect a change in mass in the graphite samples with microwave deposits, perhaps the use of a larger sample size would enhance the signal. Through the analysis of irradiated graphite with carbonaceous deposits it is clear that the deposits have a very slow oxidation rate. This is most likely why a mass loss was not detected during TGA of graphite with microwave deposits. By using an isothermal temperature program for a longer period of time, a more accurate oxidation behaviour for these samples could be obtained. Furthermore isotherms at lower temperatures but with varying oxygen percentages could be undertaken to enhance our understanding of the different samples varying oxidation profiles. Additionally further investigation of the different oxidation behaviours between Magnox and AGR graphite could be carried out.

Regarding the analysis of irradiated graphite samples this study has been based upon just six graphite specimens taken from one Magnox reactor. Further work would be necessary to confirm the findings and to assess their significance for other cores in the Magnox fleet. The work could be extended to cover more Oldbury samples including those from interstitial channel positions as well as Wylfa samples to investigate differences between two stations with differing operational histories. The investigation of the contribution of the coolant to C-14 production in the deposits could be carried out with TGA and radiochemical analysis on Oldbury samples from enclosed and vented areas. Furthermore carrying out SEM before and after sectioning would confirm that the deposit is not removed during the machining process. If used in combination with Energy Dispersive X-ray Analysis (EDAX) then information on the impurities present in the sample could be ascertained. The investigation on the morphology and distribution of the deposit is also important.

6. REFERENCES

1. World Nuclear Association . Nuclear Power Reactors. 2013.
2. anon . Chicago Pile One (CP-1). atomicarchive.com . 2013.
3. anon . Early Exploration CP-1. Argonne National Laboratory . 2013.
4. anon Cadler Hall Power Station. The Engineer 1956.
5. The Institution of Electrical Engineers Nuclear Reactor Types; The Institution of Electrical Engineers : Savoy Place, London, WC2R 0BL, 2005.
6. Jensen, S. E.; Nonbol, E. Description of the Magnox Type of Gas Cooled Reactor (MAGNOX); 1999.
7. Mackay, R. M.; Probert, S. D. Nuclear Power. Applied Energy 1996, 55 (3-4), 305-323.
8. Nonbol, E. Description of the Advanced Gas Cooled Type of Reactor (AGR); 1996.
9. World Nuclear Association . Advanced Nuclear Power Reactors. 2013.
10. European Nuclear Society . Pebble bed reactor. 2013. European Nuclear Society.
11. Gen IV International Forum . Preparing Today for Tomorrow's Energy Needs. 2013.
12. Gen IV International Forum . Very-High-Temperature Reactor. 2013.
13. Pierson, H. O. Handbook of Carbon, Graphite, Diamond and Fullerenes - Properties, Processing and Applications; Noyes Publications: 1993.
14. Hall, G.; et al The Microstructual Modelling of Nuclear Grade Graphite. Journal of Nuclear Materials 2006, 353, 12-18.
15. Marsden, B. J. Nuclear Graphite for High Temperature Reactors; EPRI: 2001.
16. Kelly, B. T. The Structure and Manufacture of Nuclear Grade Graphite, Irradiation damage in Graphite due to fast neutrons in fission and fusion systems. IAEA-TECDOC-1154: 2000.

17. Lilley, J. Nuclear Physics: Principles and Applications; 1 ed.; John Wiley & Sons Ltd: 2001.

18. Fachinger, J. Decontamination of Nuclear Graphite by Thermal Methods. 2010. Paper Presented at IAEA Technical Committe Meeting on Progress In Radioactive Graphite Waste Managment, IAEA-TECDOC-1647 (Published as CD-ROM).

19. IAEA Progress in Radioactive Graphite Waste Management. IAEA-TECDOC-1647 (Published as CD-ROM): Vienna, 2010.

20. Wareing, A.; et al Synthesis of CARBOWASTE Work Package Findings . CARBOWASTE Treatment and Disposal of Irradiated Graphite and Other Carbonaceous Waste 2013, Deliverable T-1.7.3.

21. McKinney, J.; Barlow, S. Graphite Waste Treatment and Disposal-A UK Perspective on the current opportunities and issues. IAEA-TECDOC-1647 Progress in Radioactive Graphite Waste Management . 2010.

22. Banford, A. W.; et al Integrated Waste Management Approach WP 1 Review Report - Introduction. CARBOWASTE Treatment and Disposal of Irradiated Graphite and Other Carbonaceous Waste 2009.

23. Petit, L. WP 1 Review Report – France. CARBOWASTE 2009.

24. Poskas, P. WP 1 Review Report - Russia. CARBOWASTE 2009.

25. Office for Nuclear Regulation Quarterly News Oct-Dec 2011; 2011.

26. Banford, A. W.; Eccles, H.; Metcalfe, M. D. Integrated Waste Management Approach WP1-UK Chapter. CARBOWASTE D-1.4.4. 2009.

27. Wise, M. Management of UKAEA Graphite Liabilities. 1999. Paper Presented at IAEA Technical Committe Meeting on Nuclear Graphite Waste Management, IAEA-NGWM/CD 01-00120 (Published as CD-ROM).

28. NDA Higher Activity Waste - The Long Term Management of Reactor Core Graphite Waste Credible Options (Gate A); NDA Report: 2013.

29. NDA Geological Disposal - Review of Baseline Assumptions Regarding Disposal of Core Graphite in a Geological Disposal Facility; NDA Report: 2012.

30. NDA The 2010 UK Radiaoactive Waste Inventory: Main Report; 2010.

31. DEFRA Managing Radioactive Waste Safely: Proposals for Developing a Policy for Managing Solid Radioactive Waste in the UK; 2001.

32. White, I. F.; et al . Assessment of Management Modes for Graphite from Reactor Decommissioning. Commission of the European Communities . 1984.

33. Hou, X. Rapid analysis of C^{14} and H^{3} in graphite and concrete for decommissioning of nuclear reactor. Applied Radiation and Isotopes 62, 871-882. 2005.

34. Jones, A.; McDermott, L.; Marsden, B.; Marrow, T. J. Review of the Characterization of Nuclear Graphites in UK Reactors Scheduled for Decommissioning. IAEA-TECDOC-1647 Progress in Radioactive Graphite Waste Management Papers for discussion, 99-108. 2010.

35. Pick, M. E. Magnox Graphite Core Decommissioning and Disposal Issues. IAEA-TECDOC-1647 Progress in Radioactive Graphite Waste Management Papers for discussion, 1-13. 2010.

36. Nair, S. A Model for the Global Dispersion of ^{14}C Released to the Atmosphere as CO_2. Journal of the Society for Radiological Protection 1983, 3 (2), 16-22.

37. Yim, M.; Caron, F. Life Cycle and Management of Carbon-14 from Nuclear Power Generation. Progress in Nuclear Energy 2006, 48 (1), 2-36.

38. Ramsey, C. B. Radiocarbon Dating: Revolutions in Understanding. Archaeometry 2008, 50 (2), 249-275.

39. IAEA . Management of Waste containing Tritium and Carbon-14. 2004. IAEA Technical Reports Series No. 421 Vienna.

40. Mughabghab, S. F. Atlas of Neutron Resonances; 5th ed.; Elsevier: 2006.

41. Marsden, B. J.; Hopkinson, K. L.; Wickham, A. J. The Chemical Form of Carbon-14 within Graphite;NIREX Report; 2002.

42. Mason, J. B.; Bradbury, D. Pyrolysis and its Potential use in Nuclear Graphite Disposal. IAEA-TECDOC Nuclear Graphite Waste Management Technical Committee Meeting . 2001. Paper Presented at IAEA Technical Committe Meeting on Nuclear Graphite Waste Management, IAEA-NGWM/CD 01-00120 (Published as CD-ROM).

43. Wickham, A. J.; Marsden, B. J.; Sellers, R. M.; Pilkington, N. J. Graphite Core Stability during "Care and Maintenance" and "Safe Storage". IAEA-TECDOC-1043 Technologies for gas cooled reactor decommissioning, fuel storage and waste disposal , 225-232. 1997.

44. Bradbury, D.; Wickham, A. Graphite Decommissioning - Options for Graphite Treatment, Recycling, or Disposal, including a Discussion of Safety-Related Issues;EPRI Technical Report; 2006.

45. Moskovic, R.; Heard, P. J.; Flewitt, P. E. J.; Wootton, M. R. Overview of Strength, Crack Propagation and Fracture of Nuclear Reactor Moderator Graphite. Nuclear Engineering and Design 2013, 263, 431-442.

46. Allen, G. C.; Hallam, K. R. Carbon Deposition from a y-irradaited $CO_2/CO/CH_4/C_2H_6$ gas mixture on the Manganese Oxides MnO, Mn_3O_4 and Mn_2O_3. Journal of Nuclear Materials 1997, 250 (2-3), 111-117.

47. Allen, G. C.; Hallam, K. R. Carbon Deposition from a y-irradiated $CO_2/CO/CH_4/C_2H_6$ gas mixture on Fe_3O_4. Journal of Nuclear Materials 1998, 252 (1-2), 135-144.

48. Wickham, A. J. "Caring for the Graphite Cores" Seminar "The Review of Safety at Magnox Nuclear Installations". Institute of Mechanical Engineers London 1989, 79-86.

49. Heard, P. J.; Payne, L.; Wootton, M. R.; Flewitt, P. E. J. Evaluation of surface deposits on the channel wall of trepanned reactor core graphite samples. Journal of Nuclear Materials 2014, 445 (1-3), 91-97.

50. CoRWM Managing our Radioactive Waste Safely;CoRWM Doc 700; 2006.

51. NDA Higher Activity Waste - Operational Graphite Management Strategy Credible and Preferred Options (Gate A and B); NDA Report: 2013.

52. NDA Higher Activity Waste - Strategic Position Paper on the Management of Waste Graphite; NDA Report: 2014.

53. NDA Geological Disposal - Carbon-14 Project - Phase 1 Report; NDA Report: 2012.

54. Department for Business Enterprise and Regulatory Reform BERR Meeting the Energy Challenge - A White Paper on Nuclear Power; HM Government Crown Copyright: 2008.

55. CoRWM Ninth Annual Report 2012-13; CoRWM Doc 3107: 2013.

56. Nirex The Viability of a Phased Geological Repository Concept for the Long-term Management of the UK's Radioactive Waste;Nirex Report N/122; 2005.

57. Minshall, P. C.; Sadler, I. A.; Wickham, A. J. Radiolytic Graphite Oxidation Revisited. IAEA-TECDOC-901 Graphite Moderator Lifecycle Behaviour 1996, 181-191.

58. Petit, A.; Brie, M. Graphite Stack Corrosion of Bugey-1 Reactor (Synthesis). IAEA-TECDOC-901 Graphite Moderator Lifecycle Behaviour 1996, 167-180.

59. Best, J. V.; Stephen, W. J.; Wickham, A. J. Radiolytic Graphite Oxidation. Progress in Nuclear Energy 1985, 16 (2), 127-178.

60. Brocklehurst, J. E.; et al The Effect of Radiolytic Oxidation on the Physical Properties of Graphite. Journal of Nuclear Materials 1970, 35 (2), 183-194.

61. Minshall, P. C.; Wickham, A. J. The Description of Wigner Energy and its Release from Windscale Pile Graphite for Application to Waste Packaging and Disposal. IAEA-TECDOC Nuclear Graphite Waste Management Technical Committee Meeting 2001.

62. Guppy, R. M.; McCarthy, J.; Wisbey, S. J. Technical Assessment of the Significance of Wigner Energy for Disposal of Graphite Wastes from the Windscale Piles. IAEA-TECDOC Nuclear Graphite Waste Management Technical Committee Meeting 2001.

63. Worner, J.; Botzem, W.; Preston, S. D. Heat Treatment of Graphite and Resulting Tritium Emissions. IAEA-TECDOC Nuclear Graphite Waste Management Technical Committee Meeting 2001.

64. Lexa, D.; Dauke, M. Thermal and Structural Properties of Low-fluence Irradiated Graphite. Journal of Nuclear Materials 2009, 384, 236-244.

65. Wigner, E. P. Theoretical Physics in the Metallurgical Laboratory of Chicago. Journal of Applied Physics 1946, 17 (11), 857-863.

66. IAEA Characterization, Treatment and Conditioning of Radioactive Graphite from Decommissioning of Nuclear Reactors. 2006.

67. Marsden, B. J. Irradiation Damage in Graphite. IAEA-TECDOC-901 Graphite Moderator Lifecycle Behaviour 1996, 17-46.

68. Jones, C. J.; et al Assessments of the Stresses and Deformations in an RBMK Graphite Moderator Brick. IAEA-TECDOC-901 Graphite Moderator Lifecycle Behaviour 1996, 137-149.

69. Wickham, A. J.; Rahmani, L. Graphite Dust Explosibility in Decommissioning: A Demonstration of Minimal Risk. IAEA-TECDOC Nuclear Graphite Waste Management Technical Committee Meeting 2001.

70. von Lensa, W. Treatment and Disposal of Irradiated Graphite and Other Carbonaceous Waste. ATW International Journal for Nuclear Power 2011.

71. CARBOWASTE . The Consortium - Partners. 2014.

72. Banford, A. W.; et al CARBOWASTE - An Integrated Approach to Irradiated Graphite. NNL Report Nuclear Future 2008, 4 (5).

73. Fachinger, J.; von Lensa, W.; Podruhzina, T. Decontamination of Nuclear Graphite. Nuclear Engineering and Design 2008, 238 (11), 3086-3091.

74. Podruhzina, T. Graphite as Radioactive Waste: Corrosion Behaviour Under Final Repository Conditions and Thermal Treatment. Forschungszentrum Julich 2004, Jul-4166.

75. Fromherz, T.; Mendoza, C.; Ruette, F. Chemisorption of Atomic H, C, N and O on a Cluster-model Graphite Surface. Monthly Notices of the Royal Astronomical Society 1993, 263, 851-860.

76. Gray, W. J. A Study of the Oxidation of Graphite in Liquid Water in Radioactive Waste Storage Applications. Radioactive Waste Management 1982, 3 (2), 137-149.

77. Gray, W. J.; Morgan, W. C. Leaching of ^{14}C and ^{36}Cl from Hanford Reactor Graphite;PNL-6769; Pacific Northwest Laboratory Report: 1988.

78. Gray, W. J.; Morgan, W. C. Leaching and ^{14}C and ^{36}Cl from Irradiated French Graphite;PNL-6789; Pacific Northwest Laboratory Report: 1989.

79. Costes, J. R.; De Tassigny, C.; Vidal, H. Conditioning of Graphite Bricks from Dismantled Gas-cooled Reactors for Disposal. Waste Management 1990, 10, 297-302.

80. Takahashi, R.; Toyahara, M.; Maruki, S.; Ueda, H.; Yamamoto, T. Investigation of Morphology and Impurity in Nuclear Grade Graphite, and Leaching Mechanism of Carbon 14. IAEA-TECDOC Nuclear Graphite Waste Management, Technical Committee Meeting . 2001.

81. Gulbransen, E. A.; Andrew, K. F.; Brassat, F. A. The Oxidation of Graphite at Temperatures of 600°C to 1500°C and at Pressures of 2 To 76 Torr of Oxygen. Journal of the Electrochemical Society 1963, 110 (6), 476-483.

82. Zaghib, K.; Song, X.; Kinoshita, K. Thermal Analysis of the Oxidation of Natural Graphite: Isothermal Kinetic Studies. Thermochimica Acta 2001, 371, 57-64.

83. El-Genk, M. S.; Tournier, J. P. Comparison of Oxidation Model Predictions with Gasification Data of IG-110, IG-430 and NBG-25 Nuclear Graphite. Journal of Nuclear Materials 2012, 420, 141-158.

84. Delhaes, P. Chemical vapor deposition and infiltration processes of carbon materials. Carbon 40, 641-657. 2002.

85. Marcinek, M.; Hardwick, L. J.; Zukowska, G. Z.; Kostecki, R. Microwave plasma chemical vapor deposition of graphitic carbon thin films. Carbon 48, 1552-1557. 2010.

86. Chemical Vapour Deposition: Precursors, Processes and Applications; Royal Society of Chemistry: 2009.

87. Charmond, S.; Carry, C. P.; Bouvard, D. Densification and Microstructure Evolution of Y-Tetragonal Zirconia Polycrystal Powder during Direct and Hybrid Microwave Sintering in a Single-Mode Cavity. Journal of the European Ceramic Society 2010, 30, 1211-1221.

88. Lidstrom, P.; et al Microwave Assisted Organic Synthesis- A Review. Tetrahedron 2001, 57 (589), 9225-9283.

89. Von Starck, A.; Muhlbauer, A.; Kramer, C. Handbook of Thermoprocessing Technologies: Fundamentals, Processes, Components, Safety; Vulkan-Verlag GmbH: 2005.

90. Robinson, J.; et al Understanding Microwave Heating Effects in Single Mode Type Cavities- Theory and Experiment. Physical Chemistry Chemical Physics 2010, 12, 4750-4758.

91. Handbook of Microscopy; Weinheim: 1997.

92. Ferrari, A. C.; Robertson, J. Interpretation of Raman spectra of disordered and amorphous carbon. Physical Review B 2000, 61 (20), 95-107.

93. Chen, Z. Raman Spectroscopy. 2010. Organic Electronics, National University of Singapore.

94. Jickells, S.; Negrusz, A. Clarke's Analytical Forensic Toxicology; Pharmaceutical Press: 2008.

95. Das, R. S.; Agrawal, Y. K. Raman Spectroscopy: Recent advancments, techniques and applications. Vibrational Spectroscopy 2011, 57, 163-176.

96. Russell, N. V.; et al Development of TG measurements of intrinsic char combustion reactivity for industrial and research purposes. Fuel Processing Technology 1998, 57, 113-130.

97. Fuglein, E.; Schmolzer, S. TGA Measurements on Calcium Monohydrate;Application Note 16; NETZSCH: 2012.

98. Gabbott, P. Principles and Applications of Thermal Analysis; Blackwell Publishing Ltd: 2008.

99. March, R. E.; Todd, J. F. J. Quadrupole Ion Trap Mass Spectrometry; 2nd Edition ed.; John Wiley & Sons: 2005.

100. National Diagnostics Principles and Applications of Liquid Scintillation Counting; 2004.

101. Wichenden, D. A. Analysis of Tritium and Carbon-14 in Combustible Materials using the Carbolite/AEA Technology Combustion Furnace and associated apparatus;Carbolite Process Manual MF38PR; Barloworld Scientific: 2002.

102. Bronic, I. K.; et al Intercomparison of Low-Level Tritium and Radiocarbon Measurements in Environmental Samples. The First International Conferance On Radiation And Dosimetry In Various Fields Of Research RAD 2012.

103. Jones, A. N.; et al . Microstructural characterisation of nuclear grade graphite. Journal of Nuclear Materials 381, 152-157. 2008.

104. Yang, S. J.; et al Influence of H+ ion irradiation on the surface and microstructural changes of a nuclear graphite . Fusion Engineering and Design 2012, 87, 344-351.

105. Robertson, J. Diamond-like amorphous carbon. Materials Science and Engineering 2002, 37, 129-281.

106. Ferrari, A. C. Raman spectroscopy of graphene and graphite: Disorder, electron–phonon coupling, doping and nonadiabatic effects. Solid State Communications 2007, 143, 47-57.

107. Malard, L. M.; Pimenta, M. A.; Dresselhaus, G.; Dresselhaus, M. S. Raman spectroscopy in graphene. Physics Reports 2009, 473, 51-87.

108. Sadezky, A.; et al Raman microspectroscopy of soot and related carbonaceous materials: Spectral analysis and structural information. Carbon 2005, 43 (8), 1731-1742.

109. Donato, E.; et al Wavelength-dependent Raman activity of D_{2h} symmetry polycyclic aromatic hydrocarbons in the D-band and acoustic phonon regions. Chemical Physics 2004, 301, 81-93.

110. Reich, S.; Thomsen, C. Raman Spectroscopy of graphite. Philosophical Transactions of the Royal Society 2004, 362, 2271-2288.

111. Nemanich, R. J.; Solin, S. A. First- and second-order Raman scattering from finite-size crystals of graphite. Physical Review 1979, 20 (2), 392-401.

112. Chi, S.; Kim, G. Comparison of the Oxidation Rate and Degree of Graphitization of Selected IG and NBG Nuclear Grade Graphites. Journal of Nuclear Materials 2008, 381, 9-14.

113. Wang, I.; Ting, C. Raman Spectra of Carbohydrates. Journal of the Chinese Chemical Society 1972, 19, 63-71.

114. Ozbalci, B.; Boyaci, I. H.; Topcu, A.; Kadilar, C.; Tamer, U. Rapid analysis of sugars in honey by processing Raman spectrum using chemometric methods and artificial neural networks. Food Chemistry 2013, 136 (3-4), 1444-1452.

115. Jorio, A. Raman Spectroscopy in Graphene-Based Systems: Prototypes for Nanoscience and Nanometrology. ISRN Nanotechnology 2012.

116. Wang, S.; et al Catalytic Pyrolysis of Mannose as a Model Compound of a Hemicellulose over Zeolites. Biomass and Bioenergy 2013, 57, 106-112.

117. Venderbosch, R. H.; Heeres, H. J. Pyrolysis Oil Stabilisation by Catalytic Hydrotreatment. Biofuel's Engineering Process Technology 2011, 387-411.

118. Gunstone, F. D.; Harwood, J. L.; Padley, F. B. The Lipid Handbook; 2nd Edition ed.; Chapman and Hall: 1994.

119. Shen, L.; Alexander, K. S.; Dollimore, D. A. A Thermal Analysis Study of Myristic Acid. Thermochimica Acta 2001, 367-368, 69-74.

120. Khanna, P. K.; Kulkarni, D.; Beri, R. K. Synthesis and characterization of myristic acid capped silver naoparticles. Journal of Nanoparticle Research 2008, 10 (6), 1059-1062.

121. Zhang, Z.; et al Degassing behaviour of Nanostructured Al and its composites. Metallurgical and Materials Transactions 2010, 41 (2), 532-541.

122. Milovanovic, L.; et al Thermogravimetric analysis of the total lipids extracted from the fatty tissue of fallow deer (Cervus Dama dama L). Journal of the Serbian Chemical Society 2006, 71 (12), 1281-1288.

123. Srivastava, A.; Singh, V. B. Theoretical and experimental studies of vibrational spectra of naphthalene and its cation. Indian Journal of Pure and Applied Physics 2007, 45, 714-720.

124. Xu, J.; et al Liquid-phase exfoliation of graphene in organic solvents with addition of naphthalene. Journal of Colloid and Interface Science 2014, 418, 37-42.

125. Muradov, N.; Smith, F.; Bockerman, G.; Scammon, K. Thermocatalytic decomposition of natural gas over plasma-generated carbon aerosols for sustainable production of hydrogen and carbon. Applied Catalysis A: General 2009, 365 (2), 292-300.

126. Thomsen, C.; Reich, S. Raman Scattering in Carbon Nanotubes. Topics in Applied Physics 2007, 108, 115-232.

127. IAEA Irradiation Damage in Graphite due to Fast Neutrons in Fission and Fusion Systems. IAEA-TECDOC-1154, 2000, Appendix 2.

128. Lee, J. J.; Ghosh, T. K.; Loyalka, S. K. Oxidation Rate of Nuclear-grade Graphite NBG-18 in the Kinetic Regime for VHTR Air Ingress Accident Scenarios. Journal of Nuclear Materials 2013, 438, 77-87.

129. Levy, M. Oxidation of Pyrolytic Graphite in Air Between 1250° and 1850°F. Industrial and Engineering Chemistry Product Research and Development 1962, 1 (1), 19-23.

130. Xiaowei, L.; Jean-Charles, R.; Suyuan, Y. Effect of Temperature on Graphite Oxidation Behaviour. Nuclear Engineering and Design 2004, 227, 273-280.

131. Mowforth, C. W. The Reactivity with Air of Magnox Moderator Deposit;Nuclear Electric; 1991.

132. Boothby, R. M.; et al Assessment of the 2002 Graphite Monitoring Data from Oldbury Reactor 2 and their Implementation in Fault Study Codes;BNFL Report; 03.

133. Currie, L. A. Limits for Qualitative Detection and Quantitative Determination. Analytical Chemistry 1968, 40 (3), 586-693.

134. American National Standard Performance Criteria for Radiobioassay. Health Physics Society 1996, HPS N13.30.